

# **Interaction of metal and oxide surfaces with thin films of polar phthalocyanines**

## **Dissertation**

der Mathematisch-Naturwissenschaftlichen Fakultät  
der Eberhard Karls Universität Tübingen  
zur Erlangung des Grades eines  
Doktors der Naturwissenschaften  
(Dr. rer. nat.)

vorgelegt von  
M.Sc. Małgorzata Polek  
aus Zabrze (Polen)

Tübingen  
2021

Gedruckt mit Genehmigung der Mathematisch-Naturwissenschaftlichen Fakultät der Eberhard Karls Universität Tübingen.

Tag der mündlichen Qualifikation: 28.02.2022

Dekan: Prof. Dr. Thilo Stehle

1. Berichterstatter: Prof. Dr. Thomas Chassé

2. Berichterstatter: Prof. Dr. Marcus Scheele

## **Abstract (in English)**

In the first part of this thesis, interface properties of polar phthalocyanines (Pc's): chloroaluminum(III) phthalocyanine (AlClPc) and fluoroaluminum(III) phthalocyanine (AlFPc) are investigated in form of thin films deposited on two types of silver surfaces: a single crystal and a foil. The samples were analyzed with X-ray and ultraviolet photoemission spectroscopy (XPS and UPS). A strong interaction between the organic material and silver surface has been found, which is independent of silver substrate type used. The molecules undergo a loss of their central atom ligand, with the molecule ring staying intact. After de-attachment, the central atom ligand forms a bond with silver surface leading to the formation of Ag-Cl and Ag-F bonds on the surface of silver. What is more, roughness of the substrate surface influences the interface properties. An additional intensity is formed close to the Fermi edge for monolayer thick films. It is present only on substrates with high roughness and is an indication of gap states formation.

In the second part of thesis, interface properties of chloroaluminum(III) phthalocyanine (AlClPc) at the interface to two rutile titanium dioxide single crystal surfaces: (001) and (100) surface, have been studied with XPS and UPS. Additionally, the substrates were characterized with low energy electron diffraction (LEED) to provide information on surface structure and reconstruction. A strong interaction has been found between nitrogen atoms of phthalocyanine ring and titanium dioxide surface. The interaction is stronger on the (001) surface than the (100) surface due to their different surface structure, leading to the lower reactivity of the latter one. The reactivity can be varied with number of defects in the crystal structure. The interaction was found to depend on the amount of defects present. As a consequence, using oxygen during preparation steps decreases the amount of defects and allows to quench the interaction.

Furthermore, investigation of film growth on TiO<sub>2</sub> substrates was performed using mainly microscopy methods: atomic force microscopy and scanning electron microscopy (AFM, SEM). Decrease of substrate signal intensity observed in XPS provided complementary information on film growth. It has been found that the surface type has a strong influence on the AlClPc growth mode since the organic films have a layer-island growth on the (001) surface and possible island-only growth on the (100) surface. Introduction of defects influences the film morphology since the islands are more dense and smaller in size on oxygen treated ("defect-free") surface, while the island distribution on a reduced (defect-rich) (100) surface is scarce, and the islands are bigger in size.

Based on the results of experiments presented in this thesis, it was found that the interaction of phthalocyanines can be controlled with the substrate surface type: although charge transfer from the molecule to the substrate is observed on both surfaces, the interaction with silver influences the phthalocyanine center, while interaction with titanium dioxide influences the phthalocyanine ring.

Additionally, the reactivity of phthalocyanine molecules towards the titanium dioxide single crystals is dependent on the amount of defects present, thus can be controlled through adjustment of sample preparation conditions. The type and preparation of  $\text{TiO}_2$  surface has influence on film growth mode as well.

### **Zusammenfassung (auf Deutsch):**

Im ersten Teil der Dissertation wurden die Grenzflächeneigenschaften polarer Phthalocyanine (Pc's) untersucht. Es wurden hierbei Chloraluminium(III)-phthalocyanin (AlClPc) und Fluoraluminium(III)-phthalocyanin (AlFPc) in Form von Dünnschichtproben verwendet, die auf zwei unterschiedlichen Silberoberflächen abgeschieden wurden: Silber Einkristall und Silber Folie. Die Proben wurden mit Röntgen- und Ultraviolett-Photoemissionsspektroskopie (XPS und UPS) analysiert. Dabei wurde eine starke Wechselwirkung zwischen den organischen Materialien und den Silbersubstraten beobachtet, die unabhängig vom Silbersubstrattyp ist. Die Moleküle verlieren ihren Zentralatomliganden, wobei der Molekülring intakt bleibt. Der Zentralatomligand bildet eine Bindung mit der Silberoberfläche, was zur Bildung von Ag-Cl und Ag-F auf der Silberoberfläche führt. Darüber hinaus beeinflusst die Rauheit der Substratoberfläche die Grenzflächeneigenschaften. Eine zusätzliche Intensität wird nahe der Fermi-Kante für monolagendicke Filme gebildet. Es ist nur auf Substraten mit hoher Rauheit vorhanden und ist ein Hinweis auf die Bildung von Lückenzuständen.

Im zweiten Teil der Arbeit wurden die Grenzflächeneigenschaften von Chloraluminium(III)-phthalocyanin (AlClPc) an der Grenzfläche zu zwei Rutil-Titandioxid-Einkristalloboberflächen: (001) und (100)-Oberfläche, mit XPS und UPS untersucht. Zusätzlich wurden die Substrate mit niederenergetischer Elektronenbeugung (LEED) charakterisiert, um Informationen über Oberflächenstruktur und Rekonstruktion zu erhalten. Dabei wurde eine starke Wechselwirkung zwischen den Stickstoffatomen des Phthalocyaninrings und der  $\text{TiO}_2$ -Oberfläche gefunden. Die Wechselwirkung ist auf der (001)-Oberfläche stärker als auf der (100)-Oberfläche. Dies beruht auf der geringeren Reaktivität und Struktur der (100)-Oberfläche. Die Reaktivität kann mit der Anzahl der Defekte in der Kristallstruktur variiert werden. Es wurde festgestellt, dass die Wechselwirkung zwischen Pc's und  $\text{TiO}_2$ -Oberfläche von der Menge der vorhandenen Defekte abhängt. Infolgedessen verringert die Verwendung von Sauerstoff während der Präparationsschritte die Anzahl der Defekte und ermöglicht damit die Wechselwirkung aufzuheben.

Weitere Untersuchungen des Filmwachstums auf  $\text{TiO}_2$ -Substraten wurden hauptsächlich mit den Mikroskopiemethoden (AFM und SEM) durchgeführt. Die bei XPS beobachtete Abnahme der Substratsignalintensität lieferte ergänzende Informationen zum Filmwachstum. Es hat sich herausgestellt, dass der Oberflächentyp einen starken Einfluss auf den AlClPc-Wachstumsmodus hat, da die organischen Filme ein Schicht-Insel-Wachstum auf der (001)-Oberfläche und ein mögliches Insel-

Wachstum auf der (100)-Oberfläche aufweisen. Die Einführung von Defekten beeinflusst die Filmmorphologie, da die Inseln auf einer sauerstoffbehandelten (defektfreien) Oberfläche dichter und kleiner sind, während die Inselverteilung auf einer reduzierten (defektreichen) (100) Oberfläche gering ist und die Inseln eine größere Fläche aufweisen.

Als Ergebnis der in dieser Dissertation vorgestellten Experimente ist festzustellen, dass die Wechselwirkung von Phthalocyaninen durch den Oberflächentyp gesteuert werden kann: Obwohl auf beiden Oberflächen ein Ladungstransfer vom Molekül zum Substrat beobachtet wird, beeinflusst das Silber das Phthalocyaninzentrum und das Titandioxid den Phthalocyaninring. Darüber hinaus hängt die Reaktivität von Phthalocyaninmolekülen gegenüber den Titandioxid-Einkristallen von der Menge der vorhandenen Defekte ab und kann somit durch Anpassung der Probenvorbereitungsbedingungen gesteuert werden. Die Art und Vorbereitung der  $\text{TiO}_2$ -Oberfläche hat ebenfalls Einfluss auf den Filmwachstumsmodus.

## TABLE OF CONTENTS

<b>1.</b>	<b>INTRODUCTION AND MOTIVATION .....</b>	<b>9</b>
<b>2.</b>	<b>THEORETICAL BACKGROUND.....</b>	<b>11</b>
2.1	RELATION BETWEEN STRUCTURE AND PROPERTIES OF SOLIDS.....	11
2.2	PHthalOCYANINES.....	12
2.3	SUBSTRATES.....	13
2.3.1	Metal substrates - Silver .....	14
2.3.1.1	Foil .....	14
2.3.1.2	Single Crystal (100) .....	14
2.3.2	Wide gap semiconductors - TiO <sub>2</sub> .....	14
2.4	ANALYTICAL METHODS .....	16
2.4.1	Photoemission Spectroscopy (PES) .....	16
2.4.1.1	X-ray Photoelectron Spectroscopy (XPS).....	17
2.4.1.2	Ultra Violet Photoelectron Spectroscopy (UPS) .....	20
2.4.2	Low Energy Electron Diffraction (LEED).....	22
2.4.3	Atomic Force Microscopy (AFM) .....	26
2.4.4	Scanning Electron Microscopy (SEM) .....	28
<b>3.</b>	<b>EXPERIMENTAL SETUP .....</b>	<b>29</b>
3.1	MATERIALS.....	29
3.2	SAMPLE HOLDERS.....	29
3.3	SUBSTRATE PREPARATION .....	31
3.4	MEASUREMENT EQUIPMENT .....	31
3.4.1	Vacuum system .....	31
3.4.2	X-ray photoelectron spectroscopy (XPS).....	32
3.4.3	Ultraviolet photoelectron spectroscopy (UPS).....	33
3.4.4	Low energy electron diffraction (LEED).....	33
3.4.5	Atomic force microscopy (AFM).....	34
3.4.6	Scanning Electron Microscopy (SEM) .....	34
3.5	FILM DEPOSITION .....	34
3.6	DETERMINATION OF FILM THICKNESS.....	35
3.7	DETERMINATION OF ORGANIC FILM COMPOSITION .....	37
<b>4.</b>	<b>RESULTS AND DISCUSSION .....</b>	<b>40</b>
4.1	INTERACTION BETWEEN HALOGEN SUBSTITUTED ORGANIC SEMICONDUCTORS (ALClPc AND ALFPc) AND SILVER SUBSTRATES .....	41
4.1.1	AlClPc on Ag(100) single crystal.....	41
4.1.1.1	Characterization of clean Ag(100) surface .....	41
4.1.1.2	LEED patterns - Ag(100) single crystal surface structure .....	43
4.1.1.3	Characterization of AlClPc thin films on silver single crystal.....	43
4.1.1.4	Reaction of chlorine ligand with Ag(100) surface .....	47
4.1.1.5	Valence band region and work function .....	49
4.1.1.6	Interaction with silver substrates vs. phthalocyanine molecular orientation .....	51
4.1.2	AlClPc on silver foil .....	52

4.1.2.1	Characterization of clean Ag foil .....	52
4.1.2.2	Characterization of AlClPc thin films on silver foil.....	54
4.1.2.3	Reaction of chlorine ligand with silver foil .....	55
4.1.2.4	Valence band region, work function and energy level alignment.....	57
4.1.2.5	Influence of substrate roughness.....	59
4.1.3	AlFPc on Ag foil.....	60
4.1.3.1	Ag foil - substrate characterization .....	60
4.1.3.2	Characterization of AlFPc thin films on silver foil.....	61
4.1.3.3	Reaction of fluorine ligand with silver foil.....	63
4.1.3.4	Valence band spectra of AlFPc films.....	64
4.1.4	Chapter summary .....	66
4.2	INTERACTION BETWEEN HALOGEN SUBSTITUTED ORGANIC SEMICONDUCTOR MOLECULES (ALCLPC) AND TiO <sub>2</sub> (100) SUBSTRATE. ....	67
4.2.1	Characterization of a clean TiO <sub>2</sub> (100) surface at different degrees of reduction .....	67
4.2.1.1	Substrate overview - differences resulting from two types of preparation.....	67
4.2.1.2	Ti 2p and O 1s spectra - determination of defects amount .....	68
4.2.1.3	LEED patterns - Influence of defect on TiO <sub>2</sub> (100) surface structure .....	70
4.2.1.4	Microscopy images of TiO <sub>2</sub> (100) surface preparation stages.....	75
4.2.2	Characterization of AlClPc films on TiO <sub>2</sub> (100) surface .....	77
4.2.2.1	Influence of phthalocyanine deposition on TiO <sub>2</sub> (100) core level spectra .....	77
4.2.2.2	Interaction of TiO <sub>2</sub> (100) with molecule ring.....	79
4.2.2.3	Phthalocyanine metal center and central metal ligand core levels .....	82
4.2.2.4	Electronic properties of AlClPc films on TiO <sub>2</sub> (100) .....	84
4.2.2.5	Energy level diagrams.....	86
4.2.2.6	AlClPc film growth – microscopy images.....	87
4.2.2.7	Island shape explanation.....	93
4.2.3	Chapter summary .....	95
4.3	INTERACTION BETWEEN HALOGEN SUBSTITUTED ORGANIC SEMICONDUCTOR MOLECULES (ALCLPC) AND TiO <sub>2</sub> (001) SUBSTRATE .....	96
4.3.1	Characterization of a clean TiO <sub>2</sub> (001) surface at different degrees of reduction .....	96
4.3.1.1	Substrate overview – influence of preparation procedure.....	96
4.3.1.2	Ti 2p and O 1s spectra – variation of defects amount with reduction degree.....	97
4.3.1.3	LEED patterns - Influence of defect on TiO <sub>2</sub> (001) surface structure .....	99
4.3.1.4	Microscopy images of TiO <sub>2</sub> (001) preparation stages .....	102
4.3.2	Characterization of AlClPc films on TiO <sub>2</sub> (001) surface .....	105
4.3.2.1	Influence of phthalocyanine deposition on TiO <sub>2</sub> (001) core level spectra .....	105
4.3.2.2	Interaction of TiO <sub>2</sub> (001) with molecule ring.....	106
4.3.2.3	Phthalocyanine metal center and central ligand related core levels.....	110
4.3.2.4	Electronic properties of AlClPc films on TiO <sub>2</sub> (001) .....	112
4.3.2.5	Energy level diagrams.....	115
4.3.2.6	AlClPc film growth - substrate signal attenuation.....	116
4.3.2.7	Microscopy images of AlClPc films .....	117
4.3.3	Chapter summary .....	119
<b>5.</b>	<b>CONCLUSIONS.....</b>	<b>121</b>
<b>6.</b>	<b>APPENDIX .....</b>	<b>124</b>
6.1	ABBREVIATIONS.....	124
6.2	FITTING TABLES.....	125

6.2.1	AICIPc on Ag(100) .....	125
6.2.2	AICIPc on Ag foil.....	126
6.2.3	AIFPc on Ag foil.....	127
6.2.4	AICIPc on TiO <sub>2</sub> (100).....	128
6.2.5	AICIPc on TiO <sub>2</sub> (001).....	131
6.3	SUPPORTING INFORMATION – ALCLPc ON TiO <sub>2</sub> (001) (5% Ti <sup>3+</sup> ) .....	134
6.4	SUPPORTING INFORMATION – ALCLPc ON TiO <sub>2</sub> (001) (50% Ti <sup>3+</sup> ) .....	136
<b>7.</b>	<b>LIST OF REFERENCES.....</b>	<b>137</b>
<b>8.</b>	<b>LIST OF PUBLICATIONS .....</b>	<b>146</b>
8.1	PEER-REVIEWED PAPERS .....	146
8.2	CONFERENCE CONTRIBUTIONS .....	146

### 1. Introduction and Motivation

The organic semiconductors rise opportunity for low cost devices with layer architecture, due to the possibility of preparation of thin films of such materials by several coating processes like evaporation, printing or spin coating. These methods are well established and broadly available.

The open questions that appear frequently considering organic devices are about their efficiency and stability. The same questions apply to the components of a device. For this reason, it is important to learn about the interactions at the interfaces of such building materials. Reactions at the interfaces might influence or even quench the charge transfer between the building blocks, deeming the device less efficient or useless. In this work the interactions at the interfaces of phthalocyanines (semiconducting organic molecules) and silver as well as titanium dioxide (both used as electrodes in devices) are investigated. It is shown that variation of the substrate (here silver and titanium dioxide) influences differently the phthalocyanine molecule which either reacts by its center or ring. Considering that the charge transfer from and to phthalocyanine molecule might happen at different parts of the molecule, changing the electrode material might block or promote the charge transfer to different parts of the phthalocyanine.

Additionally, careful characterization of the substrates themselves is crucial in understanding the possible interactions with the molecules deposited at their surfaces. This is important since different crystal planes of metal oxides vary in physical and chemical properties. This fact can be used further to vary the interaction with the molecules deposited at the metal oxide surface. Furthermore, the presence of defects in metal oxides influences the substrate properties. The defects are a major parameter defining the properties of metal oxide. Due to the need of characterization of substrate surface and interfaces between materials, a set of surface sensitive methods has to be used. In this work photoemission spectroscopy (divided into X-ray photoemission spectroscopy, and ultraviolet photoemission spectroscopy), low energy electron diffraction as well as microscopy methods are used to fully investigate the organic/metal and organic/metal oxide systems. The advantage of photoemission spectroscopy is that it is a non-destructive method, so that the samples can be measured with other techniques, even after several XPS and UPS measurements.

Specially synthesized molecules of the class of phthalocyanines are chosen to study correlations between molecular properties such as dipole moments or reactivity and their growth and electronic properties. The studies will be carried out using complementary spectroscopic techniques: X-ray and ultra violet photoemission spectroscopy, as well as microscopy techniques (AFM, SEM), which should provide wide and detailed experimental information on these physical properties.

## **1. Introduction and Motivation - 2.1 Relation between structure and properties of solids**

The properties of organic films can be modified through variation of substrate temperature and the use of magnetic field<sup>1</sup> during deposition. The variation of substrate type<sup>2</sup> or introduction of defects can also lead to modification of the properties, as shown within the scope of this work.

## 2. Theoretical background - 2.1 Relation between structure and properties of solids

### 2. Theoretical background

This chapter focuses on the principles behind the scientific methods applied in the experiments presented in this work, as well as the description of the materials used. This should give the reader an insight into the material types used in the semiconductor devices and analytical tools available to probe the interfaces between these materials.

#### 2.1 Relation between structure and properties of solids

The matter surrounding us can be differentiated based on many parameters. One of them is the ability of materials to conduct electricity. Typically, one describes materials with a band model. The requirement for the conduction of charges are partially filled bands from which charges may be either removed or added.<sup>3</sup>

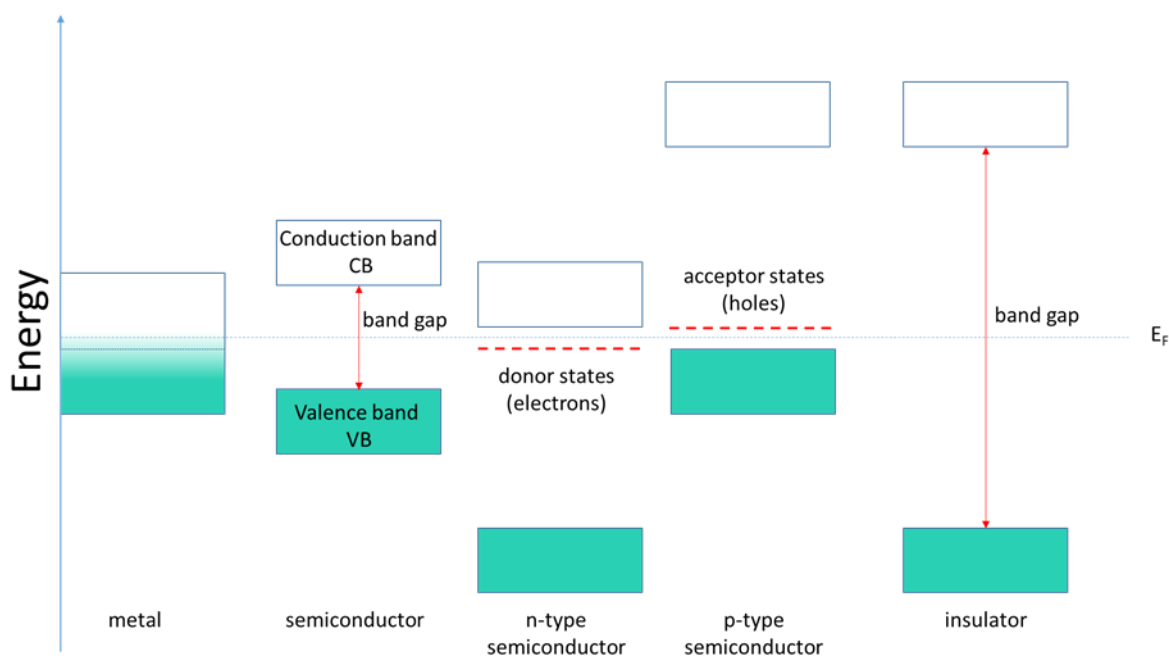


Figure 2.1 Band diagram of materials differing by their conductivity at the temperature  $T = 0$  K. From left: metal, semiconductor, n-type semiconductor, p-type semiconductor and insulator.

A band diagram of materials differing by their ability to conduct electricity is presented in Figure 2.1. One can clearly recognize, they differ in the size of band gap and position of Fermi level (at the temperature of 0 K, it is the highest energy level that electrons can occupy).<sup>4</sup> The common feature of semiconductors, whether organic or inorganic<sup>5, 6</sup>, is that they can be doped with additional charge donors or charge acceptors (resulting in n-type or p-type semiconductor) to improve their conductivity and adjust their electronic structure.<sup>3</sup> If the structure of an insulator is modified it can be promoted to become a semiconductor. This can be done through introducing defects in the material structure (for example point defects in ideal  $\text{TiO}_2$  single crystal), because they can serve as charge donors or

## 2. Theoretical background - 2.2 Phthalocyanines

acceptors too. The structure modifications introduce additional electronic bands available for charges to occupy. The presence of defects influences both conductivity and reactivity of the semiconductor, since it can give or receive charges needed for a chemical bond to be formed. A change in structure influences the properties of a material.

### 2.2 Phthalocyanines

Phthalocyanines are organic semiconductors with a system of conjugated pi-bonds. The simplest phthalocyanine is a planar ring consisting of four isoindole units with two hydrogen atoms in the center. The molecule can be adjusted by introduction of a central metal atom to form a phthalocyanine metal complex. In that case, the two hydrogens in the middle of the molecule are removed, and the four pyrrole nitrogen atoms marked with green circle in Figure 2.2 are attached to the metal atom in the center of the molecule. The bridging nitrogen atom marked in red circle has different chemical surrounding, but is still very close in binding energy to the pyrrole nitrogen. Two type of carbon atoms are present in the ring as well. The pyrrole carbon marked in blue circle and benzene carbon marked with magenta circles.

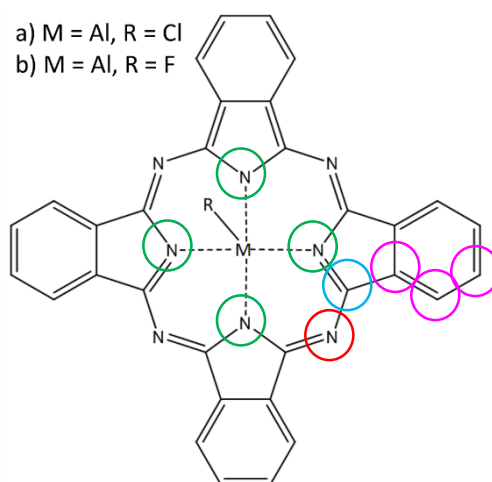


Figure 2.2 Chemical formula of a phthalocyanine molecule: a) chloroaluminum (III) phthalocyanine, b) fluoroaluminum (III) phthalocyanine. The circles mark two types of nitrogen and carbon atoms in the molecule (see main text for explanation).

Metal phthalocyanines are chemically and thermally stable. Their structural similarity to porphyrin complexes combined with accessibility in terms of the cost and large scale preparation makes them attractive as catalysts.<sup>7</sup> The phthalocyanine ring can be modified further through introduction of ligands either at the periphery of the ring, or at the central metal atom, perpendicular to the phthalocyanine ring plane. Modifications of the phthalocyanine ring allow a change of the molecule electronic properties, i.e. if hydrogen atoms of CuPc, a p-type semiconductor, are replaced with fluorine, the resulting  $\text{F}_{16}\text{CuPc}$  molecule is an n-type semiconductor.<sup>8</sup>

## 2. Theoretical background - 2.3 Substrates

The axially substituted phthalocyanines can be used as building blocks of solar cells<sup>9</sup>, due to their electronic properties and the possibility to evaporate them in form of thin films.<sup>10</sup> The periphery-substituted Pcs can be used as sensitizers in dye sensitized solar cells DSSC to replace the more expensive and less durable ruthenium (II) sensitizers<sup>11</sup> This shows the flexibility of phthalocyanines in terms of properties adjustment through molecule structure modification.

In this work, the focus is given to the polar phthalocyanines consisting of a phthalocyanine ring, a metal center with a ligand attached at the metal center along the molecule symmetry axis. The presence of axial ligand gives the molecules a non-planar geometry and a permanent dipole moment. Polar phthalocyanines provide an insight into the relation between molecule structure and thin film properties.<sup>10</sup> Upon deposition, the molecules can adopt different adsorption configurations in which the polar axial group is either facing vacuum (upward orientation) or the substrate surface (downward orientation).<sup>12-14</sup> This can influence the interface properties of the phthalocyanines.<sup>15</sup> Due to their permanent dipole moment, the orientation of the molecules within a thin film can be controlled with the external electromagnetic fields.<sup>1</sup>

An example of a polar phthalocyanine is AlClPc which molecular structure is presented in Figure 2.2a. It can be seen that the molecule has a system of conjugated  $\pi$ -bonds within a chlorine atom protruding out of the ring plane, giving the molecule  $C_{4v}$  symmetry<sup>13</sup> As stated before, due to presence of the axial ligand, the molecule exhibits a permanent dipole moment of 3.7 D.<sup>15</sup> This polar phthalocyanine sublimes intact in the form of monomers.<sup>16</sup> As it will be shown in the next chapter, the axial ligand can undergo chemical reactions upon adsorption on silver substrate.<sup>17</sup>

The axial ligand of polar-phthalocyanine can be adjusted to change the dipole moment value. As an example, the substituent at the metal atom can be changed from chlorine to fluorine atom resulting in the fluoroaluminum phthalocyanine seen in Figure 2.2b.

### 2.3 Substrates

Several substrates were used to model the interfaces within an electronic device. In the group of silver substrates, the surface order was varied between the less ordered silver foil and the silver single crystal with (100) oriented surface. In the group of titanium dioxide substrates, single crystals with (100) and (001) surface orientation were used. It allowed to investigate how variation in reactivity of  $TiO_2$  surface influences phthalocyanine molecules, since both surface orientations are expected to differ in reactivity. The differences in interaction of organic molecules and substrates from each groups will be discussed in Chapter 4.

### 2.3.1 Metal substrates - Silver

Silver is a metal with electron configuration of  $[\text{Kr}] 4d^{10} 5s^1$ . Its d shell is fully occupied with electrons. It is conductive in room temperature and has the highest conductivity of all untreated metals.<sup>18</sup> Due to its excellent conductivity it is used frequently for fabrication of electrodes in electronic devices. While the material itself is not transparent, it is possible to fabricate silver grids<sup>19</sup>, which are flexible and transparent, and can be used in the flexible organic solar cells.

#### 2.3.1.1 Foil

The silver foil serves as a model of an imperfect silver surface. While having rather good purity, the surface is not ordered. As it is shown later, the roughness of the silver foil has influence on the extent of chemical reactions between phthalocyanine molecules and the silver substrate.

The rough silver foil surface differs from ordered single crystal surface not only by its surface roughness but also by the electronic properties like work function which value is 4.2 eV. The foil is an example of a substrate with higher roughness, a non-ideal type of a surface, closer to the real life application electrodes.

#### 2.3.1.2 Single Crystal (100)

Silver single crystal has a fcc (face centered cubic) structure. The silver atoms in the (100) plane all have equal spacing. Silver single crystal planes differ from each other by their work function, the (100) plane (marked in orange, see Figure 2.3) has work function value of 4.6 eV.<sup>20</sup> The silver single crystal is used in this work as a model reactive metal surface, due to its long range order of atoms at the crystal surface.

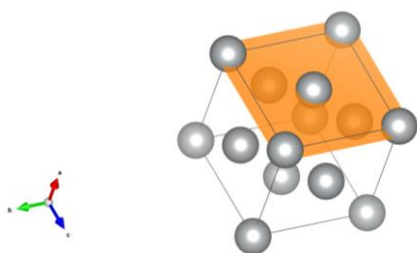


*Figure 2.3 Silver face centered cubic crystal structure with (100) plane marked in orange, the unit cell is marked with black lines forming a cube.*

### 2.3.2 Wide gap semiconductors - $\text{TiO}_2$

Titanium dioxide, a material belonging to inorganic semiconductors, exists in several polymorph forms. Among them rutile is the most stable form of  $\text{TiO}_2$  at high temperatures. The stability of  $\text{TiO}_2$  polymorphs is influenced by their structure. Due to the smallest amount of shared edges and corners between the coordination octahedral in rutile, it is the most stable polymorph of  $\text{TiO}_2$  (according to

## 2. Theoretical background - 2.3 Substrates

the third Pauling rule).<sup>21</sup> A list of stable, metastable and high pressure  $\text{TiO}_2$  polymorphs can be found in the work of Hanaor et al.<sup>22</sup> The rutile  $\text{TiO}_2$  single crystal is composed of Ti atoms with formal oxidation state 4+ and oxygen atoms with oxidation state 2-. Due to the electron configuration of titanium, it is possible that titanium atom is six fold coordinated to oxygen atoms, forming an octahedron.<sup>23</sup> Each oxygen atom is bound to three titanium atoms. A unit cell of rutile is shown in Figure 2.4a while the arrangement of the octahedrons in the rutile crystal is shown Figure 2.4b. Comment

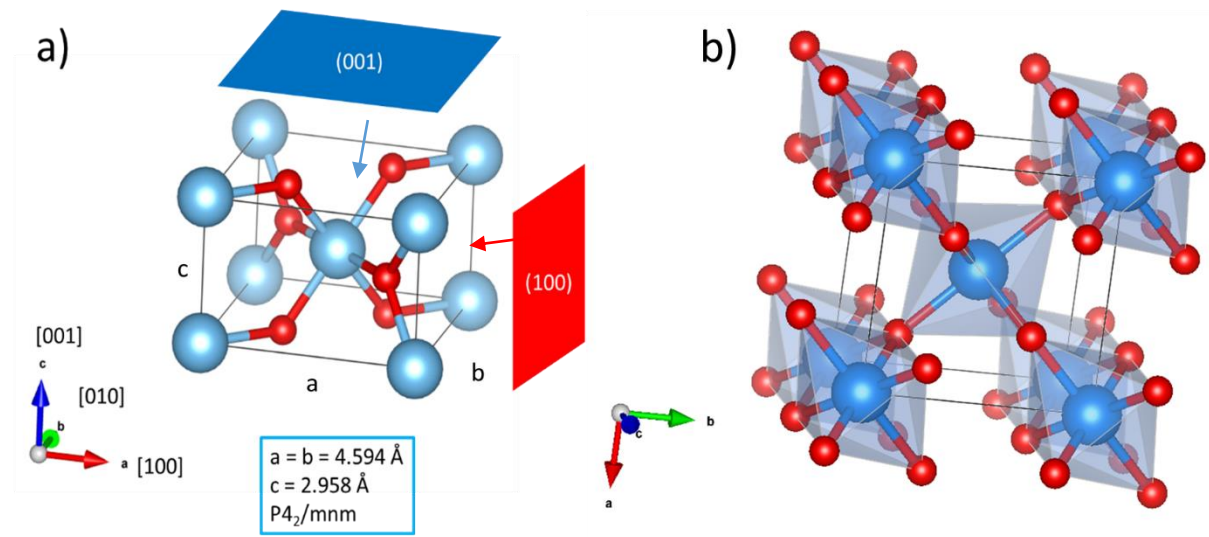


Figure 2.4  $\text{TiO}_2$  rutile unit cell with: a) (100) and (001) planes marked in red and blue respectively, b) octahedrons formed by six oxygen atoms surrounding one Ti atom. The oxygen atoms are marked as small red spheres and titanium atoms are the big blue spheres.

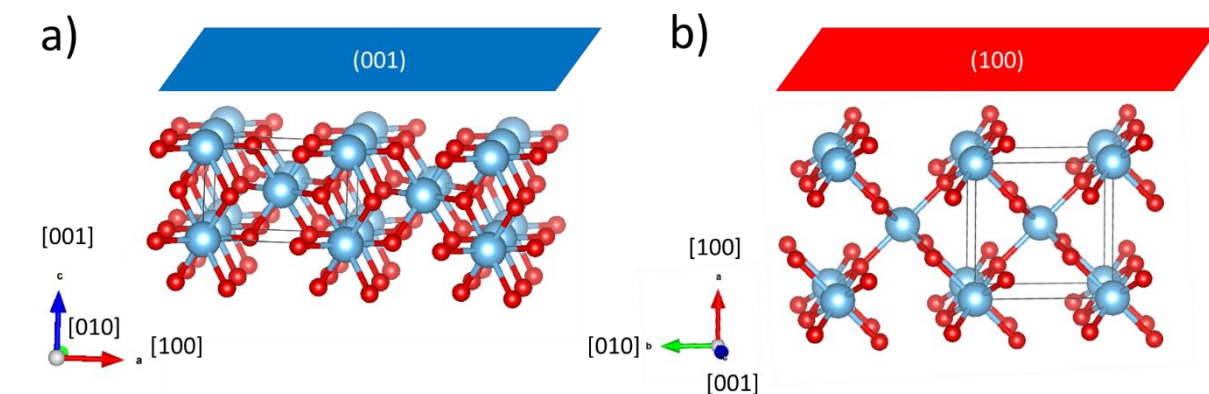


Figure 2.5 Ideal surface termination of a  $\text{TiO}_2$  rutile: a) (001) and b) (100) surface.

Figure 2.5 shows an ideal surface termination of  $\text{TiO}_2$  rutile (001) and (100) surfaces. In the ideal termination the surface Ti atoms are 4-fold coordinated for the (001) surface, and 5-fold coordinated for the (100) surface. The difference in surface Ti coordination might explain why the (001) surface is more reactive in comparison to the (100) surface.

While a high purity  $\text{TiO}_2$  rutile single crystal is an insulator, reduction methods allow to introduce defect states, making the crystal a semiconductor.<sup>23</sup> A direct effect of reduction are oxygen vacancies which

## 2. Theoretical background - 2.4 Analytical methods

result in  $\text{Ti}^{3+}$  atoms around the vacancy due to the charge left from the missing oxygen atom. An oxygen vacancy is an example of point defect. There can be line defects and  $\text{Ti}^{3+}$  atom agglomerates present in the  $\text{TiO}_2$  crystal as well. The band gap of rutile is 3.0 eV wide<sup>22</sup> and the maximum of defect states within the band gap is around 1.0 eV binding energy.<sup>24</sup> These defect states derive from Ti 3d orbitals and are metallic in character.<sup>25</sup>

Within this work, rutile single crystals with two distinct surface orientations were used. These were the (001) and (100) orientations. They are marked on the rutile unit cell model shown in Figure 2.4a with blue and red planes. The two planes differ in atom arrangement and properties.<sup>26</sup> It is expected that they will interact with the environment in a different manner.

### 2.4 Analytical methods

Analysis of interfaces requires atomically clean experimental environment. This is the reason why sample preparation as well as the analytical techniques used in this work, are performed in ultra-high vacuum (UHV) conditions. The low pressure within the vacuum system (base pressure  $p = 1 \cdot 10^{-9}$  mbar) decreases the possible interactions of the sample with its environment to minimum. There are no particles in the environment which could cause inelastic scattering of the probed electrons, which would lead to energy loss and invalid results about the kinetic energy of an electron, which is a fingerprint of its chemical environment in photoelectron spectroscopy methods. Another advantage of a UHV system is, that one can have several analytical methods possible within one system, without the need of removal of the vacuum prepared sample into air where the atomically clean substrates would be instantly contaminated with gas molecules in air. Next three chapters include a short description of UHV techniques used in this work.

Following the analysis in vacuum, microscopic techniques were used. This was possible due to the air stability of the evaporated thin films. With these techniques the surface morphology could be investigated. The microscope techniques are described in chapter 2.4.3 and 2.4.4.

#### 2.4.1 Photoemission Spectroscopy (PES)

Photoemission spectroscopy is based on a photoelectric effect, in which electrons are emitted from a material when exposed to an electromagnetic radiation of the energy  $h\nu$ . Depending on the energy region of photons used in PES, the technique is divided into X-ray photoelectron spectroscopy and Ultra Violet Photoelectron spectroscopy, both of which will be explained in detail in the following two chapters. A simplified depiction of the photoemission process in XPS and UPS is shown in Figure 2.6.

## 2. Theoretical background - 2.4 Analytical methods

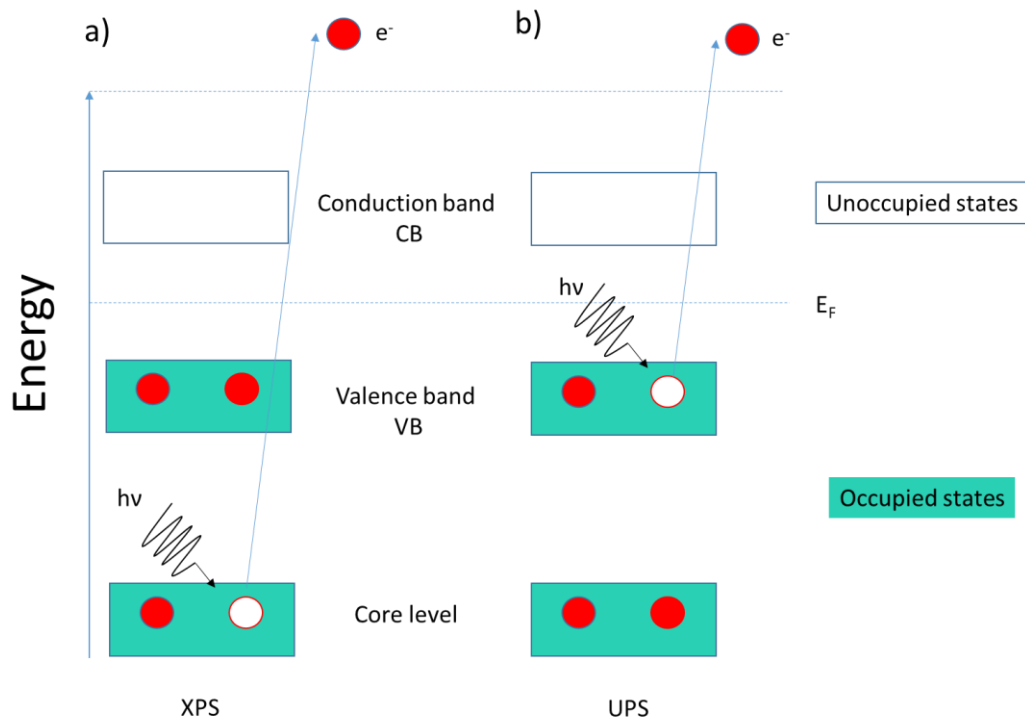


Figure 2.6 Photoemission processes: a) XPS, b) UPS.<sup>27</sup>

Both techniques probe the occupied states within an atom. In XPS, core level electrons are probed, while in UPS, due to the lower energy of radiation used, only the valence band electrons are investigated.

### 2.4.1.1 X-ray Photoelectron Spectroscopy (XPS)

X-ray photoemission spectroscopy (XPS) uses electromagnetic radiation in the range of soft X-rays with energies between 100 eV and 10 keV. Photons of the energy  $h\nu$  from the soft X-rays regime eject electrons from core levels within atoms. The probing electromagnetic radiation energy has to be of the magnitude of the probed distances in the sample. In XPS this is frequently the energy of  $Al_{K\alpha}$  ( $h\nu = 1486.7 \text{ eV}$ ) and  $Mg_{K\alpha}$  ( $h\nu = 1253.7 \text{ eV}$ ) monochromatic radiation. The ejected electrons are analysed in a spectrometer, equipped with a hemispherical analyser, which sorts the electrons by their kinetic energy.<sup>28</sup> Since the kinetic energy depends on the energy of incident photons, photoemission spectra are shown with binding energy scale. Binding energy is the energy required to bind an electron to the atom. To leave the atom, the electron needs to exceed the binding energy and work function, which is the minimum amount of energy required to remove an electron from an electrically neutral solid in vacuum.<sup>29</sup> Therefore, the kinetic energy is equal to the difference of photon energy, binding energy and work function (see Eq. 1).

We can write for kinetic energy:

$$E_K = h\nu - E_B - \phi_m \quad (\text{Eq. 1})$$

## 2. Theoretical background - 2.4 Analytical methods

Where  $E_B$  is binding energy,  $E_K$  is kinetic energy,  $h\nu$  is photon energy and  $\phi_m$  is the work function of a sample. The formula can be rewritten for binding energy as follows:

$$E_B = h\nu - E_K - \phi_m \quad (\text{Eq. 2})$$

During photoemission measurements, the sample is in electrical contact with spectrometer, so the contact potential difference between the work function of sample  $\phi_m$  and spectrometer  $\phi_s$  (See Eq. 3), due to the difference in their local vacuum level, has to be taken into consideration.<sup>30</sup>

$$\Delta\phi = (\phi_m - \phi_s) \quad (\text{Eq. 3})$$

The measured kinetic energy of an emitted electron is therefore:

$$E_{\text{meas Kin}} = h\nu - E_B - \phi_m + \Delta\phi = h\nu - E_B - \phi_s \quad (\text{Eq. 4})$$

In consequence, the measured kinetic energy  $E_{\text{meas Kin}}$  is independent of the sample work function. The maximum kinetic energy is measured for electrons emitted from the Fermi level.<sup>31</sup> The relations between the excitation, kinetic and binding energy as well as the sample and spectrometer work function are shown in Figure 2.7 below.

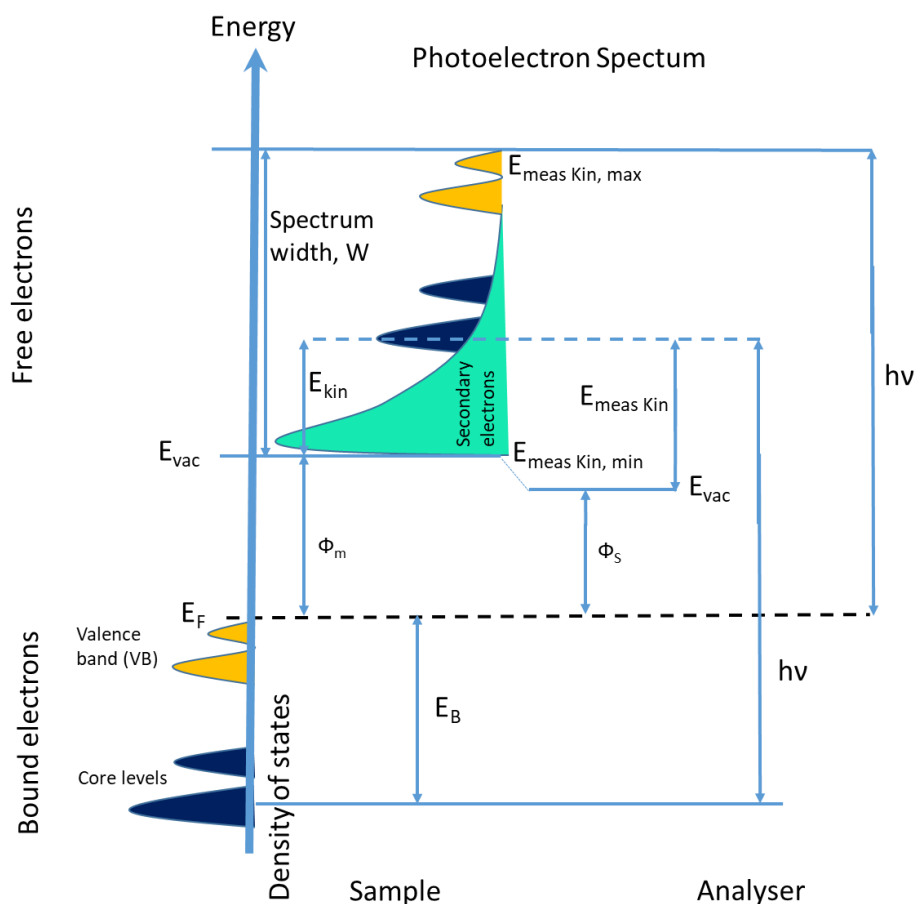


Figure 2.7 The photoemission process in XPS and the relation between sample and spectrometer energy levels.

## 2. Theoretical background - 2.4 Analytical methods

Since electrons at different core levels as well as electrons from the same core level, but belonging to different atoms have different binding energy, their kinetic energy will also differ, when photoexcited. Based on this principle, the X-ray photoemission spectroscopy, which enables detection of electrons with different kinetic energies, becomes a precise qualitative analysis technique for solid samples. Even small changes in binding energy introduced by a change in a chemical environment of the atom can be detected, like for example a change in oxidation state or creation of a new chemical bond. The information can be acquired by taking a survey spectrum of an unknown sample, electrons emitted at a specific kinetic energy will be present as peaks on a binding energy scale. Since each core-level electron of an atom has a specific kinetic and binding energy the signals of an unknown sample can be identified based on reference tables with binding energies of elements and their respective core-levels within different types of materials. Due to the short attenuation length of the photoemitted electrons only a depth of few nanometres into the solid can be examined with XPS. This makes the technique very surface sensitive, and a perfect tool to examine surfaces of solids, thin films and interfaces between materials.

XPS method enables the quantitative analysis of the sample as well, since the area under the detected peak is related to the amount of electrons taking part in photoemission process from the related core level. The peak areas taken from survey spectrum have to be divided with their respective empirical or theoretically calculated sensitivity factors. A peak fit of a core level signal allows to distinguish the composition of the sample.<sup>32</sup>

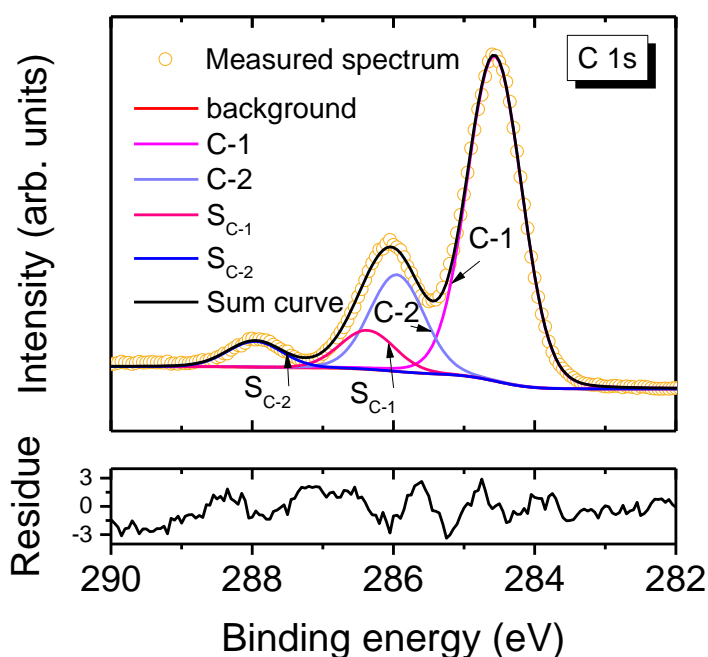


Figure 2.8 An example of a peak fit: C 1s core level spectra of a thick AlClPc film.

## 2. Theoretical background - 2.4 Analytical methods

An example of peak fitting procedure is shown based on the C 1s spectrum in Figure 2.8. The spectrum marked with yellow circles has been fitted with a Tougaard background and 4 component peaks, which represent 2 types of carbon atoms in AlClPc molecule (C-1 and C-2 components marked with magenta and light blue line) with their corresponding satellite signals ( $S_{C-1}$  and  $S_{C-2}$  marked as dark pink and dark blue lines). The sum of the 4 component peaks gives a resulting sum curve (black line). The residue curve below the fitted spectrum shows how exact is the peak fit (how much the sum curve deviates from the measured spectrum).

### 2.4.1.2 Ultra Violet Photoelectron Spectroscopy (UPS)

Similar to XPS, the UPS is based on the fact that electrons are removed from a material upon irradiation with photons. While UPS follows the same principle as XPS, it differs from the previously described method by lower excitation energy, below 100 eV, which means that only electrons with low binding energy can be excited from the sample. In practice, it means that only outer region of an atom electron cloud, the valence band (VB) is probed as seen in Figure 2.6b. Frequently in UPS, a helium lamp is used to irradiate the samples with photon of energies 21.2 eV and 40.8 eV corresponding to He I and He II lines. The technique allows probing the electronic structure of the sample.

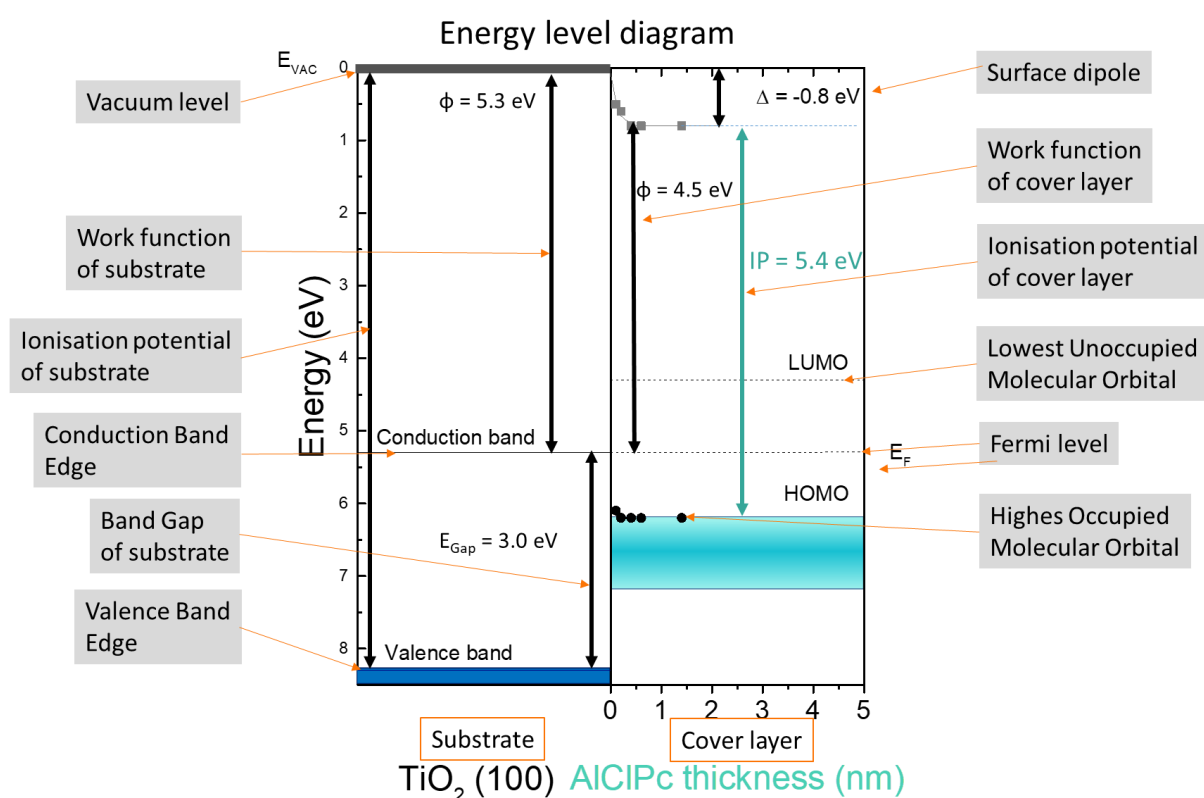


Figure 2.9 Example of an energy level diagram based on the UPS data, with exception of LUMO, which has to be probed with complementary techniques like inverse photoelectron spectroscopy (IPES).

## 2. Theoretical background - 2.4 Analytical methods

An example of an energy level diagram is shown in Figure 2.9 with the main components marked with orange arrows. Within the measurement region for organic semiconductors the position of HOMO (highest occupied molecular level) can be registered, as well as a shift in the peaks position in relation to the Fermi Edge. Ionization potential can be determined as well, by adding the work function of the material and the position of HOMO onset determined from the VB spectrum.

The work function of a sample can be obtained, by correcting for the potential  $\Delta\phi$ , by taking the width of the photoelectron spectrum:

$$\phi_m = h\nu - (E_{\text{meas Kin,max}} - E_{\text{meas Kin,min}}) \quad (\text{Eq. 5})$$

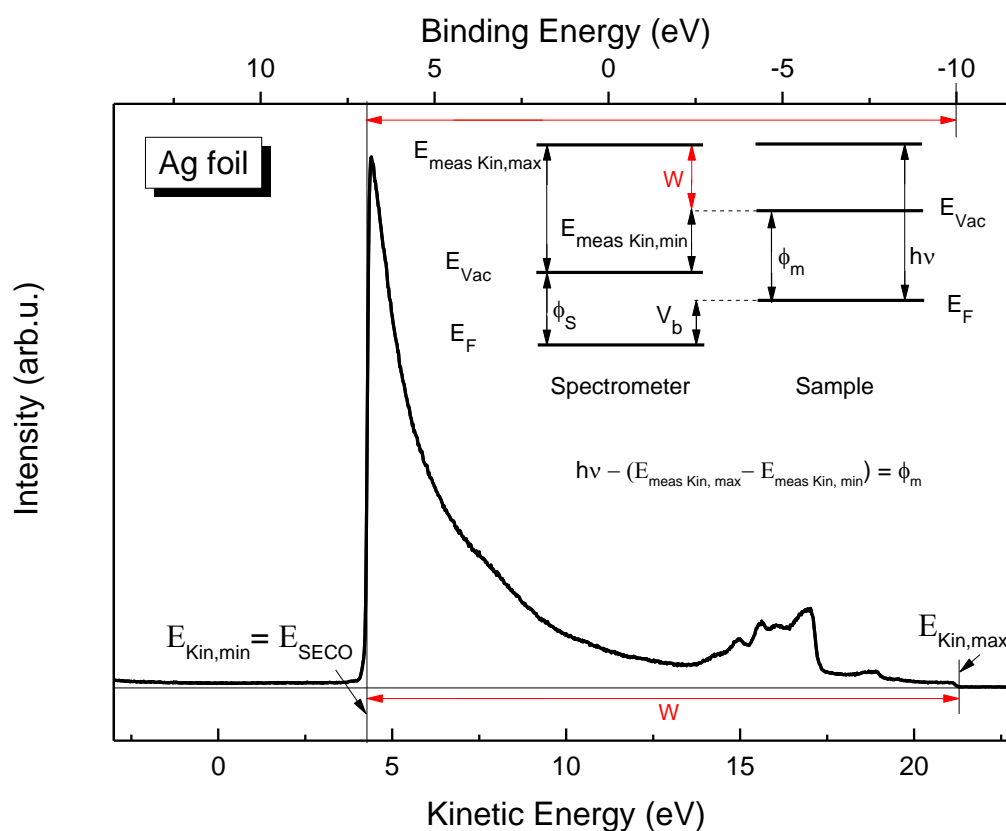


Figure 2.10 Secondary electron cut-off measured for a silver foil sample at the bias voltage  $V_b$  of 10V. The inset shows the energy levels between the spectrometer and sample, as well as the formula used to calculate the work function of the sample  $\phi_m$ .

$E_{\text{meas Kin,max}}$  is the maximum measured kinetic energy of an electron emitted from the Fermi level and  $E_{\text{meas Kin,min}}$  is the minimum measured kinetic energy in the photoelectron spectrum, as shown in Figure 2.10. The minimum kinetic energy  $E_{\text{meas Kin,min}}$  occurs in the spectrum at so called secondary electron cut-off (SECO) because most of the signal consists of low kinetic energy secondary electrons, and the spectrum is suddenly “cut-off” due to the local vacuum level.

All electrons leaving the sample with energy below  $E_{vac}$  have insufficient kinetic energy to be detected, and do not contribute to the spectrum. Even electrons whose kinetic energy is near zero may not reach the spectrometer, due to insufficient energy. Therefore, when measuring the SECO region of the spectrum, a bias voltage is applied to the sample, to accelerate the lowest kinetic energy electrons into the spectrometer, as shown in Figure 2.10 energy diagram inset. The bias voltage  $V_b$  offsets all of the energy levels in the sample. That is why Eq. 5 is still valid.<sup>31</sup>

### 2.4.2 Low Energy Electron Diffraction (LEED)

The crystal substrates have a specific atom arrangement at the surface. While the surface is ordered in “as received” crystal, there are still contaminations at the surface, which can come from polishing materials or simply are adsorbed from air. The preparation methods (described in chapter 3.3) allow to obtain clean surfaces. However, due to the sputtering and high temperature used, they will also influence the surface order. In case of  $TiO_2$  crystal defect will be created during the cleaning procedure. To confirm that the surface atoms long range order is preserved low energy electron diffraction is used. The principle of this method is the diffraction of low energy electrons from the sample surface. The technique uses the particle-wave duality, the wave character of electrons. The low energy electrons have wavelengths equal to few Angstroms, which matches the interatomic distances in crystals, making them perfect probes to investigate the long range order of a crystal lattice, which acts towards them as a diffraction grating. At low energy the inelastic mean free path of electrons is short. It means they can diffract only from the outermost layers of crystal lattice, making LEED a surface sensitive method.

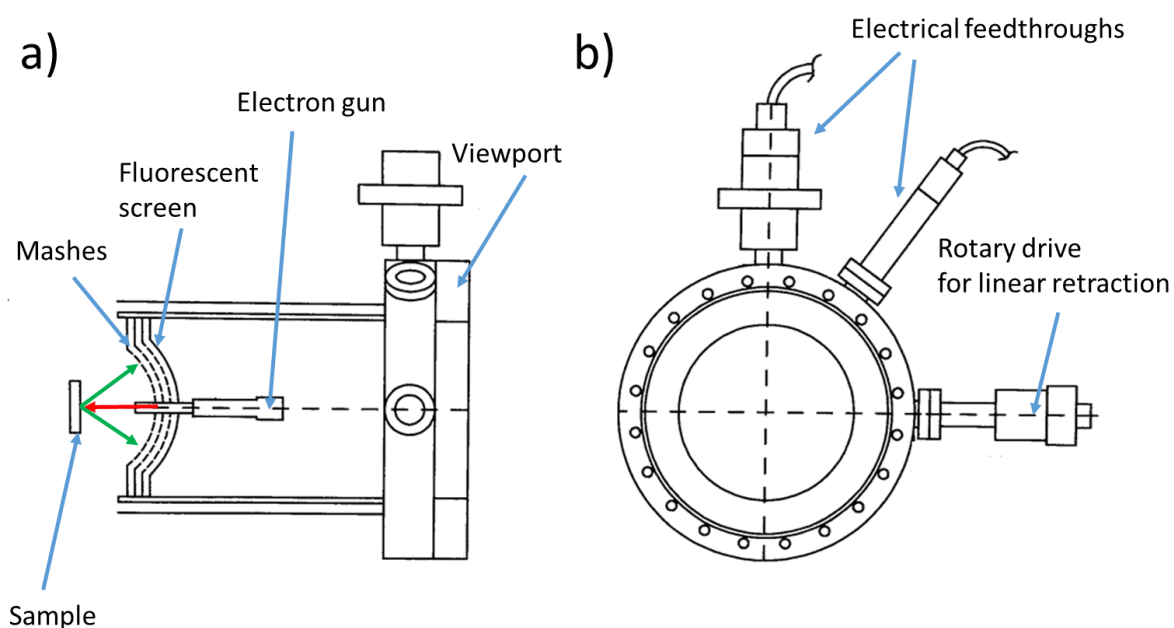


Figure 2.11 Schematic image of LEED equipment: a) side view, b) front view.<sup>33</sup>

## 2. Theoretical background - 2.4 Analytical methods

A LEED set-up is shown in Figure 2.11. The equipment is mounted in an ultra-high vacuum chamber to avoid contamination of the surface and diffraction of electrons from gas atoms. The apparatus is moved with a rotary drive towards the sample. The sample surface is irradiated with a beam of low energy electrons normal to the surface, coming from an electron gun. The electrons diffracted from the sample surface pass by a system of gratings, which filters out the inelastically scattered electrons and accelerates them on their way to the fluorescent screen, where they are detected in form of a diffraction pattern (spots).

The principle of LEED can be explained with the kinematic theory of electron diffraction and the particle-wave character of the electrons. The latter means that a beam of electrons with momentum  $p$  has a wavelength  $\lambda$ , described by the relation given by de Broglie in Eq. 6:

$$\lambda = \frac{h}{p} \quad (\text{Eq. 6})$$

where  $h$  is Planck constant.

The electrons of the incident beam are diffracted by the crystal lattice. The constructive interference occurs if Laue condition is fulfilled: the difference between wave vectors of elastically scattered electrons has to be equal to the reciprocal lattice vector as shown in Eq. 7:

$$k_f - k_i = g \quad (\text{Eq. 7})$$

$k_i$  – vector momentum of the incident electron beam

$k_f$  – vector momentum of the diffracted electron beam

$g$  – lattice vector of two-dimensional reciprocal lattice of the surface plane

The angular displacement of electrons represents momentum transfer parallel to the surface. The translation symmetry perpendicular to the surface is limited due to a short mean free path of electrons with low energy. In other words, the detected LEED spots represent a parallel momentum transfer and are the effect of the constructive interference of diffracted waves.

The equation describing the conservation of momentum parallel to the surface is given below:

$$k_{f,\parallel} - k_{i,\parallel} = g \quad (\text{Eq. 8})$$

$k_{i,\parallel}$  – vector momentum of the incident electron parallel to the surface

$k_{f,\parallel}$  – vector momentum of the diffracted electron parallel to the surface

## 2. Theoretical background - 2.4 Analytical methods

$g$  – lattice vector of two-dimensional reciprocal lattice of the surface plane

Using the relation between momentum  $p$  and kinetic energy  $E$ , where  $\hbar$  is the reduced Planck constant:

$$p = \sqrt{2mE} = \hbar k \quad (\text{Eq. 9})$$

and the relation between momentum and de Broglie wavelength, one can write the equation for the momentum parallel to the surface as:

$$k_{i,\parallel} = \sqrt{\frac{2mE}{\hbar^2}} \sin\theta \quad (\text{Eq. 10})$$

The lattice vector of the two-dimensional reciprocal lattice is given by a sum of two primitive vectors  $A$  and  $B$  multiplied by integers  $h$  and  $k$  respectively:

$$g = hA + kB \quad (\text{Eq. 11})$$

The LEED spots along the  $A$  and  $B$  vector directions are labelled with the  $h$  and  $k$  integers.

LEED pattern can be used to extract the dimensions of the unit of a crystal lattice from the dependence of the angle  $\theta$  for each spot along symmetry directions versus the incident beam energy (Eq. 10), because the distribution of diffracted electrons depends on the geometry of atoms at the crystal surface.

What is more, LEED gives information about surface domains as well as surface reconstruction, that is, a situation when the surface of crystal assumes different atom arrangement than the bulk crystal.

The LEED spots can be viewed according to Ewald Sphere (in Figure 2.12), a construction which provides a geometric representation of the momentum conservation relationships in terms of  $k_i$  and  $k_f$  versus  $A$  and  $B$ . In this figure, rods parallel to  $k_{i,\parallel}$  represent momenta supplied by multiples of primitive vector  $B$  in the horizontal direction such that diffracted beams have momentum  $k_{f,\parallel}$  due to momentum transfer  $S$ . The intersection of these lines in two dimensions defines the direction and magnitude of  $k_{f,\parallel}$ .<sup>34</sup>

## 2. Theoretical background - 2.4 Analytical methods

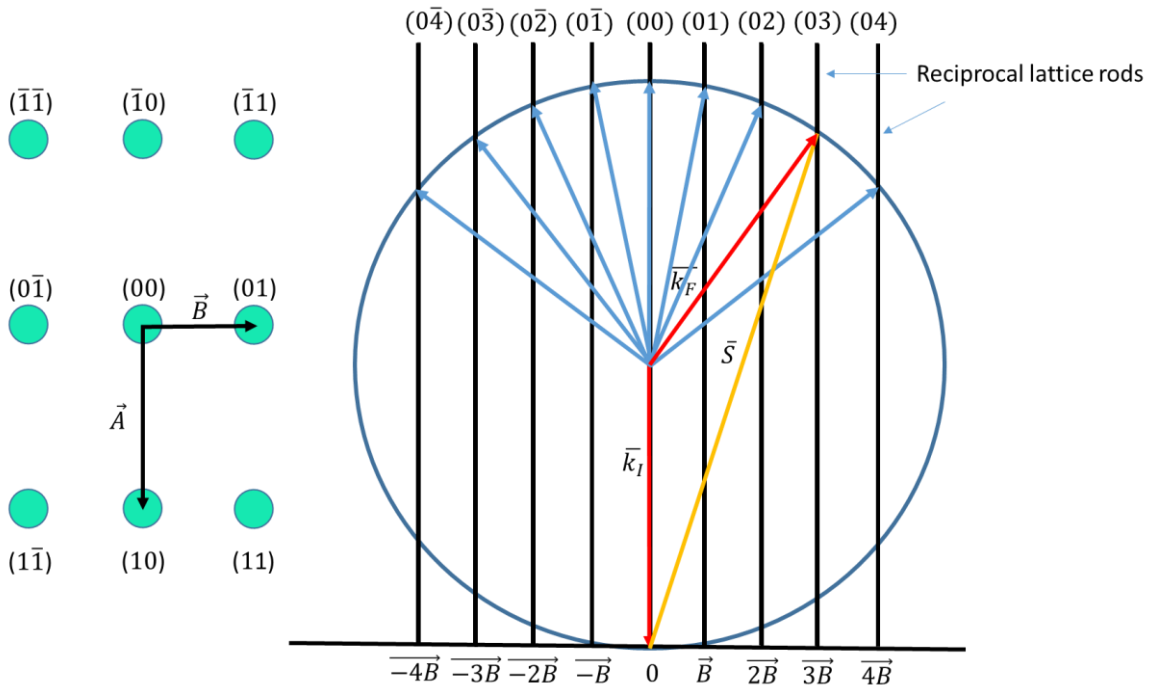


Figure 2.12 Example of a (110) surface LEED pattern (left) and the corresponding Ewald sphere with the rods of the reciprocal lattice (right). Momentum transfer  $S$  along  $B$  direction is marked with a yellow line.<sup>34</sup>

Figure 2.13 shows the relation between the vectors describing surface lattice and the reciprocal lattice, based on the definition of the reciprocal lattice vectors<sup>35</sup> (Eq. 12)

$$\vec{a}_i \cdot \vec{a}_j^* = 2\pi\delta_{ij} = \begin{cases} 2\pi & \text{if } i = j \\ 0 & \text{if } i \neq j \end{cases} \quad i, j = 1, 2 \quad (\text{Eq.12})$$

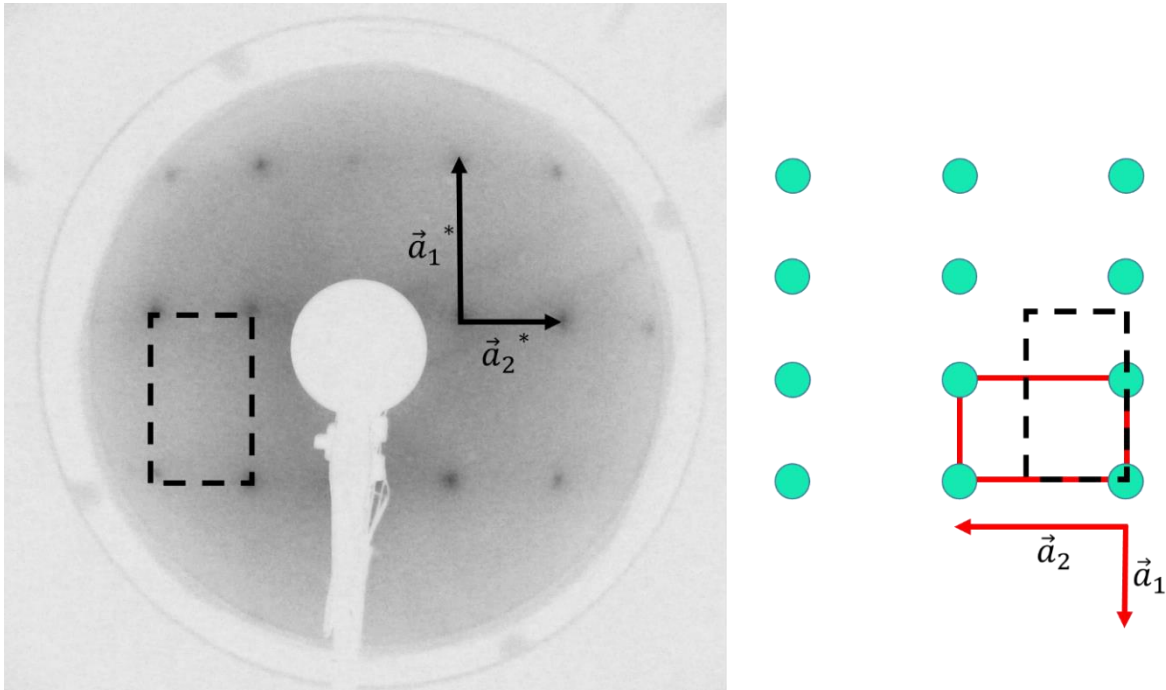


Figure 2.13 A LEED pattern with spots representing a crystal lattice in a reciprocal space and vectors defining the unit of the crystal mesh marked in black (left); crystal lattice in real space with vectors marked in red (right).



## 2. Theoretical background - 2.4 Analytical methods

when the tip oscillates freely in the air. As the tip approaches the surface and forces between the tip and the sample surface start to act, the oscillation amplitude decreases. In order to keep the oscillation amplitude constant during a scan, the feedback loop maintains a constant RMS of the oscillation signal reaching the photodetector.<sup>38</sup> Figure 2.14 shows a feedback loop in a tapping mode. The laser beam is reflected from the tip of a cantilever oscillating around its resonant frequency. When the tip is engaged with the sample (when it starts scanning the sample surface), the tip-sample interactions decrease the tip oscillation. Due to change in tip oscillation a change in laser beam reflection is detected at the photodiode. The signal from photodiode is recalculated to the RMS amplitude signal. RMS (Root Mean Square) is a measure of surface roughness, and in mathematical terms, it expresses the standard deviation of the Z-axis of the measured surface. Based on the RMS amplitude signal the feedback loop adjusts the Z-piezo to keep the constant amplitude of tip oscillation above the surface. At each X,Y-position of the scanner, the Z-position is saved by the computer to maintain a constant oscillation amplitude. At the same time, the saved dataset of tip vertical position in a X,Y-array gives the topographic image of the scanned surface.<sup>39</sup> An example of an AFM image with its surface profile is shown in Figure 2.15a and b. The data processing software mentioned in Chapter 3.4.5, allows the acquisition of the surface parameters listed in Figure 2.15c as well as a 3D surface model (Figure 2.15d). For the sake of this work, the peak to peak distance given by the minimum and maximum height in the surface profile as well as RMS roughness will be used to compare the data between the experiments.

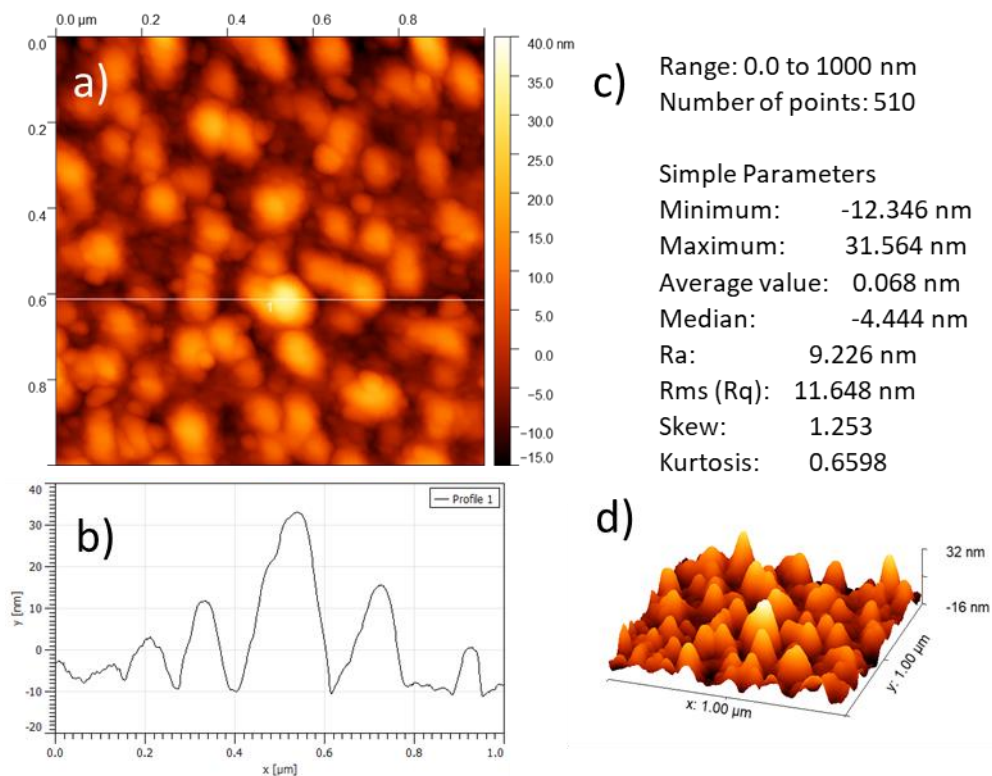


Figure 2.15 An example of AFM data: a) an 1  $\mu\text{m}$  x 1  $\mu\text{m}$  AFM image, b) surface profile marked as a white line in the AFM image, c) sample profile parameters and, d) 3D model of the sample surface.

## 2. Theoretical background - 2.4 Analytical methods

The advantage of the tapping mode is, it allows to image fragile samples which would be otherwise damaged if contact mode was used. The measurement can be performed both in air and under native liquid conditions. The thin films of AlClPc fall into the category of fragile samples, since it is possible to scratch them away with an AFM tip. Using tapping mode in this work allowed to decrease the possibility of damaging the organic thin film as well as accumulation of organic material on the tip, leading to artefacts in the AFM image or breaking the probing tip.

### 2.4.4 Scanning Electron Microscopy (SEM)

In SEM, a sample is irradiated with an electron beam, so called primary electron beam. Due to the interaction of electrons with the sample surface secondary electrons (SE), back-scattered electrons (BSE) and X-ray radiation are produced. These are detected with different detectors available inside the microscope.

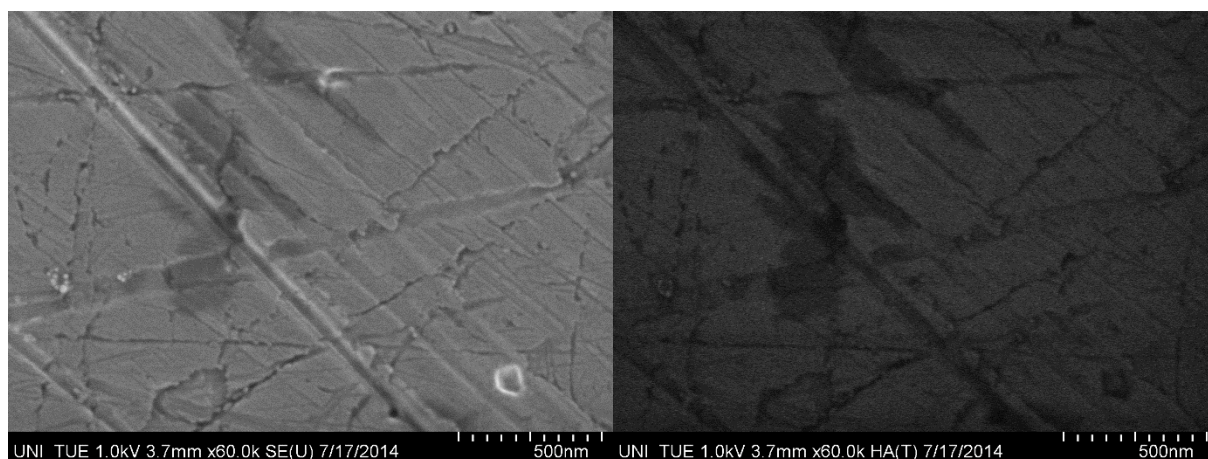


*Figure 2.16 Exemple of a SEM data acquired through (SE) secondary electrons (left) and (BSE) back-scattered electrons (right) at the same spot of the sample.*

The secondary electrons come from the sample surface, which gives the information about topography of the sample, while back-scattered electrons come from deeper regions of the sample, and are sensitive to the material type investigated. Depending on the atomic number  $Z$ , the elements scatter different amount of electrons back to the detector, upon interaction with the primary beam. This results in a different material contrast in a SEM image, allowing to distinguish between materials, which differ in composition, present at the surface. In Figure 2.16 one can see that the left image based on secondary electrons provides more information about the surface topography, while image in the right, based on back-scattered electrons, shows less topographical information in favor of a stronger contrast related to  $Z$ -number. Combined, they provide information on both topography and enable the distinction between the surface components. What is more, the X-ray quanta can be detected and analyzed in the same device with EDXS (Energy-Dispersive X-ray Spectroscopy) and enable a qualitative and quantitative analysis of the surface species.

### 3. Experimental setup

## 3. Experimental setup

This chapter focuses on description of experimental setup, preparation of samples and data evaluation procedures.

### 3.1 Materials

#### Substrates:

- Indium foil, Heraeus Fainchemikalien und Forschungsbedarf GmbH, purity grade 4N
- Silver foil, Mateck Material-Technologie & Kristalle GmbH, purity grade 3N5
- Silver single-crystals:
  - Ag(100), Mateck Material-Technologie & Kristalle GmbH, diameter = 8 mm, thickness 2 mm, Purity grade 5N, with a surrounding groove and a flat marking the second orientation
  - Ag(100), SPL.EU Crystals, Surface Preparation Laboratory, diameter = 8 mm, thickness 2 mm, Purity grade 5N with a surrounding groove and a flat marking the second orientation
- Titanium dioxide single crystals:
  - TiO<sub>2</sub>(001), SurfaceNet GmbH, dimensions 8 mm x 8 mm, thickness 2 mm
  - TiO<sub>2</sub>(001), SurfaceNet GmbH, dimensions 10 mm x 10 mm, thickness 1 mm
  - TiO<sub>2</sub>(100), SurfaceNet GmbH, dimensions 10 mm x 10 mm, thickness 1 mm

#### Gases:

- Argon (Westfalen AG, purity grade 5.0)
- Oxygen (Westfalen AG, purity grade 5.0)

#### Organic molecules

- Aluminium (III) Chloride Phthalocyanine, synthesized in the group of Dr. Tamara V. Basova (Nikolaev Institute of Inorganic Chemistry, Novosibirsk, Russia) was prepared via reaction of 1,2-dicyanobenzene and anhydrous aluminum(III) chloride in quinoline media at 230 °C<sup>40</sup>
- Aluminium (III) Fluoride Phthalocyanine (Nikolaev Institute of Inorganic Chemistry & Novosibirsk State University, Novosibirsk, Russia)
- FeClTPP, 5,10,15,20-Tetraphenyl-21H,23H-porphine iron(III) chloride, Sigma-Aldrich Chemie GmbH, purity grade ≥94% (HPLC)

### 3.2 Sample holders

Two types of sample holders were used in the photoelectron spectroscopy methods. The first type (Figure 3.2.1a) were sample holders without heating, made of stainless steel with a possibility to fix a

### 3. Experimental setup - 3.2 Sample holders

sample between two screws, or with tantalum wires or tantalum foils (depending on the size and shape of the sample) spot welded to the sample holder surface. This type of sample holder was used for silver and indium foil substrates.

The second type of sample holders were the once with a possibility to heat the sample with resistive heating. A tantalum wire inside  $\text{Al}_2\text{O}_3$  isolation tubes was fixed (Figure 3.1b) within or (Figure 3.1c and d) under the plate where the sample holder was mounted. When electric current was applied, the wire produced heat due to resistive heating, heating the sample holder top plate together with the sample. By controlling the current and voltage with a power supply, the temperature could be controlled. The temperature was measured indirectly with a pyrometer.

The heatable sample holders were used in experiments with single crystal substrates. The last example (Figure 3.1c) was particularly good for the preparation of the  $\text{TiO}_2$  single crystals, due to the large surface area of the top plate, since the size of  $\text{TiO}_2$

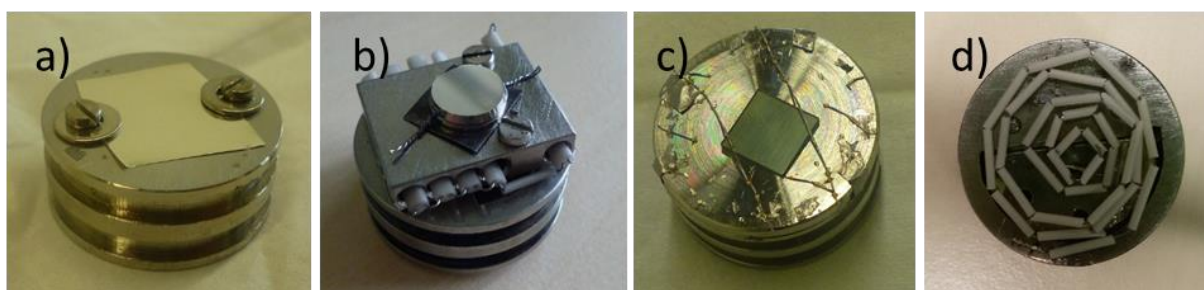


Figure 3.1 Sample holder: a) without heating, b) with resistive heating within the top plate, c) with resistive heating under the top plate (outside/external view), d) with resistive heating under the top plate (inside view of the sample holder with the tantalum filament in form of a spiral).

AFM Sample holder (see Figure 3.2a) was a round, polished, stainless steel plate, with diameter = 15 mm and thickness = 1 mm. The samples were attached to the holder with a piece of a double sided adhesive carbon tape (SPI Supplies, USA, width = 8mm), to fix the sample on the sample holder.

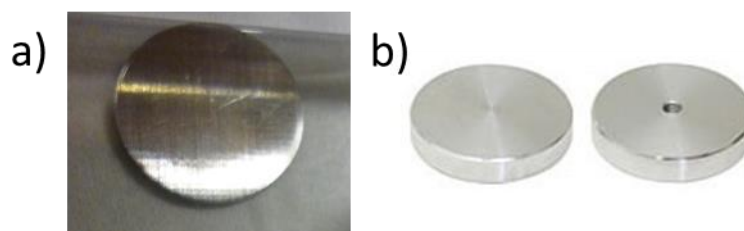


Figure 3.2 Sample holders a) AFM, b) SEM (top and bottom view).

SEM sample holder (Figure 3.2b) was a standard Hitachi holder, a circular plate with a screw to fix it in the microscope holder. The sample was fixed on the holder with a carbon tape to provide the electrical contact.

### 3. Experimental setup - 3.3 Substrate preparation

#### 3.3 Substrate preparation

The indium foil samples were prepared ex-situ. The outer layer of indium was removed by simply scratching it away with a spatula, to remove the oxidized top layer, leaving the shiny surface free for the powder samples to be pressed into the indium foil. It allowed to investigate the quality of powder materials and record reference spectra, to be sure that the molecules were intact before and after their evaporation.

The silver foil bought from MaTeck Material Technologie & Kristalle GmbH was cleaned within the vacuum system with sputtering cycles. Sputtering with argon ions was enough to remove the foil surface contamination (mostly carbon). The typical energy of foil sputtering was 1 kV. 5 sputtering cycles of 30 minutes were usually enough to obtain a clean surface. If contaminations were still present on silver, the sample angle towards the sputter gun was varied to remove the rest carbon from the surface.

The silver (100) single crystals bought at MaTeck Material Technologie & Kristalle GmbH and Surface Preparation Laboratory were prepared by alternating steps of sputtering and annealing. The first sputtering cycles, lasting 30 minutes, were done at higher energy 1.5 kV to remove the polishing agents from the “as received” crystal (mostly carbon, from possibly diamond paste). In the following cycles the energy was decreased to 0.8 kV, to avoid damaging the sample surface. The annealing was done at 900 K. Usually, 9 cycles were enough to clean an “as received” silver crystal. After thick organic films were evaporated, 13 sputtering-annealing cycles were needed to remove organic film from the single crystal surface and obtain a proper surface reconstruction.

The TiO<sub>2</sub> rutile single crystals purchased at SurfaceNet GmbH, were cleaned by sputtering and annealing cycles, to obtain reduced surface with surface defects. For defect rich samples, longer sputtering and shorter annealing was applied. For only slightly reduced crystals, the annealing step was longer, and the sputtering time was reduced. To obtain the defect free surface, the samples were treated with oxygen at pressure  $p_{O_2} = 10^{-6}$  mbar.

Depending on the TiO<sub>2</sub> surface, the temperature used for annealing was 600 °C for the TiO<sub>2</sub>(001) surface<sup>41</sup> and 635 °C for TiO<sub>2</sub>(100) surface,<sup>42</sup> while sputtering energy was first 1 kV in the first sputtering-annealing cycle and later 0.8 kV in the following cycles, to reduce the damaging of the surface. The time of annealing was longer at the beginning (1 h) later it was decreased to 30 min.

#### 3.4 Measurement equipment

##### 3.4.1 Vacuum system

The following 3 sections are focusing on methods available within one vacuum system (shown in Figure 3.3). The laboratory had three ultrahigh vacuum multichamber systems available. While their

### 3. Experimental setup - 3.4 Measurement equipment

geometry differed, the main components of such systems are the same. In the vacuum equipment description the main focus will be given the equipment with a monochromatized X-ray source, since most experiments presented in this work were performed there.

To achieve and maintain ultrahigh vacuum conditions (base pressure of  $2 \times 10^{-10}$  mbar) within the multi-chamber vacuum system several types of vacuum pumps (membrane-, gitter-, sublimation- and turbo-pumps) are used. The systems architecture can be explained along the path the sample travels in the equipment.

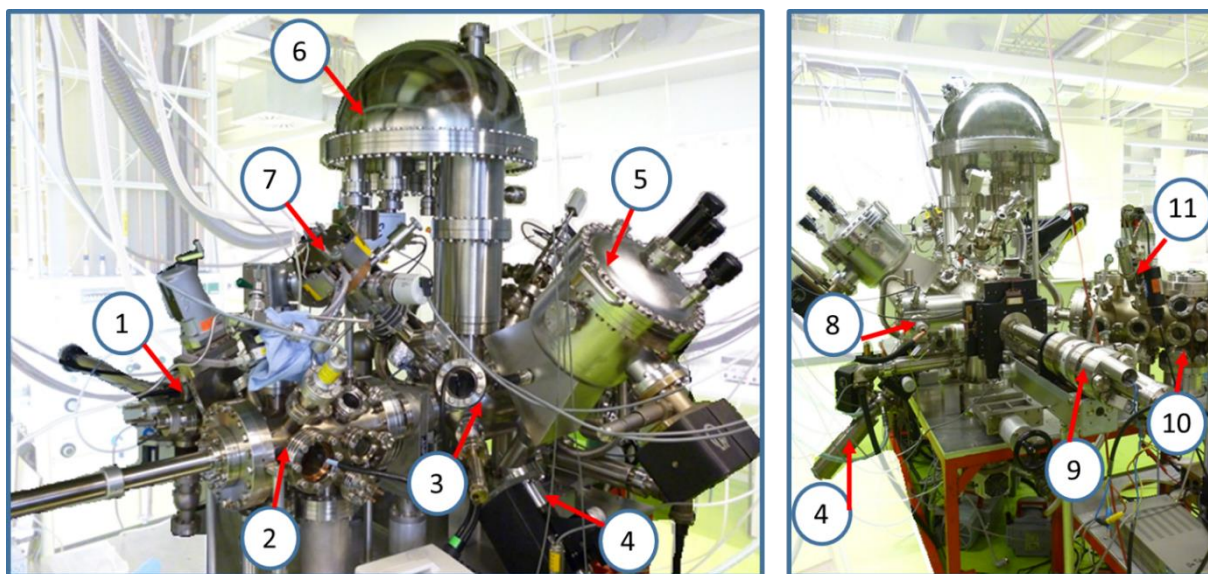


Figure 3.3 Vacuum system. 1 - Load lock, 2 – substrate preparation chamber, 3 – analysis chamber, 4 – X-Ray source, 5 – monochromator, 6 – hemispherical analyser, 7 – Helium lamp, 8 – LEED, 9 – analysis chamber manipulator, 10 – organic film preparation chamber, 11 –microbalance.

The sample is placed on a transfer bar in a load lock, which is pumped down, till the pressure (usually around  $10^{-8}$  mbar) allows opening the valve to preparation chamber and sample transfer. Preparation chamber is equipped with a manipulator where the sample can be annealed and a sputter gun with Argon gas line attached. For preparation of  $\text{TiO}_2$  additional gas line with an oxygen lecture bottle was attached. From preparation chamber the sample can be moved to analysis chamber with another transfer bar. Analysis chamber is equipped with a hemispherical analyzer, monochromatized and standard X-ray source, UV-lamp and LEED equipment. The analysis chamber manipulator allowed heating, but it was avoided to keep the base pressure of the chamber in  $10^{-10}$  mbar range. By moving the manipulator sample can be transferred it into the second preparation chamber (the organic chamber), equipped with a transfer bar, and evaporation cell to prepare thin films and a microbalance (INFICON Holding AG) to monitor the evaporation rate.

#### 3.4.2 X-ray photoelectron spectroscopy (XPS)

The XPS measurements were performed within the analysis chamber of the UHV system. Three systems were used in this work. Their equipment is listed below:

### 3. Experimental setup - 3.4 Measurement equipment

- 1) A spectrometer with an X-ray source with a monochromator (XR 50 M, SPECS) and a Phoibos 150 Hemispherical Energy Analyzer (SPECS). Excitation energy used:  $h\nu = 1486.7$  eV.
- 2) A spectrometer with a non-monochromatic X-ray source (DAR 400) and a Hemispherical Energy Analyzer (EA 125, Omicron). Excitation energy used:  $h\nu = 1253.6$  eV.
- 3) A spectrometer with a non-monochromatic X-ray source (XR 50 SPECS) and a Hemispherical Energy Analyzer (Phoibos 100, SPECS). Excitation energy used:  $h\nu = 1486.6$  eV.

The first setup was used in all experiments done on TiO<sub>2</sub> rutile single crystals, AlFPC on Ag foil, as well as powder measurement on indium foil. The second setup was used in the experiments with AlClPc on Ag foil. The third setup was used in experiment with AlClPc on Ag(100) single crystal and powder measurements on indium foil. The excitation energy used in the XPS experiments was 1486.7 eV (Al K<sub>α</sub>) when monochromatic radiation was used and either 1486.6 eV (Al K<sub>α</sub>) or 1253.6 eV (Mg K<sub>α</sub>) for non-monochromatic sources.

X-ray photoelectron spectroscopy was used to characterize the purity of the substrate and organic material, qualitative and quantitative analysis of the organic thin films and the interface between organic film and the substrate. Peak fitting of XPS spectra was performed using the program Unifit 2011.<sup>43</sup>

#### 3.4.3 Ultraviolet photoelectron spectroscopy (UPS)

The three UHV systems were equipped with helium lamps used as excitation sources in UPS measurements. These were (SPECS UVS 300 A) helium lamp (spectrometer 1) or home-made helium discharge lamps (spectrometer 2 and 3) type UVS 10/35. Corresponding hemispherical analyzers were used, as listed in chapter 3.4.2. The excitation energy of a helium lamp used in the UPS experiments was 21.2 eV. To measure secondary electron cut-off, a power supply (Knick DC-Calibrator S 252) was used to apply negative bias voltage to the sample (-7 V and -10 V).

#### 3.4.4 Low energy electron diffraction (LEED)

The diffraction measurements were performed in spectrometer 1 and 3 with SpectaLEED equipment from Omicron GmbH and VG Microtech Instruments respectively, to characterize the substrate surface structure and reconstruction. The LEED diffraction patterns were displayed on a fluorescent screen and recorded with a camera in form of digital photographs.

#### 3.4.5 Atomic force microscopy (AFM)

A Nanoscope IIIa atomic force microscope (AFM) from Veeco Instruments was used to obtain AFM images. Sample topography was probed in a tapping mode. The data was evaluated with a freeware software WSxM 5.0 Develop 6.5<sup>44</sup> and Gwyddion.<sup>45</sup> The AFM measurements were performed in air. To decrease the influence of air exposure, the samples were measured directly after being taken out of UHV chamber after XPS, UPS and LEED measurements were performed.

#### 3.4.6 Scanning Electron Microscopy (SEM)

A scanning electron microscope, model Hitachi SU8030, was used for surface characterization of thin films in TiO<sub>2</sub> experiments. The microscope is equipped with three electron detectors, and a Bruker Quantax 6G, type 200, EDXS detector (EDXS, energy-dispersive X-ray spectroscopy)). All SEM measurements were performed by Elke Nadler in the SEM laboratory of the Institute of Physical and Theoretical Chemistry (University of Tübingen).

### 3.5 Film deposition

The organic films were evaporated from home-made evaporation cell (see Figure 3.4). The cell consist of a heater with a space for a ceramic Al<sub>2</sub>O<sub>3</sub> crucible, (from Friatec AG, Division Keramik, length = 25 mm) connected to a flange with a feed-through for a thermocouple and resistive heating pins. To decrease the vacuum chamber walls contamination with the organic material evaporating from the cell, a metal screen made of tantalum foil was mounted around the heater.

An empty crucible was filled with organic material and placed in the evaporator cell. The cell was mounted in organic film preparation chamber. The cell was heated together with the chamber, to remove the water and improve the vacuum after the chamber was opened. After achieving the proper vacuum within the chamber the powder was slowly degassed in stepwise manner at the temperature below the evaporation temperature of the material. After degassing, the temperature of the evaporation cell was increased to the evaporation temperature of the material. The evaporation was observed with a quartz microbalance (INFICON Holding AG). The temperature was increased with a power supply (Hewlett Packard E 3616 A) till a constant evaporation rate was observed. AlClPc was evaporated at rates of about 1–2 Å/min. At a constant evaporation rate the sample holder with a clean substrate was moved over the evaporator cell and turned around to face it. The evaporation time was varied depending on how thick the evaporated film was expected to be.

### 3. Experimental setup - 3.6 Determination of film thickness

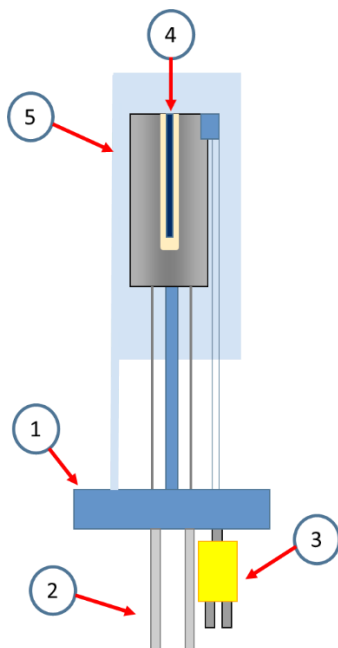


Figure 3.4 Evaporation cell: 1 – flange, 2 – resistive heating connections/pins, 3 – thermocouple connection, 4 – crucible with powder organic material, 5 – metal screen.

#### 3.6 Determination of film thickness

The samples presented in this work can be described in a simplified way as a system consisting of a thin film A, evaporated on a substrate B. Information about film thickness  $d_A$  can be derived from XPS measurements. Based on Lambert-Beer principle it can be written that the intensity of an XPS signal coming from a clean substrate  $I_{B,0}$  decreases to the value of  $I_B$ , when an organic film of thickness  $d_A$  is evaporated on top of substrate B (see Eq. 13). This is under assumption that the substrate is covered by layers of organic molecules, and all layers are continuous (meaning, a new layer will start to form, when the first layer completely covers the substrate).

$$I_B = I_{B,0} e^{-\frac{d_A}{\lambda_A \cos \theta}} \quad (\text{Eq. 13})$$

The opposite can be written for the intensity of the electrons coming from the organic film A. The intensity  $I_A$  increases as the thickness of organic film  $d_A$  increases:

$$I_A = I_{A,\infty} (1 - e^{-\frac{d_A}{\lambda_A \cos \theta}}) \quad (\text{Eq. 14})$$

$I_{A,\infty}$  is the intensity of a signal from thick organic film, with thickness exceeding the information depth of XPS measurement. Theta is the take-off angle of the emitted electrons. The  $\lambda_A$  is the mean free path of electrons coming from the organic film A. It depends on the kinetic energy of the electrons and can be calculated from the formula describing the empirical model found by M.P. Seah and W. A. Dench<sup>46</sup> valid for the organic materials:

$$\lambda_A = 49E^{-2} + 0.11E^{1/2} \quad (\text{Eq. 15})$$

Where E is the kinetic energy of the electrons produced in the photoionization process.

### 3. Experimental setup - 3.6 Determination of film thickness

A quotient of the Eq. 13 and Eq. 14 is:

$$\frac{I_A}{I_B} = \frac{I_{A,\infty}(1 - e^{-\frac{d_A}{\lambda_A \cos\theta}})}{I_{B,0}e^{-\frac{d_A}{\lambda_A \cos\theta}}} \quad (\text{Eq. 16})$$

It can be rearranged to give the following equation:<sup>30</sup>

$$d_A = \lambda_A \cdot \cos\theta \cdot \ln\left(1 + \frac{I_A I_{B,0}}{I_B I_{A,\infty}}\right) \quad (\text{Eq. 17})$$

In practice instead of intensities  $I_A$  and  $I_B$  the areas under the XPS signals of measured elements are used to determine the layer thickness. This is why the stoichiometric relationships of these elements must be taken into account by the additional factors  $\chi_B$  and  $\chi_A$ . The intensities  $I_{B,0}$  and  $I_{A,\infty}$  can be derived from the sensitivity factors  $\sigma_B$  and  $\sigma_A$ , which are derived from the calculated atomic cross-sections of pure elements.<sup>47</sup> What is more, mean free path depends on the amount of particles in a unit volume. This relation can be obtained by dividing the  $\lambda_A$  through the organic material density  $\rho$ .

$$\lambda = \frac{\lambda_A}{\rho} \quad (\text{Eq. 18})$$

For further simplification, it can be assumed that the photoelectrons in the substrate and organic film have the same mean free path equal to  $\lambda_A$ . In summary, the following relationship for organic film thickness  $d_A$  is obtained from all simplifications:

$$d_A = \lambda \cdot \cos\theta \cdot \ln\left(1 + \frac{I_A \cdot \chi_B \cdot \sigma_B}{I_B \cdot \chi_A \cdot \sigma_A}\right) \quad (\text{Eq. 19})$$

This model can be used if the layer-by-layer growth is valid. Other types of growth are layer-island growth, and island growth see Figure 3.5. In this case the calculated film thickness will be underestimated. Atomic force microscope and scanning electron microscope can give insight into the island height (AFM), shape and size and distribution (AFM, SEM).

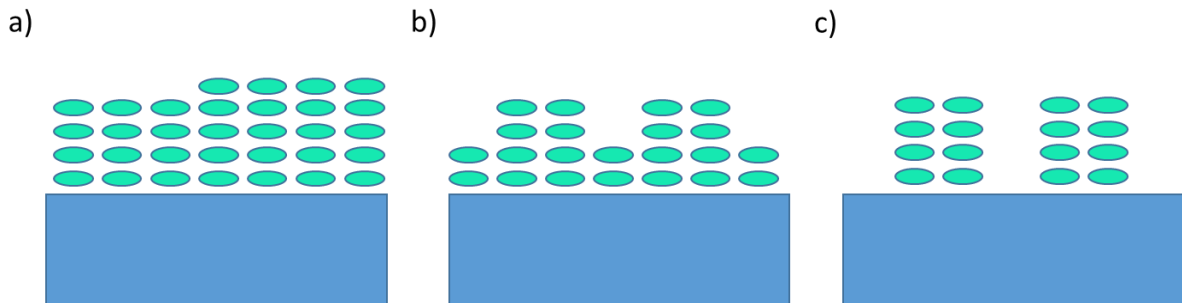


Figure 3.5 Film growth types: a) Layer-by-Layer (Frank-van der Merwe), b) Layer-Island (Stranski-Krastanov), c) Island (Volmer-Weber) model.<sup>48</sup>

### 3. Experimental setup - 3.7 Determination of organic film composition

#### 3.7 Determination of organic film composition

An XPS survey spectrum of powder material (if enough powder was available for such procedure) was taken to examine the composition of a freshly synthesized material. It also served as a future reference for the evaporated thin films in further experiments. Survey spectra of AlClPc powder on indium foil, the indium foil substrate and bulk AlClPc film are given below.

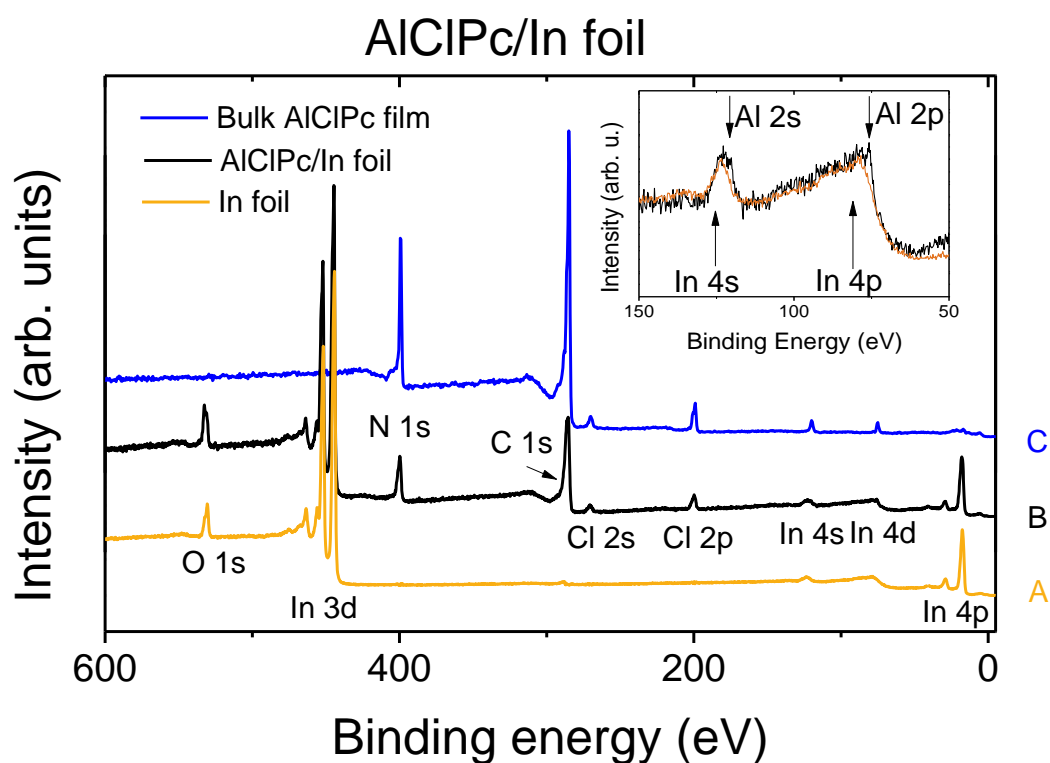


Figure 3.6 XPS Survey spectrum of a) indium foil reference, b) AlClPc powder pressed into indium foil and c) AlClPc bulk film deposited by evaporation. Excitation energy used to record all spectra was 1486.7 eV (Al  $K_{\alpha}$ ).

To measure an XPS spectrum of powder AlClPc, the material was pressed into an indium foil (Figure 3.6, spectrum A). The powder survey spectrum (Figure 3.6, spectrum B) was taken with Al K alpha radiation (1486.6 eV) and the core level peak area was measured using the program Unifit 2014.<sup>43</sup> As expected, the survey spectrum B, shows signals associated with the AlClPc powder (N 1s, C 1s, Cl 2s, Cl 2p, Al 2s, Al 2p). When compared, powder spectrum and spectrum of AlClPc bulk film (Figure 3.6, spectrum C) show the same AlClPc signals. The area of each core-level peak, divided by its photoionization cross-section is proportional to the quantity of the corresponding atom in the AlClPc molecule. The aluminium core levels overlap with the 4s and 4p core level of indium as seen in Figure 3.6 inset. To calculate the area of the aluminium peaks, reference spectrum of indium foil (spectrum A) was subtracted. Since the sample was ex-situ prepared, oxygen and carbon signal are already present in the in the indium foil reference spectrum, which can be seen in Figure 3.6, spectrum A.

### 3. Experimental setup - 3.7 Determination of organic film composition

The measured peak areas were divided by the corresponding photoionization cross-sections at the energy 1486.6 eV (see Table 1, column A<sup>47, 49</sup>). The results were then divided by a common factor. The final result for each core-level is given in the Table 1 column B, showing the composition of the AlClPc powder. In column C the expected amount of atom, based on the stoichiometry of the AlClPc molecule is given.

The amount of carbon and nitrogen in column B follows closely the value expected from the stoichiometry of AlClPc molecule. It is a proof that the phthalocyanine ring stayed intact and did not undergo degradation upon irradiation with X-rays. A clear discrepancy in the amount of aluminium, between the stoichiometric values and the experiment, comes from the very low atomic cross-section of aluminium core levels at the given experimental X-ray energy. This means, the Al 2p and Al 2s core levels will have very poor intensity (see Figure 3.6). Since the signals are just above the level of noise, even for a powder sample, it is impossible to measure amount of Al precisely. However, since the value in column B is in the same range as the expected value in column C, we assume that the thin film follows the stoichiometric relations between the amounts of atoms within the AlClPc molecule also in case of aluminium and chlorine atoms.

*Table 1. Calculation of the AlClPc powder composition: A) the photoionisation cross-sections of corresponding core-levels at  $h\nu = 1486.7 \text{ eV}$ ,<sup>47, 49</sup> B) the composition of AlClPc powder based on the experimental data, C) the composition of AlClPc molecule based on its stoichiometry.*

Core level name	A	B	C
C 1s	0.01367	32.00	32
N 1s	0.02451	7.90	8
Al 2p	0.00729	1.50	1
Cl 2p	0.03103	1.97	1
Al 2s	0.01020	1.16	1
Cl 2s	0.02299	1.25	1

The next step was to evaporate organic material and investigate the composition of a thin film. Following evaporation of the organic molecules, a survey spectrum was always taken to examine the composition of the sample. In the experiments where AlClPc was evaporated on TiO<sub>2</sub>, the Al 2p signal overlaps with Ti 3s signal. Due to the overlap and low intensity, at low film coverage (for example 0.4 nm, corresponding data in Table 2A), it is impossible to accurately measure the peak area under the Al 2p signal. However, at higher coverage (for example 2.0 nm as in Table 2B), and the same evaporation procedure, the film shows almost stoichiometric composition.

### 3. Experimental setup - 3.7 Determination of organic film composition

Table 2. Composition of AlClPc film evaporated on an oxygen treated TiO<sub>2</sub>(100): A) 0.4 nm thick film, B) 2.0 nm thick film.

Stoichiometry relations in AlClPc thin films		
	A	B
Core-level name	0.4 nm	2.0 nm
C 1s	32.0	32.00
N 1s	7.87	7.80
Al 2p	1.99	1.00
Cl 2p	1.49	1.00
Al 2s	1.89	1.20

Based on the investigation on the AlClPc composition, we are able to say that the evaporated films follow the stoichiometric composition of the AlClPc molecule.

## 4. Results and Discussion

In this chapter the results of experiments involving AlClPc and AlFPc at the interface to metal substrates as well as AlClPc at the interface to wide band gap substrates will be discussed and compared. The chapter is divided into three parts. In the first part an interaction of aluminium (III) chloride phthalocyanine with silver substrates is discussed and is later compared with the interaction of aluminium (III) fluoride phthalocyanine at the interface to silver foil. The second part focuses on the interaction of AlClPc at the interface to titanium dioxide rutile single crystal with (100) oriented surface. In part 3, the interaction between AlClPc and titanium dioxide (001) oriented surface is discussed. Influence of substrate preparation on the interaction plays an important role and will be the main focus of the last two subchapters.

## 4. Results and Discussion - 4.1 Interaction between halogen substituted organic semiconductors (AlClPc and AlFPc) and silver substrates

### 4.1 Interaction between halogen substituted organic semiconductors (AlClPc and AlFPc) and silver substrates

Silver is a reactive substrate generating strong interactions with phthalocyanines, porphyrines and other related small molecules.<sup>50-52</sup> In order to observe the possible interactions at the interface to silver substrates, clean substrates are prepared and characterized, to rule out an influence from possible metal contaminations like copper or rhodium. Afterwards, thickness dependent core level spectra related to the organic molecules are discussed. This way information about a possible chemical interaction of both chloroaluminum (III) phthalocyanine (AlClPc) and fluoroaluminum (III) phthalocyanine (AlFPc) with silver substrates can be gained. Parts of this chapter were published in a peer-reviewed paper.<sup>17</sup> They are reprinted with permission from Reference 17. *Copyright 2016 American Chemical Society.*

#### 4.1.1 AlClPc on Ag(100) single crystal

##### 4.1.1.1 Characterization of clean Ag(100) surface

The discussion on AlClPc interface with silver substrates begins with the substrate of high order: silver single crystal with the (100) surface orientation.

An overview spectrum of a clean Ag(100) single crystal surface is shown as a green line in Figure 4.1, together with the spectrum of Ag(100) substrate after the deposition of 2.6 nm AlClPc film (black line). The AlClPc specific core level signals will be discussed in Chapter 4.1.1.3. The green labeled spectrum belonging to the clean substrate exhibits typical signals of silver, with no additional signals, which might potentially indicate presence of contaminations, which could either overlap or be mistaken for either substrate or organic film signals. The most intensive signal is the Ag 3d peak, which is found at 368.3 eV binding energy, as expected from the literature.<sup>53</sup>

The Ag 3d core level spectra depicted in Figure 4.2 show same peak form and binding energy position for both clean substrate and upon consecutive deposition of AlClPc films. No new peak arise upon adsorption of organic molecules.

4. Results and Discussion - 4.1 Interaction between halogen substituted organic semiconductors (AlClPc and AlFPc) and silver substrates

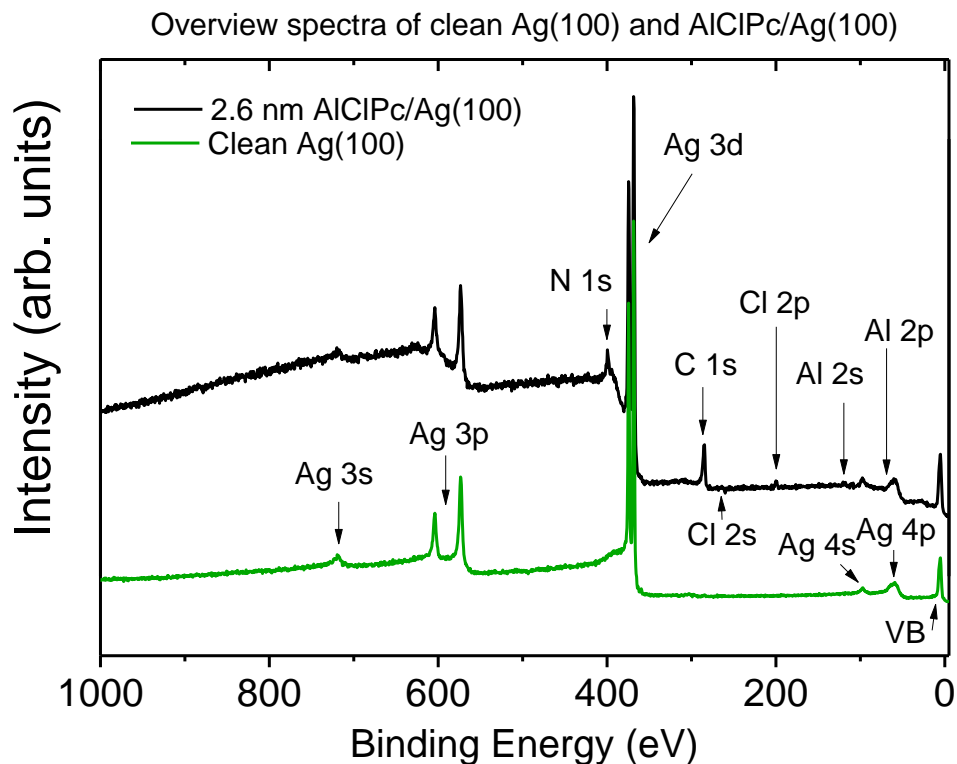


Figure 4.1 Overview spectrum of clean Ag(100) single crystal substrate (green line) and 2.7 nm thick AlClPc film on Ag(100) substrate (black line). Spectra recorded with non-monochromatic Al K $\alpha$  radiation,  $h\nu = 1486.6$  eV.

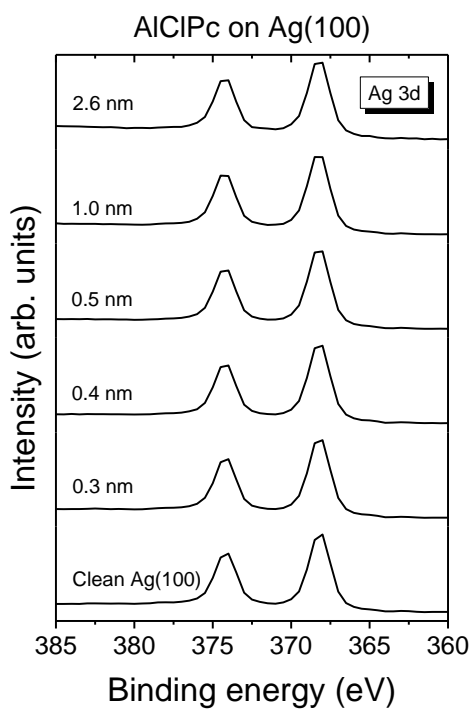


Figure 4.2. Ag 3d core level spectra of a clean Ag(100) crystal and substrate spectra upon consecutive AlClPc evaporation. Spectra recorded with non-monochromatic Al K $\alpha$  radiation,  $h\nu = 1486.6$  eV.

#### 4. Results and Discussion - 4.1 Interaction between halogen substituted organic semiconductors (AlClPc and AlFPc) and silver substrates

##### 4.1.1.2 LEED patterns - Ag(100) single crystal surface structure

The preparation procedure described in Chapter 3.3 results in a clean Ag surface (see XPS overview spectrum, Figure 4.1). Sputtering removes the contaminations from the substrate surface, leads however to destruction of the surface order. Annealing causes the implanted argon atoms to be released, the surface is smoothed and the bulk defects are removed.<sup>54</sup> The fact that the surface is clean, does not mean the atoms at the surface are still ordered in the initial arrangement. Following the preparation steps, silver single crystal was characterized with LEED to investigate if the Ag(100) single crystal surface sustained its long range order. Diffraction patterns at different energies were taken, to compare the data with literature results.

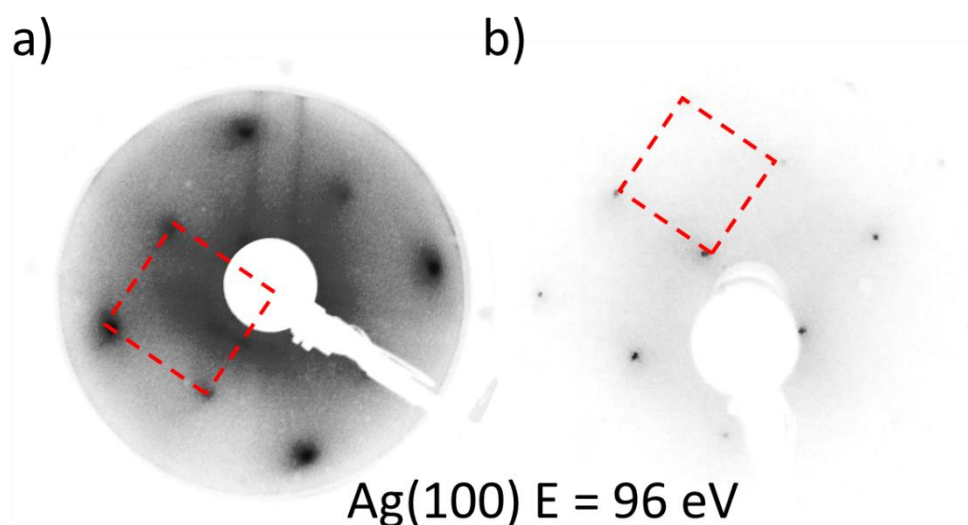


Figure 4.3. LEED diffraction pattern of an Ag(100) single crystal surface measured at 96 eV beam energy: a) after 3 sputtering and annealing cycles, b) after 7 sputtering and annealing cycles.

Figure 4.3a shows an Ag(100) surface after 3 cycles of sputtering and annealing at the beam energy of 96 eV. The pattern shows clear (1 x 1) reconstruction of the surface, with a unit cell marked with a square. The spots are yet very broad and blurred. Figure 4.3b shows an Ag(100) surface measured after 7 sputtering and annealing cycles at the same beam energy. Silver sample shows the same diffraction pattern, but due to longer annealing the spots became smaller and sharper as observed in literature.<sup>55</sup> No additional spots were visible in the measured diffraction pattern. That means that the surface is free of contamination (as confirmed with XPS). The spot size and sharpness confirms that the surface consists of large, flat areas with (100) ordered atoms.

##### 4.1.1.3 Characterization of AlClPc thin films on silver single crystal

As seen in Figure 4.1 (spectrum at the top, marked with black line), an overview spectrum of AlClPc thick film evaporated on a clean Ag(100) surface shows the typical core level signals: Al 2p, Al 2s, Cl 2p,

#### 4. Results and Discussion - 4.1 Interaction between halogen substituted organic semiconductors (AlClPc and AlFPc) and silver substrates

Cl 2s, C 1s, N 1s in the order of increasing binding energy. Since the chlorine 2s and aluminum 2s signals are less intensive than the 2p core levels of the same atom, they will not be further discussed.

Table 3. Stoichiometric relations between AlClPc core level peaks on following substrates: Ag(100), Ag foil and AlFPc core level peaks on Ag foil substrate.

	AlClPc molecule	AlClPc/Ag(100)	AlClPc/Ag foil		AlFPc/Ag foil
Thickness [nm]	Stoichiometric	0.3	0.4	Thickness	1.4
<b>C</b>	32	31.83	31.72	<b>C</b>	31.42
<b>N</b>	8	8.00	8.00	<b>N</b>	8.00
<b>Cl</b>	1	0.93	1.04	<b>F</b>	1.45

The stoichiometric relations between the core level peak areas match the stoichiometric relation of the atoms within the AlClPc molecule presented in Table 3. The values are normalized on nitrogen intensity.

Below the detailed core level spectra of carbon and nitrogen are shown in Figure 4.4a and b, as a function of AlClPc coverage. All spectra were measured using Al<sub>Kα</sub> ( $h\nu = 1486.7 \text{ eV}$ ) photon energy. Both core level signals have been fitted with a set of peaks, representing the possible contributions from carbon and nitrogen atoms with different chemical neighborhood. To model the fitted peaks, a Voigt function, a convolution of a Lorentzian and Gaussian line profile, was used. The Lorentzian peak width describes the (core-hole) lifetime broadening, while Gaussian width is related to the experimental resolution of the spectrometer. Further contributions to the Gaussian line width can be experimental artifacts, such as an unequal environment of the considered atom, different adsorption sites, or small layer-dependent energy shifts.

The C 1s signal has been fitted with four components. The benzene ring carbons of phthalocyanine molecule, linked with either other carbons or hydrogen atoms, are close on the binding energy scale and cannot be resolved in the XPS measurements so they are fitted with a single (C-1) component. Second contribution to the fit is the (C-2) component, corresponding to pyrrole carbons, bound to nitrogen atoms. The two remaining components of the fit are the ( $S_{C-1}$  and  $S_{C-2}$ )  $\pi$ - $\pi^*$  satellites<sup>56</sup> of (C-1) and (C-2) peaks respectively. The Lorentzian peak width is found to be 0.31 eV for the thickest AlClPc film and is kept constant for C 1s signals at all film coverages.

#### 4. Results and Discussion - 4.1 Interaction between halogen substituted organic semiconductors (AlClPc and AlFPC) and silver substrates

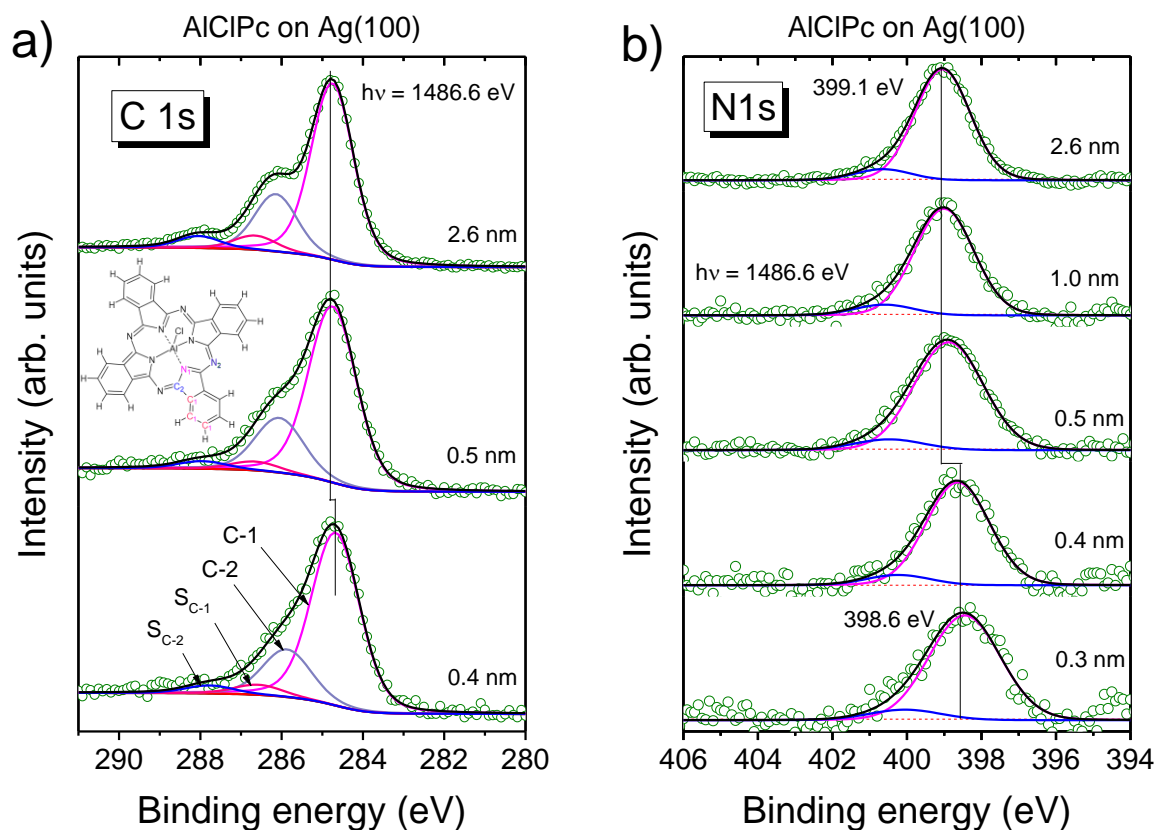


Figure 4.4 Thickness dependent core level spectra AlClPc on Ag(100) substrate: a) C 1s, b) N 1s. All spectra were measured with non-monochromatic Al K $\alpha$  radiation,  $h\nu = 1486.6$  eV. Reprinted with permission from Reference 17. Copyright 2016 American Chemical Society.

Although the Lorentzian width is kept constant, the spectra in Figure 4.4 manifest a thickness dependent broadening, with minimum width at the highest film thickness. Nevertheless, under an assumption that the intensity ratio between C-2 and C-1 contributions with their corresponding satellite signals stays constant, and variation of the Gaussian peak width, all of the spectra can be described by the same peak shape model. The intensity ratio between the peaks describing both types of carbon atoms matches the stoichiometric ratio of 0.33 between the pyrrole and benzene carbon atoms in phthalocyanine molecule, as shown in the inset of Figure 4.4a. The energy separation between the main peak and its satellite was set to 1.9 eV, as found in literature value.<sup>57</sup> For this fitting model the Gaussian peak width increases from 1.1 eV for the 2.6 nm film, up to 1.2 eV for the coverage of 0.4 nm, which is close to a monolayer (ML). Based on the crystal structure of AlClPc, the monolayer is estimated to be 0.35 nm.<sup>58</sup> What is more, the energetic distance between C-1 and C-2 increased from 1.2 eV for the 0.4 nm film to 1.4 eV for the 2.6 nm film. Furthermore, the  $S_{C-2}$  satellite intensity at the interface is suppressed. For 2.6 nm film their contribution to the total signal area is 5% (both  $S_{C-1}$  and  $S_{C-2}$ ), while for 0.4 nm film the contribution decreases to 4% and 3% respectively (see: Fitting parameters in Table 4).

#### 4. Results and Discussion - 4.1 Interaction between halogen substituted organic semiconductors (AlClPc and AlFPC) and silver substrates

Minor changes in peak shape may suggest that there is no direct involvement of macrocycle in a strong interaction between silver substrates and the phthalocyanine molecules.<sup>59</sup> That is, carbon atoms do not form new bonds with other atoms in the measured system. A shift in binding energy position of C 1s peak for 0.4 nm thick film can be explained by electrostatic screening of electrons in thin film by metal surface,<sup>60</sup> due to formation of mirror charges at the substrate surface. Due to presence of image charges, the core level electrons in monolayer thick films experience stronger screening, which leads to a shift of core level spectrum to a lower binding energy. Variation in the distance between C-1 and C-2 upon increase in film thickness cannot be however explained only with different screening of molecules in first monolayer and in thick film. Also, parts of phthalocyanine ring can be screened differently by the metal substrate as observed for MgPc on Au foil.<sup>61</sup> The interaction between AlClPc ring and silver substrate can be site-specific, due to the non-planar shape of the molecule, and different distance between pyrrole and benzene carbons to the silver surface. What is more, the energy difference between the carbon components can be caused by a charge rearrangement within the phthalocyanine molecule directly at the substrate surface, due to interaction with the metal surface, which is not experienced by the molecules of the bulk film (2.6 nm) as observed in case of CuPc and ZnPc on gold and silver substrates.<sup>52</sup> What may also contribute to the change in the energetic distance between C-1 and C-2 are complex bidirectional charge transfer processes observed for related systems as well.<sup>52, 61-63</sup> Fitting parameters of C 1s core level spectra are summarized in Table 4.

Additional information on possible interactions with the substrate can be acquired from the thickness dependent N 1s core level spectra shown in Figure 4.4b. Due to an overlap of nitrogen spectra with the Ag 3d signal, the background of reference signal has been subtracted for the clarity of the signals shown. The bulk 2.6 nm film has been fitted with a main peak at 399.0 eV and its corresponding satellite peak, 1.6 eV higher in binding energy. The main peak corresponds to the two types of nitrogen atoms present in the AlClPc molecule. The energy separation between the two nitrogen signals is reported to be 0.28 eV<sup>64</sup>, which is too close to be properly resolved in the experimental setup that have been used to obtain these results. All N 1s core level spectra presented in Figure 4.4b can be fitted with the same set of peaks. No new signals arise at lower film thickness. The slightly higher background noise between 394 eV and 395 eV is an artefact, an effect caused by the background subtraction procedure. The only difference between the bulk 2.6 nm and 0.4 nm film in terms of peak shape is the peak width, which is higher at the lower AlClPc coverage, similar to the C 1s core level spectra, which also undergoes broadening at the 0.4 nm thickness. The peak position of 0.4 nm film signal is at 398.6 eV, which is 0.4 eV lower than the bulk signal. Similar to the carbon spectrum of the 0.4 nm AlClPc film the energetic shift of N 1s core level to lower binding energy can be explained by core hole screening effects. The fitting parameters are summarized in Table 5 in part 6.2 of Appendix.

#### 4. Results and Discussion - 4.1 Interaction between halogen substituted organic semiconductors (AICIPc and AIFPc) and silver substrates

##### 4.1.1.4 Reaction of chlorine ligand with Ag(100) surface

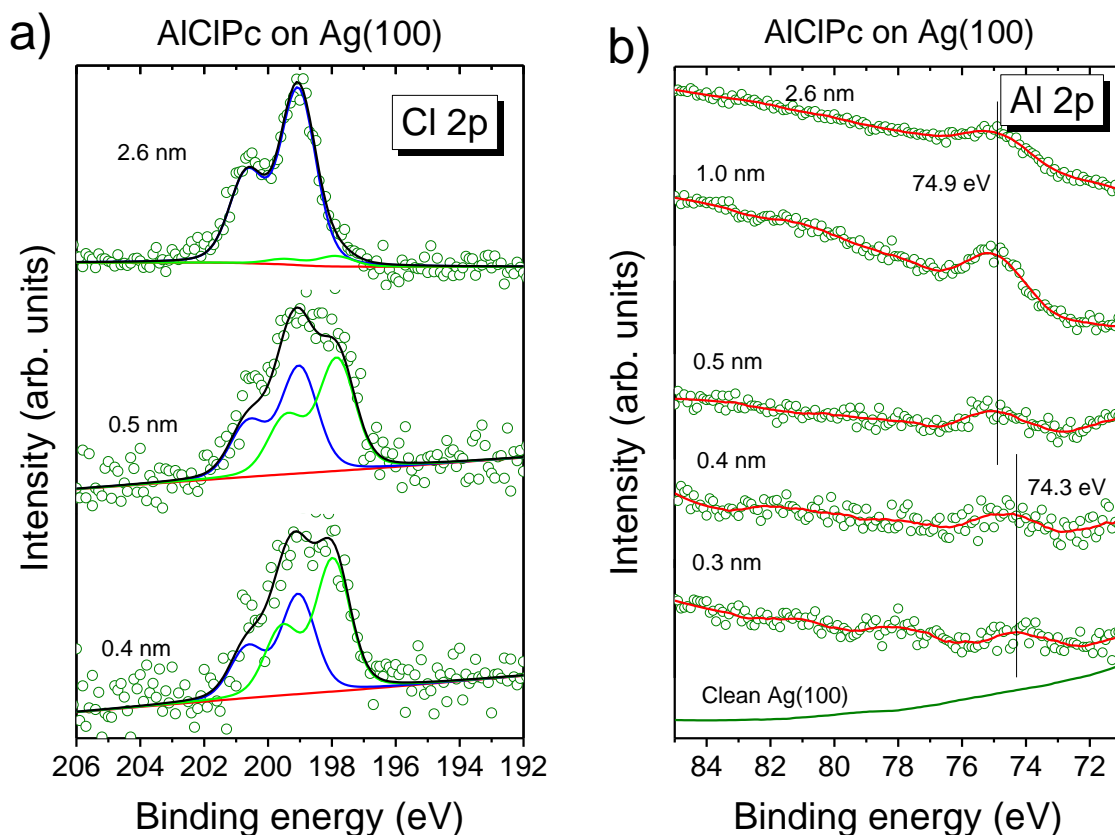


Figure 4.5 Thickness dependent Cl 2p core level spectra of AICIPc films on Ag(100) substrate. Spectra recorded with non-monochromatic Al K $\alpha$  radiation,  $h\nu = 1486.6$  eV.

A single AICIPc molecule possesses one chlorine atom. That means, only one chlorine signal is expected in the Cl 2p spectra. Due to the spin-orbit coupling, the Cl 2p signal has a form of a doublet peak. A fitting procedure performed on thickness dependent Cl 2p core level spectra, shows however, that a fit with a single doublet peak is not possible. The peak shape varies clearly as a function of film thickness, this is why a second doublet is needed to fit the peak shape properly. The Lorentz width of both doublets is kept at 0.3 eV and the Gauss width varies only slightly between 1.1 eV and 1.2 eV for bulk and thin film. In the spectra of 2.6 nm bulk film, the position of the Cl 2p<sub>3/2</sub> peak is located at 199.1 eV and the Cl 2p<sub>1/2</sub> peak is at 200.7 eV, which gives the energy separation of 1.6 eV, as expected from literature<sup>53</sup>. The small contribution from a second chlorine species is marked with a doublet peak with Cl 2p<sub>3/2</sub> and Cl 2p<sub>1/2</sub> peaks at 197.9 eV and 199.5 eV respectively. Detailed fitting parameters of Cl 2p spectra can be found in Appendix: Table 6.

The energy difference in position of doublets describing both chlorine species is much higher than the 0.5 eV shift seen in N 1s core level spectra, and cannot be explained simply by the core hole screening. The energy difference of 1.1 eV between the two doublets, points to an interaction at the interface

#### 4. Results and Discussion - 4.1 Interaction between halogen substituted organic semiconductors (AlClPc and AlFPc) and silver substrates

and presence of two chlorine species with different chemical environment present in the investigated samples. We assign the intensive doublet at 199.1 eV in Figure 4.5a to the chlorine atom of intact AlClPc molecule, bound to the aluminum atom in the center of the phthalocyanine under investigation. The intensity of the peak describing the second chlorine species at low binding energy is maximal at the lowest film coverage of 0.4 nm, and is assigned to an interface species. The binding energy of second doublet is close to that of a chlorine atom bound to silver as shown in literature for chlorine adsorbed on Ag(110) surface<sup>65</sup> or for AgCl electrodes<sup>66</sup>, so the second chlorine species binding energy position points to the formation of Ag-Cl bond at the interface to silver single crystal. The bond between aluminum and chlorine in AlClPc is likely to break. It is known that in thin films of AlClPc the chlorine ligand will be removed from AlClPc to form  $(PcAl)_2O$   $\mu$ -(oxo)dimers if water is present<sup>67</sup>. No additional peak was seen in the Ag 3d core level spectra. This is due to the fact that the Ag 3d5/2 peak maximum for a Ag-Cl bond appears at 358.1 eV which is only 0.2 eV away from the metallic silver Ag 3d5/2 peak measured in a reference spectrum at 358.3 eV as seen in Figure 4.2. Since the energy difference is low, the peaks cannot be resolved properly.

However, a change in binding energy position is seen in Al 2p core level spectra (shown in Figure 4.5b) upon background subtraction. The background presence would complicate the analysis of broad Al 2p peak. Due to poor quality of spectra in the monolayer region, more spectra in the film thickness series are shown, to better visualize the change of peak position, which changes from 74.9 eV for 2.6 nm film to 74.3 eV for the lowest film thickness. The binding energy of the Al 2p signal of 2.6 nm is typical for a Al-Cl bond of AlClPc, and the binding energy of the same bond present in  $AlCl_3$ .<sup>68</sup> This result is compatible with Cl 2p spectra of 2.6 nm film, where most of the chlorines are bound to AlClPc. The Al 2p peak position of the 0.4 nm thick film is only 0.6 eV lower in binding energy, due to the loss of chlorine atom. The peak position is still higher than the binding energy of metal Al (73 eV, as recorded in literature<sup>69</sup>), which confirms, that the aluminum atom is still part of the phthalocyanine molecule. The energy difference is similar to the one observed for N 1s core level spectra and is likely due to the core hole screening effects.

Based on the observation of increase of intensity of the reactive chlorine species at the interface, as well as the binding energy position of the doublet describing the reactive species in the fitting procedure it can be concluded that there is a strong interaction between chlorine atom and the Ag substrate. As a result, Al-Cl bond is broken and Ag-Cl bond is formed. As a consequence, bond formation may also occur between silver and the AlPc. If such bond with the remaining phthalocyanine does not form, the reaction at the surface could be an alternative method to obtain an AlPc, a molecule with magnetic properties.

#### 4. Results and Discussion - 4.1 Interaction between halogen substituted organic semiconductors (AICIPc and AIFPc) and silver substrates

##### 4.1.1.5 Valence band region and work function

The UPS data giving insight on electronic structure of the investigated systems are given below. The thickness dependent UPS spectra of AICIPc on Ag(100) single crystal substrate are shown in Figure 4.6a. The excitation energy of a helium lamp used in the UPS experiments was He I,  $h\nu = 21.2$  eV, at normal emission. At the film thickness of 2.6 nm, the features of clean silver are not visible anymore, while the AICIPc related features in valence band spectrum are fully developed, which implies that the silver substrate is fully covered at this thickness. The HOMO (highest occupied molecular orbital) peak can be found at 1.6 eV for the bulk film.

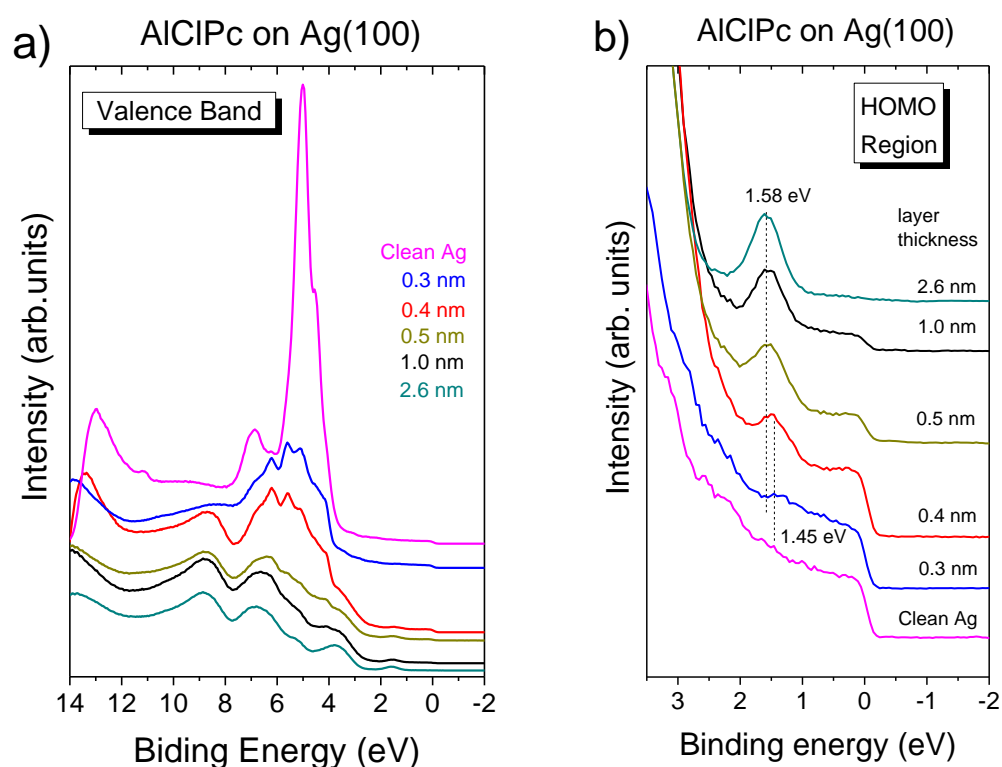


Figure 4.6. AICIPc on Ag(100): a) thickness dependent UPS valence spectra, b) thickness dependent valence band spectra HOMO region. Spectra measured with He I radiation,  $h\nu = 21.2$  eV. Reprinted with permission from Reference 17. Copyright 2016 American Chemical Society.

For better visualization of the HOMO peak, the valence band spectra are zoomed into the binding energy region of HOMO peak in Figure 4.6b. The position of HOMO peak is constant for films between 2.6 nm and 0.5 nm. The peak seems to broaden at 0.4 nm thickness, and the peak maximum is shifted to 1.45 eV at 0.3 nm thick film. The difference in binding energy between both HOMO positions is 0.13 eV. This value is close to the energy difference between Cl-up and Cl-down AICIPc molecules on Au(111) surface, where the molecules take a random up and down distribution in a monolayer, and do not form a bilayer. On gold substrate the as-grown films of AICIPc displayed two HOMO peaks. The one at low binding energy was attributed to Cl-down configuration, while the high binding energy HOMO

#### 4. Results and Discussion - 4.1 Interaction between halogen substituted organic semiconductors (AlClPc and AlFPc) and silver substrates

peak was connected with Cl-up configuration<sup>10</sup>. This is in line with the findings from Cl 2p spectra where not all molecules in 0.4 nm film (which around the ML thickness) react, indicating presence of both Cl-up and Cl-down configurations of AlClPc present at the interface to Ag(100). While there is a small minor shift in the HOMO peak position, no additional signals are visible in the HOMO region at any film thickness.

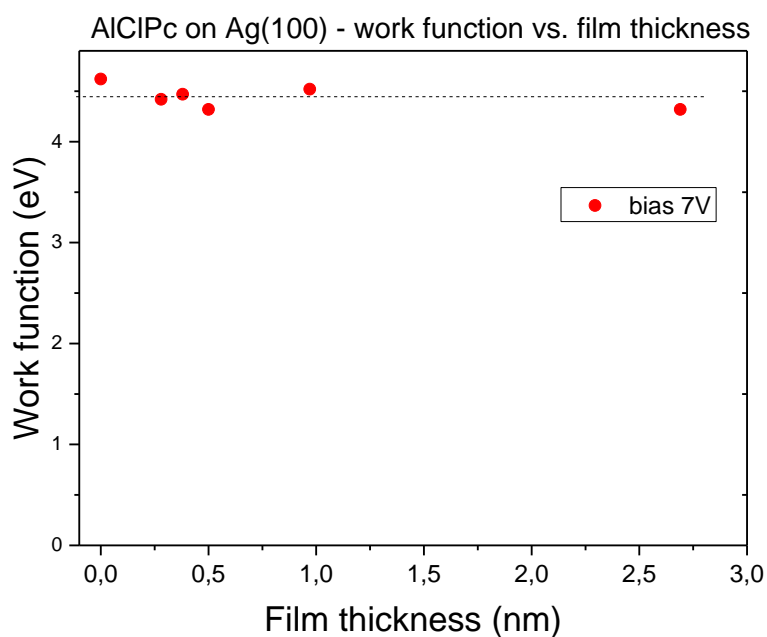


Figure 4.7 Work function of AlClPc films on Ag(100) substrate vs. film thickness.

The work function of clean Ag(100) (value shown in Figure 4.7 at film thickness equal to 0 nm) was found to be 4.6 eV. Upon adsorption of AlClPc film, the work function decreases to 4.4 eV and oscillates around the value of 4.45 eV for consecutive film depositions. At the film thickness of 2.6 nm, work function reaches the value of 4.3 eV. The decrease in work function may be due to formation of an interface dipole or redistribution of metal electrons (Cushion Effect) after adsorption of phthalocyanine molecules and decrease of metal work function.<sup>70</sup> The ionization potential of AlClPc is the sum of AlClPc work function and AlClPc HOMO peak onset. With the work function of 4.3 eV and onset of HOMO peak found at 1.1 eV the ionization potential of thick (2.6 nm) AlClPc film is easily calculated to be 5.4 eV.

## 4. Results and Discussion - 4.1 Interaction between halogen substituted organic semiconductors (AIClPc and AIFPc) and silver substrates

### 4.1.1.6 Interaction with silver substrates vs. phthalocyanine molecular orientation

Complementary methods like X-ray absorption spectroscopy (XAS) may give information on the molecules orientation.

The orientation of molecules closest to the substrate surface, as well as the type of interaction they may undergo at the interface, can influence the properties of a device remarkably. The adsorption geometry can affect the complex charge transfer processes, in which central metal atom and the phthalocyanine macrocycle may be involved, as discussed in literature.<sup>52, 62, 63, 71</sup>

Based on the X-ray absorption spectroscopy results it was determined in literature<sup>72</sup> that the AIClPc molecules in (ultra-)thin films on both Au and Ag foils as well as Ag(111) single crystal are lying flat on the substrate surface, that is, the phthalocyanine macrocycle in the films is oriented parallel to the substrate surface. An almost perfect lying adsorption geometry is reported for AIClPc molecules on an ordered surface of Ag(111) single crystal, whereas a certain degree of disorder might be expected for the molecules on foils induced by the substrate morphology.

A polar phthalocyanine like AIClPc, may adsorb in one of two geometries, either dipole-up (Cl-down) or dipole-down (Cl-up).<sup>15</sup> On surfaces, where the interaction of AIClPc at the interface is of comparable strength as on silver substrate, such as copper and indium tin oxide (ITO), randomly distributed dipoles were observed. On the other hand, AIClPc is reported to adsorb in the Cl-up configuration on graphite or graphene layers.<sup>15, 73-75</sup>

DFT calculations for AIClPc on Cu(111), point toward a strong charge accumulation at the interface between copper surface and the chlorine atom, adsorbed in the Cl-down configuration, caused by the electron transfer from the bonded Cu atoms.<sup>15</sup>

Planar metal phthalocyanines (MPcs) often adsorb in a flat lying geometry on single crystal metal substrates, parallel to the substrate surface, while on polycrystalline surfaces, the molecules are tilted with respect to the substrate surface.<sup>50, 71, 76</sup> In case of copper phthalocyanine (CuPc) on Au foil, the interfacial layer of phthalocyanine molecules is highly ordered with molecules adsorbing in flat lying geometry. The order is preserved until around 0.8 nm film thickness, above which, the molecules orientation changes towards standing molecules with the Pc ring plane perpendicular to the substrate surface.<sup>76</sup> In comparison to the AIClPc film, the gold substrate has a significantly higher free surface energy. Microscopically, among others, a charge redistribution and polarization effects at the interface to gold have to be taken into account. Hence, the molecular orientation in first few layers of molecules, directly at the interface to gold can be understood by the strong molecule-substrate interaction.<sup>76</sup> At higher film thickness the influence of substrate becomes negligible. As a result, change in molecular orientation occurs.

#### 4. Results and Discussion - 4.1 Interaction between halogen substituted organic semiconductors (AlClPc and AlFPC) and silver substrates

However, in case of AlClPc on gold and silver foil, the flat lying molecular orientation is preserved in films with thickness up to 4 nm. It appears that the presence of axial chlorine ligand, leading to the dipole moment of to the phthalocyanine plane, promotes maintaining of the initial molecular orientation throughout the film, at film thicknesses where the influence of substrate would be otherwise negligible. The maximization of dipole-dipole interaction energy might be the driving force behind the “lock-in” of the initial orientation. Similar behavior was discussed for polar subphthalocyanines on the surface of Cu(111), where by combining the dipole-up and dipole-down intact molecules a binary system could be created. Furthermore, a discrete well-defined bilayer and trilayer triangular nanocrystallites were observed.<sup>77</sup> Another example is the growth of titanyl-phthalocyanine (TiOPc)<sup>78</sup> and vanadyl-phthalocyanine (VOPc).<sup>79</sup> As a consequence of a strong dipole–dipole interaction, also AlClPc molecules keep the lying orientation even at a film thickness when the interaction with gold is negligible, contrary to the nonpolar CuPc on Au foil.<sup>76</sup>

##### 4.1.2 AlClPc on silver foil

We continue the discussion with characterization of a less ordered, closer to application conditions, substrate of silver foil. This substrate does not have an ordered surface. It is expected to have increased roughness too. In the application conditions where silver is used as for example electrodes, the surface is far from ideally ordered.

###### 4.1.2.1 Characterization of clean Ag foil

An overview spectrum of a clean silver foil is shown in Figure 4.8 (green line). The composition of the AlClPc film deposited on Ag foil is shown in Table 3 (see Chapter 4.1.1.3). It matches the stoichiometric relations between atoms in AlClPc molecule as well as the stoichiometric relations of AlClPc film deposited on Ag(100) single crystal surface.

#### 4. Results and Discussion - 4.1 Interaction between halogen substituted organic semiconductors (AICIPc and AIFPc) and silver substrates

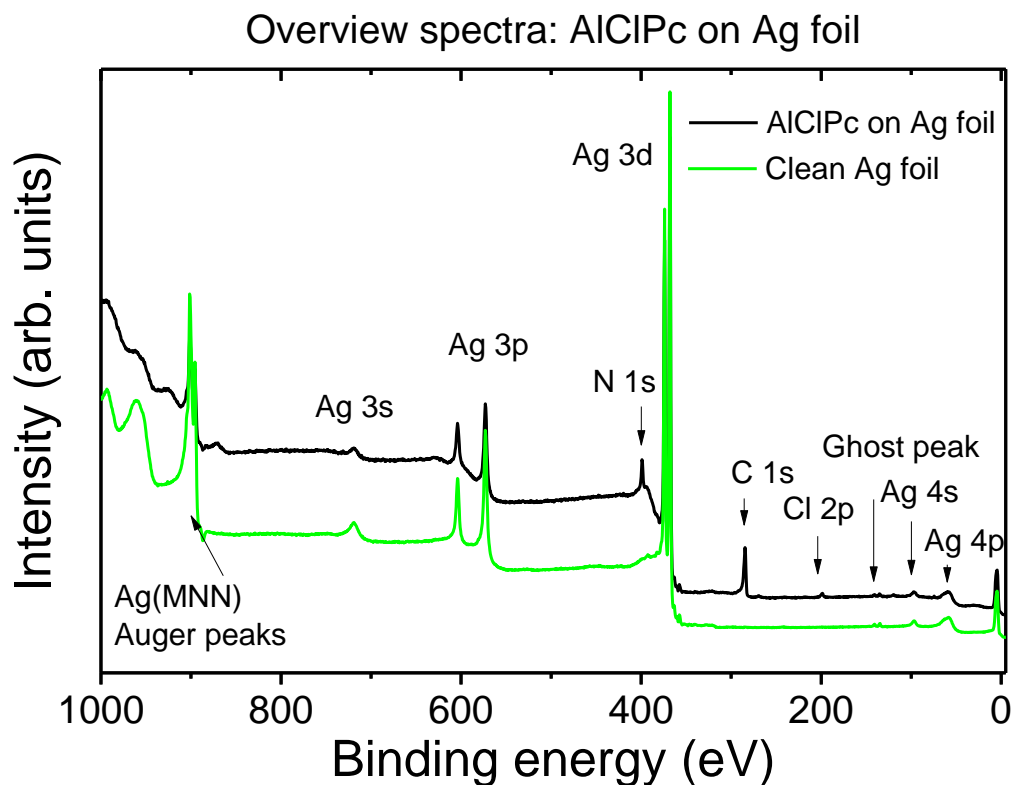


Figure 4.8 XPS overview spectra of clean Ag foil (green line) and AICIPc film on Ag foil (black line). Both spectra were acquired with non-monochromatic Mg  $K_{\alpha}$  radiation,  $h\nu = 1253.6$  eV

The Ag overview spectrum shows two types of additional peaks, which are not related to any contaminations. The first contribution comes from the Auger peaks above 900 eV. For non-monochromatized Al  $K_{\alpha}$  (1487.6 eV) excitation energy, the Auger peaks, which have fixed kinetic energy, appear above 1000 eV binding energy. The overview spectra in Figure 4.8 were measured with non-monochromatized Mg  $K_{\alpha}$  (1253.6 eV) excitation energy, causing the Auger peaks to appear within the range of the overview spectrum presented here. The second, less intensive contribution is a small doublet at binding energy exactly 233 eV lower than the Ag 3d peak. This small signal is a ghost peak, due to the presence of both Al and Mg in a twin anode of the X-ray standard source. While Mg anode is used, some electrons of Al anode are excited and as they hit the sample they cause appearance of ghost peaks lower in binding energy by the value equal to energy difference of Al and Mg  $K_{\alpha}$  radiation. No other, substrate unrelated signals appear in the spectrum, pointing to a clean substrate. The second overview spectrum (black line) belongs to the AICIPc film on Ag foil, with typical phthalocyanine related core level signals. These will be discussed in detail in further part of this chapter.

## 4. Results and Discussion - 4.1 Interaction between halogen substituted organic semiconductors (AICIPc and AIFPc) and silver substrates

### 4.1.2.2 Characterization of AICIPc thin films on silver foil

The thickness dependent core level spectra of carbon, shown in Figure 4.9, can be fitted with the same model as described in Chapter 4.1.1.3. As observed for the films evaporated on the Ag(100) surface, the intensity ratio between the C-1 and C-2 peaks with their corresponding satellites matches the stoichiometric ratio of 3:1 in the phthalocyanine molecule, meaning that the phthalocyanine macrocycle is intact and does not take part in a strong chemical interaction with silver foil.

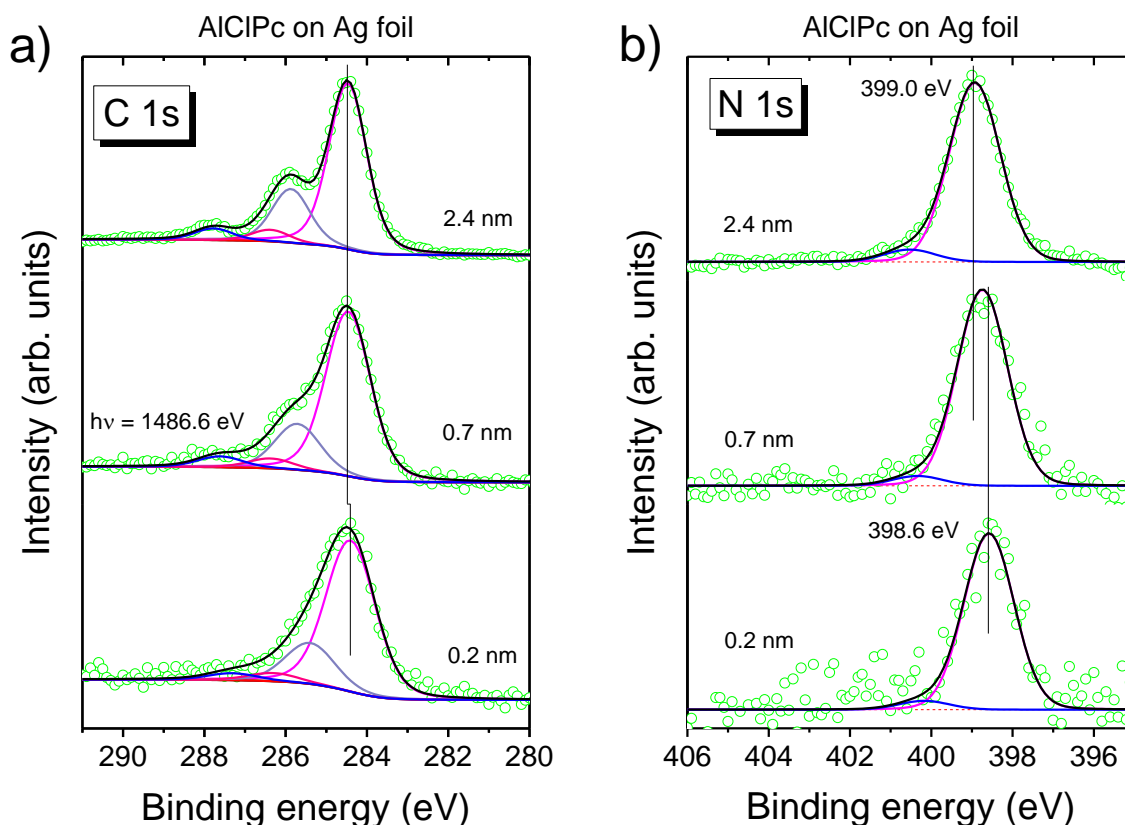


Figure 4.9 Thickness dependent core level spectra of AICIPc on Ag foil: a) C 1s and b) N 1s. Non-monochromatic Mg  $K_{\alpha}$  radiation,  $h\nu = 1253.6$  eV, was used to acquire all spectra shown in this figure.

When compared to the C 1s core level spectra broadening of AICIPc on Ag(100) substrate, the thickness dependent C 1s peak broadening on the Ag foil is even stronger. For a thick film of 2.4 nm, the Gaussian peak width value is equal to 0.9 eV, while for the lowest coverage, 0.2 nm thick film, the peak width increases to 1.3 eV. The energetic distance between the C-1 and C-2 components was found to be 1.4 eV for the 2.4 nm thick film. Similar value was observed for the bulk AICIPc film on Ag(100) and Ag(111)<sup>17</sup> substrates. While the energetic distance for 0.2 nm film was found to be 1.0 eV, which is even lower than the distance observed for monolayer coverage on Ag(100) surface (see Chapter 4.1.1.3). On both substrates the change in energetic distance between the two carbon types can be explained by the different polarization screening at the interface and bulk films. In case of films

#### 4. Results and Discussion - 4.1 Interaction between halogen substituted organic semiconductors (AlClPc and AlFPc) and silver substrates

deposited on Ag foil, the effects are even stronger and may point to a different charge distribution for AlClPc molecules through their macrocycles in the bulk film compared to the molecules in the direct contact with the Ag foil surface. The exact fitting parameters of spectra depicted in Figure 4.9a are found in Appendix: Table 7.

As observed for AlClPc on Ag(100) all N 1s core level peaks in Figure 4.9b of AlClPc on Ag foil can be fitted with the same model. Detailed fitting parameters of N1s spectra can be found in Table 8. No new peaks arise with decreasing film thickness. The only difference between the bulk and ML-region films is peak position on the binding energy scale which is 399.0 eV for 2.4 nm thick film, and 398.6 eV for 0.2 nm film. The 0.4 eV shift in binding energy can be explained by the core hole screening effects. There is a change in energetic distance of C-1 and C-2 features, as well, which can be attributed to a different polarization screening of atoms at the metal interface. The large change observed on Ag foil may indicate a different charge distribution via the macrocycle for bulk film AlClPc molecules and phthalocyanine molecules in direct contact with the silver substrate.

##### 4.1.2.3 Reaction of chlorine ligand with silver foil

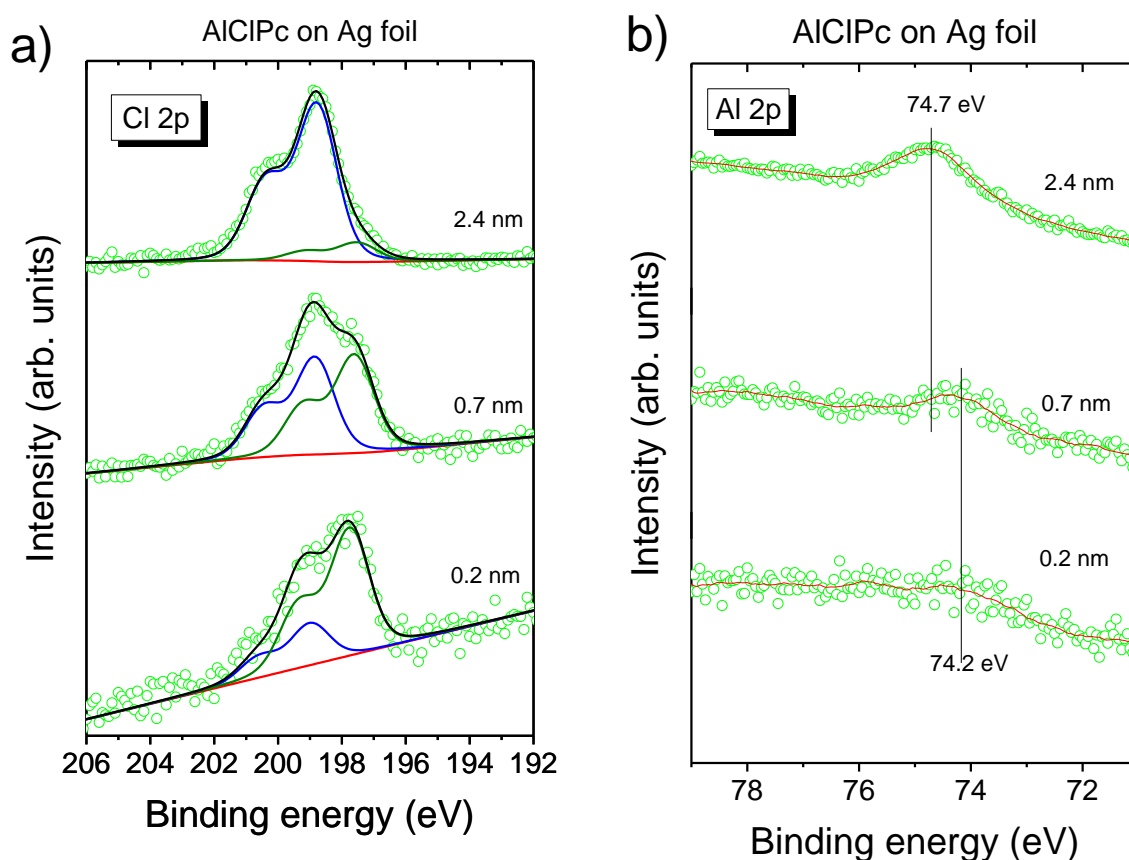


Figure 4.10 Thickness dependent core level spectra of AlClPc on Ag foil: a) Cl 2p and b) Al 2p. Non-monochromatic Mg  $K_{\alpha}$  radiation,  $h\nu = 1253.6$  eV, was used to acquire all spectra shown in this figure.

#### 4. Results and Discussion - 4.1 Interaction between halogen substituted organic semiconductors (AIClPc and AlFPc) and silver substrates

The Cl 2p core level spectra presented in Figure 4.10 were fitted with two doublet peaks. For a bulk film an intensive doublet peak at 198.8 eV labeled as Cl-1 is accompanied by a second signal, fitted with a doublet labeled Cl-2, which is found at 197.5 eV binding energy. The energy separation is kept constant throughout the fitting procedure. At 0.7 nm film thickness the contribution of both doublets is almost equal, while for a 0.2 nm film, the second doublet dominates the spectrum. The exact fitting parameters of Cl 2p spectra can be found in Appendix: Table 9. The doublets can be ascribed to bulk chlorine at the central metal atom of phthalocyanine and an interface species. As explained for the Ag(100) surface, the low binding energy of the first species matches the values found in literature for a chlorine atom bound to silver.<sup>65, 66</sup> Due to the strong interaction with silver substrate at the interface, the chlorine atoms detaches from phthalocyanine molecule and forms a chloride with silver.

The strong interaction at the interface to silver seems to be independent from the substrate surface type, as it is observed on polycrystalline Ag foil, single-crystalline surfaces, like Ag(100) and Ag(111)<sup>17</sup>. Careful fitting of Cl 2p spectra on both types of silver surface, reveals that non-reacted chlorine is present also at coverages in the monolayer range. It might be connected with random distribution of dipole-up and dipole-down configurations of AIClPc molecule, similar to another polar phthalocyanine, VOPc which strongly interacts with the nickel (111) single crystal surface<sup>80</sup>. The strong chemical interaction with the silver surface might be preferred if the molecules are oriented with their chlorine atom downwards, in the direction of silver substrate.

Signals connected with interface species in Cl 2p spectra were observed for a related system: chloro[subphthalocyaninato]-boron(III) on Ag(111) surface<sup>81</sup>. In case of the same molecule on Cu(111) surface, a combination of scanning tunneling microscopy (STM) measurements and density functional theory (DFT) calculations has shown that the molecules adsorb either in dipole-down configuration (with the chlorine atom pointing towards vacuum side of the interface), or they dechlorinate<sup>82</sup>. It is in good agreement with the results on AIClPc on silver surfaces presented in this work, where only part of the molecules react at the interface.

The XPS results on Al 2p thickness dependent spectra are in line with the results on Ag(100) surface, where the Al 2p peak is shifted to lower binding energy, by about 0.6 eV, in the monolayer region of film thickness. In case of AIClPc on Ag foil, the binding energy difference between the bulk and monolayer film is slightly smaller, 0.5 eV indicating a change in chemical neighborhood of the aluminum atom at the interface to silver foil.

#### 4. Results and Discussion - 4.1 Interaction between halogen substituted organic semiconductors (AICIPc and AIFPc) and silver substrates

##### 4.1.2.4 Valence band region, work function and energy level alignment

The valence band spectra of AICIPc on Ag foil are shown in Figure 4.11a. As in case of AICIPc on Ag(100) surface the AICIPc features are fully developed at film thickness above 2 nm. The position of the HOMO peak is found at 1.6 eV for bulk AICIPc film (2.4 nm thick), as seen in the HOMO region of valence band spectra shown Figure 4.11b. The same energy was registered for AICIPc on Ag(100) surface, suggesting a similar energy level alignment (shown later in Figure 4.13). Furthermore, the HOMO peak position at films with thickness in the monolayer region is shifted to slightly lower binding, at 1.35 eV, which is also the case on the Ag(100) surface.

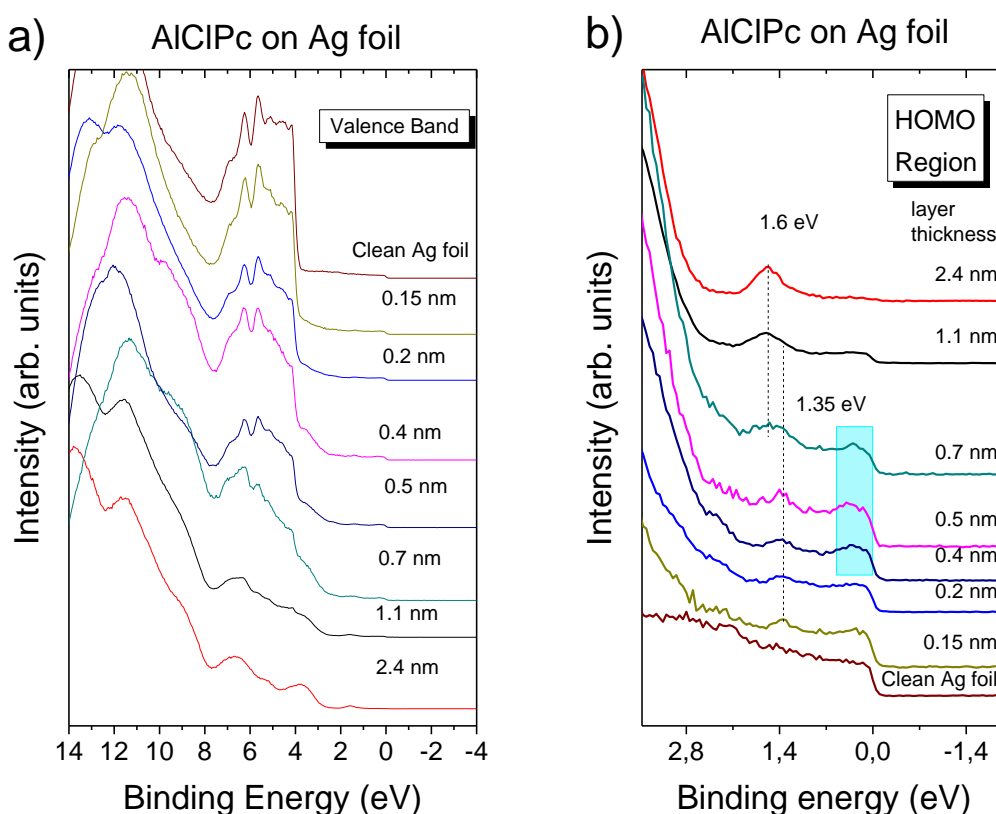


Figure 4.11. Thickness dependent UPS spectra of AICIPc on Ag foil: a) Valence band, b) Valence band HOMO region. All spectra were acquired with He I radiation,  $h\nu = 21.2$  eV. Reprinted with permission from Reference 17. Copyright 2016 American Chemical Society.

Despite the similarities between the UPS data recorded for AICIPc on Ag(100) single crystal and Ag foil, their behavior of AICIPc is not exactly the same. On closer inspection, the spectra of AICIPc films in monolayer region measured on Ag foil clearly exhibit an additional intensity in the energy region of Fermi level ( $E_F$ ), marked with a blue rectangle in Figure 4.11b. Such additional intensity was not observed for low coverages of AICIPc on Ag(100), as well as Ag(111) surface<sup>17</sup>, indicating that such interface state is absent on single-crystalline silver substrates.

#### 4. Results and Discussion - 4.1 Interaction between halogen substituted organic semiconductors (AICIPc and AIFPc) and silver substrates

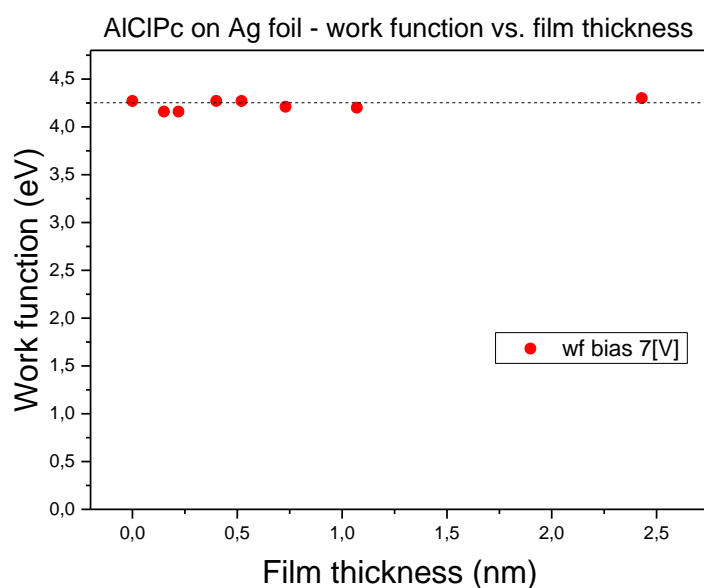


Figure 4.12 Work function of an AICIPc/Ag foil system plotted against the organic film thickness.

The work function of AICIPc/Ag foil system is plotted against the AICIPc film thickness in Figure 4.12. The data points were collected based on SECO position measured with UPS. For a clean silver foil, the work function was measured to be 4.3 eV. After deposition of AICIPc films the work function stays almost constant. At the film thickness of 2.4 nm, the value of work function is still measured to be 4.3 eV. It seems that no interface dipole is formed.

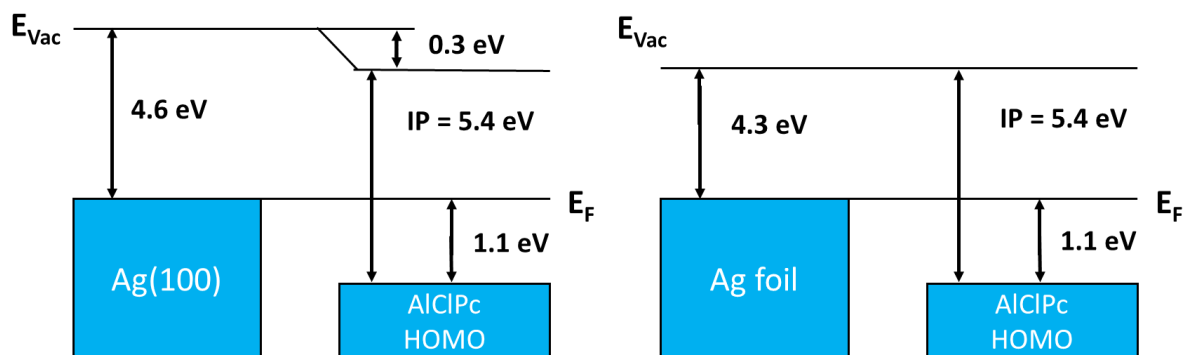


Figure 4.13. Energy level alignment for AICIPc thick film on Ag(100) (left), and AICIPc thick film on Ag foil (right). Reprinted with permission from Reference 17. Copyright 2016 American Chemical Society.

The information on energy level alignment taken from UPS data of thick AICIPc films (film thickness in the 2-3 nm region) on both Ag(100) and Ag foil is compared in Figure 4.13. For both cases the HOMO onset of AICIPc is located at 1.1 eV. Change of Ag substrate does not influence the ionization potential of AICIPc, which is 5.4 eV on both substrates. The only difference is that the work function of the Ag substrates differs by 0.3 eV. This indicates that the Fermi level is pinned at the same position in the gap of the organic semiconductor.

## 4. Results and Discussion - 4.1 Interaction between halogen substituted organic semiconductors (AICIPc and AIFPc) and silver substrates

### 4.1.2.5 Influence of substrate roughness

As explained in Chapter 4.1.2.4, the formation of an interface state is observed for AICIPc thin films on polycrystalline substrate (Ag foil), while it is absent on a single-crystalline surface of Ag(100) crystal. This leads to a question if the substrate roughness has influence on the interaction mechanism between AICIPc and silver surface. Alternatively, the interaction could be affected by a different preparation procedure for silver foil and single crystal. Silver foil surface might have increased reactivity due to a missing final annealing step in its preparation.

To test how these parameters contribute to the presence of an interface state the interface properties of AICIPc were tested on a Ag(100) single crystal, which was annealed in temperatures above 750°C, which resulted in partial damage of the single-crystalline structure of the surface. Figure 4.14 (a and b) presents valence band spectra of AICIPc on the highly annealed substrate, zoomed into the HOMO region as well as an AFM image of the strongly annealed Ag(100) surface. The AFM image shows a mixture of two regions. The first region marked in yellow, with a constant relative height of 2 nm, are terraces of the original silver crystal surface, which preserved their single-crystalline character (they are large enough, that spots in the diffraction image could be observed in LEED measurements). However, major part of the sample is covered with the second region in which silver islands of different sizes are present, due to the high temperature used during annealing, which was likely above the melting point of the surface. These contribute to the total root-mean square (RMS) roughness of the sample, which is 1.9 nm for the image shown in Figure 4.14b.

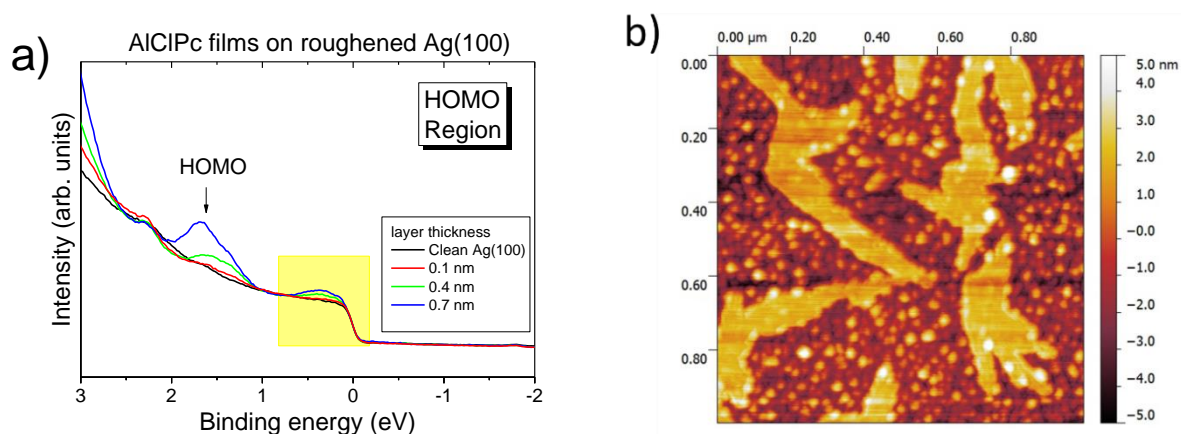


Figure 4.14 AICIPc on silver single-crystal surface treated with in temperature above 750°C: a) thickness dependent UPS valence spectra (measured with He I radiation,  $h\nu = 21.2$  eV), HOMO region of a Ag(100) single crystal surface which has been roughened upon annealing, enhanced intensity near Fermi energy is observed, similar to AICIPc on Ag foil; b) AFM Image ( $1 \mu\text{m} \times 1 \mu\text{m}$ ) of a Ag(100) single crystal surface which has been damaged upon annealing. Reprinted with permission from Reference 17. Copyright 2016 American Chemical Society.

#### 4. Results and Discussion - 4.1 Interaction between halogen substituted organic semiconductors (AIClPc and AIFPc) and silver substrates

The thickness dependent valence band spectra of AIClPc on the highly annealed Ag(100) surface (Figure 4.14a) are normalized to the same height of the bands in the range between 0.8 eV and 1.0 eV of. An additional intensity just above the Fermi level is present, as was the case of Ag foil. It is possible, that the interface state arises from molecules adsorbed on the polycrystalline islands, in regions between the terraces with crystalline character. The final annealing step of the substrate, however, seems not to affect the interaction mechanism at the interface.

##### 4.1.3 AIFPc on Ag foil

###### 4.1.3.1 Ag foil - substrate characterization

An overview XPS spectrum of a clean silver foil (red line) and a thick AIFPc film evaporated onto Ag foil (black line) are shown in Figure 4.15. The red spectrum shows only contributions from Ag substrate. Possible contaminations like adventitious carbon, are below the detection limit of a surface sensitive XPS measurement. Typical signals of AIFPc can be seen in the black spectrum within the energy range shown in the Figure 4.15. Clear C 1s, N 1s peaks and slightly smaller F 1s and Al 2s peaks are seen. Due to low intensity and overlap with substrates' Ag 4p signal and the Al 2p peak is not well visible.

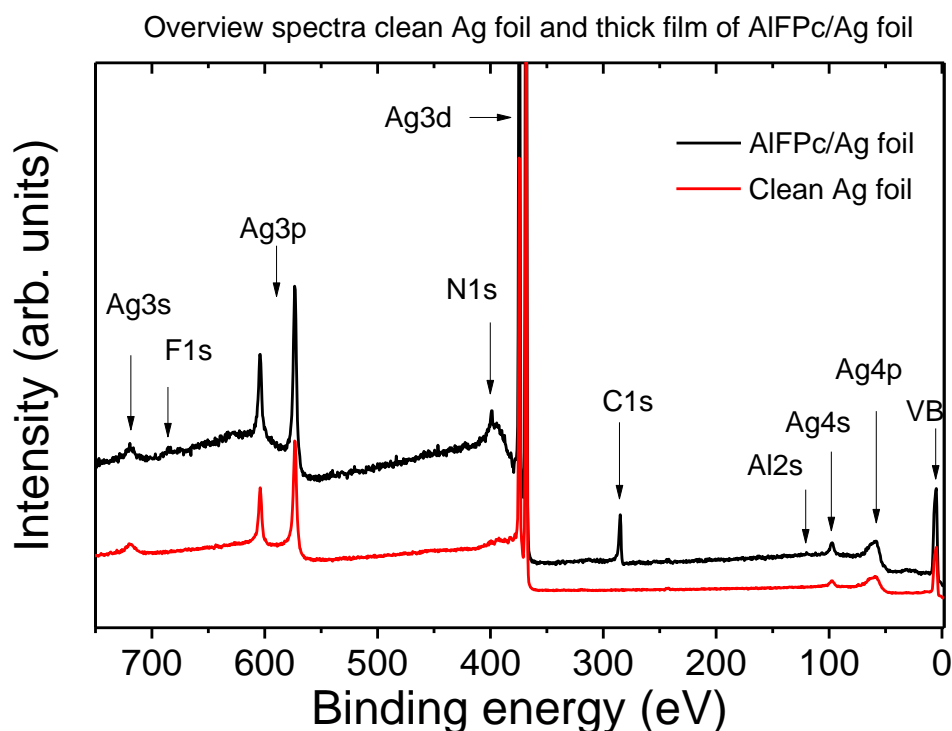


Figure 4.15 Overview spectra of clean Ag foil (red line) and thick (1.6 nm) AIFPc film deposited on Ag foil (black line). Spectra measured with monochromatic Al K $\alpha$  radiation,  $h\nu = 1486.7$  eV.

#### 4. Results and Discussion - 4.1 Interaction between halogen substituted organic semiconductors (AlClPc and AlFPc) and silver substrates

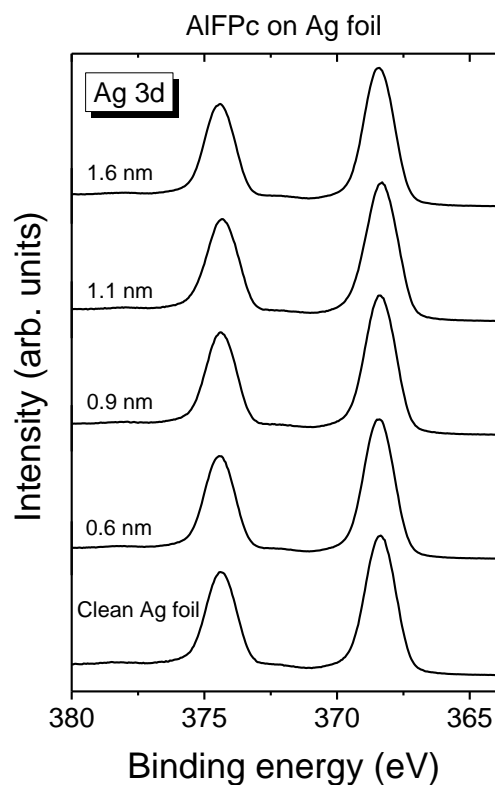


Figure 4.16 Ag 3d core level spectra of clean Ag foil, followed by Ag 3d spectra of Ag foil after deposition of AlFPc films at different coverage. Spectra measured with Al K $\alpha$  radiation,  $h\nu = 1486.7$  eV.

Figure 4.16 shows the Ag 3d core level spectrum of clean Ag foil and Ag 3d spectra after AlFPc evaporation of consecutive films. It is a doublet peak at 368.4 eV binding energy, with energy separation of 6 eV as expected from literature for clean silver.<sup>53</sup> The peak binding energy position and shape do not change after AlFPc evaporation, nor does the peak separation and peak width.

##### 4.1.3.2 Characterization of AlFPc thin films on silver foil

In previous chapters (Chapter 4.1.1 and 4.1.2) breaking of the Al-Cl bond of AlClPc molecule was described. Taking into consideration the difference in electronegativity of atoms within Al-Cl and Al-F bonds, it is expected that the latter bond might be stronger, as the difference in the electronegativity between the atoms is higher. For this reason, AlFPc might be more chemically stable when evaporated on silver surface. To investigate interactions between these two materials, AlFPc films were studied on Ag foil. The film composition (found in Table 3, see Chapter 4.1.1.3) corresponds to the stoichiometric relations in the AlFPc molecule. The related C 1s and F 1s spectra are shown in Figure 4.17.

#### 4. Results and Discussion - 4.1 Interaction between halogen substituted organic semiconductors (AIClPc and AIFPc) and silver substrates

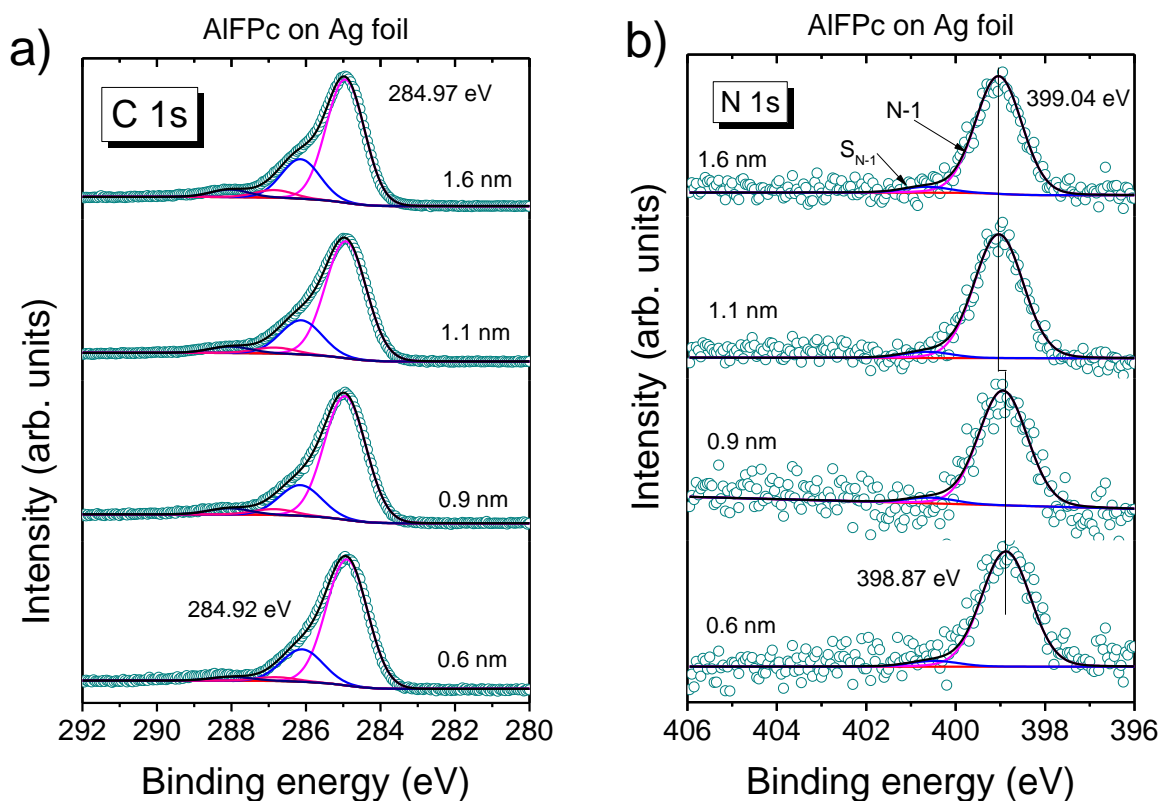


Figure 4.17 Thickness dependent core level spectra of AIFPc on Ag foil: a) C 1s, b) N 1s. Spectra measured with Al K $\alpha$  radiation,  $h\nu = 1486.7$  eV.

The C 1s spectrum in Figure 4.17a can be described by the same fitting parameters as C 1s core level of AIClPc on silver substrates. The ratio between the C-C & C-H to C-N bonds is 3:1 as expected from the AIFPc molecule stoichiometry, showing that the macrocycle is intact. The fitting parameters for C 1s core level of AIFP on Ag foil can be found in Appendix (Table 10). For the lowest AIFPc coverage of 0.6 nm, the binding energy distance between C-1 and C-2 components is 1.2 eV, which is lower than the value of 1.4 eV observed for bulk phthalocyanine films. Similar behavior was observed for AIClPc and can be explained by the charge transfer across the interface or different charge distribution within the phthalocyanine macrocycle at the interface to silver substrate.

The N 1s peak overlaps with Ag 3d peak, this is why background was subtracted from core level spectra in Figure 4.17b. This procedure allows to present the N 1s peaks, introduces however additional noise to the signals, especially in spectra at low AIFPc coverages. For the highest film thickness of 1.6 nm, the peak shape of N 1s core level spectra can be fitted with a main peak at 399.04 eV representing both types of nitrogen present in the AIFPc molecule. These are too close to each other and cannot be resolved in the equipment used for the experiment. There is a satellite peak ( $S_{N-1}$ ) present 1.6 eV higher in binding energy than the main N-1 component. The Lorentzian and Gaussian widths are kept constant

#### 4. Results and Discussion - 4.1 Interaction between halogen substituted organic semiconductors (AIClPc and AlFPc) and silver substrates

for all coverages throughout the fitting procedure. At lower coverages, the N 1s core level spectra can be fitted with the same fitting model, the only difference is, that the main component N-1 is at slightly lower binding energy: 398.87 eV. The shift is smaller than the one observed for AIClPc on Ag foil, and can be explained by the core hole screening effects. The fitting parameters of N 1s fits are summarized in Appendix 6.2.3 (Table 11).

##### 4.1.3.3 Reaction of fluorine ligand with silver foil

The changes in Al 2p and F 1s will be discussed based on their XPS spectra shown in Figure 4.18. The original Al 2p spectra (teal circles) in Figure 4.18a, were smoothed (black curve) for better visualization of the peaks after background subtraction. The ambiguous features in the binding energy range between 73.0 eV and 72.0 eV are artefacts from the background subtraction procedure. For thick film of 1.6 nm, the Al 2p peak lies at 74.9 eV binding energy. The same position is observed for the peak of 1.1 nm thick film. However, below 1 nm film thickness the peak shifts to 74.7 eV binding energy. The shift is similar in direction and magnitude to the one observed in N 1s core level spectra, pointing to the same core hole screening effects for both nitrogen and aluminum atoms in the 2-3 ML region.

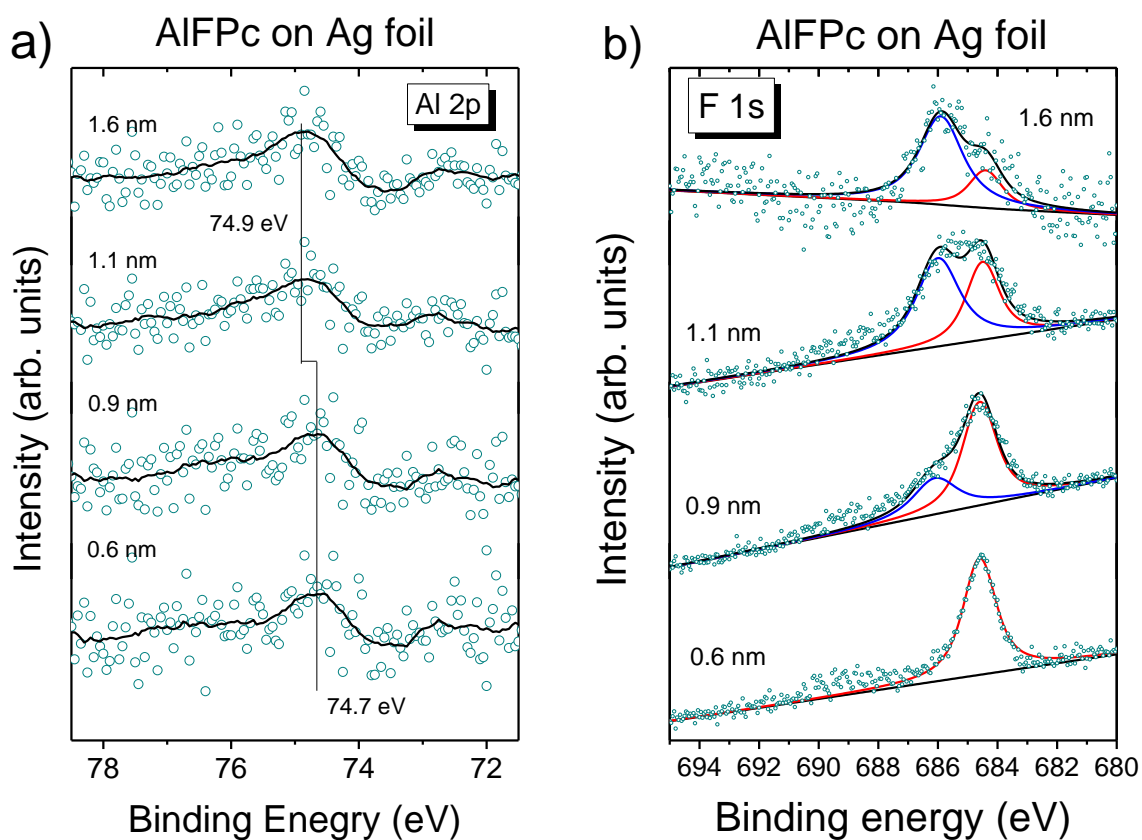


Figure 4.18 Thickness dependent core level spectra of AlFPc on Ag foil: a) Al 2p, b) F 1s. Spectra measured with Al K $\alpha$  radiation,  $h\nu = 1486.7$  eV.

#### 4. Results and Discussion - 4.1 Interaction between halogen substituted organic semiconductors (AIClPc and AIFPc) and silver substrates

Unlike Al 2p core level spectra where only shift in peak position is observed, the F 1s spectra shown in Figure 4.18b exhibit a thickness dependent peak shape variation. The spectrum of film with lowest thickness (0.6 nm, which is between 1 and 2 monolayers of AIFPc) exhibits only one distinct signal at binding energy of 684.6 eV.

With increasing film thickness, a second peak develops at 686.0 eV binding energy. The high binding energy peak is related to a fluorine atom with bulk AIFPc properties, while the low binding energy peak is related to fluorine atoms present only at the interface to silver. Such interface species is expected to form upon breaking of Al-F bond and formation of Ag-F bond, similar to what happens with the Al-Cl bond of AIClPc molecules. The binding energy position of F 1s signal for the Ag-F bond is expected to be lower than the fluorine signal measured for the bulk AIFPc. According to the literature, the binding energy of an Ag-F bond is about 683 eV.<sup>83-85</sup>

##### 4.1.3.4 Valence band spectra of AIFPc films

Following with the UPS results, one can see that the shape of HOMO peak also changes with the increasing film thickness.

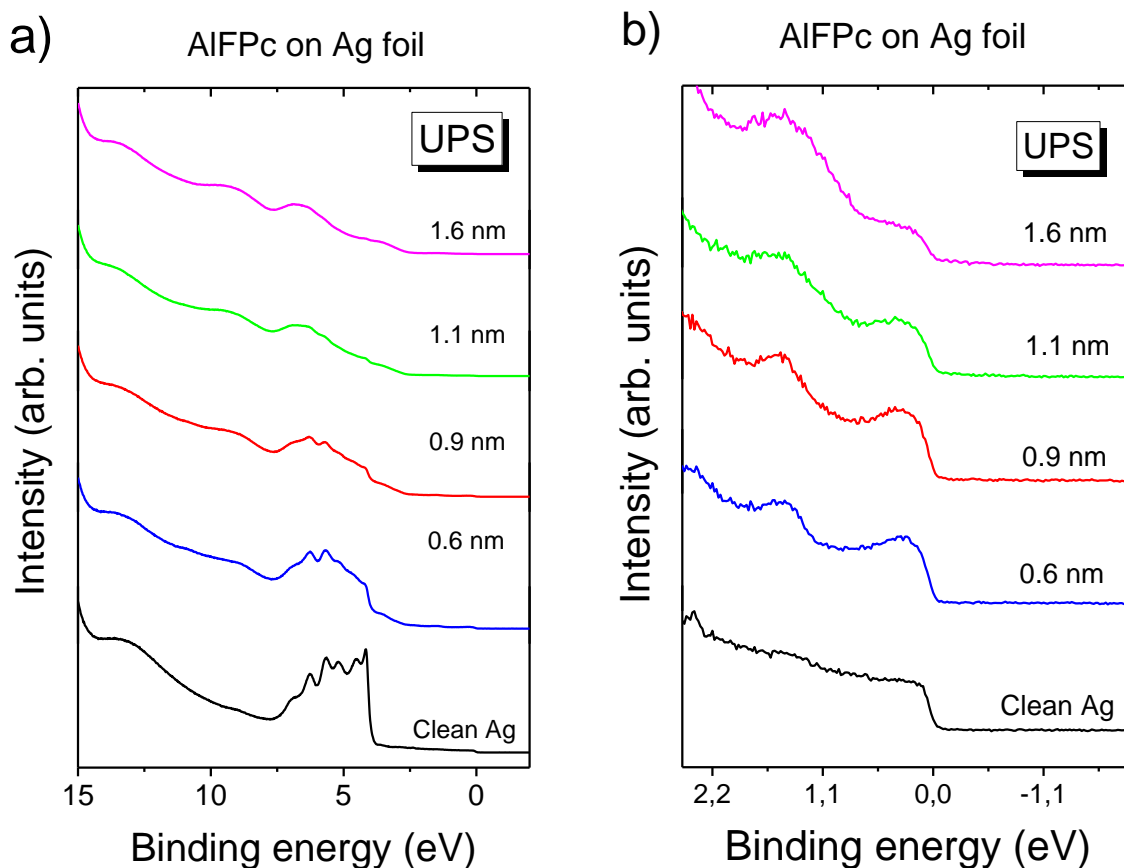


Figure 4.19 Thickness dependent UPS spectra of AIFPc on Ag foil: a) Valence band, b) Valence band, HOMO region. Spectra measured with He I radiation,  $h\nu = 21.2$  eV.

#### 4. Results and Discussion - 4.1 Interaction between halogen substituted organic semiconductors (AICIPc and AIFPc) and silver substrates

The related data showing the development of valence band spectra are presented in Figure 4.19a. In case of 1.6 nm thick AIFPc film, the valence band spectrum shows the features of bulk AIFPc film features. The magnification of valence band spectrum with binding energy up to 2.5 eV is shown in Figure 4.19b to provide more details on the HOMO region of the valence band spectra.

What is more, when comparing the valence band spectra of clean substrate and the 0.6 nm AIFPc film in the Fermi energy region, one can see an additional intensity present close to the Fermi edge at low coverages (see Figure 4.20), another similarity to AICIPc on Ag foil.

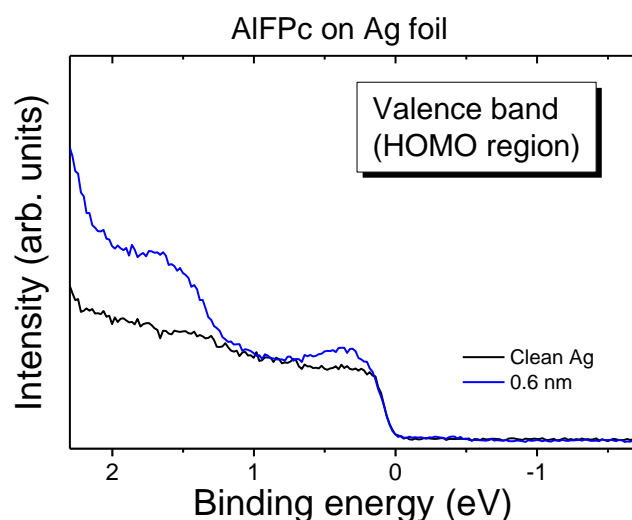


Figure 4.20 HOMO region of AIFPc on Ag foil. Spectra measured with He I radiation,  $h\nu = 21.2$  eV. Reprinted with permission from Reference 17. Copyright 2016 American Chemical Society.

A peak within this energy region in photoemission spectrum can be explained by so-called “gap states”, in particular, those observed for reactive metal-organic interfaces. Formation of such interface states could be explained by interfacial doping effects caused by charge transfer across the interface, which are accompanied by a (partial) filling of the (former) LUMO (lowest unoccupied molecular orbital), as is the case for  $\text{CuPcF}_4$  deposited on silver.<sup>86</sup> Gap states formation may result in strong coupling to the metal states for particular molecules, which can also lead to surface induced aromatic stabilization of substantially charged molecular monolayers and a metallic behavior.<sup>87</sup> The roughness of a polycrystalline substrate, such as silver foil, seems to support formation of such interface states. In this context, the roughness with magnitude of the molecule size would be important. For foils, the presence of single-crystalline terraces, with heights similar to the molecule size can be excluded, as well as for highly annealed single crystals. Furthermore, the energy distance between C 1s core level components C-1 and C-2 of AICIPc is distinctly smaller at the interface to silver foil, so it can be assumed that the phthalocyanine macrocycle takes part in this interaction. Nevertheless, for AICIPc on  $\text{Ag}(111)$ <sup>17</sup> and  $\text{Ag}(100)$ , the absence of gap states and minor change in the energy difference between the C 1s components at the interface, points to the fact that the macrocycle of AICIPc on silver single-crystals

#### 4. Results and Discussion - 4.1 Interaction between halogen substituted organic semiconductors (AlClPc and AlFPc) and silver substrates

stays almost unaltered, even though the chlorine atom reacts with silver surface at the interface. This means, that the AlClPc can be attached to the silver surface without a serious change in its physical properties. The states close to Fermi level were detected for FePc on silver single-crystal as well, as shown in literature.<sup>59, 88</sup> In case of FePc on Ag(111), however, these states may have different origin. It has been shown that the formation of gap states is a result of an interaction between the central metal atom of FePc with the substrate.<sup>59</sup>

##### 4.1.4 Chapter summary

The photoelectron spectroscopy results have shown that both AlClPc and AlFPc molecules undergo a chemical reaction at the interface to silver substrates with their central metal ligand. A peak fit analysis of Cl 2p and F 1s core level spectra allows to detect formation of Cl-Ag and F-Ag bonds, which is independent of the silver substrate type used. The reaction happens at the interface to both polycrystalline and single-crystalline substrates. Although Al-F bond is expected to be stronger than Al-Cl bond, the high reactivity of silver causes both bonds to break. At the same time, the phthalocyanine ring stays intact. Changes observed in the C 1s and N 1s core level spectra are less profound, but noticeable. A shift of core level signals to lower binding energy spectra for films in the 1-2 ML region has been observed in N 1s and C 1s peaks. The highest difference between ML and bulk films was observed for AlClPc on Ag(100) (0.6 eV and 0.29 eV for N 1s and C 1s respectively), for AlClPc on Ag foil it was 0.36 eV and 0.07 eV, while for AlFPc it was only 0.16 eV and 0.05 eV (See Appendix: 6.2.1, 6.2.2, 6.2.3 Fitting parameters). This indicates that the screening and charge rearrangement effects causing the shift are stronger on crystalline substrate than on silver foil.

Although the reaction was found to take place independent from the silver substrate type used, differences were detected with ultra-violet photoelectron spectroscopy. It was found that an additional intensity close to the Fermi edge for monolayer coverages of AlClPc and AlFPc is present only on silver foil, while absent on Ag(100) single crystal. Comparison of Ag foil UPS data with the ones measured for Ag(100) single-crystalline substrate treated in temperatures above 750°C revealed that gap states are formed even on Ag(100) substrate, if it's roughness was increased with thermal treatment, as confirmed with AFM measurements. This leads to the conclusion, that substrate roughness may influence the strength of the observed interaction.

#### 4. Results and Discussion - 4.2 Interaction between halogen substituted organic semiconductor molecules (AlClPc) and TiO<sub>2</sub>(100) substrate.

##### 4.2 Interaction between halogen substituted organic semiconductor molecules (AlClPc) and TiO<sub>2</sub>(100) substrate.

In the following part, the properties of AlClPc on TiO<sub>2</sub> rutile single crystal surface will be discussed based on the photoemission spectroscopy results. In this chapter, TiO<sub>2</sub>(100) surface prepared in presence and absence of oxygen will be characterized, following by detailed description of AlClPc thin films and the AlClPc/TiO<sub>2</sub> interface. The interaction between AlClPc and TiO<sub>2</sub> will be discussed. Parts of this chapter were published in a peer-reviewed paper<sup>89</sup>. They are reproduced from Reference 89 with permission from the PCCP Owner Societies.

##### 4.2.1 Characterization of a clean TiO<sub>2</sub>(100) surface at different degrees of reduction

###### 4.2.1.1 Substrate overview - differences resulting from two types of preparation

The rutile TiO<sub>2</sub>(100) single crystal surface has been prepared with two procedures described in Chapter 3.3: the surface prepared in presence of oxygen and reduced TiO<sub>2</sub> surface prepared in absence of oxygen, marked as “O<sub>2</sub> treatment” and “absence of O<sub>2</sub>” in figures presented in the following chapters. The outcome of both preparations was obtaining clean substrates differing in the amount of defects present at the surface.

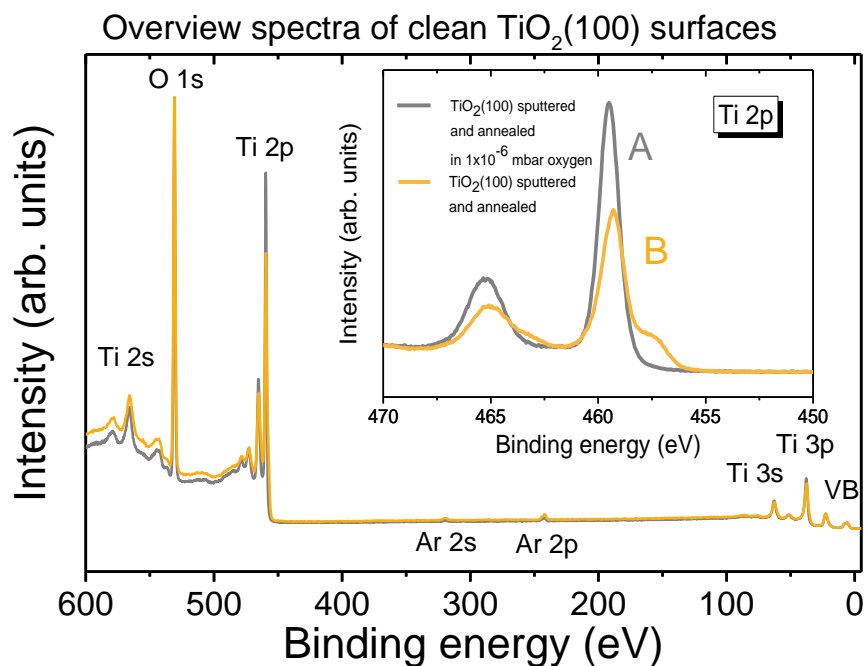


Figure 4.21 An XPS overview spectra of: a) clean TiO<sub>2</sub>(100) surface treated with oxygen, b) clean TiO<sub>2</sub>(100) surface prepared in absence of oxygen. Spectra measured with Al K $\alpha$  radiation,  $h\nu = 1486.7$  eV.

#### 4. Results and Discussion - 4.2 Interaction between halogen substituted organic semiconductor molecules (AlClPc) and TiO<sub>2</sub>(100) substrate.

Overview spectra of clean TiO<sub>2</sub>(100) surfaces (oxygen treated - gray line, reduced - yellow line) are shown in Figure 4.21. The spectrum constitutes of typical titanium dioxide signals, the most intensive ones being Ti 2p and O 1s core level peaks in the binding energy region between 450 eV and 550 eV. In low binding energy region, below 150 eV, Ti 3s and Ti 3p core levels are present, while the most intensive contribution in the valence band region stems from O 2p electrons. Although no contamination related signals can be detected (most common are carbon and calcium), there is a small contribution from argon ions which were implanted into the surface during the sputtering procedure. At the first glance the both preparation procedures resulted in the same spectrum of TiO<sub>2</sub>(100) surface. The differences cannot be detected, without zooming into the TiO<sub>2</sub> specific core level signals, clearly visible in the inset of Figure 4.21 containing Ti 2p peaks of oxygen treated (gray line) and reduced (yellow line) TiO<sub>2</sub>(100) surfaces, which will be discussed in detail in next chapter.

##### 4.2.1.2 Ti 2p and O 1s spectra - determination of defects amount

As mentioned in the previous subchapter, the oxygen treated and reduced TiO<sub>2</sub>(100) differ by the shape of substrate related core level spectra. Detailed Ti 2p core level spectra of clean TiO<sub>2</sub>(100) surface following both preparations are shown in Figure 4.22. The components of Ti 2p core level spectra were identified with a fitting procedure.

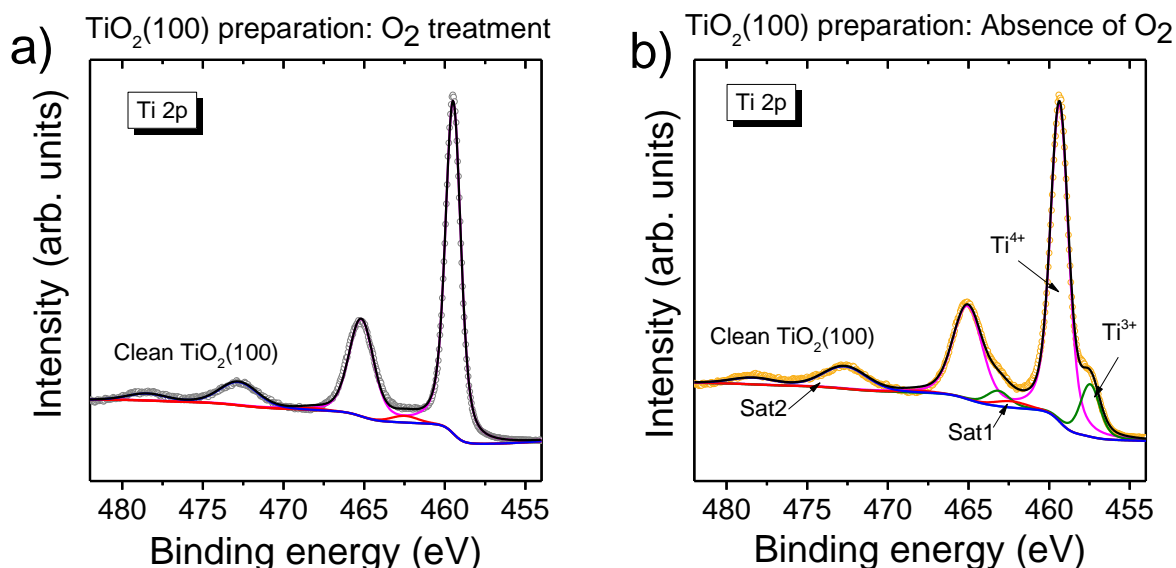


Figure 4.22 Ti 2p spectra of a clean TiO<sub>2</sub>(100) surface: a) treated with oxygen during all annealing steps and b) prepared without oxygen, resulting in the presence of reduced Ti<sup>3+</sup> ions. A fitting procedure has been performed on both spectra, underlining their different composition. Spectra measured with Al K $\alpha$  radiation,  $h\nu = 1486.7$  eV. Reproduced from Ref. 89 with permission from the PCCP Owner Societies.

The Ti 2p core level spectrum of a clean TiO<sub>2</sub>(100) surface treated with oxygen during preparation (Figure 4.22a), can be described with three doublet peaks, as described in literature.<sup>90</sup> The Ti 2p<sub>3/2</sub> component of the first doublet lies at 459.5  $\pm$  0.1 eV (this value was found for several samples) was

#### 4. Results and Discussion - 4.2 Interaction between halogen substituted organic semiconductor molecules (AIClPc) and TiO<sub>2</sub>(100) substrate.

identified as Ti<sup>4+</sup> ions typically found in the TiO<sub>2</sub> crystal lattice. This is the most intensive contribution to the Ti 2p signal, and is used as the main peak in the fitting procedure. The main doublet exhibits a spin-orbit splitting of 5.7 eV, as expected for TiO<sub>2</sub> in the literature.<sup>91</sup> The remaining two doublets, which are found 3eV and 13.3 eV (marked as Sat1 and Sat2 in Figure 4.22b) higher in binding energy than the main peak, originate from loss structures.<sup>90</sup>

As for the TiO<sub>2</sub>(100) surface prepared in absence of oxygen (Figure 4.22b), three doublets are not enough to fit the Ti 2p spectrum. A low binding energy shoulder of the Ti 2p peak, requires use of a fourth doublet. The additional doublet is situated 1.9 eV lower on binding energy scale than the main doublet and can be assigned to reduced titanium at 3+ oxidation state: Ti<sup>3+</sup>.<sup>91-94</sup> Titanium atoms at lower oxidation states were not detected. The Ti<sup>2+</sup>, for example, is expected between 3.0 eV and 3.4 eV lower in binding energy than the main peak,<sup>91-94</sup> however, no such contribution is observed in the discussed spectra. The relative amount of reduced Ti<sup>3+</sup> species was calculated based on the intensities of Ti<sup>4+</sup> and Ti<sup>3+</sup> related doublets, according to the following ratio: (Ti<sup>3+</sup>)/(Ti<sup>3+</sup> + Ti<sup>4+</sup>). Intensities of satellite (loss) peaks were not included in calculation, assuming that their contribution is similar for different Ti species with respect to the main doublet. For the Ti 2p spectrum presented in Figure 4.22b, the relative amount of reduced Ti<sup>3+</sup> species is about 16%.

Formation of defects on TiO<sub>2</sub>(100) surface prepared in absence of oxygen, has influence on both shape and position of the Ti 2p peak. A shift towards lower binding energy (459.3 ±0.1 eV), as compared to the oxygen treated surface, indicates a shift in Fermi level, due to an increased number of defect states present in the TiO<sub>2</sub> band gap (see TiO<sub>2</sub> valence band spectra in Chapter 4.2.2.4). What is more, broadening of the Ti 2p main component is observed for reduced TiO<sub>2</sub> surface. The broadening effect increases with an increase in sputtering dose, which can be explained by an increase in the number of defects within TiO<sub>2</sub> substrate,<sup>95</sup> leading to an increase in number of inequivalent Ti<sup>4+</sup> sites.<sup>89</sup> Fitting parameters of Ti 2p spectra presented in Figure 4.22 are found in Table 12 and Table 13 in Appendix 6.2.3.

Variation in preparation procedure of TiO<sub>2</sub>(100) substrate leads also to changes in O 1s core level signals. Fitted O 1s spectra are shown in Figure 4.23. For substrate prepared in presence of oxygen during annealing (Figure 4.23a), the O 1s spectrum is dominated by a component at 530.8 eV (denoted as O-1), which stems from oxygen atoms in the bulk TiO<sub>2</sub> crystal. A small second contribution at the higher binding energy (denoted O-2), may indicate one of the following: oxygen atoms in the neighborhood of titanium atoms at lower oxidation state than the Ti<sup>4+</sup> present in the bulk<sup>96, 97</sup> hydroxyl groups<sup>98, 99</sup> or other oxygen species present at the surface.

#### 4. Results and Discussion - 4.2 Interaction between halogen substituted organic semiconductor molecules (AlClPc) and TiO<sub>2</sub>(100) substrate.

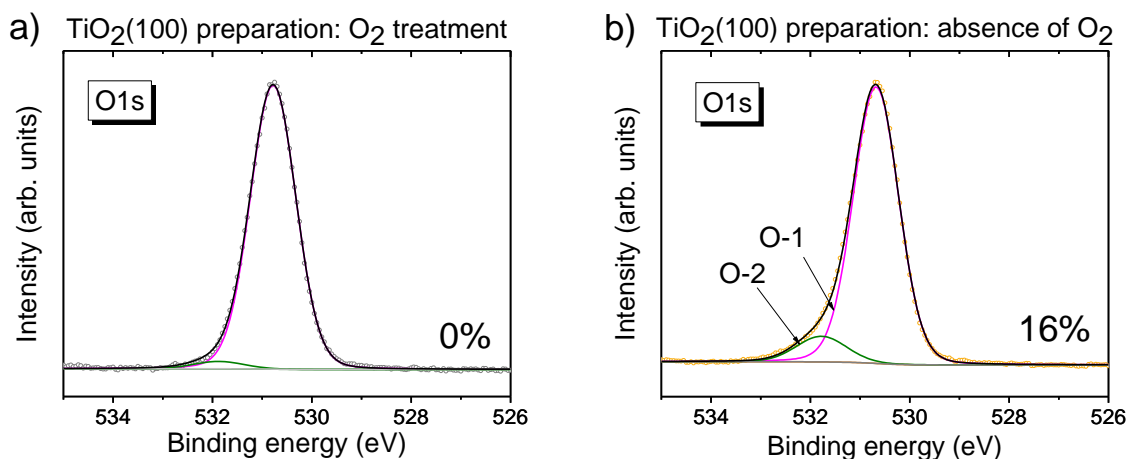


Figure 4.23 O1s spectra of clean TiO<sub>2</sub>(100) substrate: surface with: a) 0% and b) 16% defects. Spectra measured with Al K $\alpha$  radiation,  $h\nu = 1486.7$  eV. Reproduced from Ref. 89 with permission from the PCCP Owner Societies.

The O 1s spectrum of surface prepared in absence of oxygen has both O-1 and O-2 components present, however, the ratio between them has changed, as the relative intensity of the second component has increased. This indicates, that defect structures now present in the crystal contribute to the O-2 component. As a matter of fact, it was frequently reported that the binding energy position of oxygen atoms bound to Ti<sup>3+</sup> is 1.4 eV higher than the bulk TiO<sub>2</sub> oxygen atoms O-1.<sup>96, 97, 99, 100</sup> The binding energy difference obtained from the peak fit of O 1s presented in this work is equal to 1.1 eV, which is in reasonable agreement with the literature value. Detailed fitting parameters of O 1s spectra can be found in Table 14 of Appendix. What is more, presence of other oxygen species like adsorbed water molecules<sup>101</sup> or chemisorbed oxygen<sup>100</sup> can be ruled out, since their signals are expected at higher binding energies, where no signals were detected.

##### 4.2.1.3 LEED patterns - Influence of defect on TiO<sub>2</sub>(100) surface structure

As described in Chapter 2.4.2, LEED results provide information about the long-range order of the sample. In case of transition metal oxides like TiO<sub>2</sub>, the LEED pattern is expected to be more complicated, since the surface orientation and preparation conditions influence surface reconstruction. The presence of defects like point defects, steps and dislocations between large domains cannot be excluded in case of oxides. While LEED is not the main technique to investigate such defects, some of their fingerprints can be observed with this technique.<sup>54</sup> The XPS measurements are followed with a LEED technique to check how the preparation parameters described in Chapter 3.3 influence the surface order of rutile TiO<sub>2</sub> single crystal (100) and surface.

The TiO<sub>2</sub>(100) surface annealed in oxygen atmosphere, was measured with LEED setup at 80 eV and 130 eV primary beam energy. The corresponding diffraction patterns are shown in Figure 4.24 (a and b). Both of them display a clear array of small, sharp spots. The crystal lattice of the rutile TiO<sub>2</sub>

#### 4. Results and Discussion - 4.2 Interaction between halogen substituted organic semiconductor molecules (AICIPc) and TiO<sub>2</sub>(100) substrate.

(100) surface is marked with red rectangle. The spots exactly match the distances between the atoms in rutile unit cell. No additional spots, apart from the first order diffraction spots, can be seen in the LEED pattern, neither at lower nor at higher primary beam energy. The observed spot arrangement is identical with diffraction patterns of a (1 x 1) reconstructed TiO<sub>2</sub>(100) surface presented in literature,<sup>102</sup> which were measured at the same beam energy.

Since the TiO<sub>2</sub>(100) surface is more stable than the TiO<sub>2</sub>(001), the (1 x 1) reconstruction of a defect free surface can be obtained easily at mild sputtering and annealing conditions if oxygen is used. Both images show that the sample has sustained its long range order after preparation procedure.

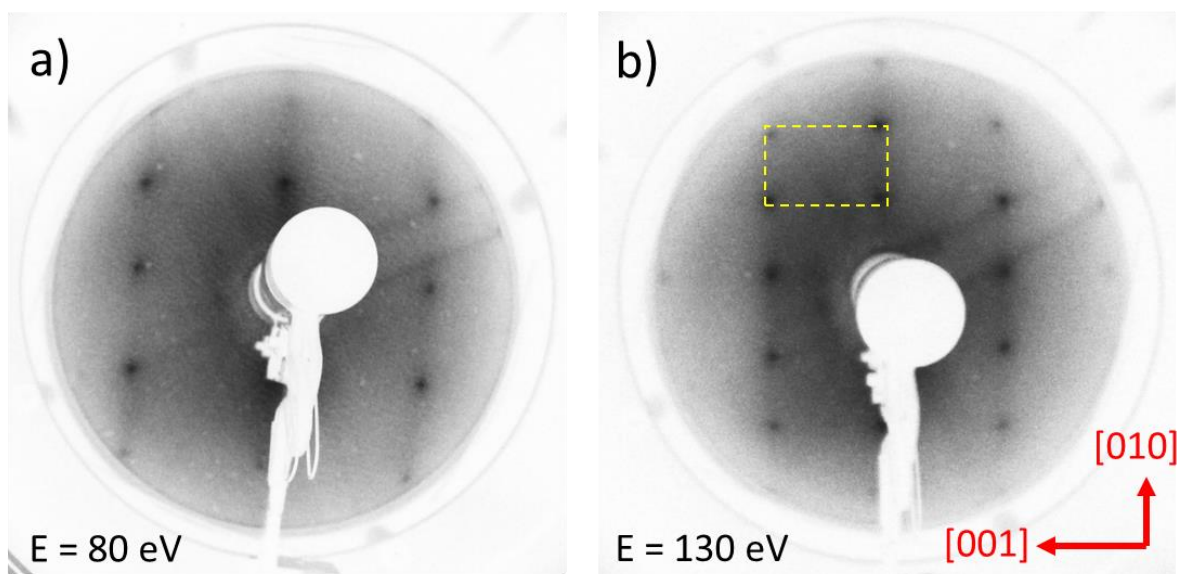


Figure 4.24 LEED diffraction pattern of TiO<sub>2</sub>(100) surface prepared in presence of oxygen, measured at a) 80 eV and b) 130 eV incident beam energy.

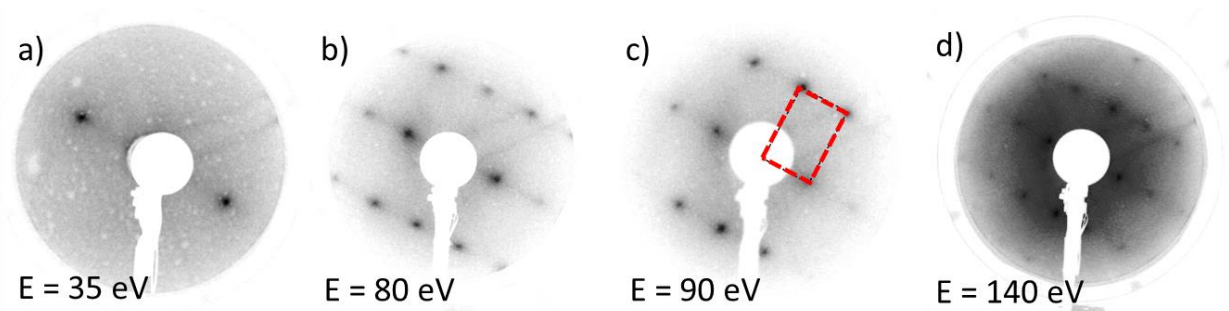


Figure 4.25 LEED patterns series reproduced for a second TiO<sub>2</sub>(100) oxygen treated substrate at: a) 35 eV, b) 80 eV, c) 90 eV, d) 140 eV primary electron beam energy.

Second series of LEED patterns shown in Figure 4.25 confirms that the data can be reproduced using the same preparation conditions on a second TiO<sub>2</sub>(100) single crystal surface treated with oxygen. In Figure 4.25 a-d the LEED patterns were measured at 35, 80, 90 and 140 eV primary beam energy.

#### 4. Results and Discussion - 4.2 Interaction between halogen substituted organic semiconductor molecules (AlClPc) and TiO<sub>2</sub>(100) substrate.

At 35 eV beam energy only the primary spots are visible with no streaks, split or satellite spots seen between the first-order spots.

The diffraction patterns of a reduced TiO<sub>2</sub>(100) surface, on the other hand, exhibit additional features between the primary spots. The corresponding diffraction patterns are shown in Figure 4.26. It can be seen that all LEED patterns show streaks along the [010] direction. At lower energies, where diffraction spots are the sharpest, one can see two additional spots along the [010] direction, between the first order spots describing the rutile unit cell. These spots can be seen at 66 eV and 80 eV as well. The unit cell is marked as a yellow rectangle in Figure 4.26. The spots are less sharp than the diffraction pattern of oxygen treated (100) surface, where defects are not present. With increasing beam energy the background of the patterns becomes more intensive, making it difficult to observe spots at 130 eV. In this case only streaks along the [010] are visible. The increased background intensity indicates presence of defects.

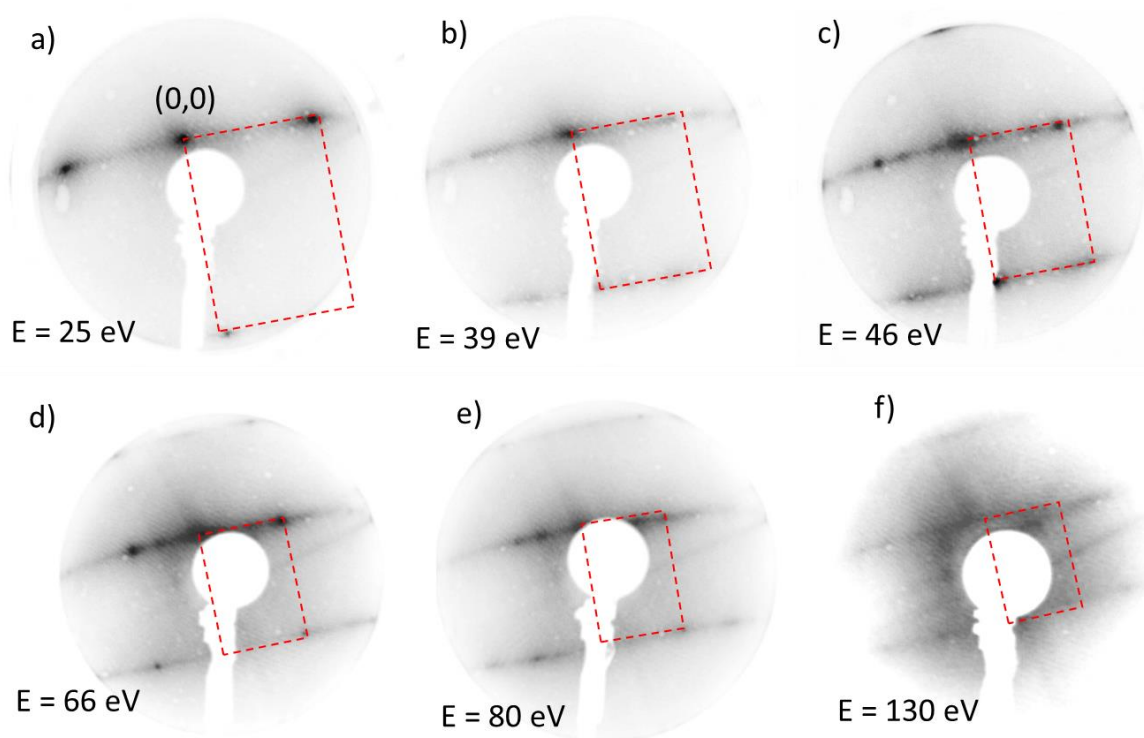


Figure 4.26 LEED images of a reduced TiO<sub>2</sub>(100) surface (12% defects) prepared without the oxygen treatment. The images were measured at the following energies: a) 25.1 eV, b) 39 eV, c) 46 eV, d) 66 eV, e) 80 eV, f) 130 eV.

The additional spots present in a LEED pattern can be explained with the surface reconstruction. According to literature the additional spots between the primary spots indicate a (1 x 3) reconstruction of the oxygen deficient TiO<sub>2</sub>(100) surface.<sup>103-105</sup> The TiO<sub>2</sub>(100) surface undergoes a reconstruction from the nominally stoichiometric (1 x 1) surface to a (1 x 3) microfaceted surface when annealed in vacuum

#### 4. Results and Discussion - 4.2 Interaction between halogen substituted organic semiconductor molecules (AIClPc) and TiO<sub>2</sub>(100) substrate.

above 600 °C.<sup>105</sup> The additional spots in pattern measured at E = 46 eV are not as sharp as the (1 x 1) spots. They however point to the (1 x 3) reconstruction of the sputtered and annealed TiO<sub>2</sub>(100) surface.<sup>105</sup> The diffraction pattern can be seen in Figure 4.27. For the sake of comparison, LEED pattern of an oxygen treated (100) surface measured at the same beam energy is shown as well.

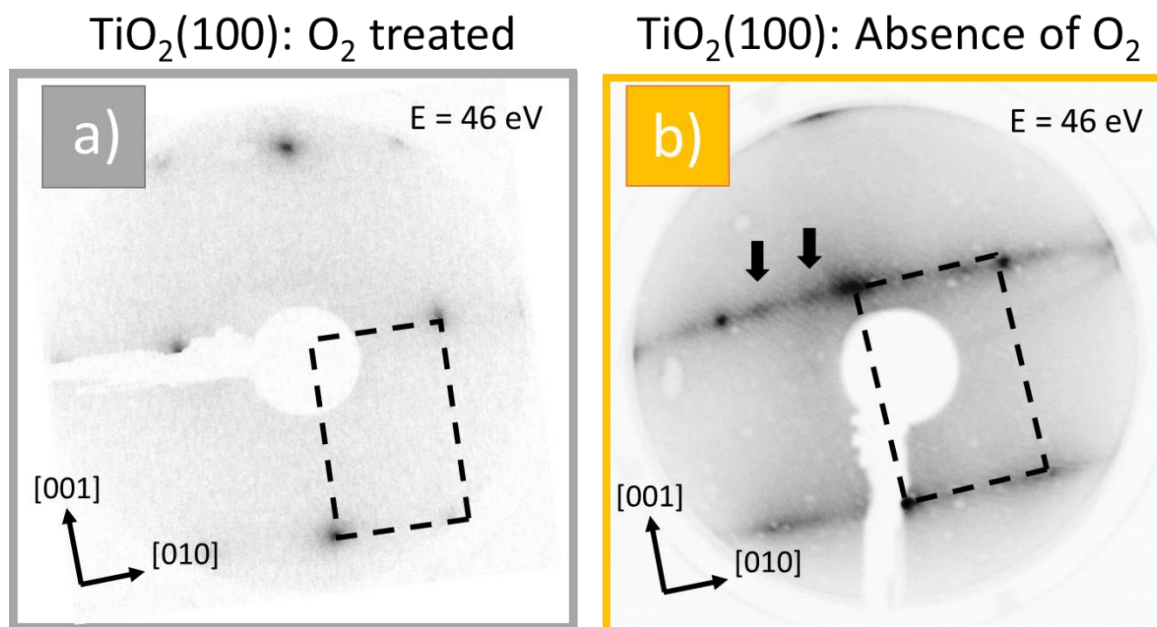


Figure 4.27 LEED pattern of TiO<sub>2</sub>(100) surface measured at 46 eV: a) oxygen treated, b) prepared in absence of oxygen. The rutile unit cell is marked as yellow rectangle. The crystal directions are marked with white arrows. Additional spots of possible (1 x 3) reconstruction are marked with white arrows.

The same pattern was observed in literature at the 46 eV primary beam energy for a (1 x 3) reconstructed rutile TiO<sub>2</sub>(100) surface.<sup>106</sup> A similar diffraction pattern can be seen in literature at E = 27 eV, although the patterns shown in Figure 4.26 is not as sharp as the literature ones.<sup>107</sup> Models of both surface reconstructions are shown in Figure 4.28.<sup>104, 105</sup>

#### 4. Results and Discussion - 4.2 Interaction between halogen substituted organic semiconductor molecules (AlClPc) and TiO<sub>2</sub>(100) substrate.

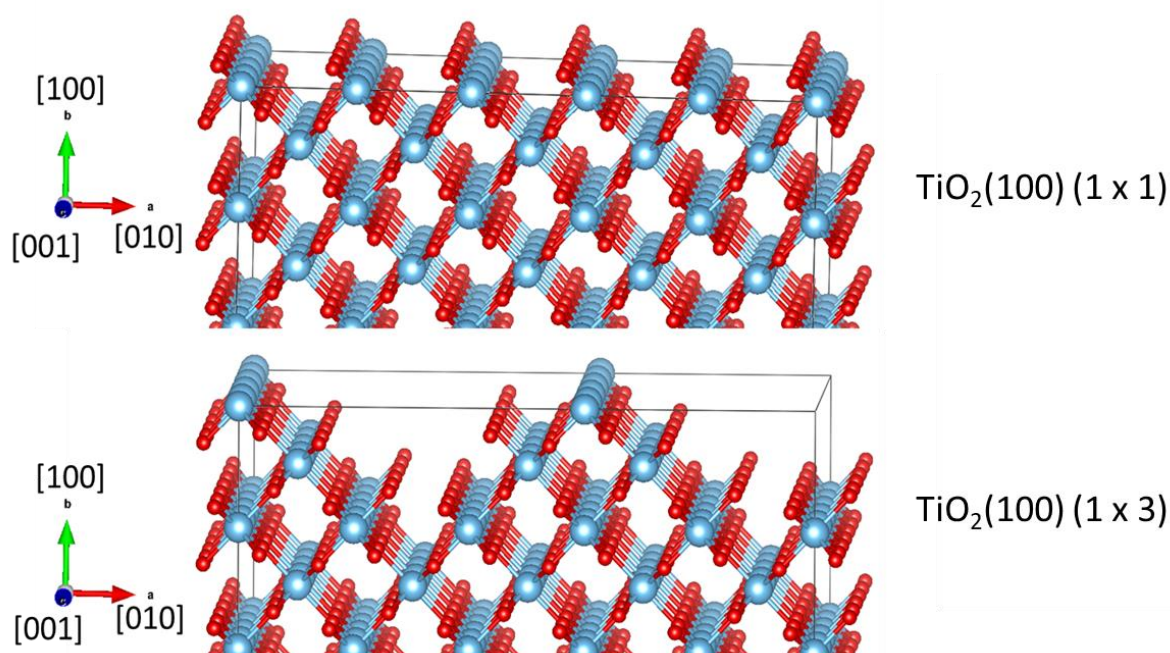


Figure 4.28 The (1 x 1) and (1 x 3) reconstructed TiO<sub>2</sub>(100) surface, at top and bottom of the Figure respectively.

The TiO<sub>2</sub>(100) surface is terminated with oxygen atoms. In case of (1 x 1) reconstructed rutile TiO<sub>2</sub>(100) surface the titanium atoms are five-fold coordinated instead of six-fold coordination, to maintain the charge neutral surface. (See Figure 4.28 (top)).<sup>105</sup> The TiO<sub>2</sub>(100) surface undergoes faceting upon annealing around 600 °C. To decrease the energy of the surface and increase the number of six-fold coordinated Ti atoms, the low-energy (110) facets are formed<sup>108</sup>, as shown in Figure 4.28 (bottom). Small terraces run along the [010] direction. The reconstruction results in an increased number of unsaturated Ti cations at the row edge.<sup>105</sup> It was found with the RHEED technique that the large area terraces formed at the (100) surface, at the preparation temperature used in this work, were longer along the [001] direction and shorter in the [010] direction.<sup>105</sup>

The (1 x 3) LEED pattern was also observed for a vicinal (stepped) TiO<sub>2</sub>(100) (1 x 1) surface.<sup>103</sup> It was found that the observed steps in [010]-direction are a continuation of (110) plane microfacets, which form the basis of the (1 x 3) reconstruction.<sup>107</sup> Also, the authors of reference 106 confirm the presence of steps with average height of 0.5 nm.<sup>106</sup> The formation of steps explains the presence of streaks in the LEED patterns.

According to the literature<sup>109</sup> if steps of varying width are present at the crystal surface, a spot and streak pattern will be seen in the LEED image, as can be observed in Figure 4.26. Additionally, if the step orientation varies at random, a change between sharp and diffuse spot can be seen<sup>109</sup>, which seems to be the case if patterns a, b and c in Figure 4.26 are compared. The fact that even the same spot (i.e the (00) spot) seem to broaden, depending on the beam energy used, is caused due to the high density of point defects (proven by XPS technique for the reduced TiO<sub>2</sub>(100) surface).

#### 4. Results and Discussion - 4.2 Interaction between halogen substituted organic semiconductor molecules (AlClPc) and TiO<sub>2</sub>(100) substrate.

The streaks have been observed for the TiO<sub>2</sub>(110) surface as well. A LEED pattern of TiO<sub>2</sub>(110) with a calcium monolayer adsorbed at the surface, shows streaks between the spots belonging to the primary pattern of (1 x 1) TiO<sub>2</sub>(110) reconstructed surface, which do not belong to the Ca LEED pattern. The authors explain these streaks as a sign of lack of in-phase correlation in consequence of an existing certain degree of disorder at the TiO<sub>2</sub> surface. This disorder the authors relate to the oxygen deficiencies in the surface layer, due to the UHV preparation.<sup>110</sup> Further, it has been observed for a highly reduced TiO<sub>2</sub>(110) surface, that the streaks between the LEED spots, initially thought to be the (1 x 2) surface reconstruction, were signs of the formation of the Ti<sub>2</sub>O<sub>3</sub> row fragments.<sup>111</sup>

Different TiO<sub>2</sub>(100) surface reconstruction models were proposed in literature based on SXRD<sup>112</sup> and first-principle simulations<sup>113</sup>. They however support the microfaceted surface structure. Formation of stepped terraces of various width in the [010] direction matches the reconstruction direction of facets with (110) surface. The presence of streaks and diffuse spots, shows that the width and arrangement of terraces is random. We can conclude from the LEED data (supported by AFM roughness profiles in next chapter: 4.2.1.4) that steps in a random array are present at the (100) surface. Since the steps at the TiO<sub>2</sub> surface act as catalytic and dissociation centers<sup>103</sup>, it is expected that the reduced surface will be more prone to react with the phthalocyanine thin films.

##### 4.2.1.4 Microscopy images of TiO<sub>2</sub>(100) surface preparation stages

In this chapter clean TiO<sub>2</sub>(100), which underwent 5 annealing and 3 sputtering cycles, is characterized with AFM. Oxygen atmosphere was used during the annealing step. A clean and smooth surface can be seen in Figure 4.29 where no bright spots can be seen in the image, which would indicate presence of higher elements at the surface.

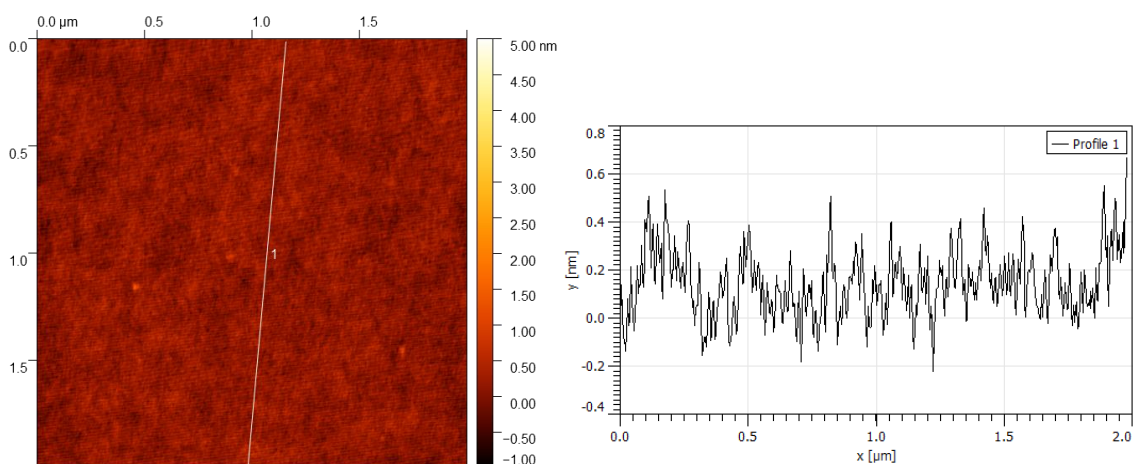


Figure 4.29 A 2 μm x 2 μm image of a clean TiO<sub>2</sub>(100) surface treated with oxygen.

#### 4. Results and Discussion - 4.2 Interaction between halogen substituted organic semiconductor molecules (AlClPc) and TiO<sub>2</sub>(100) substrate.

The profile of a surface in Figure 4.29 was taken. The minimum of the curve is at -0.225 nm and the maximum is at 0.668 nm. The RMS is 0.138 nm, indicating a very low roughness of the surface. The roughness value is in the same range as the roughness of a clean (001) surface.

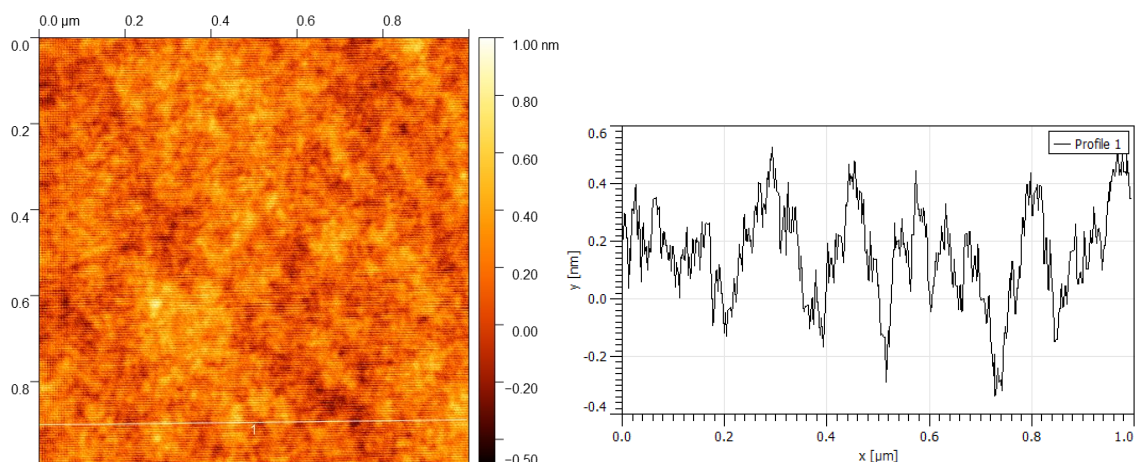


Figure 4.30 A 1 μm x 1 μm AFM image of a clean TiO<sub>2</sub>(100) surface (left) and the surface profile 1 (right).

A clean rutile TiO<sub>2</sub>(100) surface has low RMS of 0.167 nm, the minimum of a profile taken at the surface presented in Figure 4.30 has minimum and maximum at -0.336 nm and 0.527 nm respectively. Although the surface is very smooth, at closer look the profile of the surface shows small hills with the width between 50 and 200 nm. These could be grains and terraces formed due to sputtering and subsequent annealing as in the case of the (001) surface.

If one zooms in more on the clean substrate, a network of TiO<sub>2</sub> atoms is seen at the surface. Considering the information from the unit cell size and LEED reconstruction, one would expect rows of atoms. Meanwhile the, rows are short and perpendicular to each other, forming a network of rectangles similar to the TiO<sub>2</sub>(001) surface.<sup>114-116</sup> Formation of such structures is possibly due to the low annealing temperature used for preparation of the substrates used in this work. A rather poorly resolved 200 nm x 200 nm AFM image of the same surface shows a mosaic structures of short rows at the surface of the oxygen treated TiO<sub>2</sub>(100) single crystal (Figure 4.31).

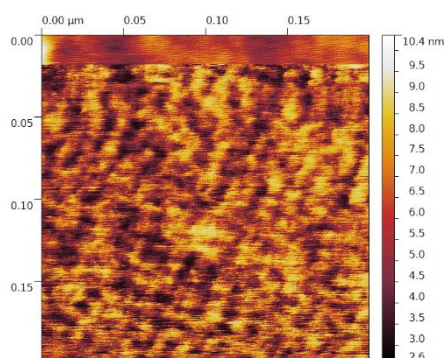


Figure 4.31 AFM image (200 nm x 200 nm) of a clean TiO<sub>2</sub>(100) surface.

#### 4. Results and Discussion - 4.2 Interaction between halogen substituted organic semiconductor molecules (AlClPc) and TiO<sub>2</sub>(100) substrate.

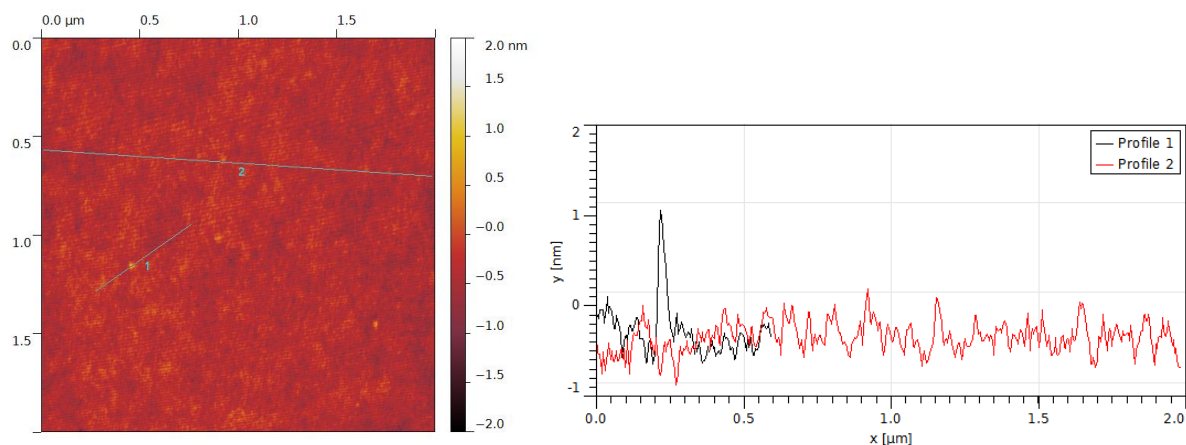


Figure 4.32 AFM image ( $2\ \mu\text{m} \times 2\ \mu\text{m}$ ) of a clean TiO<sub>2</sub>(100) single crystal surface (left), and two line profiles of the clean TiO<sub>2</sub>(100) surface prepared in presence of oxygen.

Figure 4.32 shows a clean TiO<sub>2</sub>(100) surface prepared in presence of oxygen. It is flat with RMS of 0.138 nm, as opposed to “as received” TiO<sub>2</sub> crystal surface, which shows very high RMS value above 4.1 nm, as will be shown later in Chapter 4.3.1.4. The height variation in the Profile 2 (red line) is not higher than 1 nm. There are random spikes present in Profile 1 (black line), but their height is no more than 2 nm, which is just 1 nm more than the height in Profile 2.

#### 4.2.2 Characterization of AlClPc films on TiO<sub>2</sub>(100) surface

##### 4.2.2.1 Influence of phthalocyanine deposition on TiO<sub>2</sub>(100) core level spectra

Influence of phthalocyanine deposition on substrate will be investigated based on substrate related core level spectra. Figure 4.33 shows Ti 2p spectra of substrates prepared in presence (a) and absence (b) of oxygen with AlClPc films at different coverage. Both spectra series were fitted with the model used for clean TiO<sub>2</sub> substrate given in Chapter 4.2.1.2 for spectra presented in Figure 4.22. The changes between the Ti 2p spectrum before and after evaporation of AlClPc are hardly visible. No new peaks arise upon AlClPc adsorption. Lack of new peaks below 456 eV binding energy allows to exclude presence of bonds like Ti-N or Ti-C<sup>53</sup>, which reside in this energy region. Detailed peak fit parameters (see. Appendix 6.2.3 Table 12 and Table 13) reveal that the energetic shift of Ti 2p signal upon AlClPc adsorption is smaller than  $\pm 0.1\ \text{eV}$ , which points to an absence of Fermi level shift as a result of surface doping due to adsorption of molecules. Most likely, the high number of states in the gap of TiO<sub>2</sub> semiconductor determines the position of the Fermi level and is not varied distinctly by the AlClPc adsorption.<sup>89</sup>

As for the intensity of the defect peaks, there is a slight decrease in the relative intensity of Ti<sup>3+</sup> component, when compared to the ratio seen for a clean substrate prepared in absence of oxygen. Lower oxidation states of titanium like Ti<sup>2+</sup> were not detected.

#### 4. Results and Discussion - 4.2 Interaction between halogen substituted organic semiconductor molecules (AlClPc) and TiO<sub>2</sub>(100) substrate.

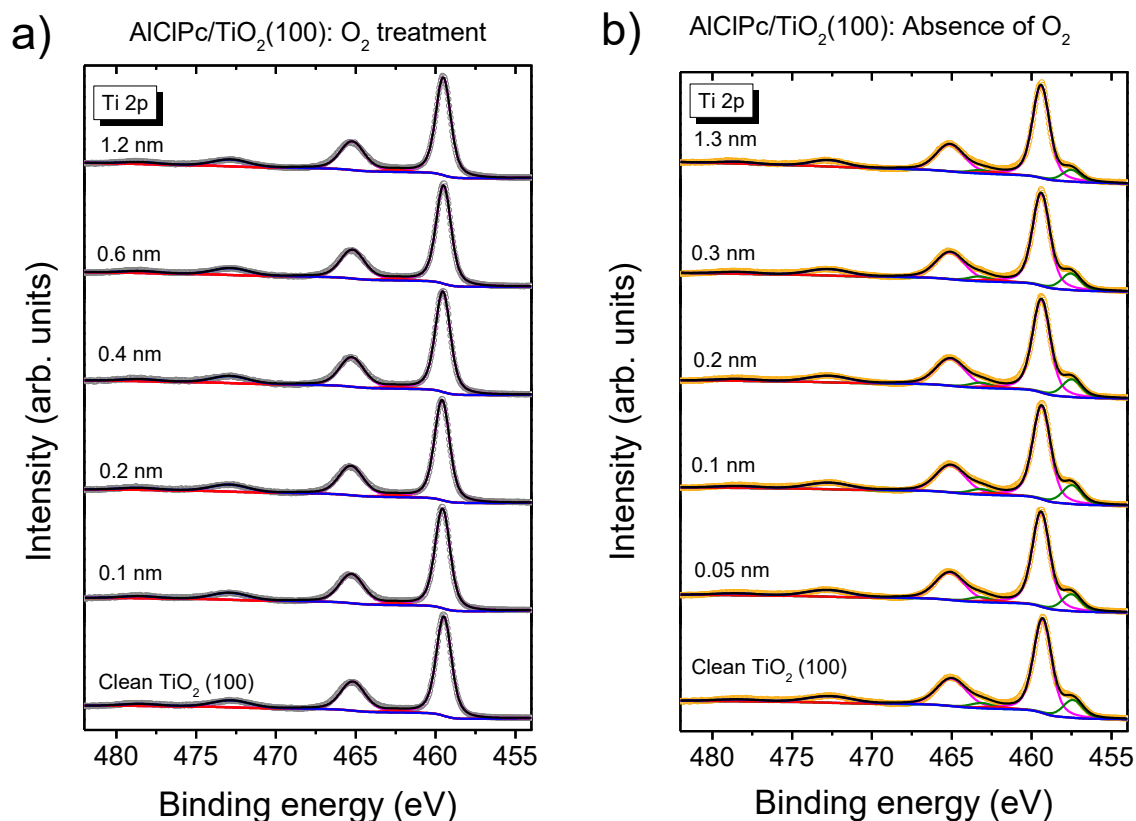


Figure 4.33 Substrate-related Ti 2p spectra of: a) AlClPc films on TiO<sub>2</sub>(100) treated with oxygen, b) AlClPc films on TiO<sub>2</sub>(100) reduced surface. Spectra measured with Al K $\alpha$  radiation,  $h\nu = 1486.7$  eV. Reproduced from Ref. 89 with permission from the PCCP Owner Societies.

Two series of O 1s core level spectra belonging to TiO<sub>2</sub> crystals that underwent both preparations are shown in Figure 4.34. No changes in O 1s core level spectra were observed upon consecutive deposition of AlClPc films. The peak shape is unaffected by deposition of molecules, with a constant O-2 component intensity and peak width, for each series of O 1s spectra in Figure 4.34. The fitting parameters used for clean TiO<sub>2</sub>(100) substrate (see Table 14) can be used throughout the series. The lack of changes due to phthalocyanine adsorption indicates the absence of newly formed bonds with oxygen atoms of TiO<sub>2</sub> single crystal.

#### 4. Results and Discussion - 4.2 Interaction between halogen substituted organic semiconductor molecules (AlClPc) and TiO<sub>2</sub>(100) substrate.

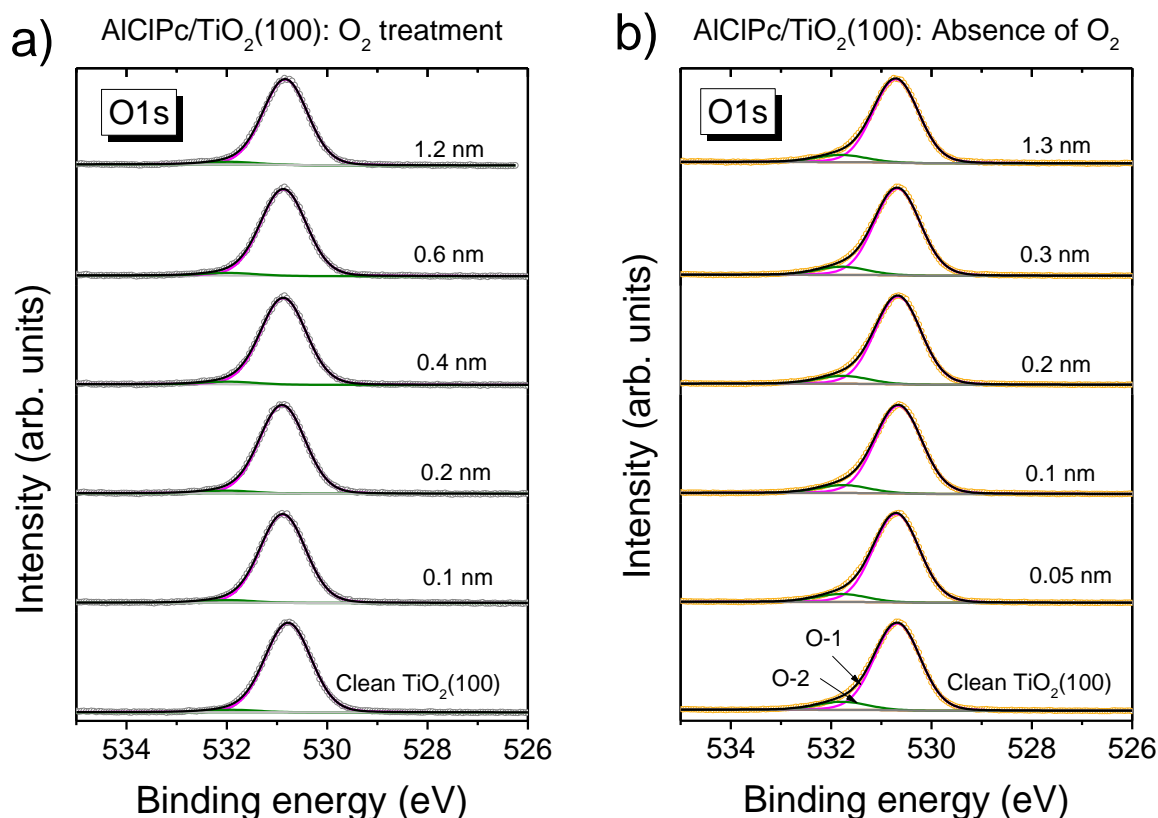


Figure 4.34 O 1s core level spectra of TiO<sub>2</sub>(100) surface: a) treated in oxygen, b) prepared in absence of oxygen, before and after AlClPc films deposition. Spectra measured with Al K $\alpha$  radiation,  $h\nu = 1486.7$  eV. Reproduced from Ref. 89 with permission from the PCCP Owner Societies.

##### 4.2.2.2 Interaction of TiO<sub>2</sub>(100) with molecule ring

Adsorbate-related core level spectra give a direct insight into possible chemical reactions of deposited films at the interface to the substrate. Thickness dependent C 1s core level spectra of AlClPc films deposited on TiO<sub>2</sub>(100) substrate prepared in presence and absence of oxygen are compared in Figure 4.35. The film thicknesses presented there range between sub-monolayer (sub-ML) and multilayer (bulk film). The C 1s spectra of the thickest film can be described with four components as explained in literature for AlClPc and related phthalocyanines.<sup>17, 56, 57</sup> The components are connected with the following parts of phthalocyanine molecule: aromatic carbon of benzene rings (marked as C-1), pyrrole carbon bonded with nitrogen atom (C-2) and their corresponding  $\pi - \pi^*$  satellites ( $S_{C-1}$  and  $S_{C-2}$ ). The energy distance between the carbon related peaks and their satellites is 1.8 eV (C-1 –  $S_{C-1}$  satellite) and 2 eV (C-2 –  $S_{C-2}$  satellite).<sup>17, 56, 57</sup> All fitting parameters of C 1s core levels are summarized in Table 15 (Appendix 6.2.3).

4. Results and Discussion - 4.2 Interaction between halogen substituted organic semiconductor molecules (AlClPc) and TiO<sub>2</sub>(100) substrate.

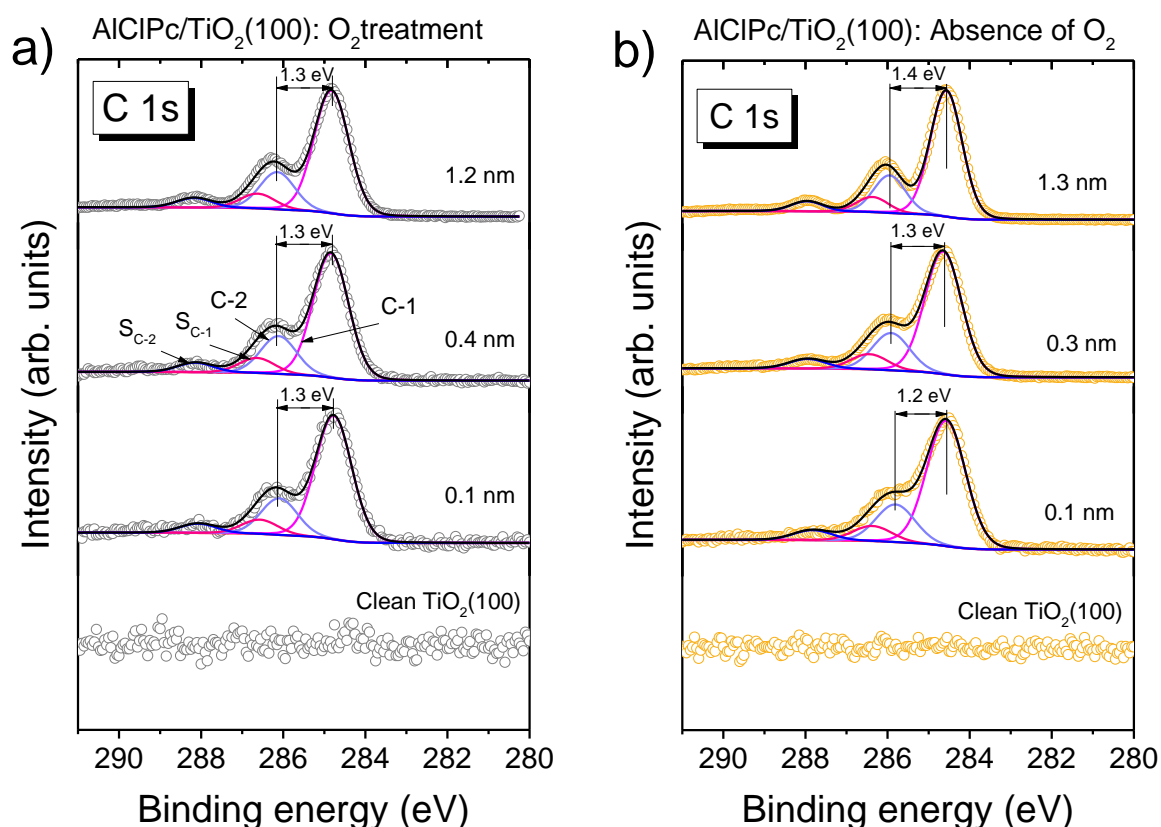


Figure 4.35 Thickness dependent C 1s core level spectra of AlClPc evaporated on differently prepared TiO<sub>2</sub>(100) surfaces: a) AlClPc on TiO<sub>2</sub>(100) prepared in presence of oxygen, b) AlClPc on TiO<sub>2</sub>(100) prepared in absence of oxygen. All spectra can be described by the same peak shape and were measured with Al K $\alpha$  radiation,  $h\nu = 1486.7$  eV. Reproduced from Ref. 89 with permission from the PCCP Owner Societies.

Thickness-dependent C 1s spectra presented in Figure 4.35 show hardly any changes, indicating that the molecules stay intact after deposition on TiO<sub>2</sub>(100) surface. No hints of molecules oxidation can be seen, as reported in the literature for FePc on TiO<sub>2</sub>(110) surface, which underwent different preparation.<sup>88</sup> The main component of C 1s core levels in Figure 4.35, at all AlClPc film thicknesses and both TiO<sub>2</sub> preparations, can be found between 284.8 eV and 284.6 eV. The ratio between components belonging to the two carbon types (C-1+S<sub>C-1</sub>:C-2+S<sub>C-2</sub>) is 3:1, which corresponds also to the stoichiometric ratio between these carbons in the phthalocyanine molecule under investigation, for all film thicknesses. The spectra are slightly broadened as the film thickness decreases, which can be particularly seen for AlClPc on reduced TiO<sub>2</sub>(100) surface (Figure 4.35b). At 1.3 nm and 0.1 nm film thickness the Gaussian width of C 1s peaks is 0.9 and 1.1 eV respectively. Such broadening was observed for other interfaces and can be understood by inhomogeneous adsorption sites on the more defect-rich surface.<sup>92, 117</sup> What is more, a small but significant change in the components C-1 and C-2 separation (see. Black double arrows in Figure 4.35 (a and b) seen for the reduced surface (0.2 eV

#### 4. Results and Discussion - 4.2 Interaction between halogen substituted organic semiconductor molecules (AICIPc) and TiO<sub>2</sub>(100) substrate.

binding energy difference between sub-ML and bulk film) may indicate differences in charge distribution in molecules at the interface, as compared to the molecules in bulk. Such behavior was also observed on metal surfaces.<sup>89</sup>

Further information on phthalocyanine ring interaction with interface can be found in N 1s core level spectra shown in Figure 4.36, depicting thickness dependent spectra of AICIPc on TiO<sub>2</sub>(100) surface prepared in presence and absence of oxygen. The reference spectrum of a clean TiO<sub>2</sub>(100) surface exhibits no initial nitrogen signal for both preparations. Spectra of bulk-like AICIPc films of 1.2 nm and 1.3 nm (on oxygen treated and reduced surface respectively) have typical shape of bulk AICIPc films seen also on other substrates.<sup>17, 57</sup> Both spectra were fitted with two components: the main peak N-1 (magenta curve) with its corresponding satellite S<sub>N-1</sub> (blue curve). The main peak is related to two types of nitrogen atom found in AICIPc, these are: pyrrole nitrogen bound to the aluminium atom in the centre of the molecule and the bridging nitrogen atom (see. Figure 2.2, nitrogen atoms are marked respectively with green and red circle). Fitting parameters are found in Appendix 6.2.4: Table 16.

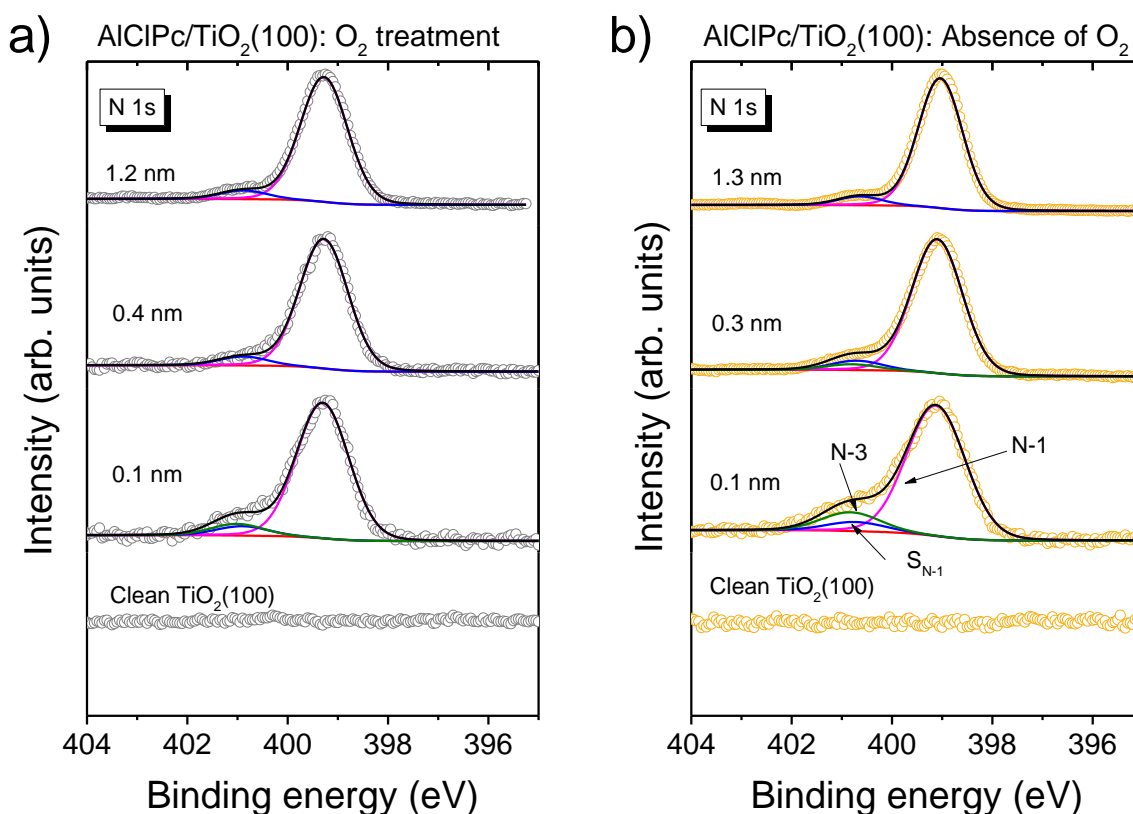


Figure 4.36 Thickness dependent N 1s core level spectra of AICIPc evaporated on differently prepared TiO<sub>2</sub>(100): a) AICIPc on TiO<sub>2</sub>(100) prepared in presence of oxygen, b) AICIPc on TiO<sub>2</sub>(100) prepared in absence of oxygen. An interface component (green) is visible in both cases. All spectra were measured with Al K $\alpha$  radiation,  $h\nu = 1486.7$  eV. Reproduced from Ref. 89 with permission from the PCCP Owner Societies.

#### 4. Results and Discussion - 4.2 Interaction between halogen substituted organic semiconductor molecules (AlClPc) and TiO<sub>2</sub>(100) substrate.

While both nitrogen atoms have different chemical environment, the energy separation between them is small, which makes it unable to resolve them properly in the XPS spectrum. A chemical shift between the two nitrogen types was reported to be 0.28 eV.<sup>64</sup> The binding energy position of the N-1 component, on oxygen treated and reduced TiO<sub>2</sub>(100) surface, was determined to be 399.3 eV and 399.1 eV. The position is almost independent from film thickness. The less intense shake-up satellite S<sub>N-1</sub> is found 1.6 eV higher in binding energy than the main peak. The relative intensity of S<sub>N-1</sub> peak is around 6.0%, which is in good agreement with related phthalocyanines.<sup>56, 92, 118</sup> The binding energy position of peaks measured for higher coverage films, match well the values recorded for multilayer AlClPc films deposited on silver substrates (as shown in Chapter 4.1) pointing to a similar equilibrium energy level alignment on both silver and titanium dioxide substrates.

If N 1s spectra of the highest and lowest film thickness in Figure 4.36 are compared, a clear increase in intensity in the binding energy region of shake-up satellite is seen. What is more, the spectra of low coverages are broadened, as was also observed for C 1s spectra belonging to the same samples. It is unlikely that the satellite will increase in intensity at the interface. The satellite peaks are often suppressed at interfaces.<sup>119</sup> To properly describe N 1s spectra shown in Figure 4.36, there is a need of introduction of an additional component (N-3 marked with green curve). This interface component is visible for both oxygen treated and reduced TiO<sub>2</sub>(100) surface, although for the former one it is visible only for 0.1 nm thick film, while on the latter it is observed also at higher film thickness of 0.3 nm. If satellites intensity is being kept constant for all film thicknesses, when compared, the 0.1 nm thick films in Figure 4.36a and b show interface component intensity of 7% and 12% (of the total N 1s intensity) for oxygen prepared and reduced TiO<sub>2</sub>(100) surface. The additional component is situated at 401.0 eV, 1.7 eV higher than N-1 main peak.

##### 4.2.2.3 Phthalocyanine metal center and central metal ligand core levels

Although there is a clear hint of formation of an interface component in N 1s core level spectra, the phthalocyanine center related spectra of Cl 2p and Al 2p do not show any clear signs of a strong interaction at the interface. The corresponding spectra are shown in Figure 4.37 and Figure 4.38 respectively. Due to a high noise, the spectra have been smoothed (red line) to provide a more clear line shape, especially at the lowest AlClPc coverages. The Cl 2p spectra belonging to thickest films of 1.2 nm and 1.3 nm in Figure 4.37 resemble that of a typical Cl 2p doublet observed for bulk AlClPc film (see Figure 3.6). The Cl 2p peak stays constant throughout evaporation of consecutive AlClPc layers at 198.9 eV and 198.8 eV for oxygen treated and reduced TiO<sub>2</sub>(100) surface. At lower coverages however, Cl 2p spectra undergo broadening, which can be explained by inhomogeneous adsorption sites as seen

#### 4. Results and Discussion - 4.2 Interaction between halogen substituted organic semiconductor molecules (AlClPc) and TiO<sub>2</sub>(100) substrate.

for other AlClPc related spectra described previously. What is more, the stoichiometric relations between carbon, nitrogen and chlorine atoms in AlClPc films are preserved as shown in Appendix 6.2.4, Table 17.

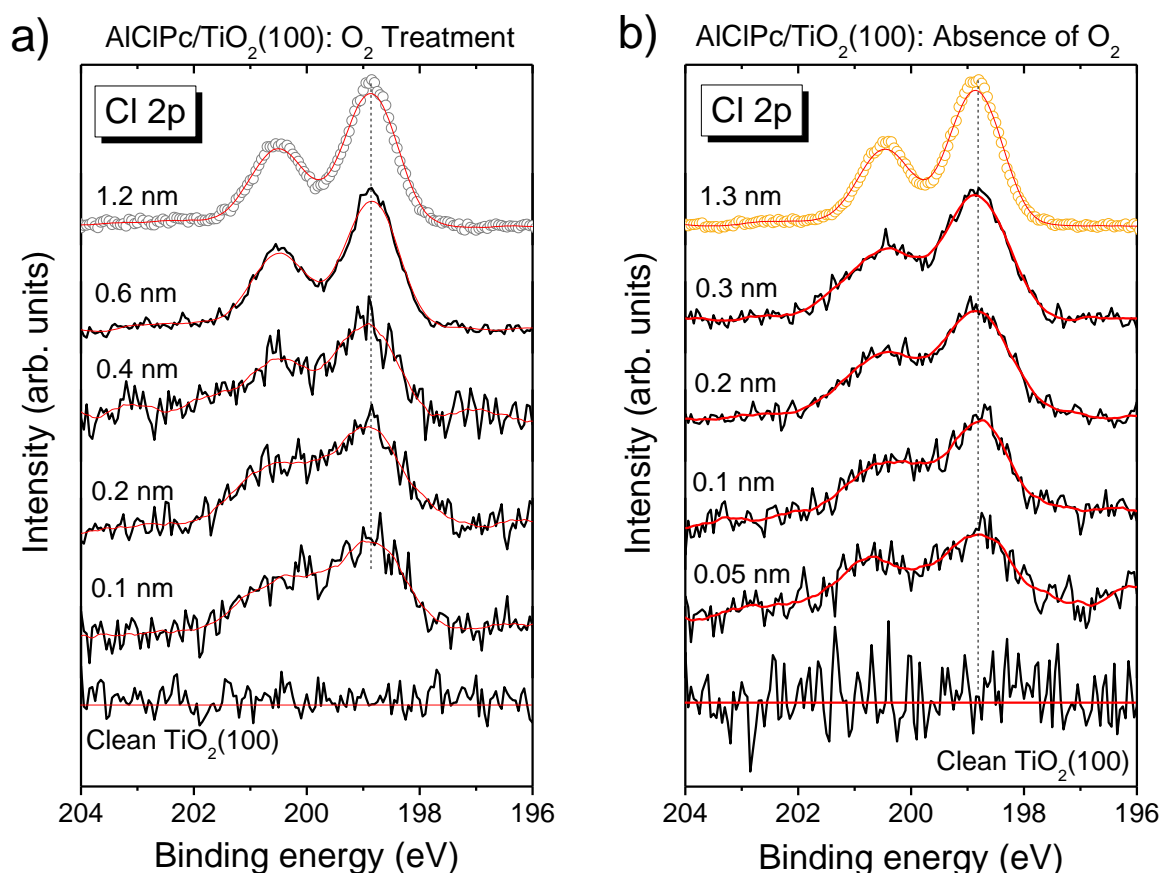


Figure 4.37 Thickness dependent Cl 2p spectra of AlClPc evaporated on a) TiO<sub>2</sub>(100) treated with O<sub>2</sub>, b) TiO<sub>2</sub>(100) prepared in absence of O<sub>2</sub>. The red lines represent the original data after smoothing procedure for the ease of data comparison. Spectra measured with Al K $\alpha$  radiation,  $h\nu = 1486.7$  eV. Reproduced from Ref. 89 with permission from the PCCP Owner Societies.

Analysis of Al 2p spectra (Figure 4.38) is difficult due to an overlap with intensive titanium background. The background contribution comes from Ti 3s peak with a broad plasmon loss structure, which is present in the same binding energy region as Al 2p peak. Due to the high intensity of Ti 3s signal changes in Al 2p signal, which is broad and has very low intensity at the sub-ML thickness, can be hardly recorded. At higher film thicknesses for both preparations the peak position is at 74.9 eV, and at lower coverage the peaks are broadened, with no shift in binding energy or any additional peaks visible in the sub-monolayer region.

#### 4. Results and Discussion - 4.2 Interaction between halogen substituted organic semiconductor molecules (AlClPc) and TiO<sub>2</sub>(100) substrate.

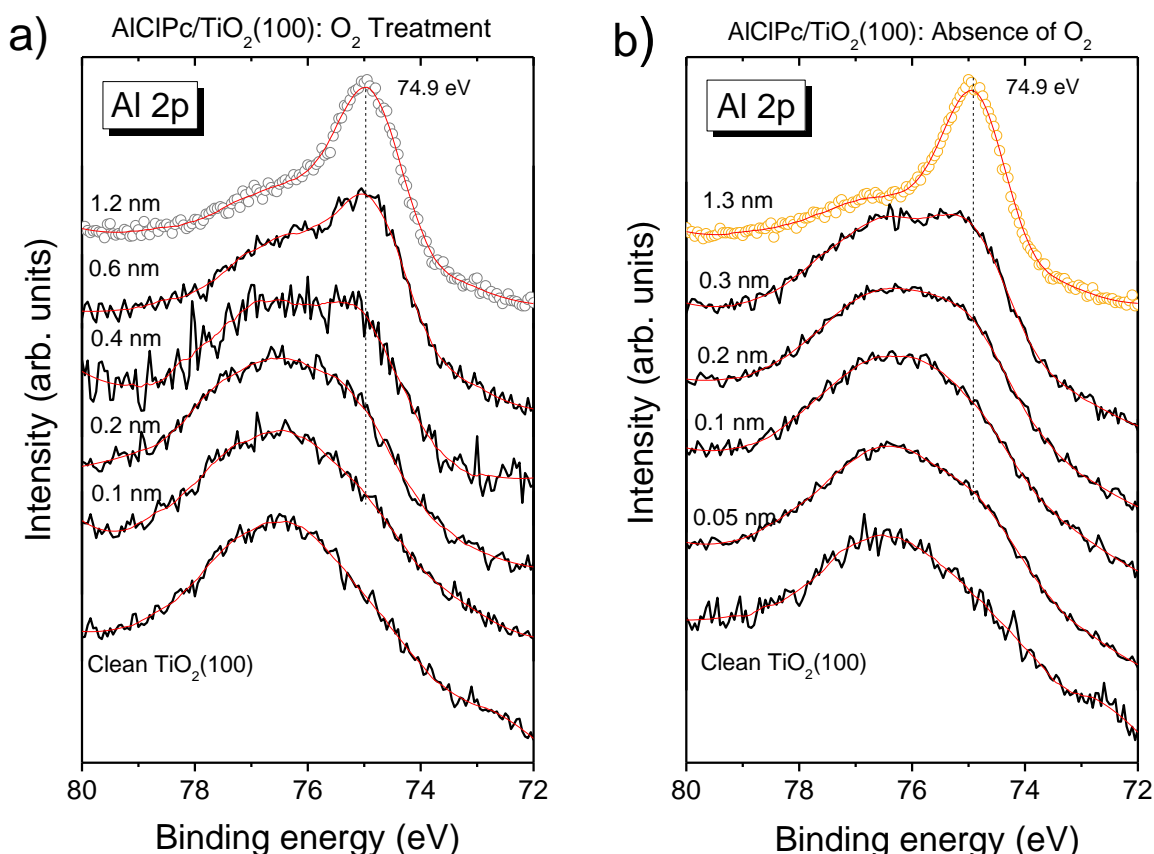


Figure 4.38 Al 2p spectra for: a) AlClPc on TiO<sub>2</sub>(100) treated with O<sub>2</sub>, b) AlClPc on TiO<sub>2</sub>(100) prepared in absence of O<sub>2</sub>. The red lines represent the original data after smoothing procedure for the ease of data comparison. Spectra measured with Al K $\alpha$  radiation,  $h\nu = 1486.7$  eV. Reproduced from Ref. 89 with permission from the PCCP Owner Societies.

##### 4.2.2.4 Electronic properties of AlClPc films on TiO<sub>2</sub>(100)

Additional information on charge transfer between materials at their interface can be gained from UPS results containing information from the valence band region of photoemission spectra. For the AlClPc/TiO<sub>2</sub> interface the analysis and interpretation of spectral features, which could be interface states can be obstructed by the presence of gap states, especially in case of reduced TiO<sub>2</sub> surface.

For AlClPc films deposited on TiO<sub>2</sub>(100) surface prepared in presence of oxygen the spectra representing secondary electron cut-off (SECO), valence band and HOMO region of valence band are shown in Figure 4.39a, b and c. From the secondary electron cut-off one can read the work function of the clean TiO<sub>2</sub>(100) substrate (5.3 eV) and observe a decrease in work function after phthalocyanine deposition with the work function of 4.5 eV for the thickest 1.2 nm film. Figure 4.39b shows a typical valence band spectrum of a clean TiO<sub>2</sub>(100) surface with O 2p states dominating the binding energy region between 3 eV and 10 eV. No intensive peak within the TiO<sub>2</sub> band gap is registered in the clean TiO<sub>2</sub> UPS spectrum, which is expected considering an almost ideal Ti 2p peak seen before in Figure 4.33

#### 4. Results and Discussion - 4.2 Interaction between halogen substituted organic semiconductor molecules (AICIPc) and TiO<sub>2</sub>(100) substrate.

for the same substrate. Some gap states are however seen in the background, indicating that the oxygen treated surface is not totally defect-free. After deposition of AICIPc film the typical phthalocyanine features increase in intensity. Spectrum of 1.2 nm thick film resembles that of a bulk phthalocyanine film. A HOMO peak (highest occupied molecular orbital) can be seen at 1.4 eV. A zoom-in to the HOMO region allows to detect the HOMO peak even at the lowest film thickness of 0.1 nm, with an almost constant HOMO peak onset value, registered between 0.8 eV and 0.9 eV (for higher thickness). The resolution of valence band spectra is not high enough to distinguish between the two configurations of AICIPc (Cl-up and Cl-down) which are otherwise would result in two distinct HOMO peak maxima. The HOMO peak at 0.1 nm film thickness is too broad for such detailed analysis.

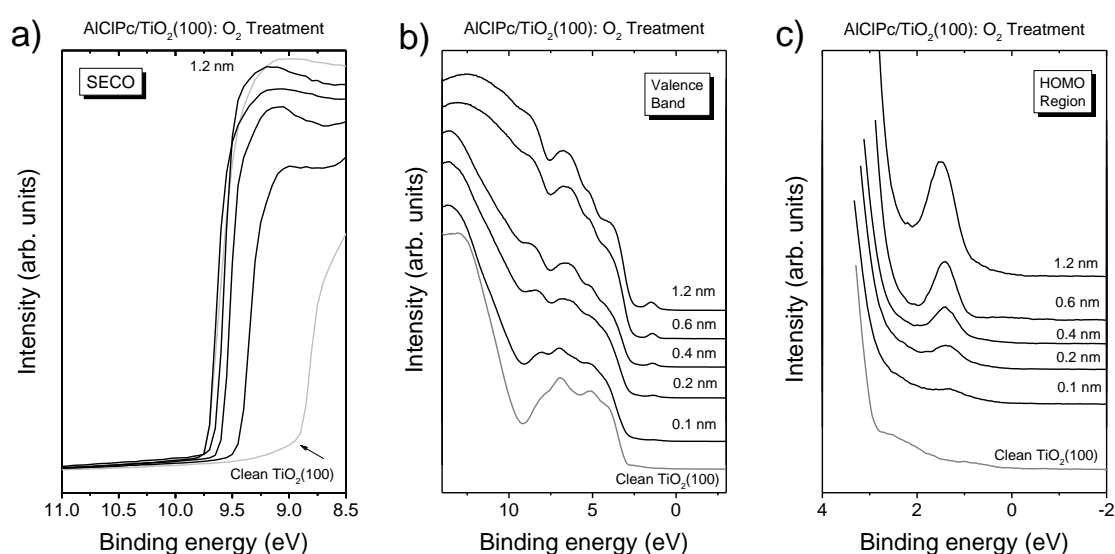


Figure 4.39 Thickness dependent UPS results measured for AICIPc films on TiO<sub>2</sub>(100) treated with oxygen: a) secondary electron cut-off, b) valence band spectra, c) valence band spectra – HOMO region. Spectra measured with He I radiation,  $h\nu = 21.2$  eV. Reproduced from Ref. 89 with permission from the PCCP Owner Societies.

For AICIPc films deposited on TiO<sub>2</sub>(100) surface prepared in absence of oxygen a similar decrease of work function is observed after the deposition of phthalocyanine molecules. The work function of clean substrate is however slightly lower, only 5.1 eV. As described in literature for differently prepared TiO<sub>2</sub> surfaces, the work function of titanium dioxide can strongly depend on sample preparation.<sup>120</sup> Valence band spectrum of a clean TiO<sub>2</sub>(100) reduced surface differs from the one for oxygen treated surface by an intensive feature at 0.9 eV. This signal is connected to the gap states due to the presence of defects on the reduced surface, as seen also in Ti 2p spectrum. In the magnified HOMO region in Figure 4.40c it can be seen that the HOMO peak overlaps with the gap states peak, rendering it difficult to give precise values of HOMO peak onset. For the thick film though (1.3 nm) it can be seen that the HOMO peak position is the same as on the oxygen treated surface (1.4 eV), and the shape of valence band

#### 4. Results and Discussion - 4.2 Interaction between halogen substituted organic semiconductor molecules (AlClPc) and TiO<sub>2</sub>(100) substrate.

spectrum is typical for AlClPc bulk. Detailed values of work function, HOMO onset and ionization potential can be found in Appendix 6.2.4, Table 18.

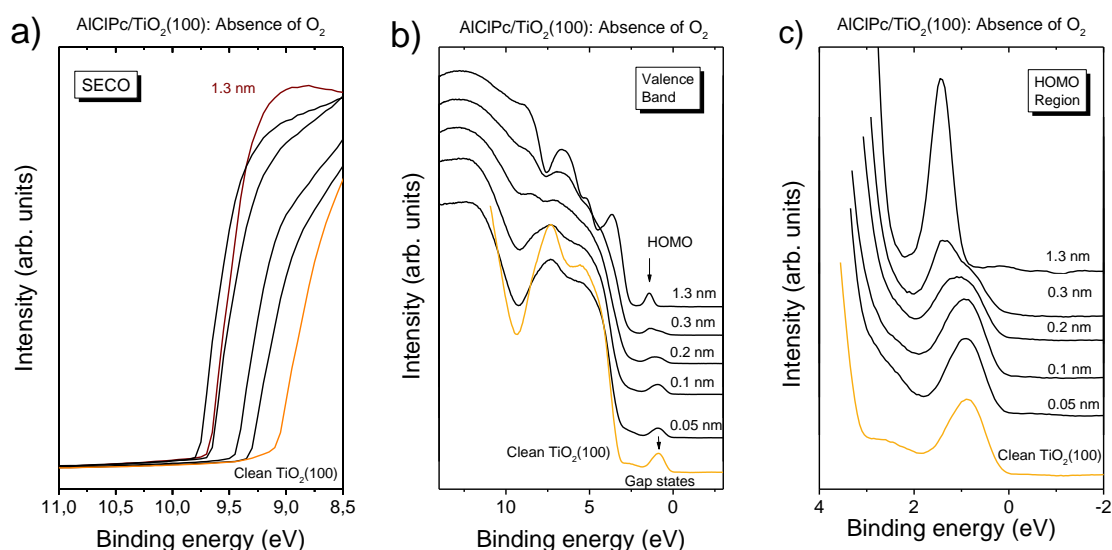


Figure 4.40 Thickness dependent UPS results measured for AlClPc films on TiO<sub>2</sub>(100) prepared in absence of oxygen: a) secondary electron cut-off, b) valence band spectra, c) valence band spectra – HOMO region. Spectra measured with He I radiation,  $h\nu = 21.2$  eV. Reproduced from Ref. 89 with permission from the PCCP Owner Societies.

##### 4.2.2.5 Energy level diagrams

All data from UPS measurements (see. Figure 4.39 and Figure 4.40) are summarized in form of energy level diagrams in Figure 4.41 for experiments on both TiO<sub>2</sub>(100) surface treated with oxygen and prepared in absence of oxygen. Both diagrams show the decrease of work function upon adsorption of AlClPc with formation of surface dipoles of -0.8 eV and -0.6 eV for defect-free and defect-rich surface respectively. The direction of the surface dipole points to possible charge transfer from molecule to titanium dioxide. The literature states that some electronic charge is transferred from the organic layer to the oxide substrate, depending on the interaction between both materials. As a result a decrease in work function is observed.<sup>121</sup> The charge transfer might not be however the only reason for the potential drops at the surface observed in the data presented below. Effects such as “push back effect”, where substrate electrons are pushed away from the surface upon adsorption of molecules, might also cause a decrease in work function of the substrate. Additionally, in case of AlClPc molecules which are polar, the direction of intrinsic molecular dipole could influence the work function, which for Cl-up configuration would actually increase the work function. A detailed discussion of influence of AlClPc and GaClPc molecular orientation on the work function can be found in recent publications.<sup>122, 123</sup> This is why a conclusion about charge transfer from the energy level diagrams only is complicated.

#### 4. Results and Discussion - 4.2 Interaction between halogen substituted organic semiconductor molecules (AlClPc) and TiO<sub>2</sub>(100) substrate.

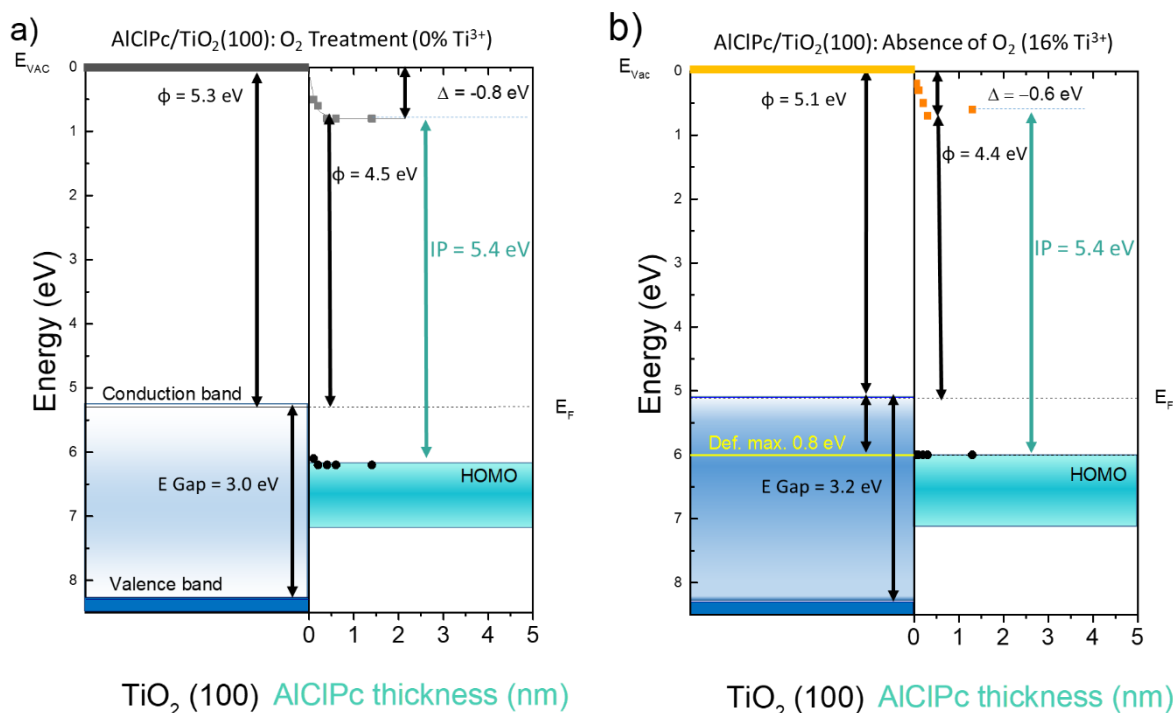


Figure 4.41 Energy level diagrams of: a) AlClPc/TiO<sub>2</sub>(100) treated with oxygen, b) AlClPc/TiO<sub>2</sub>(100) reduced. Reproduced from Ref. 89 with permission from the PCCP Owner Societies.

In both diagrams the ionization potential of a thick AlClPc films is 5.4 eV ± 0.1 eV, which is in good agreement with previously reported data.<sup>17</sup> It can be an indication that the intrinsic molecular dipoles are oriented in a similar manner, with different orientations present. What is interesting, although the defect state peak was not present in the valence band spectra of the oxygen treated TiO<sub>2</sub>(100) surface, the HOMO onset for both preparations is found between 0.9 eV and 1 eV, the binding energy position of gap states. It can be thus assumed that the HOMO peak is pinned at the defect states, also for surface where Ti<sup>3+</sup> states were not detected. It is likely that small amount of defects is present at the surface even for oxygen treated substrates, which might be caused by the defect migration to the surface during annealing step.<sup>124</sup> As recently discussed in literature, organic film work functions independent from substrate (4.5 eV for thick films for both preparations of substrates) are expected for such pinning regimes.<sup>125</sup>

##### 4.2.2.6 AlClPc film growth – microscopy images

AlClPc film growth on TiO<sub>2</sub>(100) surface will be discussed based on AFM and SEM images shown in the following chapter.

#### 4. Results and Discussion - 4.2 Interaction between halogen substituted organic semiconductor molecules (AlClPc) and TiO<sub>2</sub>(100) substrate.

AlClPc/TiO<sub>2</sub>(100): O<sub>2</sub> treatment

AlClPc/TiO<sub>2</sub>(100): Absence of O<sub>2</sub>

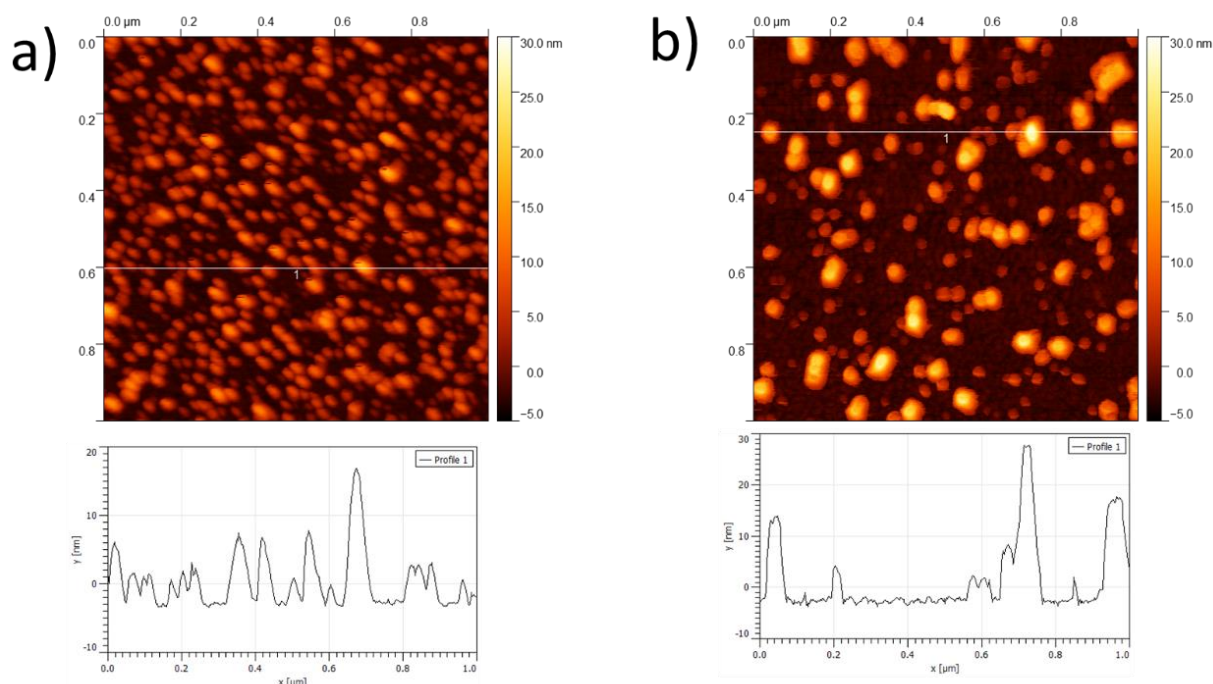


Figure 4.42 1 μm x 1 μm AFM images of AlClPc islands on TiO<sub>2</sub>(100) a) treated with oxygen (0% Ti<sub>3+</sub>) and defect-rich, b) prepared in an absence of oxygen (16% Ti<sup>3+</sup>). The AlClPc films presented in these images have thickness equal to an equivalent of a 1.2 nm and 1.3 nm layer-by-layer film respectively.

In Figure 4.42 two AFM images are included: the left one shows an equivalent of a 1.2 nm layer-by-layer AlClPc film on an oxygen treated TiO<sub>2</sub>(100) surface, while the right one shows an equivalent of 1.3 nm layer-by-layer AlClPc film on a defect-rich TiO<sub>2</sub>(100) surface, prepared in absence of oxygen. It can be seen that AlClPc molecules form islands on the both TiO<sub>2</sub>(100) surfaces independent of preparation. The large area AlClPc islands on TiO<sub>2</sub>(100) single crystal surface remind of large grain structures which were found for bulk films of AlClPc and TiOPc deposited on heated silicon substrates (with roughness of 5.08 nm and 4.18 nm), as opposed to planar phthalocyanines, which grain size and roughness were significantly smaller.<sup>126</sup> Similar shape of islands can be observed in VOPcF<sub>16</sub> (peripheral substituted polar phthalocyanine) films on the silicon substrates, when annealed at 180° C under ambient conditions. The crystallites are quadratic in shape and definitely higher in the middle than their edges.<sup>127</sup>

The island size and distribution is more uniform on oxygen treated surface, where they cover 47% of the image area. Islands with side length equal to 33.17 and 53.6 nm prevail in the AFM image. On the other hand, on reduced (100) surface the islands are scarce (23% of the image area) and they have broader size distribution. The smaller islands have the side length of 27.4 nm, whereas the big islands have the side length of 63 nm. Profiles of both images were taken: the left one shows a minimum at -

#### 4. Results and Discussion - 4.2 Interaction between halogen substituted organic semiconductor molecules (AICIPc) and TiO<sub>2</sub>(100) substrate.

3.45 nm and maximum at 16.87 nm, while its RMS is equal to 3.93 nm. The profile of image in the right, has minimum at -3.56 nm and maximum at 26.56 nm, while the RMS is 7.01 nm. That means that the islands on the defect-rich surface (right profile), are not only wider in the X-Y plane, but they are also higher (30 nm). In the left profile the islands are maximally 21 nm high.

It shows the flexibility of AICIPc molecules to form different density of islands upon a change in substrate preparation. The AICIPc film morphology could be adjusted through substrate temperature too. This diffusion is facilitated when the phthalocyanine film structure is disorganized, but the diffusion of large anions in the material may become difficult and even impossible when the phthalocyanine film is polycrystalline.<sup>128</sup> This could explain low extent of the interaction between phthalocyanine molecules and TiO<sub>2</sub>(100) surface, because crystalline AICIPc islands are formed on the substrate.

#### AICIPc/TiO<sub>2</sub>(100): O<sub>2</sub> treatment

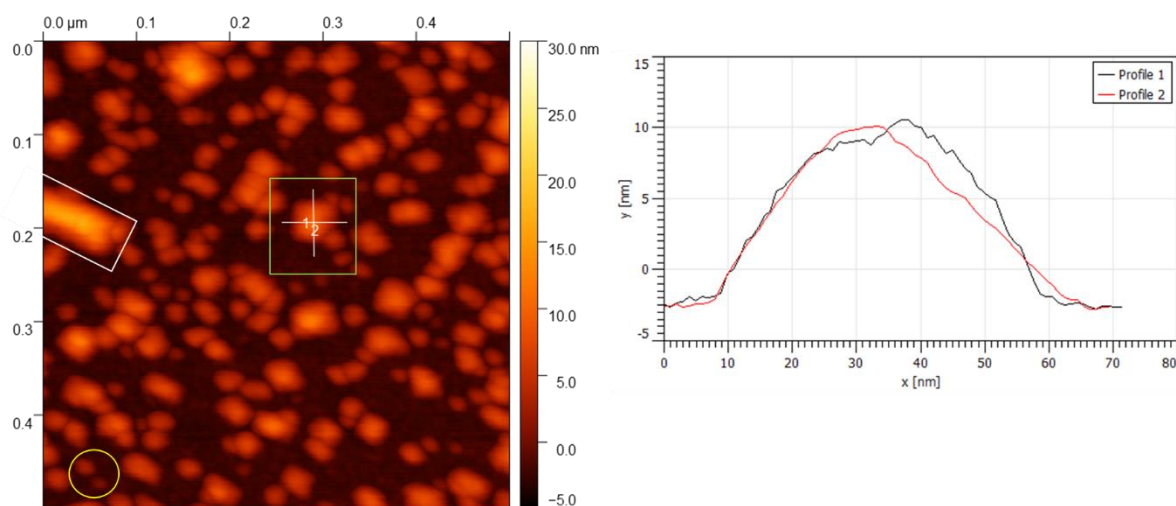


Figure 4.43 A 500 nm x 500 nm AFM image of a 1.2 nm thick AICIPc film on TiO<sub>2</sub>(100) prepared with oxygen (left) and (right) a line profile of the AICIPc islands.

Figure 4.43 shows an AICIPc film (1.2 nm) on a defect free TiO<sub>2</sub>(100) surface. Most of the islands have the same height, since they have the same colour on the height scale. One can clearly recognize the rectangular shape of the islands. Most of the islands are “free standing” especially the small islands (marked with a yellow circle). Bigger island with a clear quadratic base grow either free (green square) or grow next to each other forming a row (white rectangle). The islands are higher in the middle and lower and broader at their bottom. Considering their base is quadratic, the profile of a single island points to symmetric island geometry, either conical or pyramidal in shape, as seen in Profiles 1 and 2 (right side of the Figure 4.43).

#### 4. Results and Discussion - 4.2 Interaction between halogen substituted organic semiconductor molecules (AlClPc) and TiO<sub>2</sub>(100) substrate.

##### AlClPc/TiO<sub>2</sub>(100): Absence of O<sub>2</sub>

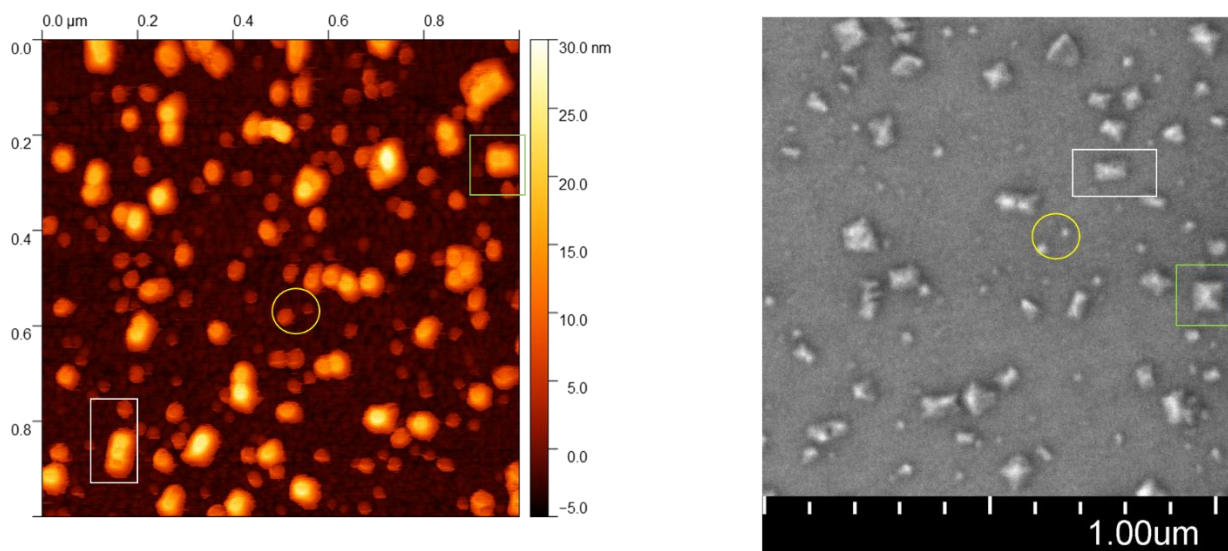


Figure 4.44 AlClPc film (1.3 nm) on TiO<sub>2</sub>(100) prepared in absence of oxygen. A 1 μm x 1 μm AFM image (left) and a 1 μm x 1 μm SEM image of the same sample measured at a different point (right).

Thin film of AlClPc (1.3 nm) on TiO<sub>2</sub>(100) prepared in absence of oxygen was measured with both AFM and SEM. Images (1 μm x 1 μm) of a sample measured with both techniques are shown in Figure 4.44. Although both images were measured at different points on the sample surface, it is possible to recognise the same forms of AlClPc islands on TiO<sub>2</sub> surface in both images of Figure 4.44. There are groups of small islands (marked with yellow circle), big single-standing islands (green square) and rows of small islands or a long rectangular island (white rectangle). These are the same structures as those observed on the (100) surface prepared with oxygen. Due to a good resolution and image contrast of SEM image, one can see that the islands have rectangular base. They are actually small crystals, pyramidal in their form. Figure 4.45 reveals that most of the square based pyramids are pointing in the direction away from the substrate (red arrows). However, there are also pyramidal crystals which are lying on their side (yellow arrows).

4. Results and Discussion - 4.2 Interaction between halogen substituted organic semiconductor molecules (AlClPc) and TiO<sub>2</sub>(100) substrate.

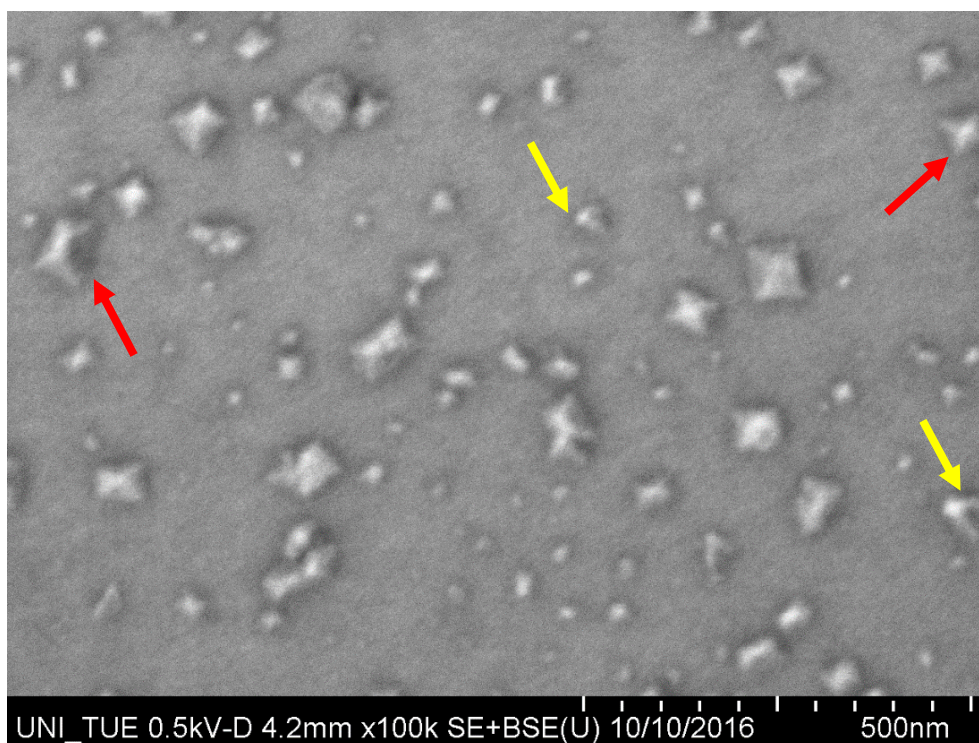


Figure 4.45 AlClPc on TiO<sub>2</sub>(100) treated without oxygen forms different sizes of crystallites, as well as different direction of growth: upwards (red arrows), sideways (yellow arrows).

If one changes the contrast of the SEM image (Figure 4.46), one can recognize the mosaic background of TiO<sub>2</sub>(100) substrate as seen in Figure 4.31.

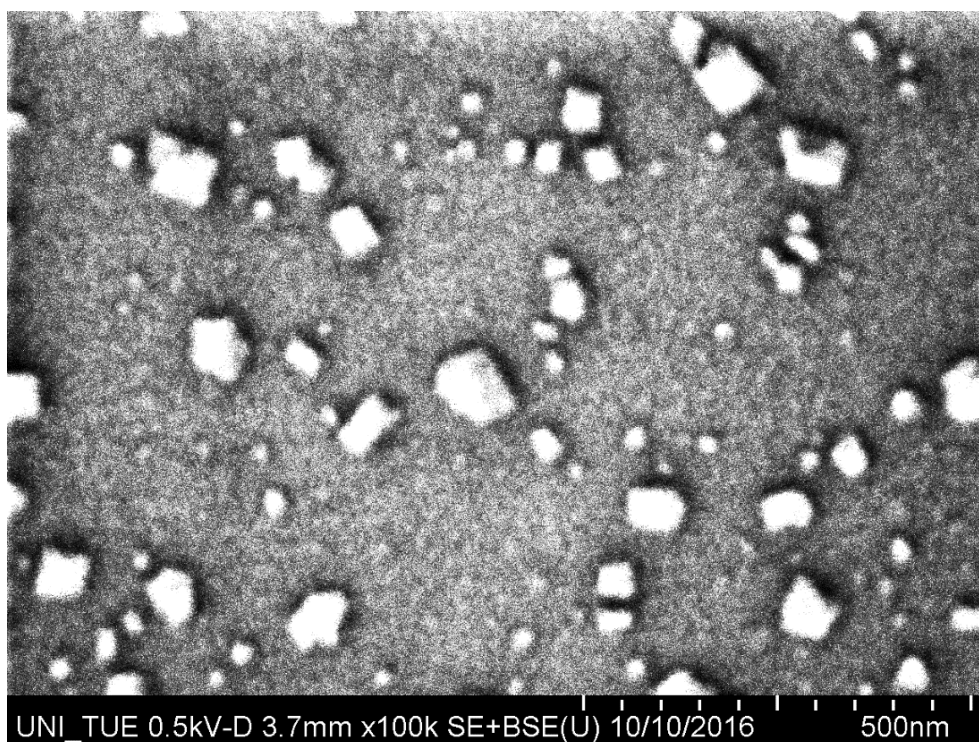


Figure 4.46 SEM image of AlClPc on TiO<sub>2</sub>(100) prepared in absence of oxygen.

#### 4. Results and Discussion - 4.2 Interaction between halogen substituted organic semiconductor molecules (AlClPc) and TiO<sub>2</sub>(100) substrate.

The question arises if AlClPc evaporated onto TiO<sub>2</sub>(100) surface grows in the same mode (Stranski-Krastanov growth) as on the TiO<sub>2</sub>(001) surface. The following procedure was used to find this information: The AFM images of AlClPc film on defect free and defect-rich TiO<sub>2</sub>(100) surface were normalized between the maximum height of an island and the island base. To better describe it, the flat area at the base of the islands was masked in blue, as show in Figure 4.47.

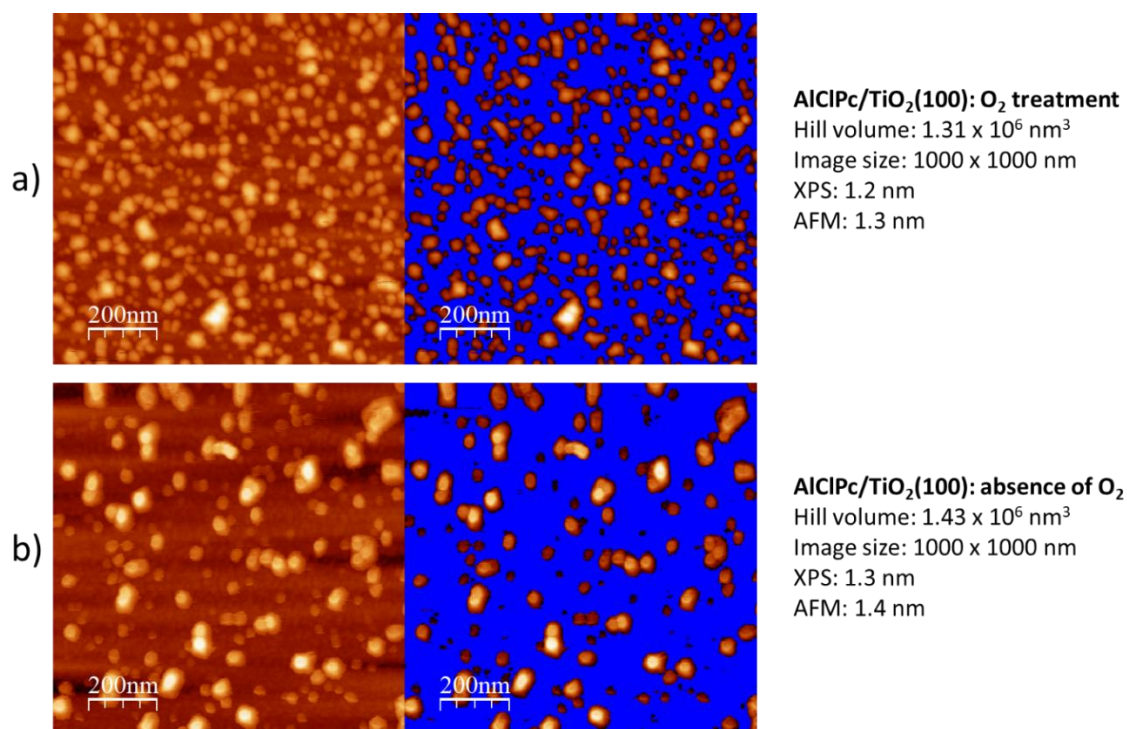


Figure 4.47 The AlClPc islands on TiO<sub>2</sub>(100): a) defect free and b) defect-rich surface. The blue area, at the level of island base, masks the flat space between the islands.

The volume of detected islands was then calculated with the use of the WSxM Software<sup>129</sup>. The total volume of the islands was later divided by the total area of the image, giving the height of a fully closed layer, with volume equivalent to that of the total island volume. The height is then compared with the layer thickness calculated with the layer-by-layer model. The results are as follows. The film thickness on defect free surface was found to be 1.3 nm while the calculated value was 1.2 nm. In case of defect-rich surface the film was found to be 1.4 nm thick, while it was calculated to be 1.3 nm with the layer-by-layer model. The results obtained from AFM measurements are very close to the film thickness calculated based on the XPS signals, which might lead to the idea that the substrate below the islands is not covered with a fully closed monolayer of phthalocyanine molecules. Especially because a monolayer of AlClPc is around  $0.35 \text{ nm}^{58}$ , so the difference between the AFM and XPS results would have to be higher with the latter value higher. The assumption of a fully closed layer with islands on top is less likely than the island-only growth. The film thickness results based on other AFM images

#### 4. Results and Discussion - 4.2 Interaction between halogen substituted organic semiconductor molecules (AIClPc) and TiO<sub>2</sub>(100) substrate.

ended up in similar range with AFM thickness matching the XPS one with an error margin below a monolayer thickness.

##### 4.2.2.7 Island shape explanation

One of the explanations for the formation of pyramidal shaped islands can be adsorption of molecules around the defects at the substrate surface. If the substrate surface is not atomically flat (we do have information, that the clean TiO<sub>2</sub>(100) oxygen treated surface includes small grains/rows, and that the surface prepared without oxygen exhibits defects in Ti 2p XPS signal) the defects can act as the nucleation centres<sup>130</sup>, i.e. for metals.<sup>131</sup> The screw dislocations are a particular defect type (see Figure 4.48) which can act as a crystallization centre for this specific spiral pyramid growth. Presence of screw dislocations in TiO<sub>2</sub> is possible and can for example be an effect of uneven temperature distribution during the cooling process of TiO<sub>2</sub>.<sup>132</sup> The dislocations were reported for the (100) rutile TiO<sub>2</sub> surface.<sup>133</sup> Even a high temperature annealing (1300°C) was not able to remove all dislocations in powder TiO<sub>2</sub> samples,<sup>129</sup> so although we do not observe the dislocations in the AFM images, their presence at the surface is possible, due to lower temperature of sample preparation (see Chapter 3: Experimental).

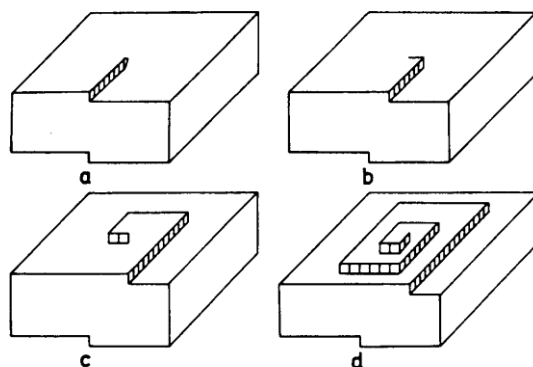


*Figure 4.48 The mechanism of crystal growth starting at a screw dislocation. Formation of consecutive steps (a-d) enabling a spiral pattern formation (see text below).*

The molecules adsorbed at the dislocation form an island that grows along the dislocation forming a step. (Figure 4.48a). The step advances, as the next molecules attach, creating second step (Figure 4.48b). Growth of the second step generates an edge for molecules to attach, creating third step (Figure 4.48c) it is followed with fourth step, and continues (Figure 4.48d) till a spiral island is formed. This type of growth requires less energy than a layer mechanism<sup>134</sup> explaining why island-growth is more preferential if dislocations are available. This would also support the idea that the growth on the (100) surface is more likely to be island-only growth.

A clean defect-free rutile TiO<sub>2</sub>(001) surface has low roughness, however small (not well resolved) grains are visible in the AFM image of a clean substrate. The (100) surface, due to its smoothness was difficult

#### 4. Results and Discussion - 4.2 Interaction between halogen substituted organic semiconductor molecules (AlClPc) and TiO<sub>2</sub>(100) substrate.

to resolve properly in an AFM image, however a profile of a clean rutile TiO<sub>2</sub>(100) surface shows small hills indicating formation of grains on the surface during the cleaning process with subsequent sputtering and annealing cycles. The boundaries between the grains can include dislocations, which act as electron traps as well.<sup>135</sup> These will be attractive to phthalocyanine molecules, which upon adsorption transfer the negative charges to the TiO<sub>2</sub> (based on our UPS measurements, there is a charge transfer from phthalocyanine molecule into TiO<sub>2</sub>). This would explain the occurrence of defects as the preferential adsorption sites for AlClPc on TiO<sub>2</sub>. The phthalocyanines adsorbed at the dislocations will then act as seeds for an island growth in form of a spiral which can be observed for other small organic molecules<sup>136 137</sup>.

In case of reduced TiO<sub>2</sub> surface, as mentioned before, the available experiments indicate presence of defects. The main indicator of defects presence is the Ti<sup>3+</sup> of Ti 2p peak in the XPS spectrum. The second is the defect related peak in UPS spectra with the Ti 3d character. Additionally, even if the Ti<sup>3+</sup> peak is not seen in Ti 2p spectrum, it is known that there can still be minor amount of defects present on the rutile surface<sup>124</sup>. The XPS and UPS results however, are not enough to tell about the type of defect present. Point defects contribute to the Ti<sup>3+</sup> signal, while the Ti atoms at the dislocation core were found to contribute to both Ti<sup>3+</sup> and Ti<sup>4+</sup> components.<sup>133</sup>

Indication of the presence of this type of defects can be found using XAS data. According to literature, the reduced rutile TiO<sub>2</sub> shows a Ti-L edge XAS spectrum resembling the one of Ti<sub>2</sub>O<sub>3</sub>.<sup>135</sup> With increasing oxygen non-stoichiometry of a rutile TiO<sub>2</sub> surface, the surface structure resembles more the Ti<sub>2</sub>O<sub>3</sub>.<sup>138</sup> It means that the strongly reduced surface cannot be treated as a TiO<sub>2</sub> surface anymore. A comparison of Ti-L edges measured with electron energy loss near-edge structure spectroscopy<sup>139</sup> shows the difference between the TiO<sub>2</sub> rutile and Ti<sub>2</sub>O<sub>3</sub> Ti-L edge. The authors of reference 135 state that the area of the sample resulting in the reduced like XAS spectrum belongs to the dislocation in the TiO<sub>2</sub> structure, while the bulk area, without the dislocations present, shows a typical Ti-L XAS spectrum of TiO<sub>2</sub>.<sup>135</sup> Similar effect is seen in XAS spectrum of rutile TiO<sub>2</sub>(100) substrate<sup>140</sup> where the intensity of the XAS Ti-L peak at 459.0 eV increases with the presence of defects of the defect-rich rutile TiO<sub>2</sub>(100), while the feature A peak at 457.0 eV photon energy decreases.<sup>135</sup>

While the pyramidal shape of the islands can be explained by the growth on top of a screw dislocation, the rectangular shape of the base of the pyramids can be explained by the strong corner diffusion. As the islands grow with subsequent evaporation of AlClPc, the diffusion of the molecules to the corners of the island base leads to the rectangular shape of the base<sup>141</sup>, instead of a circular base expected from the spiral growth of the island at the dislocation. Phthalocyanine themselves exhibit also growth with a screw dislocation outcrop in their own crystal structure, as is the case of metal free

#### 4. Results and Discussion - 4.2 Interaction between halogen substituted organic semiconductor molecules (AlClPc) and TiO<sub>2</sub>(100) substrate.

phthalocyanine. Although the morphology of the H<sub>2</sub>Pc crystals is needle like, the growth shows an elongated spiral growth<sup>142</sup> which could also explain the rectangular shape of the pyramid base. Alternatively the islands may follow the direction of polishing scratches, which were not completely removed by annealing.

##### 4.2.3 Chapter summary

AlClPc molecules undergo an interaction with the TiO<sub>2</sub>(100) surface through the nitrogen atom, while carbon atoms and the center of the molecule are not affected. All spectra undergo broadening in the monolayer region due to different adsorption sites as a consequence of presence of defects, which is seen the best on the defective surface with 16% of Ti<sup>3+</sup> contribution. Although (100) surface is not the most reactive type among all low index TiO<sub>2</sub> single crystal surfaces, the surface geometry allows interaction with the phthalocyanine molecules especially if the substrate was prepared in absence of oxygen and surface defects are present. The intensity of N-3 component decreases when number of defects decreases (due to oxygen treatment in sample preparation), indicating that defects are the mediators of the phthalocyanine/TiO<sub>2</sub> interaction. The oxygen treated TiO<sub>2</sub>(100) surface does not show presence of Ti<sup>3+</sup> component in Ti 2p spectra, however, based on the ultra violet photoemission spectroscopy, there is an evidence of some surface defects still available, which explains why the AlClPc molecules still have a chance to interact in the film thickness region below a monolayer. The HOMO pinning indicating presence of defects, even on the oxygen treated surface, is present for both sample preparations. Upon AlClPc adsorption no new defect states are created, as the Ti<sup>3+</sup> intensity does not increase. The system work function decreases followed by formation of surface dipoles. A possible charge transfer from the organic film to the substrate is observed.

The microscopy measurements (both AFM and SEM) confirm the existence of islands TiO<sub>2</sub>(100) surface. The latter technique has shown that AlClPc molecules form pyramidal crystallites. The islands form regardless of the surface reduction degree. The amount of defects however, influences the size and distribution of islands. At higher percentage of Ti<sup>3+</sup> islands are bigger and scarcer, while for almost defect free surface the islands are denser and smaller in size. Since the amount of defects influences the island size and density, it has direct influence on film roughness. AlClPc films on reduced TiO<sub>2</sub>(100) surface show higher RMS values than on oxygen treated surface. The growth of AlClPc islands on (100) surface based on the AFM measurements is either layer-island or island only, however, the morphology of the crystallites indicates the island-only mode. The surface roughness increases with film thickness. In thinner films the islands are more broad and flat, while they grow higher in the thick films, which influences the film roughness.

## 4. Results and Discussion

### 4.3 Interaction between halogen substituted organic semiconductor molecules (AlClPc) and TiO<sub>2</sub>(001) substrate

In this chapter, an interaction of AlClPc at the interface to rutile TiO<sub>2</sub>(001) surface will be discussed. The amount of defects in TiO<sub>2</sub> single crystal has been varied with the use of two preparation procedures (preparation with oxygen treatment and in absence of oxygen). Clean substrate, as well as AlClPc thin films will be characterized by means of photoemission spectroscopy. The different surface reconstructions of TiO<sub>2</sub>(001) surface will be discussed based on the images obtained with low energy electron diffraction. Parts of this chapter were published in a peer-reviewed paper<sup>89</sup>. They are reproduced from Reference 89 with permission from the PCCP Owner Societies.

#### 4.3.1 Characterization of a clean TiO<sub>2</sub>(001) surface at different degrees of reduction

##### 4.3.1.1 Substrate overview – influence of preparation procedure

A preparation procedure described in Chapter 3 resulted in a clean rutile TiO<sub>2</sub>(001) single crystal surface. An XPS overview spectra of the 3 stages of TiO<sub>2</sub>(001) surface preparation are shown in Figure 4.49. The top spectrum marked in with red line (spectrum A) shows the TiO<sub>2</sub>(001) surface “as received”. Although substrate specific core level signals (Ti 2p and O 1s) are visible, the substrate is clearly dirty. High intensity of C 1s and N 1s signals points to a huge amount of carbon, as well as nitrogen at the crystal surface. All signals in the overview spectrum are shifted by around 10 eV to higher binding energy, due to the charging effects of a, yet insulating, TiO<sub>2</sub> crystal. The next spectrum (blue line, spectrum B) shows a substrate after 3 preparation cycles. No charging of the sample occurs anymore because through sputtering and consecutive annealing defects are introduced into TiO<sub>2</sub> structure. Formation of defects (i.e. oxygen vacancies, which act as electron donors) leads to presence of charge carriers in TiO<sub>2</sub> single crystal, making it an n-type semi-conductor.<sup>143</sup> Carbon signal decreased drastically, while nitrogen signal is not visible anymore. A calcium signal appeared, due to bulk contaminations transport to the surface during annealing step. The substrate specific signals are now well developed, and their position matches the literature values.<sup>143</sup> The last spectrum (green line, spectrum C) shows a clean TiO<sub>2</sub>(001) surface, with only substrate specific peaks present and a small amount of implanted argon ions, due to the sputtering procedure. The spectrum did not shift anymore. Since the overview spectrum presented here belongs to the TiO<sub>2</sub>(001) crystal prepared in the absence of oxygen, a shoulder in Ti 2p peak is present, as seen in the inset of Figure 4.49. The details of Ti 2p peak will be discussed in the next chapter.

#### 4. Results and Discussion - 4.3 Interaction between halogen substituted organic semiconductor molecules (AlClPc) and TiO<sub>2</sub>(001) substrate

The preparation procedure of oxygen treated TiO<sub>2</sub>(001) surface resulted in the same overview spectrum as shown in Figure 4.49 Spectrum C, with the exception of no shoulder present in the Ti 2p peak.

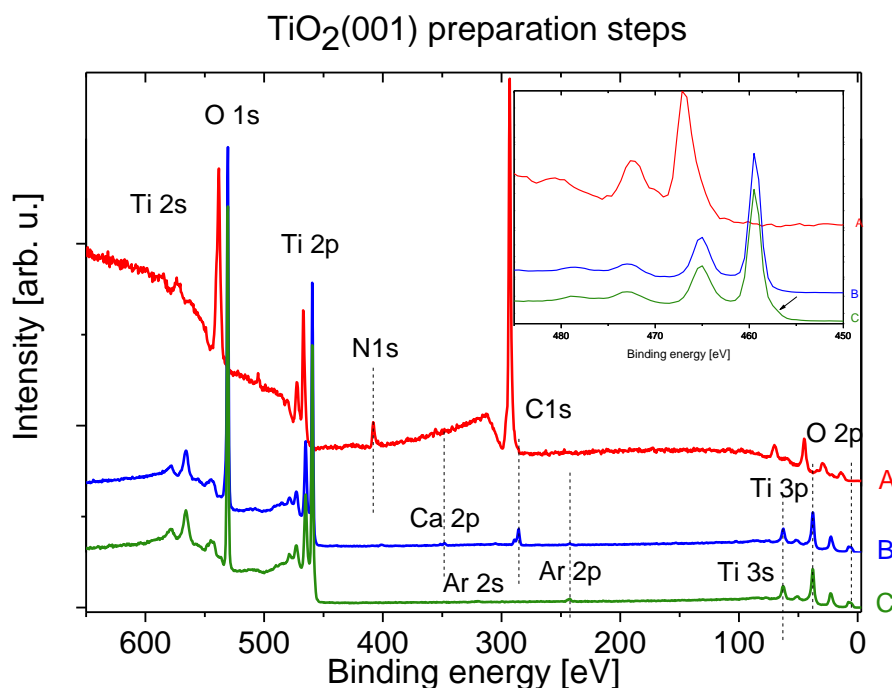


Figure 4.49 XPS spectra of A – as received, B – sputtered and annealed (3 cycles) and C – clean TiO<sub>2</sub>(001) single crystal. Spectra measured with Al K $\alpha$  radiation,  $h\nu = 1486.7$  eV.

##### 4.3.1.2 Ti 2p and O 1s spectra – variation of defects amount with reduction degree

Four Ti 2p spectra of clean TiO<sub>2</sub>(001) surface are presented in Figure 4.50a. They were fitted according to the fitting model described in chapter 4.2.1.2. The spectra show (001) surface at four different degrees of reduction. The top spectrum (magenta), belongs to a substrate, which was treated in oxygen during annealing. It shows only a contribution from Ti<sup>4+</sup> atoms, indicating that no defects are present at the surface. The three remaining spectra belong to substrates prepared in absence of oxygen, with increasing sputtering time. Substrate with the shortest sputtering time is shown in blue. The contribution of defect related Ti<sup>3+</sup> doublet is 5%. As the sputtering time increases, the intensity of Ti<sup>3+</sup> doublet increases to 12% for substrate depicted with green spectrum. The last, purple spectrum belongs to a defect-rich substrate. Due to a very high degree of reduction (50%) the spectrum shows contributions from Ti<sup>3+</sup> and Ti<sup>2+</sup> as well (1.9 eV and 3.3 eV lower in binding energy than the Ti<sup>4+</sup> peak). The effect of spectra broadening upon defect formation is clearly visible in Ti 2p spectrum of defect-rich sample. The Gaussian width of Ti 2p<sub>3/2</sub> peak is 1.45 eV while the width of the same peak for defect-free sample is only 0.8 eV (at constant Lorentz width value of 0.5 eV).

#### 4. Results and Discussion - 4.3 Interaction between halogen substituted organic semiconductor molecules (AICIPc) and TiO<sub>2</sub>(001) substrate

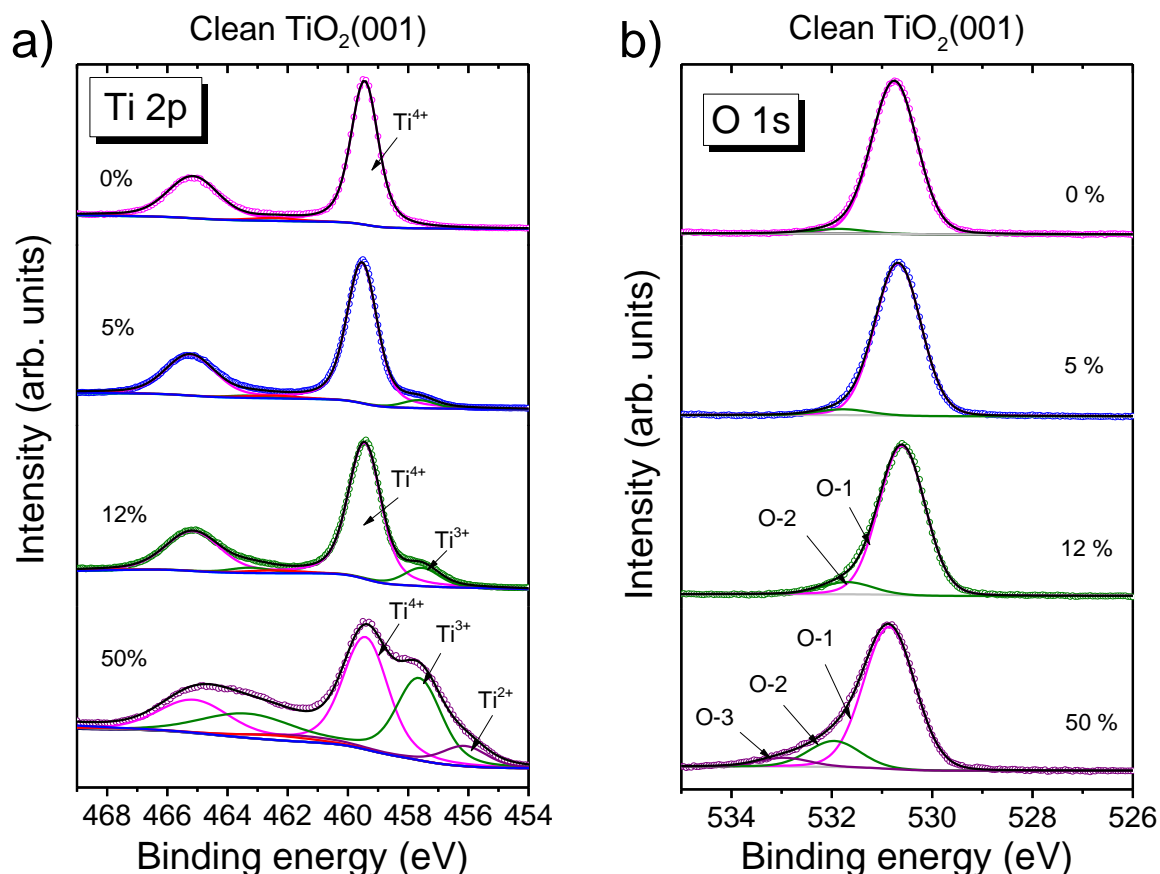


Figure 4.50 Spectra of clean TiO<sub>2</sub>(001) surface: a) Ti 2p core level, b) O 1s core level. Spectra from top to bottom: magenta - 0%, blue - 5%, green - 12% and purple - 50% defect contribution. Defects are represented by Ti<sup>3+</sup> and if present, Ti<sup>2+</sup> peak in the fitted model. Spectra measured with Al K $\alpha$  radiation,  $h\nu = 1486.7$  eV.

Presence of defects is mirrored in O 1s spectra (Figure 4.50) of the same TiO<sub>2</sub>(001) sample series. Two contributions: O-1 connected with bulk oxygen atoms, and O-2, connected with oxygen atoms around defects are visible for the samples with 0%, 5% and 12% Ti<sup>3+</sup>. The intensity of O-2 contribution becomes visibly higher as the relative amount of Ti<sup>3+</sup> increases. The peak position of O-2 contribution can be fitted at 1.1 eV binding energy higher than the bulk oxygen O-1 contribution. For the defect-rich sample, additional contribution O-3 needs to be fitted at binding energy 2.1 eV higher than the main peak. The O-3 component is likely to be oxygen atoms around Ti<sup>2+</sup> seen in Ti 2p peak fit as well. Similar to Ti 2p, a broadening of spectra with increasing sputtering time and amount of defects is seen in O 1s. The effect can be clearly seen when comparing the “defect-free” and defect-rich surface. While their Lorentz width is kept at 0.1 eV, the Gaussian width is equal to 1.0 eV and 1.3 eV respectively. Detailed fitting parameters of both core level spectra can be found in Table 19 and Table 20.

Ti 2p spectra of TiO<sub>2</sub>(001) surfaces at different reduction degree were shown above. The influence of defect amount on AICIPc films will be discussed based on samples with 0% and 12% Ti<sup>3+</sup> contribution,

#### 4. Results and Discussion - 4.3 Interaction between halogen substituted organic semiconductor molecules (AlClPc) and TiO<sub>2</sub>(001) substrate

for the sake of comparison with the TiO<sub>2</sub>(100) surface with similar amount of defects. However, the samples with higher reduction degree will be used when discussing the AlClPc film growth on reduced TiO<sub>2</sub>(001) surface, as shown in Chapter 4.3.2.7. All photoemission spectra of samples with 5% and 50% Ti<sup>3+</sup> contribution can be found in Appendix: part 6.3 and 6.4.

##### 4.3.1.3 LEED patterns - Influence of defect on TiO<sub>2</sub>(001) surface structure

To fully discuss the influence of defects on AlClPc molecules, one needs to distinguish between surface and sub-surface defects. For this reason, low energy electron diffraction (LEED) study was performed. The discussion will begin with TiO<sub>2</sub>(001) surface prepared in absence of oxygen with the XPS calculated amount of defects of 12%.

A LEED pattern of the reduced TiO<sub>2</sub>(001) surface is presented in Figure 4.51a. Since some spots are not sharp the spots are identified in a copy of the pattern in Figure 4.51b for better clarity. The pattern was recorded at primary beam energy of 44 eV. The strongest spots seen in the diffraction pattern of the reduced TiO<sub>2</sub> sample are recognized as the first order diffraction spots marked in black circles. Additional spots are present marked in black small circles. Although they are not sharp, one can recognize a pattern. According to literature, they correspond to the 1/2 and 1/4 spots, marking 13 x 6.5 Å unit cell, representing a  $(2\sqrt{2} \times 2\sqrt{2})R45^\circ$  superlattice of a reconstructed surface.<sup>41</sup>

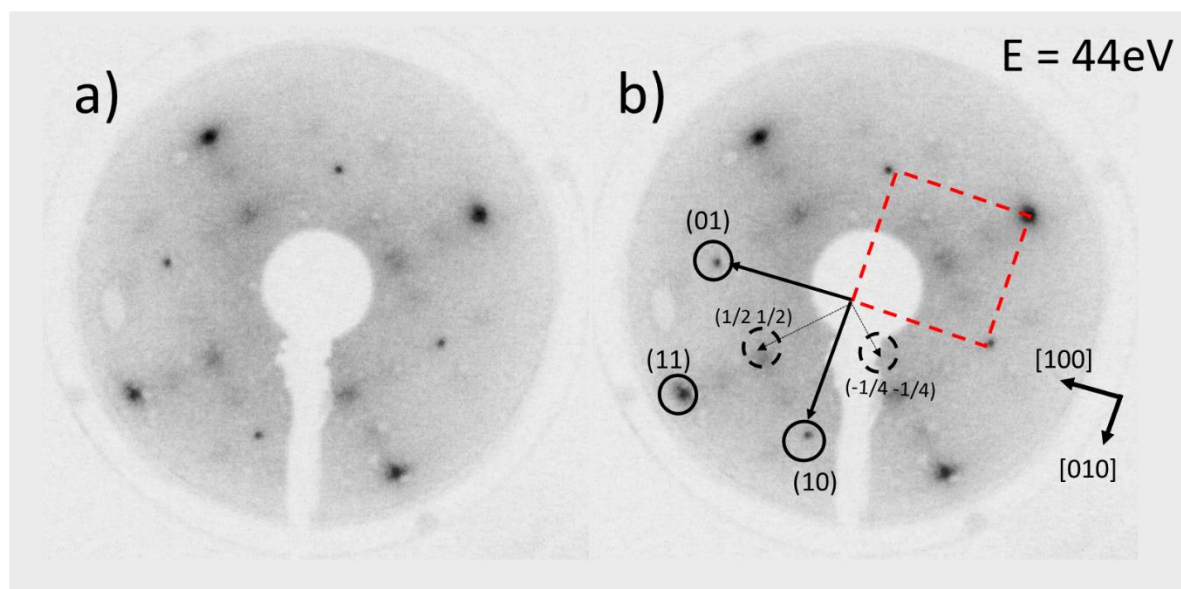


Figure 4.51 TiO<sub>2</sub>(001) reduced surface, prepared without oxygen atmosphere, E = 44 eV: a) original image, b) copy of the original image with diffraction spots identified: first order (black circles) and superlattice (black lined circles) spots. Crystal orientation directions are marked with thick black arrows. TiO<sub>2</sub>(001) surface unit cell is marked with red lined rectangle.

Such surface reconstruction is the effect of reduction through sputtering and mild annealing conditions used in the experiments presented in this work as well as in literature.<sup>41</sup> The lack of sharpness, and

#### 4. Results and Discussion - 4.3 Interaction between halogen substituted organic semiconductor molecules (AICIPc) and TiO<sub>2</sub>(001) substrate

increased background intensity around the spots is an indication of presence of defects<sup>54</sup>, which are seen in XPS Ti 2p signal as well.

The TiO<sub>2</sub>(001) surface is the least stable of all the low index rutile surfaces<sup>144</sup> because of its high surface energy<sup>145</sup> due to many dangling bonds at the surface<sup>41</sup>. The (001) surface undergoes reconstruction to lower the surface energy. Depending on the preparation conditions the outcome of the reconstruction can differ. Several models of TiO<sub>2</sub>(001) surface reconstruction in dependence of annealing temperature were proposed. Facets may be formed during heat treatment of unstable surfaces.<sup>54</sup> The authors of reference 146 state that annealing of (001) TiO<sub>2</sub> surface resulted in microfaceted surface with {011} and {114} microfacets at lower and higher annealing temperature respectively.<sup>146</sup> Further high temperature surface models have been offered, these are: reduced<sup>115</sup>, oxidized<sup>147</sup> and stoichiometric latticework like structure (a structure consisting of interlacing wide rows, running along the [110] and  $[1\bar{1}0]$  directions, with steps and narrow terraces on their slopes)<sup>148,149</sup>. There has been also a successful approach to obtain reconstruction similar to the high temperature models, using mild annealing temperature and low energy of sputtering.<sup>41</sup> The common result, of all surface reconstruction models is that a reconstructed (001) surface consists of facets. Such reconstructed surface will have potential sites for seeding crystal islands of organic molecules as explained later within this work in Chapter 4.3.2.7. Additionally, the reconstruction of the TiO<sub>2</sub>(001) surface can influence its band gap and lead to photo-oxidation reactions.<sup>150</sup> The fact that the reduced (001) surface is faceted adds to its reactivity.

To reduce the amount of defects at the surface, the TiO<sub>2</sub>(001) sample was prepared in oxygen atmosphere. LEED measurement was performed to check, if the oxygen treatment diminished the faceting of the (001) surface. The LEED pattern shown in Figure 4.52a, belongs to a TiO<sub>2</sub>(001) surface prepared in presence of oxygen, measured at 46 eV primary beam energy after 11 preparation cycles. The spots are weak and diffused. They resemble lines, which could indicate presence of steps, due to sputtering.<sup>109</sup> The second diffraction pattern presented in Figure 4.52b (right) shows a TiO<sub>2</sub>(001) surface at the 46 eV incident beam energy as well. This time the sample underwent 28 preparation cycles, where annealing time was prolonged. While the spots in Figure 4.52b are still diffused, meaning the ordered terraces have small areas, their shape becomes smaller and one can clearly recognize the (1 x 1) reconstruction pattern they form (the unit cell is marked with a yellow square). Although the annealing temperature is high enough to achieve a well-defined (1 x 1) reconstruction, the ordered areas are small.

#### 4. Results and Discussion - 4.3 Interaction between halogen substituted organic semiconductor molecules (AlClPc) and TiO<sub>2</sub>(001) substrate

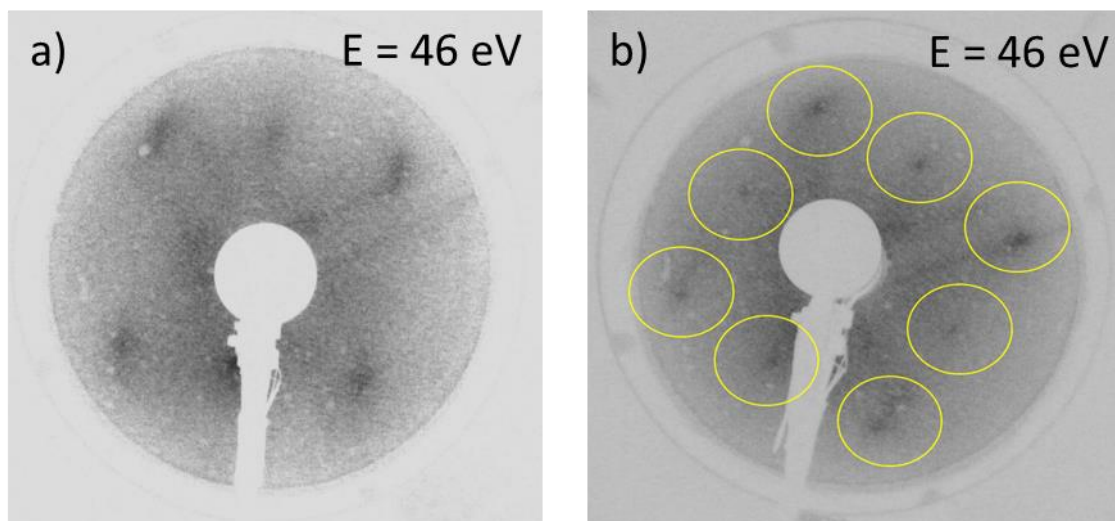


Figure 4.52 LEED pattern of a TiO<sub>2</sub>(001) surface measured at 46 eV beam energy a) after 11 preparation cycles, b) after 28 preparation cycles and increased annealing time. The diffraction spots are marked with yellow circles.

A (1 × 1) pattern of an unreconstructed TiO<sub>2</sub>(001) surface annealed in oxygen atmosphere was communicated recently in literature.<sup>144</sup> The LEED diffraction pattern was measured at 72 eV primary beam energy. Although the (001) surface is energetically the most unstable from the low index TiO<sub>2</sub> rutile surfaces the sample still exhibits a clear (1 × 1) reconstructed LEED pattern. The authors explain that the (1 × 1) pattern exists due to presence of unreconstructed (1 × 1) terraces and reconstructed facets, the latter which can stabilize the unreconstructed (1 × 1) terraces.<sup>144</sup> Using even milder annealing conditions than in literature<sup>144</sup>, the diffraction pattern still shows a (1 × 1) reconstruction, but the presence of facets cannot be excluded. Considering that such prepared surface shows a “defect free” XPS Ti 2p spectra it can be concluded that the sample is has (1 × 1) reconstruction, with many small terraces.

#### 4. Results and Discussion - 4.3 Interaction between halogen substituted organic semiconductor molecules (AIClPc) and TiO<sub>2</sub>(001) substrate

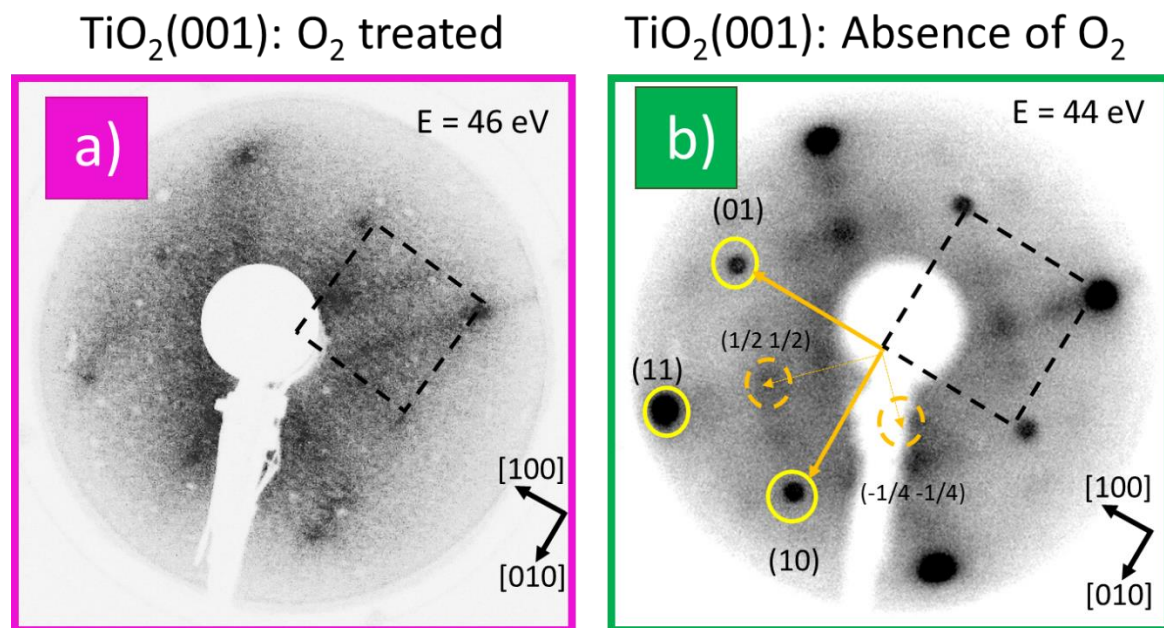


Figure 4.53 Comparison of TiO<sub>2</sub>(001) surface: a) treated with oxygen, b) prepared without presence of oxygen. Reproduced from Ref. 89 with permission from the PCCP Owner Societies.

Figure 4.53 shows a comparison of both oxygen treated and reduced TiO<sub>2</sub>(001) surfaces. It is clear, that they exhibit the same pattern of primary spots. The additional spots between the primary spots, seen on the reduced surface, are absent on the oxygen treated surface.

##### 4.3.1.4 Microscopy images of TiO<sub>2</sub>(001) preparation stages

The last method used to characterize a clean TiO<sub>2</sub> substrate was AFM. The TiO<sub>2</sub>(001) single crystal was first measured in the "as received" form, without any preparation step done yet.

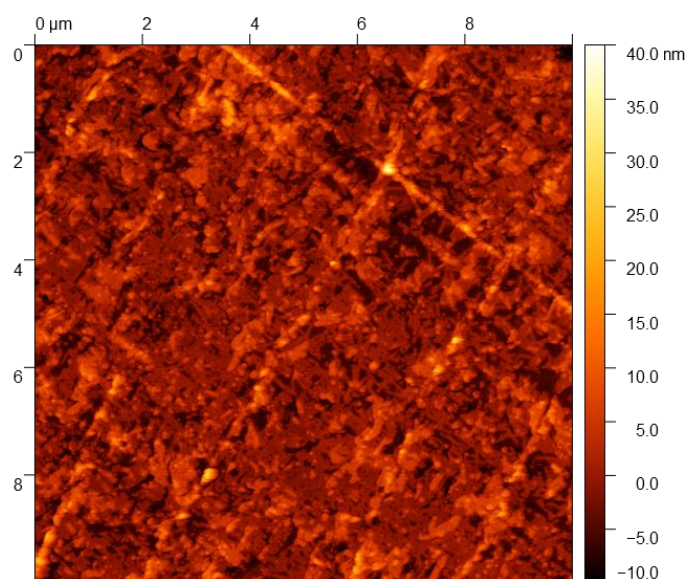


Figure 4.54 An AFM image of an "as received" TiO<sub>2</sub>(001) surface, 10 μm x 10 μm.

#### 4. Results and Discussion - 4.3 Interaction between halogen substituted organic semiconductor molecules (AlClPc) and TiO<sub>2</sub>(001) substrate

The “as received” surface is shown in Figure 4.54. The surface is covered with big patches of material. An XPS overview spectrum measured before the AFM measurement, has shown, apart from the typical TiO<sub>2</sub> peaks, an intensive carbon peak (see Chapter 4.3.1.1, Figure 4.49, red curve A).

It is most probable that the bright patches seen in Figure 4.54 are the polishing material left-overs (possibly diamond paste, which explains the source of carbon contamination in XPS). The bright lines are scratches from polishing. They appear bright, because they are likely filled with the leftover polishing agent, that is why they appear higher on the height-colour scale. The roughness of the “as received” TiO<sub>2</sub>(001) surface is obviously high, the RMS value is equal to 4.128 nm (4.1 nm)

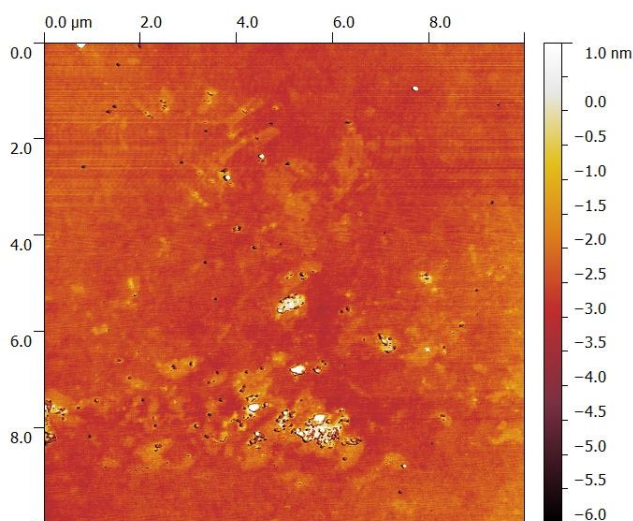


Figure 4.55 AFM image of TiO<sub>2</sub>(001) after 3 cycles of sputtering and annealing, 10 μm x 10 μm.

The AFM image of the surface taken after 3<sup>rd</sup> preparation cycle can be seen in Figure 4.55. After the sample underwent a cleaning procedure of 3 sputtering and annealing cycles, most of the polishing material is gone. The RMS of the sputtered surface decreases profoundly and is equal to 0.476 nm (0.5 nm).

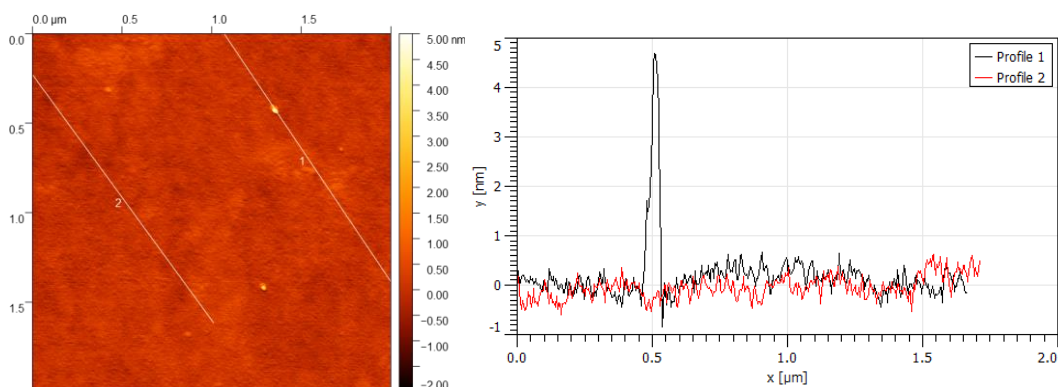


Figure 4.56 2 μm x 2 μm AFM image of a TiO<sub>2</sub>(001) surface after 3 cycles of sputtering and annealing with corresponding surface profiles.

#### 4. Results and Discussion - 4.3 Interaction between halogen substituted organic semiconductor molecules (AIClPc) and TiO<sub>2</sub>(001) substrate

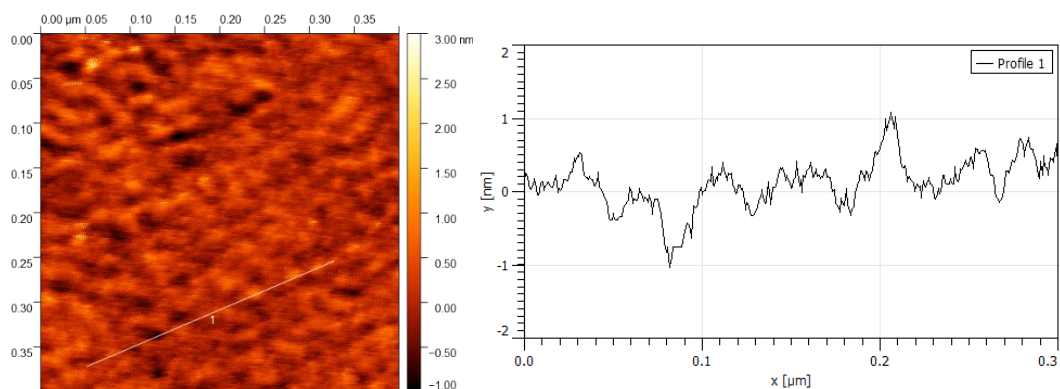


Figure 4.57 A 400 nm x 400 nm AFM image: zoom-in onto the flat area of the sputtered TiO<sub>2</sub>(001) sample with a surface line profile on the right.

A magnification at the surface sputtered surface (Figure 4.56) shows that there are still some higher particles visible (up to 6 nm) which likely contribute to the rest carbon in the XPS spectrum (see Chapter 4.3.1.1, Figure 4.49, blue curve B), but the remaining surface is flat and free from contamination. Figure 4.55 and Figure 4.56 show larger areas of the sample (10  $\mu\text{m}$  x 10  $\mu\text{m}$  and 2  $\mu\text{m}$  x 2  $\mu\text{m}$ ), the last figure (Figure 4.57) is a 400 nm x 400 nm image of the flat area of the sample. The line profile taken in Figure 4.57, shows small dips and hills present at the surface. Their height or depth however, does not exceed the value of 1.1 nm. In the height axis of the profile, the minimum value is at -1.041 nm and the maximum value is at 1.022 nm which means the surface is flat (in comparison to the TiO<sub>2</sub> with organic film as will be shown later in this chapter). The RMS is equal to 0.351 nm showing that the surface became very smooth in comparison to the “as received” single crystal.

Further sputtering and annealing (9 cycles), leads to a clean flat surface. There are still small hills present but this time, their height does not exceed 1 nm, as can be seen in the line profile taken in the Figure 4.58.

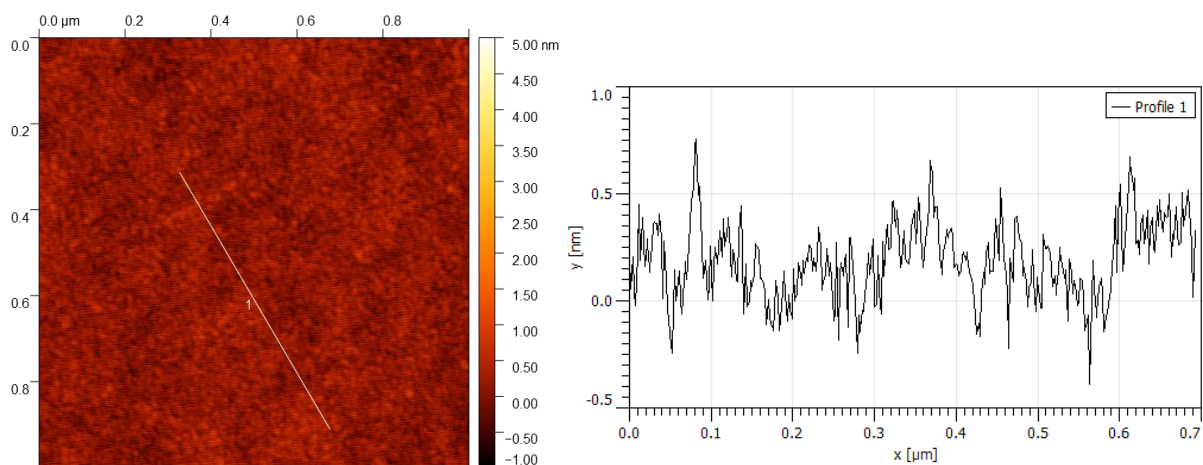


Figure 4.58 The 1  $\mu\text{m}$  x 1  $\mu\text{m}$  AFM image (left) of a clean TiO<sub>2</sub>(001) surface after 9 cycles of sputtering and annealing, with a corresponding line profile (right).

#### 4. Results and Discussion - 4.3 Interaction between halogen substituted organic semiconductor molecules (AlClPc) and TiO<sub>2</sub>(001) substrate

It is clearly visible, that the TiO<sub>2</sub>(001) surface is flat and free of contamination (according to XPS as well). The profile taken in Figure 4.58 has minimum and maximum at -0.392 nm and 0.752 nm respectively, while the RMS value decreased even more, reaching the value of 0.179 nm. This value will be considered a reference for a smooth TiO<sub>2</sub>(001) surface when discussing the roughness of the organic over-layer.

##### 4.3.2 Characterization of AlClPc films on TiO<sub>2</sub>(001) surface

###### 4.3.2.1 Influence of phthalocyanine deposition on TiO<sub>2</sub>(001) core level spectra

As in case of TiO<sub>2</sub>(100) surface, the Ti 2p core level peaks (see Figure 4.59) can be fitted with the same peak fit model for both clean substrate and for spectra after deposition of AlClPc films. The slight peak shift upon adsorption of the molecules is not more than  $\pm 0.1$  eV. In case of the TiO<sub>2</sub>(001) surface with 12% defects, a minor decrease in Ti<sup>3+</sup> component is seen for the Ti 2p peak with bulk 4.2 nm AlClPc film. No new peaks appear as a result of phthalocyanine deposition, excluding the possibility of formation of titanium at low oxidation state. No changes in O 1s core level peak were observed upon adsorption of AlClPc molecules.

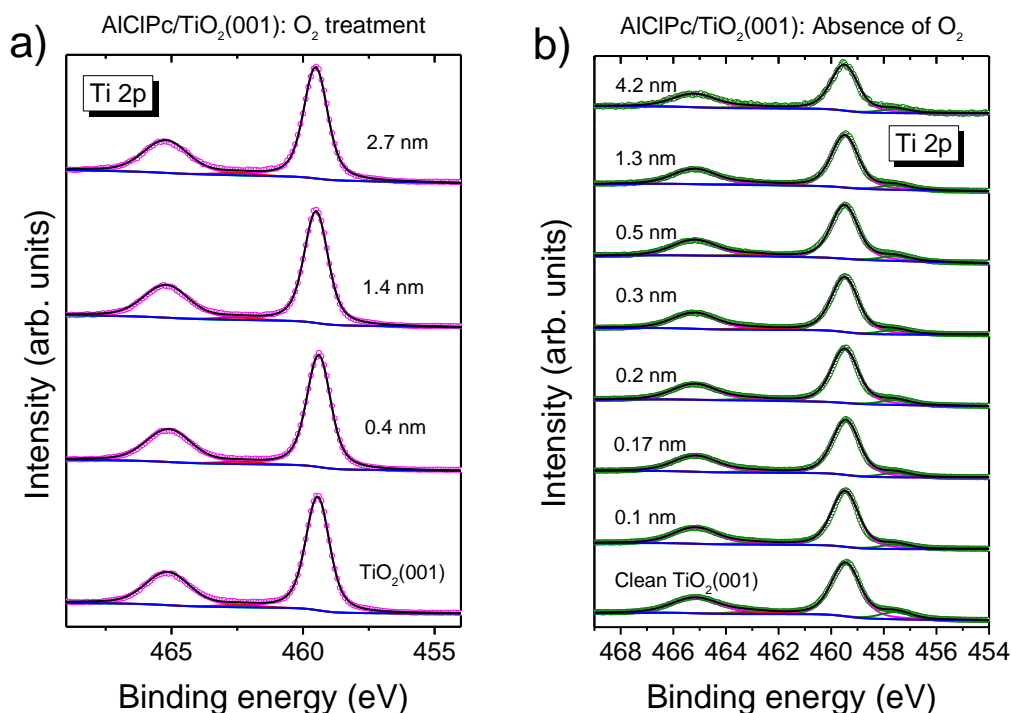


Figure 4.59 Ti 2p spectra of AlClPc on TiO<sub>2</sub>(001): a) prepared in presence and b) absence of oxygen. Spectra measured with Al K $\alpha$  radiation,  $h\nu = 1486.7$  eV. Reproduced from Ref. 89 with permission from the PCCP Owner Societies.

#### 4. Results and Discussion - 4.3 Interaction between halogen substituted organic semiconductor molecules (AlClPc) and TiO<sub>2</sub>(001) substrate

##### 4.3.2.2 Interaction of TiO<sub>2</sub>(001) with molecule ring

Properties of AlClPc films may change at the interface to the substrate, therefore organic film-related spectra are investigated below. Investigation of AlClPc properties in dependence on substrate type are performed, since TiO<sub>2</sub>(001) surface used in this experiment is expected to be more reactive than the (100) surface. C 1s spectra shown in Figure 4.60a and b belong to AlClPc films deposited on TiO<sub>2</sub>(001) single crystal surface prepared in presence and absence of oxygen.

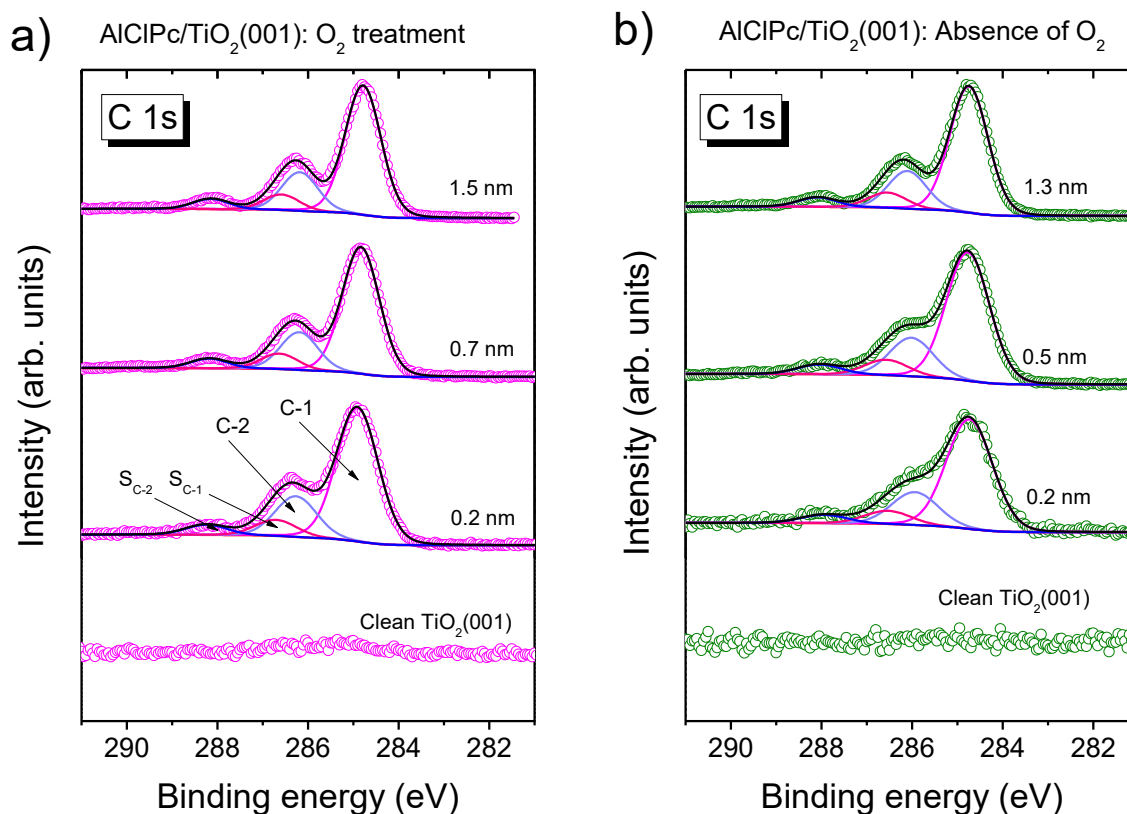


Figure 4.60 Thickness dependent C 1s core level spectra of AlClPc evaporated on differently prepared TiO<sub>2</sub>(001): a) AlClPc on TiO<sub>2</sub>(001) prepared in presence of oxygen, b) AlClPc on TiO<sub>2</sub>(001) prepared in absence of oxygen. All spectra can be described by the same peak shape. Spectra measured with Al K $\alpha$  radiation,  $h\nu = 1486.7$  eV. Reproduced from Ref. 89 with permission from the PCCP Owner Societies.

The spectra exhibit a trend observed also for TiO<sub>2</sub>(100) surface. It is possible to fit all spectra with four components representing the two types of carbon within phthalocyanine molecule with their corresponding satellites. On an oxygen treated surface (Figure 4.60a) the distance between C-1 and C-2 components is constant, and is equal to 1.4 eV, independent from film thickness. There is only a slight peak width increase at lowest film thickness, with Gaussian width of 1.0 eV for 0.2 nm film as compared to 0.9 eV for 1.5 nm film. This difference is even smaller than for oxygen treated TiO<sub>2</sub>(100) surface. Therefore it can be stated that there is little change in peak form upon phthalocyanine deposition.

#### 4. Results and Discussion - 4.3 Interaction between halogen substituted organic semiconductor molecules (AlClPc) and TiO<sub>2</sub>(001) substrate

In case of reduced surface (with 12% of Ti<sup>3+</sup> contribution), difference in Gaussian width between the lowest and highest film thickness is much larger: 1.2 eV for 0.2 nm film and 0.9 eV for 1.3 nm film. There is also bigger variation in the C-1 to C-2 component distance: 1.2 eV for 0.2 nm film and 1.4 eV for the thick film. The peak broadening in the sub-monolayer region can be explained by inhomogeneous adsorption sites as a clear response to the presence of defect on the reduced TiO<sub>2</sub>(001) surface, as was the case of reduced TiO<sub>2</sub>(100) surface. Detailed peak fit parameters can be found in Appendix 6.2.5, Table 21.

Nitrogen core level spectra provide complementary information on the state of phthalocyanine ring directly at the interface to the substrate and at higher coverage. Since the Ti 2p, O 1s and C 1s core level spectra do not undergo any dramatic changes, N 1s core level spectra might be a good probe for an interaction with the reactive TiO<sub>2</sub>(001) surface and its strength.

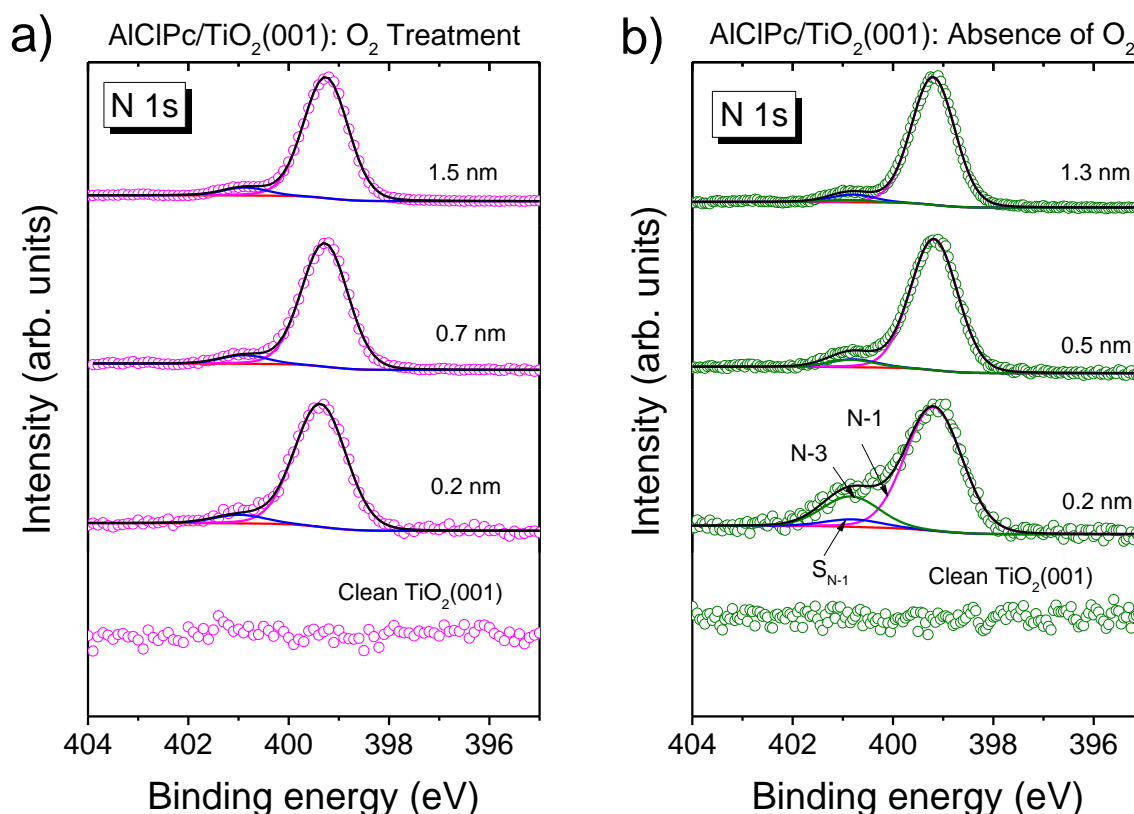


Figure 4.61 Thickness dependent N 1s core level spectra of AlClPc evaporated on differently prepared TiO<sub>2</sub>(001) surfaces: a) AlClPc on TiO<sub>2</sub>(001) prepared in presence of oxygen, b) AlClPc on TiO<sub>2</sub>(001) prepared in absence of oxygen. An interface component (N-3, green line) is only visible on surface prepared in absence of oxygen. Spectra measured with Al K $\alpha$  radiation,  $h\nu = 1486.7$  eV. Reproduced from Ref. 89 with permission from the PCCP Owner Societies.

Figure 4.61 shows N 1s spectra of AlClPc thin films on TiO<sub>2</sub>(100) surface prepared in presence and absence of oxygen (a and b respectively). Both groups presented in Figure 4.61 were fitted with peak

#### 4. Results and Discussion - 4.3 Interaction between halogen substituted organic semiconductor molecules (AlClPc) and TiO<sub>2</sub>(001) substrate

fitting model used to explain the components of N 1s core level spectra of AlClPc films deposited on TiO<sub>2</sub>(100) surface (shown in Figure 4.36). The fitting parameters can be found in Appendix 6.2.5, Table 22. Similar to the previously described surface, the binding energy position of the main N-1 component almost does not change. For oxygen treated surface it is 399.4 eV and for the reduced surface, where defects are present it is 399.2 eV. The S<sub>N-1</sub> satellite contribution lies at 1.6 eV higher binding energy for both preparations, with an intensity around 6% of the total N 1s peak intensity. For the defective (001) surface however, additional peak N-3 has to be used to describe the peak shape, due to an increase in intensity at high binding energy part of N 1s spectrum. The N-3 component is 1.7 eV higher than the main component and increases in intensity as the film thickness decreases. Such feature is not observed at the interface to the oxygen treated TiO<sub>2</sub>(001) surface. When compared to C 1s spectra on oxygen treated TiO<sub>2</sub> surface, there is a lack of changes in shape of spectra related to the phthalocyanine ring, which is a sign of an unaltered phthalocyanine ring at the interface to a surface with no defects present. What is remarkable, on (001) reduced surface the N-3 feature of 0.2 nm AlClPc film is more intensive (19% of total N 1s peak intensity) than for 0.1 nm film on TiO<sub>2</sub>(100) reduced surface (7% of total N 1s peak intensity). Such intensive feature is observed, although the contribution of Ti<sup>3+</sup> component in corresponding Ti 2p spectra is only 12% as opposed to the 16% on the reduced TiO<sub>2</sub>(100) surface (see Ti 2p spectra in Figure 4.22b and Figure 4.50b). This may suggest that on TiO<sub>2</sub>(001) reduced surface there is a preference for defects to be localized at the surface and/or the surface geometry allows an interaction with higher number of nitrogen atoms.

If number of nitrogen atoms which interact with the TiO<sub>2</sub> surface is given by the number of surface defects present or is determined by the surface geometry, this effect might be stronger at coverages in sub-monolayer region of film thicknesses. Based on the AlClPc crystal structure, a monolayer thickness is estimated to be 0.35 nm.<sup>58</sup> AlClPc sub-monolayer coverages on both TiO<sub>2</sub>(001) and TiO<sub>2</sub>(100) are compared in Figure 4.62. For the reduced TiO<sub>2</sub>(001) in Figure 4.62a, the relative intensity of the N-3 component is 37% for 0.07 nm and 19% for 0.17 nm thick film. Films with comparable thickness on reduced TiO<sub>2</sub>(100) surface (Figure 4.62b) have the following N-3 intensities: 12% and 7% at film thickness of 0.09 nm and 0.2 nm, which in both cases is lower than on the TiO<sub>2</sub>(001) surface. It shows that the preferred adsorption sites for AlClPc molecules are determined by the available defects at the surface and their number, initially.<sup>89</sup> What could happen is, when the monolayer is completed, the molecules will have less to no preferential sites available to adsorb. As a result there probability of local interaction decreases and the contribution of reacted nitrogen atoms will be reduced. The geometry of TiO<sub>2</sub>(001) surface allows interaction of more than one third of nitrogen atoms in AlClPc film. An even stronger interaction is observed for a 0.1 nm thick AlClPc film deposited on defect-rich (50% Ti<sup>3+</sup>) TiO<sub>2</sub>(001) surface where 40% of the nitrogen atoms undergo an interaction with the

#### 4. Results and Discussion - 4.3 Interaction between halogen substituted organic semiconductor molecules (AlClPc) and TiO<sub>2</sub>(001) substrate

substrate (see Appendix 6.4). Based on the experiments presented within this thesis, the (001) is evidently more reactive towards the phthalocyanine molecules as long as the substrate has defects available, that is oxygen partial pressure is not used during the preparation steps.

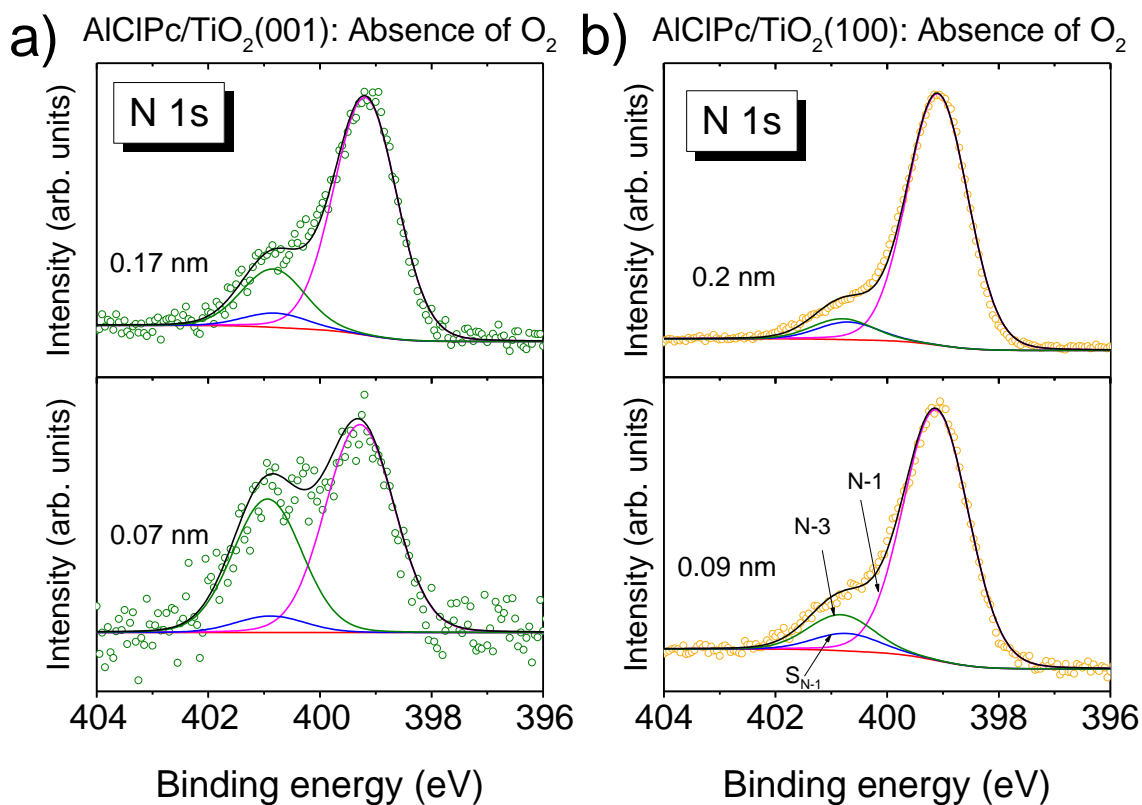


Figure 4.62 Comparison of sub-ML coverages of AlClPc on rutile a) TiO<sub>2</sub>(001) and b) TiO<sub>2</sub>(100) surfaces, both prepared in absence of oxygen. Spectra measured with Al K $\alpha$  radiation,  $h\nu = 1486.7$  eV. Reproduced from Ref. 89 with permission from the PCCP Owner Societies.

What is interesting, the interaction of phthalocyanine nitrogen with TiO<sub>2</sub> surface with defects present does not necessarily depend on the phthalocyanine type. Whether the phthalocyanine molecule is non-polar with a planar structure or polar like AlClPc presented in this work, the interaction is still observed, as was seen for both planar FePc and a ring substituted FePcF<sub>16</sub> at the interface to a defect-rich TiO<sub>2</sub> substrate.<sup>92</sup> Furthermore, as explained in Chapter 4.1.1.6, for polar phthalocyanines like AlClPc and VOPc, the adsorption geometry may influence the interface interaction, since the molecules may adsorb in Cl-, O- upwards or downwards configuration.<sup>122, 151</sup> While only single Cl-upwards configuration is observed for AlClPc at the surface of Au(111) single crystal<sup>122</sup> the same molecule exhibits both Cl-up and Cl-down configurations on Ag(111), where they are equally favored.<sup>73</sup> Presence of two molecular configurations may lead to splitting of the highest molecular orbital (HOMO) signal in the valence band spectrum,<sup>10, 13</sup> which however was not possible to resolve in the results presented within this work (see Chapters 4.2.2.4 and 4.3.2.4). If a random distribution of adsorption configurations is assumed, it is most probable that a strong interaction between the phthalocyanine

#### 4. Results and Discussion - 4.3 Interaction between halogen substituted organic semiconductor molecules (AlClPc) and TiO<sub>2</sub>(001) substrate

ring and the TiO<sub>2</sub> substrate is possible only for 50% of the molecules. The assumption can be confirmed by the N 1s spectra of AlClPc on the defect-rich (50% Ti<sup>3+</sup>) TiO<sub>2</sub>(001) surface, where almost half of the nitrogen atoms undergo an interaction with the substrate. What is more, it was shown that the four nitrogen atoms at the central metal atom of AlClPc take important role in accommodation of charges.<sup>121, 122</sup> Formation of interface states involving nitrogen atoms and substrates surface atoms was reported for phthalocyanines like ZnPc and H<sub>2</sub>Pc.<sup>121</sup> It is a possible explanation for the additional N-3 interface component, which can be seen only in N 1s spectra. Alternatively, the nitrogen atom could form a chemical bond with TiO<sub>2</sub> substrate. However, the N 1s core level signals belonging to the titanium nitride and oxynitride bonds, appear at lower binding energy than the signals registered for AlClPc.<sup>152</sup> Another more possible option is that part of nitrogen atoms of the phthalocyanine molecule are protonated, since a H-N bond is higher in binding energy than the -N= bond as shown in literature.<sup>153, 154</sup> Such protonation of bridging nitrogen atom at the periphery of the phthalocyanine ring, was used to explain the additional N 1s signal ZnPc on Cu(110) substrate. The source of the hydrogen could have been hydroxyl groups at the TiO<sub>2</sub> surface or other phthalocyanine molecules. The data presented in this work however, does not provide enough information to confirm such finding.

##### 4.3.2.3 Phthalocyanine metal center and central ligand related core levels

Further indication that the pathway for the interaction of phthalocyanine molecules at the interface to TiO<sub>2</sub> substrates leads mostly through nitrogen atoms can be based on spectra related to the central metal atom and the central ligand, perpendicular to the ring surface. Thickness dependent Cl 2p and Al 2p core level spectra are shown in Figure 4.63 and Figure 4.64 for AlClPc films deposited on substrates with 0% and 12% Ti<sup>3+</sup> component contribution.

Due to presence of noise, the spectra have been smoothed (see smoothed red line above the original data - black line) for the ease of spectra comparison. Thick films of Cl 2p spectra show a typical doublet at 199 eV and 198.9 eV for oxygen treated and reduced TiO<sub>2</sub>(001) surface respectively. The variation of peak position with the decrease of film thickness is less than ± 0.1 eV and can be assumed constant.

#### 4. Results and Discussion - 4.3 Interaction between halogen substituted organic semiconductor molecules (AICIPc) and TiO<sub>2</sub>(001) substrate

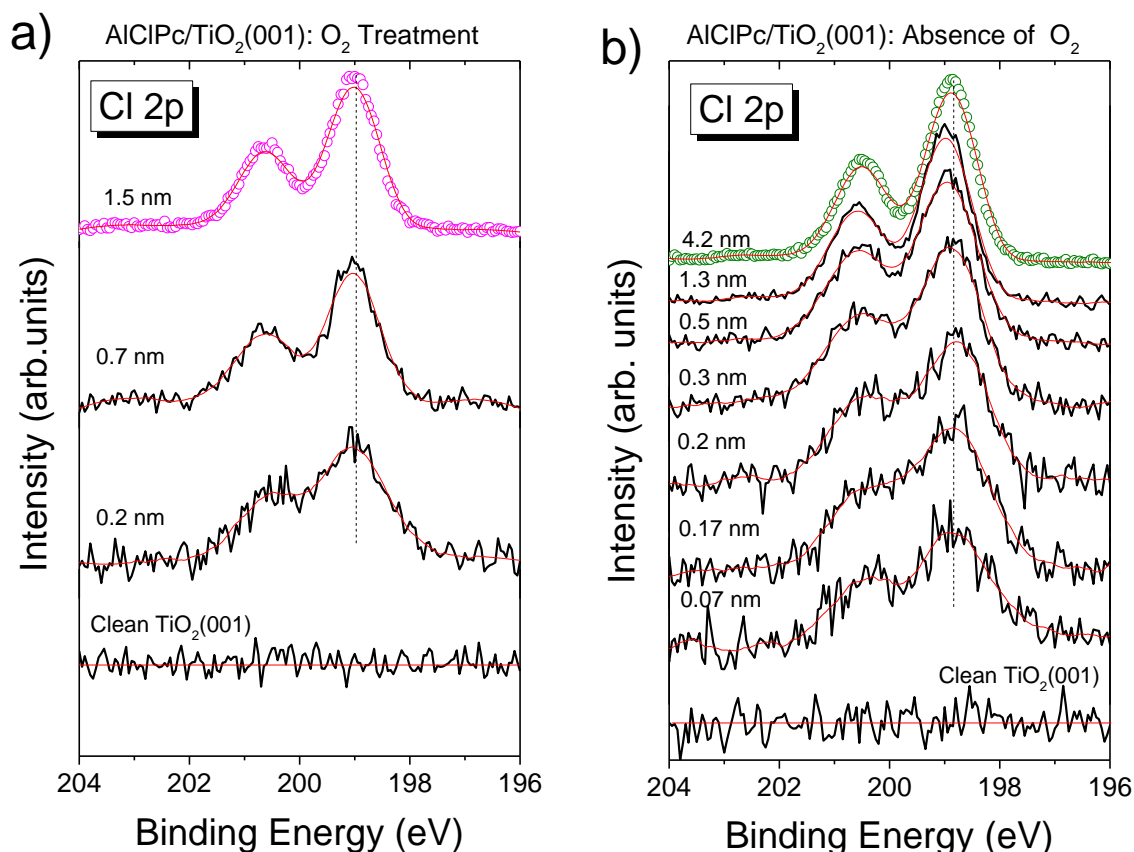


Figure 4.63 Thickness dependent Cl 2p spectra of AICIPc evaporated on: a) TiO<sub>2</sub>(001) treated with O<sub>2</sub>, b) TiO<sub>2</sub>(001) prepared in absence of O<sub>2</sub>. The red lines represent the original data after smoothing procedure for the ease of data comparison. Spectra measured with Al K $\alpha$  radiation,  $h\nu = 1486.7$  eV. Reproduced from Ref. 89 with permission from the PCCP Owner Societies.

One can clearly see that the chlorine spectra do not exhibit any additional features or even shoulders in the monolayer and sub-monolayer region as was observed on silver substrates. Formation of bonds with titanium atom is unlikely, since the signal would have to be present at low binding energy, which is not the case. The only effect present, is broadening of spectra for the smallest film coverage as was the case C 1s and N 1s spectra within this thickness region on both TiO<sub>2</sub>(100) and (001) oxidized and reduced surfaces.

The thickness dependent Al 2p core level spectra for both sample preparations are shown in Figure 4.64, however the analysis of Al 2p spectra is difficult due to the overlap with TiO<sub>2</sub> background and, high width of the Al 2p peak and noise, this is why these spectra have been smoothed as well (red line). The Al 2p spectra do not show any additional features, so there is no direct hint in the involvement of the metal center or central ligand in the interaction at the surface. Breaking of Al-Cl bonds and desorption of chlorine can be excluded based on the atomic ratios calculated from XPS results (see Table 23).

#### 4. Results and Discussion - 4.3 Interaction between halogen substituted organic semiconductor molecules (AlClPc) and TiO<sub>2</sub>(001) substrate

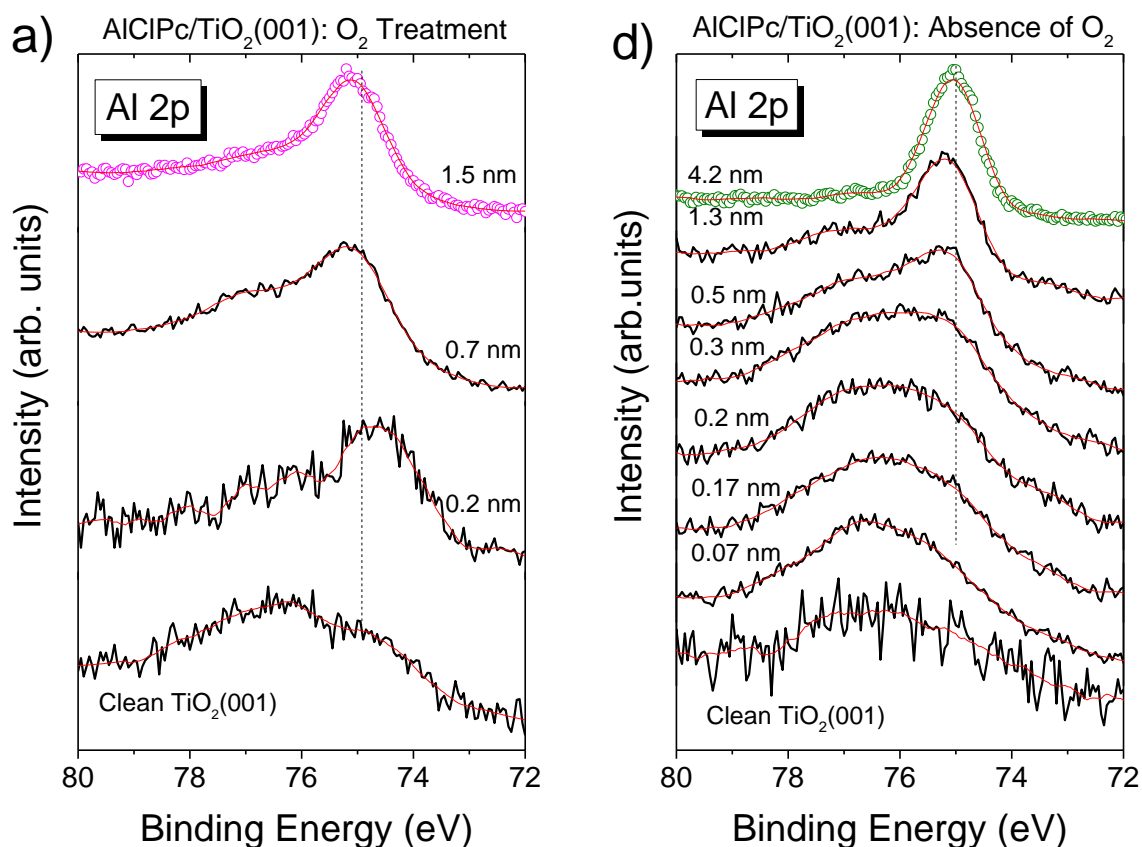


Figure 4.64 Al 2p spectra for: a) AlClPc on TiO<sub>2</sub>(001) treated with O<sub>2</sub>, b) AlClPc on TiO<sub>2</sub>(001) prepared in absence of O<sub>2</sub>. The red lines represent the original data after smoothing procedure for the ease of data comparison. Spectra measured with Al K $\alpha$  radiation,  $h\nu = 1486.7$  eV. Reproduced from Ref. 89 with permission from the PCCP Owner Societies.

##### 4.3.2.4 Electronic properties of AlClPc films on TiO<sub>2</sub>(001)

The UPS data for AlClPc films deposited on TiO<sub>2</sub>(001) surface prepared in presence and absence of oxygen are shown in Figure 4.65 and Figure 4.66 respectively. From SECO in (Figure 4.65a) one can read out the work function of a clean TiO<sub>2</sub>(001) surface which is 4.7 eV for the oxygen treated surface. Upon adsorption of AlClPc films the work function decreases to 4.4 eV as is observed for the thickest film. Since the surface was treated with oxygen to remove surface defects, the gap state signal is not present in the valence band spectra of the clean substrate. With the deposition of organic films, characteristic features of AlClPc arise, with a HOMO peak at 1.5 eV for the 1.5 nm thick film and a HOMO peak onset of 1.0 eV, which can be clearly seen in the HOMO region of the valence band spectrum in Figure 4.65c.

#### 4. Results and Discussion - 4.3 Interaction between halogen substituted organic semiconductor molecules (AICIPc) and TiO<sub>2</sub>(001) substrate

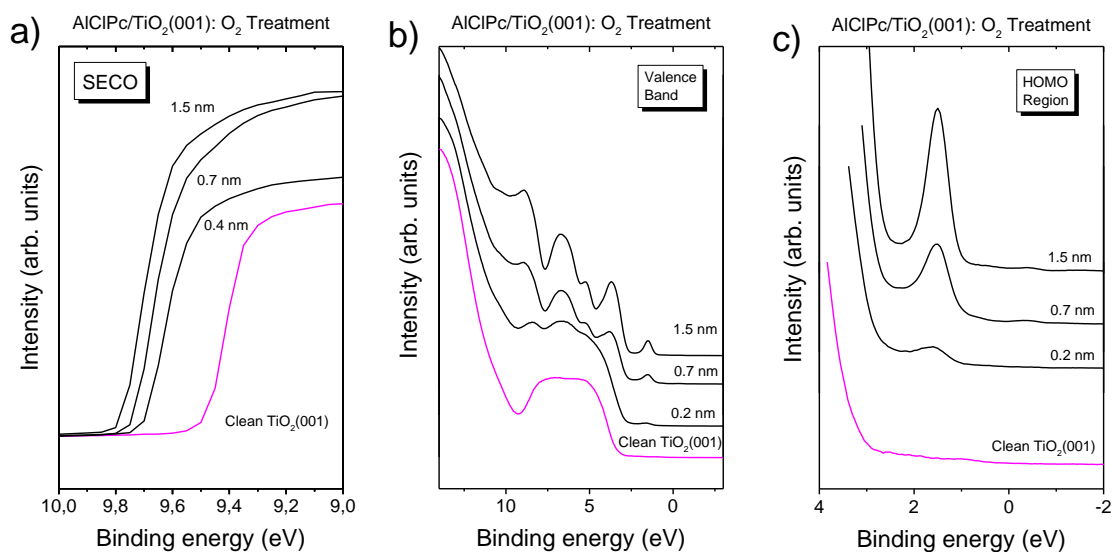


Figure 4.65 Thickness dependent UPS results measured for AICIPc films on TiO<sub>2</sub>(001) treated with oxygen: a) secondary electron cut-off, b) valence band spectra, c) valence band spectra – HOMO region. Spectra measured with He I radiation,  $h\nu = 21.2$  eV. Reproduced from Ref. 89 with permission from the PCCP Owner Societies.

The next figure (Figure 4.66a) gives information on the work function of AICIPc films on reduced (001) surface. A clean reduced TiO<sub>2</sub>(001) surface (12% of Ti<sup>3+</sup>) has work function of 4.7 eV. Upon AICIPc adsorption the work function decreases. It reaches a minimum value of 4.2 eV when the film thickness reaches the monolayer region of 0.3 nm. For the bulk film, the work function increases slightly to 4.4 eV, a value also observed for the bulk AICIPc film on the oxygen treated TiO<sub>2</sub>(001) surface.

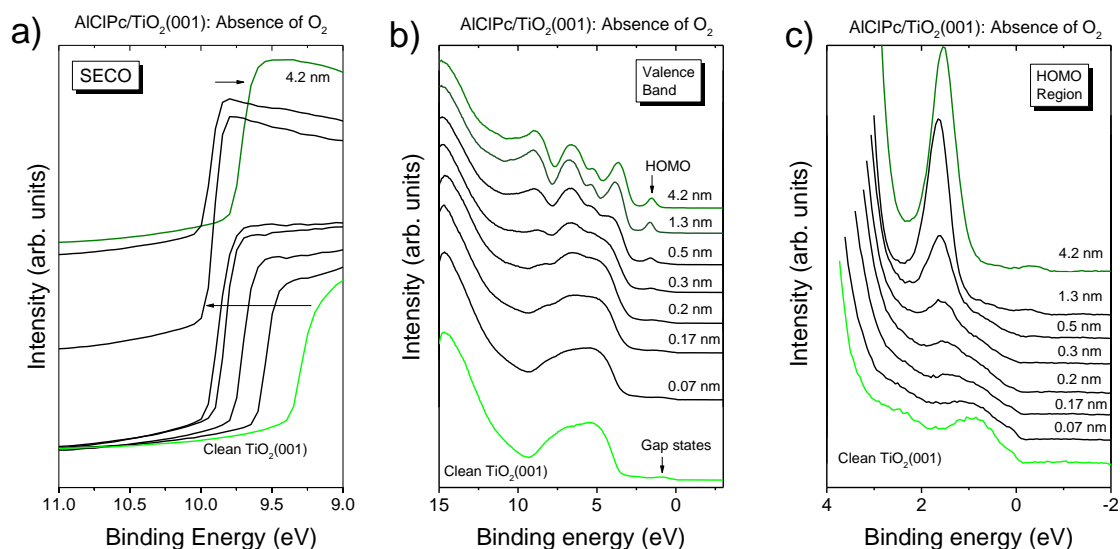


Figure 4.66 Thickness dependent UPS results measured for AICIPc films on TiO<sub>2</sub>(001) prepared in absence of oxygen: a) secondary electron cut-off, b) valence band spectra, c) valence band spectra – HOMO region. Spectra measured with He I radiation,  $h\nu = 21.2$  eV. Reproduced from Ref. 89 with permission from the PCCP Owner Societies.

#### 4. Results and Discussion - 4.3 Interaction between halogen substituted organic semiconductor molecules (AICIPc) and TiO<sub>2</sub>(001) substrate

On the other hand, the valence band spectrum of a clean TiO<sub>2</sub>(001) surface prepared in absence of oxygen shows increase in the intensity within the TiO<sub>2</sub> gap. It is expected for rutile to have a band gap of around 3.0 eV, but due to the preparation conditions the valence band edge is found at 3.4 eV. When magnified into HOMO peak region (Figure 4.66c), there is a broad peak related to gap states in spectrum of a clean substrate, with peak maximum found at around 0.8 eV. Increased background intensity within the band gap, up to Fermi edge is observed as well. Similar increase of intensity within the TiO<sub>2</sub> band gap was described in literature. In an investigation of effect of strain on 50 nm TiO<sub>2</sub> films, the additional intensity in band gap was explained as follows: application of stress causes rise in energy distribution of oxygen vacancies (n-type dopants) in the proximity of conduction band, which leads to an increase in carrier concentration (degenerate doping of TiO<sub>2</sub>) and metallic behavior of the semiconductor, as well as shift of conduction and valence band relative to Fermi edge. The authors state that the most of the carriers must come from bulk oxygen vacancies, rather than the ones located at the surface. Such semiconductor-to-metal transition upon application of strain is said to be reversible.<sup>155</sup> Based on the XPS results (see Overview spectra), the source of a strain in the reduced TiO<sub>2</sub> crystal structure might come from the implanted argon ions which can be seen in overview spectrum. The shift of conduction (and valence band) relative to Fermi edge could explain increased value of valence band onset leading to a band gap width higher than 3.0 eV, which is normally expected for rutile TiO<sub>2</sub>.

Another explanation for the additional intensity close to Fermi edge, was proposed based on investigation of anatase TiO<sub>2</sub> samples of different crystallinity. The gap states are divided into two regions: deep gap states, with maximum around 1.2 eV and shallow gap states around 0.2 eV below Fermi edge. While the deep gap states are due to under-coordinated Ti atoms in and near TiO<sub>2</sub> surface, present as an effect of oxygen vacancies formation (0D point defects), the authors postulate that the shallow gap states are due to excess electrons present at under-coordinated 4-fold Ti atoms (1D line defects). These one-dimensional defects are either step edges or imperfections of the cleavage plane. The shallow gap states are not formed due to missing oxygen within the TiO<sub>2</sub> structure. Based on their results, the authors excluded the possibility that the shallow gap states are caused due to crystal contaminations or additional titania phases. What is more, the valence band onset measured on anatase samples with shallow gap states also gave a band gap width greater than the expected value of 3.2 eV.<sup>156</sup> While both groups of authors propose different source of additional charges leading to the shallow gap states close to Fermi edge, they both agree that the source of the gap states are additional charge carriers, metallic in character, which is a characteristic of a degenerate semiconductor.

#### 4. Results and Discussion - 4.3 Interaction between halogen substituted organic semiconductor molecules (AlClPc) and TiO<sub>2</sub>(001) substrate

After deposition of AlClPc a HOMO peak arises, which intensity increases with film thickness. The HOMO peak overlaps partially with the gap states peak at lower film thicknesses, and has an onset at 0.9 eV. For a bulk like 4.2 nm film HOMO peak has maximum at 1.6 eV and onset at 1.0 eV which is close in value when compared to the oxygen treated surface. All values of work function, HOMO onset and ionization potential can be found in Table 24.

##### 4.3.2.5 Energy level diagrams

The data from Figure 4.65 and Figure 4.66 are summarized in form of energy level diagrams in Figure 4.67 for both preparations of TiO<sub>2</sub>(001) surface: oxygen treatment and absence of oxygen. As mentioned above, there is a decrease of work function upon AlClPc adsorption on both samples, followed by formation of a surface dipole: -0.3 eV and -0.5 eV for oxygen treated and reduced surface respectively. As was the case of (100) surface, the direction of surface dipole indicates a possible charge transfer from AlClPc films to the TiO<sub>2</sub> substrate. The factors influencing the work function value are discussed in 4.2.2.5 for TiO<sub>2</sub>(100) surface. Since formation of direct bonds with TiO<sub>2</sub> surface was not observed in XPS spectra, there is high chance that the decrease of work function at the interface between AlClPc and TiO<sub>2</sub> is caused by a push-back effect.

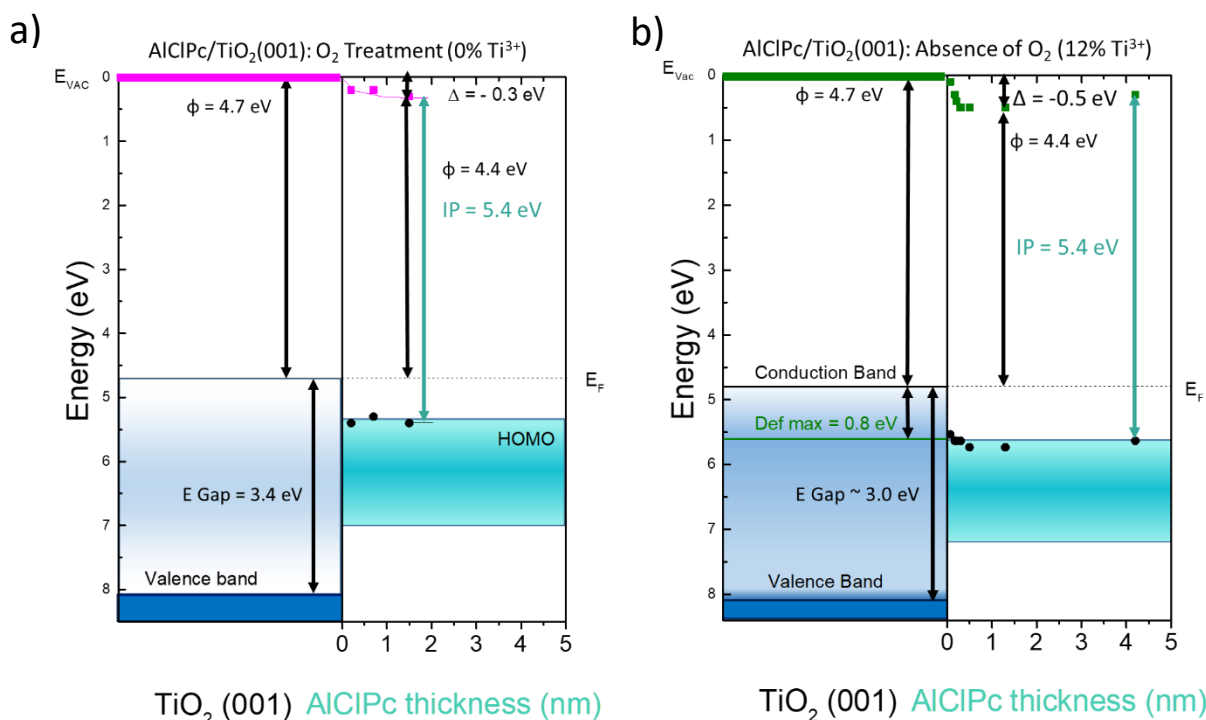


Figure 4.67 Energy level alignment for AlClPc films at the interface to TiO<sub>2</sub>(001) single crystal prepared: a) in presence of oxygen and b) absence of oxygen during preparation. Reproduced from Ref. 89 with permission from the PCCP Owner Societies.

Thick films of AlClPc for both preparations exhibit the same value of ionization potential (5.4 eV), which was observed on TiO<sub>2</sub>(100) surface and silver substrates as well.<sup>17</sup> The HOMO peak onset at low film

#### 4. Results and Discussion - 4.3 Interaction between halogen substituted organic semiconductor molecules (AlClPc) and TiO<sub>2</sub>(001) substrate

thickness is always at 1.0 eV binding energy, independent from preparation procedure. The HOMO level pinning takes place on (001) surface, similar to (100) surface. That means, even for an almost defect-free oxygen prepared TiO<sub>2</sub>(001) surface, there are few defects available at the surface for a pinning to happen, possibly due to defect migration towards the surface when the sample is heated,<sup>124</sup> or presence of step edges. It seems that the HOMO level pinning is independent on the substrate preparation and type (see (100) surface). The surfaces do however differ by the magnitude of surface dipoles formed.

##### 4.3.2.6 AlClPc film growth - substrate signal attenuation

To investigate the growth mode of AlClPc on TiO<sub>2</sub> single crystals, two approaches were used. The first one is through the measurement of substrate peak intensity decrease in XPS spectra. The second, is through microscopy: atomic force microscopy (AFM).

The absolute intensity of Ti 2p spectra shown in Figure 4.59b (TiO<sub>2</sub>(001) surface prepared in absence of oxygen, with 12% Ti<sup>3+</sup>) decreases upon consecutive deposition of AlClPc films. When plotted against the evaporation time (in seconds), the quotient of Ti 2p peak intensity at each evaporation step ( $I$ ) and the Ti 2p intensity of a clean TiO<sub>2</sub>(001) substrate ( $I_0$ ) gives a curve following an exponential decay. The data can be plotted in form of a natural logarithm  $\ln(I/I_0)$  against the evaporation time, as shown in Figure 4.68. For a layer-by-layer growth, the curve is expected to follow a straight line. In Figure 4.68 however, there is a clear break of a linear trend seen after 350 seconds of AlClPc deposition. The measurement point at this deposition time corresponds to the AlClPc film thickness of 0.5 nm. Such knick in the intensity decay points to a layer-island mode (also known as Stranski-Krastanov growth mode).<sup>157</sup> This means that first, a layer of molecules is formed. Once the layer is completed, islands of AlClPc molecules grow on top of it. As will be seen in the next part of this chapter, the presence of island is confirmed by the AFM results. The molecular orientation of phthalocyanine molecules within the film may influence it's the growth mode. The position of phthalocyanine ring, either parallel or perpendicular to the surface may promote stronger substrate-to-molecule interactions (leading to layer-by-layer growth) or stronger molecule-to-molecule interactions (leading to layer-island or island growth). It has been found that phthalocyanine molecules in a monolayer region of film thickness orient parallel to the substrate surface. At higher film thickness tilted<sup>92</sup> or even standing molecules<sup>76</sup>, perpendicular to the substrate surface, are observed.

#### 4. Results and Discussion - 4.3 Interaction between halogen substituted organic semiconductor molecules (AlClPc) and TiO<sub>2</sub>(001) substrate

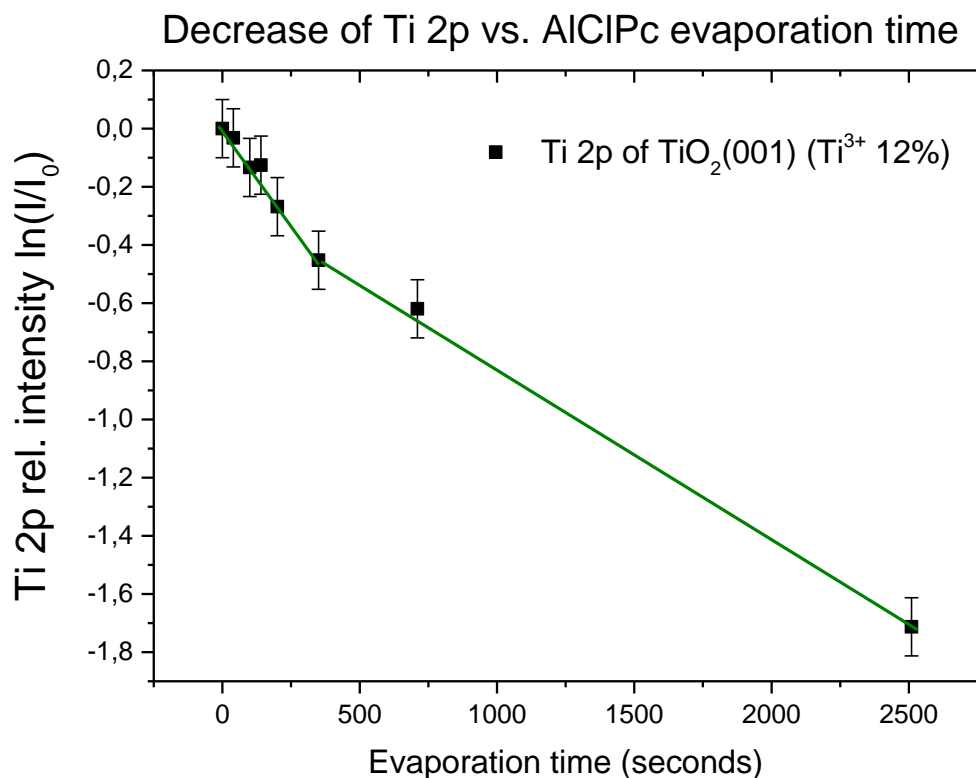


Figure 4.68 The exponential decay of the substrate Ti 2p peak upon evaporation of AlClPc films against the evaporation time (given in seconds).

##### 4.3.2.7 Microscopy images of AlClPc films

Microscopy images are helpful to confirm the findings of XPS, since they give a direct view onto the sample surface and are the simplest way to detect possible islands. TiO<sub>2</sub> substrates were characterized in chapter 4.3.1.4 for a clear picture of the state of sample before phthalocyanine evaporation. Next AlClPc thin films will be characterized in detail.

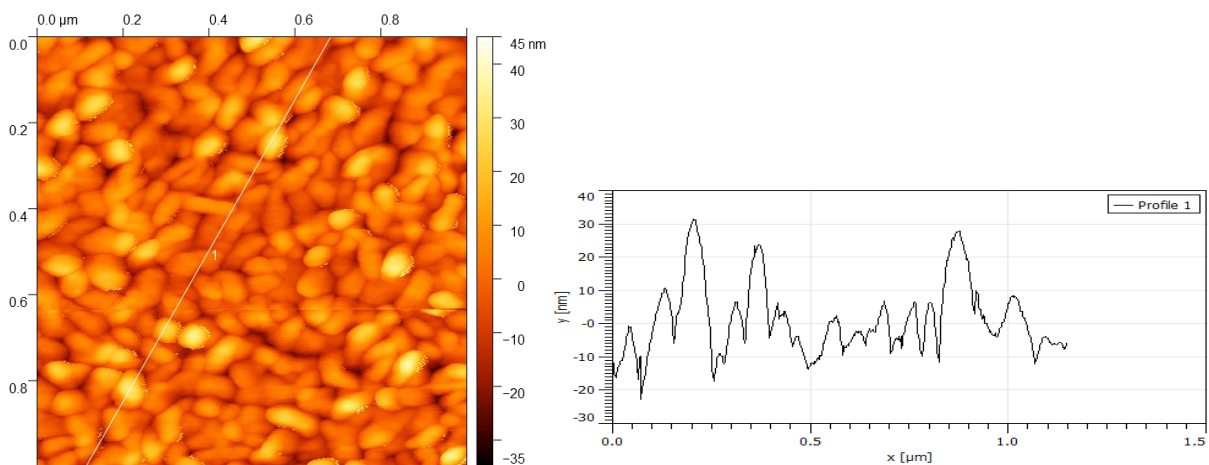


Figure 4.69 1  $\mu\text{m}$  x 1  $\mu\text{m}$  AFM image of a AlClPc thick film (evaporated in one step).

#### 4. Results and Discussion - 4.3 Interaction between halogen substituted organic semiconductor molecules (AlClPc) and TiO<sub>2</sub>(001) substrate

An image of a thick AlClPc film, evaporated in one step is shown in Figure 4.69. According to the evaporation time and rate the film thickness should be above 40 nm. The sample surface is densely populated with islands/grains of average width of 40 nm. The profile of a thick film is shown in the right side of Figure 4.69. The RMS measured at the profile is: 10.72 nm. The highest point in the profile is at 31.56 nm, while the minimum is at -22.98 on the height scale. The height difference between the minimum and maximum (peak-to-peak height) is 55 nm, which is in agreement with the evaporation parameters determined film thickness. Similar, well defined grains, were seen in thick film of another polar phthalocyanine VOPc on H-Si(111) substrate.<sup>158</sup>

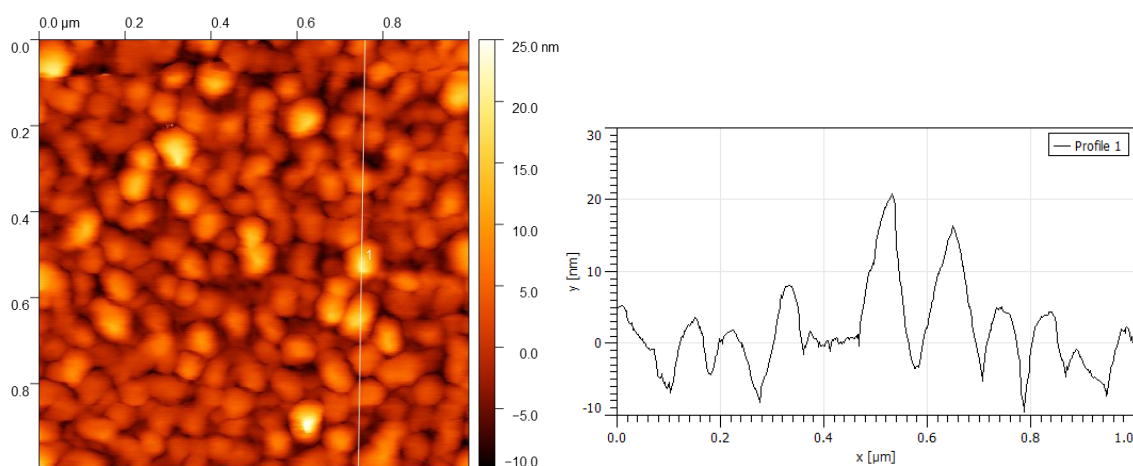


Figure 4.70 1  $\mu\text{m}$  x 1  $\mu\text{m}$  AFM image of 4.2 nm thick film of AlClPc on TiO<sub>2</sub>(001) with 12% defects.

A thin film of AlClPc with a thickness equivalent to a layer-by-layer 4.2 nm thick film (see 4.2 nm film of AlClPc on TiO<sub>2</sub>(001) treated without oxygen with 12% of Ti<sup>3+</sup> contribution to Ti 2p in Chapter 4.3.1.2) is presented in Figure 4.70. Grains are also visible at the surface of the sample. A profile of the sample surface is shown on the right side of Figure 4.70. The minimum height is at -9.09 nm and maximum is at 20.08 nm, giving the height difference of 30.7 nm. As expected it is smaller than the height difference of the grains in thick film shown in Figure 4.69. The RMS of the 4.2 nm AlClPc film is also smaller 5.84 nm. The islands/grains of the 4.2 nm film are lower and broader (average width 60 nm) and more uniform while the sample surface is less rough than the thick film.

An equivalent of a layer-by-layer 1.4 nm film on a defect-rich surface with 50% Ti<sup>3+</sup> contribution (see Supporting information, Chapter 6.4) is shown in Figure 4.71. The first difference seen in this Figure is that the size distribution of islands is broader. One can clearly see small islands coexisting with large area islands. A profile taken in the Figure 4.71 has a minimum on the height scale at -11.19 nm and maximum at 33.12 nm. The RMS of the AlClPc on the defect rich (001) surface is 11.64 nm which is much higher than on a surface with less defects. There are some flat spaces between the islands on the defect rich surface, unlike the thicker film on the surface with less defects, where the islands are more densely packed.

#### 4. Results and Discussion - 4.3 Interaction between halogen substituted organic semiconductor molecules (AlClPc) and TiO<sub>2</sub>(001) substrate

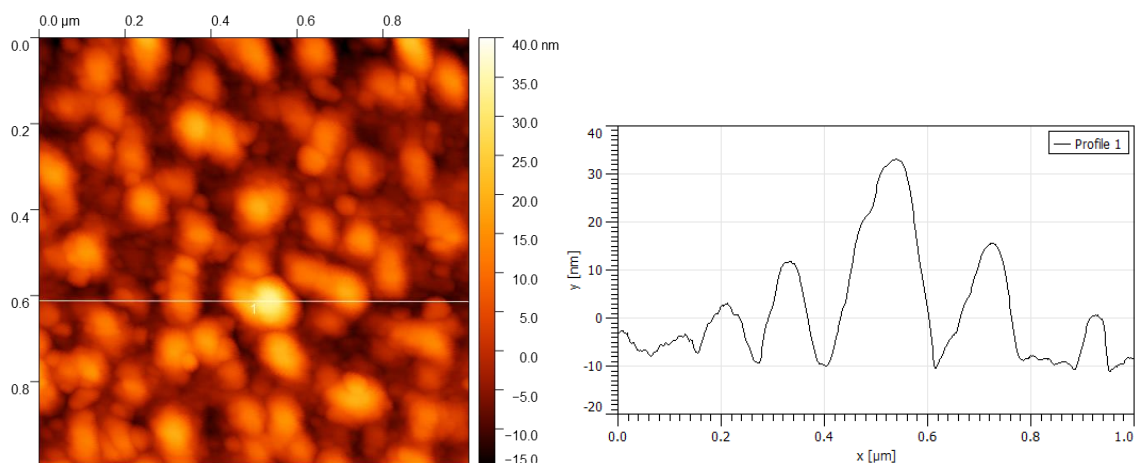


Figure 4.71 A defect-rich (50%) TiO<sub>2</sub>(001) surface covered with AlClPc film, equivalent of a 1.4 nm layer-by-layer film.

The film on the defect-rich (001) surface will be used for further comparison with AlClPc films on the defect-rich TiO<sub>2</sub>(100) surface. It can be assumed that the changes in the film morphology between the samples are due to variation in preparation of substrate surface, since all the AlClPc films presented in this chapter were evaporated with the same evaporation conditions and evaporation rate of 2 Å/min. The AFM results have confirmed presence of islands of AlClPc on TiO<sub>2</sub>(001) surface with a height greater than predicted by XPS measurements. Based on the acquired information it is likely that the growth mode is layer-island growth. An example of phthalocyanine layer-island growth can be found in literature: STM images have shown that SnPc (a non-planar phthalocyanine as AlClPc) on Ag(111) surface has similar growth mode. At the beginning the molecules grow in layer-by-layer mode, the third layer exhibits island formation, with consecutive island growth.<sup>159</sup>

##### 4.3.3 Chapter summary

A clear interaction between AlClPc with reduced TiO<sub>2</sub>(001) surface (with the characteristic Ti<sup>3+</sup> shoulder of Ti 2p spectrum and additional diffraction spots in the LEED diffraction pattern) can be seen in nitrogen core level spectra of phthalocyanine films. The interaction is reduced to minimum when the amount of defects is decreased through the use of oxygen during substrate preparation. An oxygen treated surface exhibits a (1 x 1) surface reconstruction and shows no signs of Ti<sup>3+</sup> component in Ti 2p core level spectra, which is additional indication that the degree of interaction is bound with the degree of reduction of the TiO<sub>2</sub>(001) single crystal. While nitrogen atoms clearly undergo an interaction, the other atoms within the molecule both in the ring and center of phthalocyanine seem to be unaffected. They do not exhibit any additional features, especially in the low binding energy region which could imply presence of direct bonds with titanium atoms. The binding energy of the additional nitrogen component points to a charge transfer from AlClPc to TiO<sub>2</sub>, similar to related interfaces between

#### 4. Results and Discussion - 4.3 Interaction between halogen substituted organic semiconductor molecules (AlClPc) and TiO<sub>2</sub>(001) substrate

phthalocyanines and TiO<sub>2</sub> substrates.<sup>92, 121</sup> Although no Ti<sup>3+</sup> features are present in the Ti 2p spectrum of oxygen treated TiO<sub>2</sub>(001), some defects must be present at the surface since the HOMO level is aligned with the maximum of defects states present in the TiO<sub>2</sub> band gap.

AlClPc molecules have been found to form islands on TiO<sub>2</sub>(001) surface, as observed in AFM images for surfaces at different reduction degree. A thick AlClPc film with islands of similar dimensions shows high roughness. The roughness decreases with film thickness, as seen for the film recorded on substrate with 12% Ti<sup>3+</sup> contribution. The islands areas are rather uniform. An increase in Ti<sup>3+</sup> contribution to 50% leads to a broader island size distribution. No matter the film thickness, the islands are dense on TiO<sub>2</sub>(001) substrate. This is in line with the XPS results, which show that the film grows in the layer-island (Stranski-Krastanov) mode.

## 5. Conclusions - 4.3 Interaction between halogen substituted organic semiconductor molecules (AlClPc) and TiO<sub>2</sub>(001) substrate

### 5. Conclusions

In the research presented within this thesis, it has been found that the choice of a substrate material influences the interaction at the interface with phthalocyanine films. Different parts of phthalocyanine molecule are affected if the substrate is metal (silver) or an oxide (titanium dioxide). On silver substrates the main interaction pathway is connected with the central metal ligand (chlorine atom) and on TiO<sub>2</sub> the phthalocyanine interacts mainly through nitrogen atoms of the phthalocyanine ring.

Although ionization potential of AlClPc molecule does not change much upon adsorption on Ag and TiO<sub>2</sub> and the electrons are transferred from the organic molecules to both metal and oxide substrates, the reaction pathway differs between the interfaces. In the first case, the molecule center is influenced by strong interaction with silver substrate, independently on the type of silver substrate used. The chlorine ligand detaches from the phthalocyanine molecule and forms a bond with silver substrate, leading to formation of Ag-Cl bond at the molecule-substrate interface.

The chemical reaction is related to the central metal atom ligand, while the phthalocyanine ring stays intact, which points to the presence of AlPc at the silver substrate surface. The on-surface dechlorination of phthalocyanine molecule under vacuum, through the reaction with silver substrates could be an alternative method of obtaining a reactive AlPc molecule, to the one presented in literature, where metal free phthalocyanine is metalated with aluminum atoms.<sup>160</sup> Such reactive molecule has paramagnetic properties and is interesting for possible application as a molecular magnet.

Further aspects which have to be taken into consideration, when discussing the interface between AlClPc and titanium dioxide are the surface orientation, and the degree of TiO<sub>2</sub> reduction. Both were found to have influence on extent of interaction between TiO<sub>2</sub> and AlClPc and growth mode of phthalocyanine films.

In case of reduced single crystals prepared in absence of oxygen, the molecules interact with crystal surface through the nitrogen atom. Although an interaction takes place, the remaining phthalocyanine ring atoms are only slightly affected and the phthalocyanine ring stays intact. The molecule metal center, as well as the chlorine ligand seem to be unaffected. Single crystals can be considered a model system to investigate the interaction with organic molecules. The complexity of an oxide single crystal in terms of preparation and the preparation outcome, makes of course the model more complicated, leads however to new ways to control the extent of the chemical reaction at the oxide single crystal surface. As shown in this work, the reaction probability rises on the reduced surfaces, due to the presence of defects at the crystal surface. The surfaces undergo faceting and possess several types of defects, which can act as reaction centers (point defects like oxygen vacancies, dislocations). They can

## 5. Conclusions - 4.3 Interaction between halogen substituted organic semiconductor molecules (AlClPc) and TiO<sub>2</sub>(001) substrate

as well lead to specific growth of the organic film. The LEED measurements confirm that defects are not limited to the bulk or sub-surface region of the substrates. Therefore, it might be expected that the reduced surfaces are also more prone to react with the phthalocyanine molecules. The interaction is affected by the orientation of TiO<sub>2</sub> surface. The TiO<sub>2</sub>(100) surface appears more inert compared to the TiO<sub>2</sub>(001), which is most likely related to the 5-fold coordination of surface Ti atoms, against the less energetically stable 4-fold coordinated Ti atoms on (001) surface. The number of defects in the topmost layer might also differ between both orientations. We show that interface interactions can be suppressed to a large extent for both TiO<sub>2</sub>(100) and (001) surfaces by an oxygen exposure during the annealing steps, resulting in a re-oxidation of the surface and diminishing the amount of surface defects.<sup>89</sup> The pinning of AlClPc HOMO level at TiO<sub>2</sub> defect maximum seen in valence band spectra of all samples, no matter the preparation type, points to existence of defects even in samples treated with oxygen. The amount of surface defects is never zero.

The results for AlClPc on TiO<sub>2</sub> surface show also, that nitrogen atom is an important probe for phthalocyanine interaction and should be given attention when investigating interfaces for designing any phthalocyanine based elements in a multi-layer architecture devices.

The interaction with only part of nitrogen atoms within molecule (similar behavior was observed for AlClPc/Au(111)<sup>122</sup>) points to a strong interaction of the incomplete ML with the TiO<sub>2</sub> substrate, well seen on the reduced substrates. Upon AlClPc evaporation the work function of AlClPc/TiO<sub>2</sub> system decreases, till the film thickness of around 0.3 nm where the work function value has its minimum. At this film thickness a complete monolayer of AlClPc molecules is formed (a ML thickness of AlClPc is around 0.3 nm). The film thickness at which the work function reaches its minimum value coincides with the thickness of AlClPc monolayer. It is possible, that upon formation of a complete monolayer the further layers are decoupled from the substrate, due to a stronger molecule to molecule interaction than the substrate to molecule interaction upon formation of a ML. The decoupling leads to an increase in film work function as the film thickness grows (seen for films with thickness above 1 nm). Additionally, a strong molecule to molecule interaction over the substrate to molecule interaction leads to an island growth of organic film. Such island formation was observed on all investigated TiO<sub>2</sub> substrates, as seen in AFM and SEM results.

Based on our investigations we confirm the layer-island film growth on the TiO<sub>2</sub>(001) surface and a decoupling of AlClPc film from the substrate upon a complete ML formation. Before the ML is formed, AlClPc molecules undergo a charge reorganization within the molecule, due to the interaction with TiO<sub>2</sub> substrates, which results in nitrogen atoms with two distinct chemical environments. For

## 5. Conclusions - 4.3 Interaction between halogen substituted organic semiconductor molecules (AIClPc) and TiO<sub>2</sub>(001) substrate

TiO<sub>2</sub>(100) surface from the microscopy results only, island-only growth was proposed, however in light of the work function results, the layer-island film growth might not be impossible.

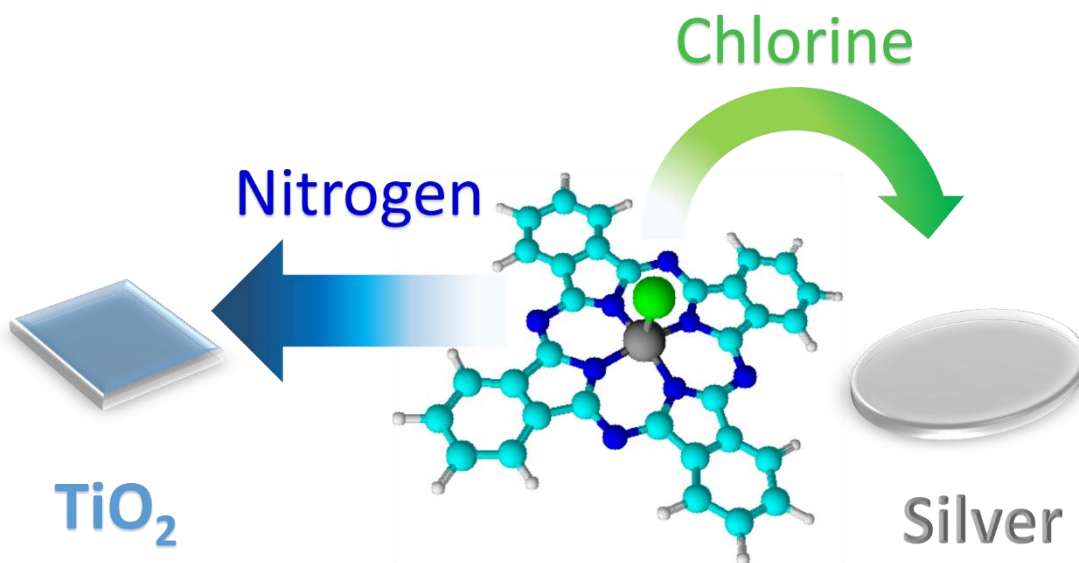


Figure 5.1. Graphic representation of interactions of AIClPc at the interface to silver and TiO<sub>2</sub> substrates.

Unlike the Ag surface, where the AIClPc molecule undergoes chemisorption and loses a chlorine atom, due to Ag-Cl bond formation with silver surface, on TiO<sub>2</sub> chlorine is not affected by a chemical reaction. The energy level alignment diagrams indicate that there is possibility of charge transfer from AIClPc film into TiO<sub>2</sub>. Charge transfer to TiO<sub>2</sub> might be the reason behind the presence of two differently charged nitrogen atoms.

## 6. Appendix

### 6.1 Abbreviations

AFM	Atomic Force Microscopy
AgCl	Silver Chloride
AgF	Silver Fluoride
AlClPc	Chloroaluminum(III) Phthalocyanine
AlFPc	Fluoroaluminum(III) Phthalocyanine
IP	Ionization Potential
ML	Monolayer
SEM	Scanning Electron Microscopy
Sub-ML	Sub-Monolayer
TiO <sub>2</sub>	Titanium dioxide
UPS	Ultra-Violet Photoelectron Spectroscopy
WF	Work Function
XPS	X-ray Photoelectron Spectroscopy

## 6. Appendix - 6.2 Fitting tables

### 6.2 Fitting tables

#### 6.2.1 AlClPc on Ag(100)

Table 4. C 1s core level fitting parameters of AlClPc on Ag(100) single crystal.

AlClPc on Ag(100)												
Thickness	Layer thickness 0.4 nm				Layer thickness 0.5 nm				Layer thickness 2.6 nm			
Peak name	C-1	C-2	Sc-1	Sc-2	C-1	C-2	Sc-1	Sc-2	C-1	C-2	Sc-1	Sc-2
GP-FWHM/eV	1.2	1.2	1.2	1.2	1.2	1.2	1.2	1.2	1.1	1.1	1.1	1.1
Position	284.46	1.2	1.9	3.1	284.75	1.31	1.9	3.21	284.75	1.39	1.9	3.29
LP-FWHM/eV	0.31	0.31	0.31	0.31	0.31	0.31	0.31	0.31	0.31	0.31	0.31	0.31
Rel. area	0.72	0.20	0.04	0.03	0.71	0.22	0.04	0.03	0.68	0.22	0.05	0.05
	0.30	$(C-2+S_{C-2})/(C-1+S_{C-1})$			0.34	$(C-2+S_{C-2})/(C-1+S_{C-1})$			0.36	$(C-2+S_{C-2})/(C-1+S_{C-1})$		

Table 5. N 1s core level spectra fitting parameters of AlClPc films on Ag(100) single crystal.

AlClPc on Ag(100)											
Thickness	0.3 nm		0.4 nm		0.5 nm		1.0 nm		2.6 nm		
Peak name	N-1	S <sub>N-1</sub>									
GP-FWHM/eV	2.20	2.20	2.16	2.16	2.13	2.13	1.83	1.83	1.69	1.69	
Position/eV	398.45	400.05	398.63	400.23	398.88	400.48	399.01	400.61	399.05	400.65	
LP-FWHM/eV	0.1	0.1	0.1	0.1	0.1	0.1	0.1	0.1	0.1	0.1	
Relative area	0.91	0.09	0.49	0.51	0.33	0.67	0.91	0.09	0.91	0.09	

Table 6. Cl 2p core level spectra fitting parameters of AlClPc films on Ag(100) single crystal.

AlClPc on Ag(100)							
Thickness		0.4 nm		0.5 nm		2.6 nm	
Doublet name		Cl -1	Cl-2	Cl -1	Cl-2	Cl -1	Cl-2
GP-FWHM/eV	P1	1.1	1.1	1.2	1.2	1.1	1.1
	P2	1.1	1.1	1.2	1.2	1.1	1.1
Position/eV	P1	199.1	198.0	199.0	197.8	199.1	197.9
	P2	200.7	199.6	200.6	199.4	200.7	199.5
LP-FWHM/eV	P1	0.3	0.3	0.3	0.3	0.3	0.3
	P2	0.3	0.3	0.3	0.3	0.3	0.3
Relative area	P1+P2	0.43	0.57	0.49	0.51	0.94	0.06

## 6.2.2 AlClPc on Ag foil

Table 7. C 1s core level fitting parameters of AlClPc on silver substrate: Ag foil.

AlClPc on Ag foil												
Thickness	Layer thickness 0.2 nm				Layer thickness 0.7 nm				Layer thickness 2.4 nm			
Peak name	C-1	C-2	S <sub>C-1</sub>	S <sub>C-2</sub>	C-1	C-2	S <sub>C-1</sub>	S <sub>C-2</sub>	C-1	C-2	S <sub>C-1</sub>	S <sub>C-2</sub>
GP-FWHM/eV	1.3	1.3	1.3	1.3	1.1	1.1	1.1	1.1	0.9	0.9	0.9	0.9
Position/eV	284.40	285.40	286.30	287.30	284.46	285.71	286.36	287.61	284.47	285.87	286.37	287.77
LP-FWHM/eV	0.3	0.3	0.3	0.3	0.3	0.3	0.3	0.3	0.3	0.3	0.3	0.3
Rel. Area	0.73	0.20	0.04	0.03	0.71	0.20	0.04	0.05	0.68	0.22	0.05	0.05
	0.25	$(C-2+S_{C-2})/(C-1+S_{C-1})$			0.33	$(C-2+S_{C-2})/(C-1+S_{C-1})$			0.37	$(C-2+S_{C-2})/(C-1+S_{C-1})$		

Table 8. N 1s core level spectra fitting parameters of AlClPc deposited on Ag foil.

AlClPc on Ag foil						
Thickness	0.2 nm		0.7 nm		2.4 nm	
Peak name	N-1	S <sub>N-1</sub>	N-1	S <sub>N-1</sub>	N-1	S <sub>N-1</sub>
GP-FWHM/eV	1.4	1.4	1.4	1.4	1.4	1.4
Position/eV	398.58	400.18	398.74	400.34	398.94	400.54
LP-FWHM/eV	0.1	0.1	0.1	0.1	0.1	0.1
Relative Area	0.95	0.05	0.95	0.05	0.94	0.06

Table 9. Cl 2p core level fitting parameters of AlClPc on Ag foil.

AlClPc on Ag foil							
Thickness		0.2 nm		0.7 nm		2.4 nm	
Doublet name		Cl -1	Cl-2	Cl -1	Cl-2	Cl -1	Cl-2
GP-FWHM/eV	P1	1.3	1.3	1.2	1.2	1.3	1.3
	P2	1.3	1.3	1.2	1.2	1.3	1.3
Position/eV	P1	199.0	197.7	198.8	197.6	198.8	197.5
	P2	200.6	199.3	200.4	199.2	200.4	199.1
LP-FWHM/eV	P1	0.3	0.3	0.3	0.3	0.3	0.3
	P2	0.3	0.3	0.3	0.3	0.3	0.3
Relative area	P1+P2	0.25	0.75	0.50	0.50	0.89	0.11

## 6. Appendix - 6.2 Fitting tables

### 6.2.3 AlFPc on Ag foil

Table 10. Fitting parameters of C 1s core level spectra of AlFPc films deposited on Ag foil.

AlFPc on Ag foil				
Film thickness 0.6 nm				
Peak name	C-1	C-2	S <sub>C-1</sub>	S <sub>C-2</sub>
GP-FWHM/eV	1.3	1.3	1.3	1.3
Position/eV	284.9	286.1	286.8	288.0
LP-FWHM/eV	0.01	0.01	0.01	0.01
rel. Area	0.73	0.20	0.04	0.03
		0.29	$(C-2+S_{C-2})/(C-1+S_{C-1})$	
Film thickness 0.9 nm				
Peak name	C-1	C-2	S <sub>C-1</sub>	S <sub>C-2</sub>
GP-FWHM/eV	1.3	1.3	1.3	1.3
Position/eV	284.9	286.1	286.8	288.0
LP-FWHM/eV	0.01	0.01	0.01	0.01
rel. Area	0.71	0.21	0.04	0.04
		0.33	$(C-2+S_{C-2})/(C-1+S_{C-1})$	
Film thickness 1.1 nm				
Peak name	C-1	C-2	S <sub>C-1</sub>	S <sub>C-2</sub>
GP-FWHM/eV	1.3	1.3	1.3	1.3
Position/eV	284.9	286.1	286.8	288.0
LP-FWHM/eV	0.01	0.01	0.01	0.01
rel. Area	0.71	0.21	0.04	0.04
		0.33	$(C-2+S_{C-2})/(C-1+S_{C-1})$	
Film thickness 1.6 nm				
Peak name	C-1	C-2	S <sub>C-1</sub>	S <sub>C-2</sub>
GP-FWHM/eV	1.2	1.2	1.2	1.2
Position/eV	284.9	286.1	286.8	288.1
LP-FWHM/eV	0.01	0.01	0.01	0.01
rel. Area	0.71	0.21	0.04	0.04
		0.33	$(C-2+S_{C-2})/(C-1+S_{C-1})$	

Table 11. Fitting parameters of thickness dependent N 1s core level spectra of AlFPc films deposited on Ag foil.

AlFPc on Ag foil								
Thickness	0.6 nm		0.9 nm		1.1 nm		1.6 nm	
Peak name	N-1	S <sub>N-1</sub>						
GP-FWHM/eV	1.2	1.2	1.2	1.2	1.2	1.2	1.2	1.2
Position/eV	398.87	400.47	398.94	400.54	399.04	400.64	399.04	400.64
LP-FWHM/eV	0.1	0.1	0.1	0.1	0.1	0.1	0.1	0.1
relative Area	0.95	0.05	0.95	0.05	0.95	0.05	0.95	0.05

6.2.4 AlClPc on TiO<sub>2</sub>(100)Table 12. Fitting parameters: Ti 2p peak of TiO<sub>2</sub>(100) prepared with oxygen treatment during an annealing step.

		AlClPc/TiO <sub>2</sub> (100): O <sub>2</sub> treatment					
		Film thickness (nm)					
		0 nm			1.2 nm		
Doublet name		Ti <sup>4+</sup>	Sat1	Sat2	Ti <sup>4+</sup>	Sat1	Sat2
Position/eV	P1	459.5	462.5	472.8	459.5	462.5	472.9
	P2	465.2	468.2	478.5	465.2	468.2	478.6
GP-FWHM/eV	P1	0.8	1.7	2.5	0.8	1.6	2.3
	P2	1.5	1.7	2.5	1.5	1.6	2.3
LP-FWHM/eV	P1	0.5	0.5	0.5	0.5	0.5	0.5
	P2	0.6	0.5	0.6	0.6	0.5	0.6
Relative Area	P1+P2	0.86	0.02	0.12	0.86	0.02	0.12

Table 13. Fitting parameters: Ti 2p peak of TiO<sub>2</sub>(100) prepared without oxygen treatment during an annealing step.

		AlClPc/TiO <sub>2</sub> (100): Absence of O <sub>2</sub>							
		Film thickness (nm)							
		0 nm				1.3 nm			
Doublet name		Ti <sup>4+</sup>	Ti <sup>3+</sup>	Sat1	Sat2	Ti <sup>4+</sup>	Ti <sup>3+</sup>	Sat1	Sat2
Position/eV	P1	459.3	457.4	462.3	472.6	459.4	457.5	462.4	472.7
	P2	465.0	463.1	468.0	478.3	465.1	463.2	468.1	478.4
GP-FWHM/eV	P1	1.0	1.1	2.1	3.1	1.0	1.1	2.0	2.7
	P2	1.9	1.4	2.1	3.1	1.8	1.3	2.0	2.7
LP-FWHM/eV	P1	0.5	0.5	0.5	0.5	0.5	0.5	0.5	0.5
	P2	0.6	0.5	0.5	0.5	0.6	0.5	0.5	0.5
Relative Area	P1+	0.74	0.14	0.02	0.11	0.78	0.10	0.02	0.10
	Ti <sup>3+</sup> /(Ti <sup>3+</sup> +Ti <sup>4+</sup> )	0.16				0.11			

Table 14. Fitting parameters: O 1s peak of TiO<sub>2</sub>(100) prepared with and without oxygen treatment during annealing.

		AlClPc/TiO <sub>2</sub> (100): O <sub>2</sub> treatment		AlClPc/TiO <sub>2</sub> (100): Absence of O <sub>2</sub>	
		Clean Substrate			
Doublet name		O-1	O-2	O-1	O-2
Position/eV		530.8	531.9	530.6	531.7
GP-FWHM/eV		1.0	1.1	1.0	1.1
LP-FWHM/eV		0.1	0.1	0.1	0.1
Relative Area		0.97	0.03	0.91	0.09

## 6. Appendix - 6.2 Fitting tables

Table 15. C 1s core level spectra fitting parameters of AlClPc films on TiO<sub>2</sub>(100) surface.

AlClPc/TiO <sub>2</sub> (100): O <sub>2</sub> treatment												
	Layer thickness 0.1 nm				Layer thickness 0.4 nm				Layer thickness 1.2 nm			
Peak name	C - 1	C - 2	S <sub>(C-1)</sub>	S <sub>(C-2)</sub>	C - 1	C - 2	S <sub>(C-1)</sub>	S <sub>(C-2)</sub>	C - 1	C - 2	S <sub>(C-1)</sub>	S <sub>(C-2)</sub>
GP-FWHM/eV	1.0	1.0	1.0	1.0	1.0	1.0	1.0	1.0	1.0	1.0	1.0	1.0
Position/eV	284.8	286.1	286.6	288.1	284.8	286.1	286.6	288.1	284.8	286.1	286.6	288.1
LP-FWHM/eV	0.1	0.1	0.1	0.1	0.1	0.1	0.1	0.1	0.1	0.1	0.1	0.1
rel. Area	0.67	0.20	0,08	0.05	0.67	0.20	0,08	0.05	0.67	0.20	0,08	0.05
	$(C-2+S_{C-2})/(C-1+S_{C-1})$		0.33		$(C-2+S_{C-2})/(C-1+S_{C-1})$		0.34		$(C-2+S_{C-2})/(C-1+S_{C-1})$		0.34	
AlClPc/TiO <sub>2</sub> (100): Absence of O <sub>2</sub>												
	Layer thickness 0.1 nm				Layer thickness 0.3 nm				Layer thickness 1.3 nm			
Peak name	C - 1	C - 2	S <sub>(C-1)</sub>	S <sub>(C-2)</sub>	C - 1	C - 2	S <sub>(C-1)</sub>	S <sub>(C-2)</sub>	C - 1	C - 2	S <sub>(C-1)</sub>	S <sub>(C-2)</sub>
GP-FWHM/eV	1.1	1.1	1.1	1.1	1.0	1.0	1.0	1.0	0.9	0.9	0.9	0.9
Position/eV	284.6	285.8	286.4	287.8	284.6	285.9	286.4	287.9	284.6	286.0	286.4	288.0
LP-FWHM/eV	0.1	0.1	0.1	0.1	0.1	0.1	0.1	0.1	0.1	0.1	0.1	0.1
rel. Area	0.67	0.20	0.08	0.05	0.67	0.20	0.08	0.05	0.67	0.20	0.08	0.05
	$(C-2+S_{C-2})/(C-1+S_{C-1})$		0.34		$(C-2+S_{C-2})/(C-1+S_{C-1})$		0.34		$(C-2+S_{C-2})/(C-1+S_{C-1})$		0.34	

Table 16. N 1s core level spectra fitting parameters of AlClPc films on TiO<sub>2</sub>(100) surface.

AlClPc/TiO <sub>2</sub> (100): O <sub>2</sub> treatment									
	Layer thickness 0.1 nm			Layer thickness 0.4 nm			Layer thickness 1.2 nm		
Peak name	N-1	S <sub>(N-1)</sub>	N-3	N-1	S <sub>(N-1)</sub>	N-3	N-1	S <sub>(N-1)</sub>	N-3
GP-FWHM/eV	1.2	1.2	1.2	1.1	1.1	1.1	1.1	1.1	1.1
Position/eV	399.3	400.9	401.0	399.3	400.9	401.0	399.3	400.9	401.0
LP-FWHM/eV	0.1	0.1	0.1	0.1	0.1	0.1	0.1	0.1	0.1
Relative Area	0.87	0.06	0.07	0.94	0.06	0.00	0.94	0.06	0.00
AlClPc/TiO <sub>2</sub> (100): Absence of O <sub>2</sub>									
	Layer thickness 0.1 nm			Layer thickness 0.3 nm			Layer thickness 1.3 nm		
Peak name	N-1	S <sub>(N-1)</sub>	N-3	N-1	S <sub>(N-1)</sub>	N-3	N-1	S <sub>(N-1)</sub>	N-3
GP-FWHM/eV	1.3	1.3	1.3	1.1	1.1	1.1	1.0	1.0	1.0
Position/eV	399.1	400.7	400.8	399.1	400.7	400.8	399.0	400.6	400.7
LP-FWHM/eV	0.1	0.1	0.1	0.1	0.1	0.1	0.1	0.1	0.1
Relative Area	0.82	0.06	0.12	0.90	0.06	0.04	0.94	0.06	0.00

Table 17. Stoichiometric relations C:N:Cl for AlClPc on (100) surface at different reduction degree.

Film stoichiometry AlClPc/TiO <sub>2</sub> (100) 0% Ti <sup>3+</sup>						
Thickness	AlClPc molecule	0.1 nm	0.2 nm	0.4 nm	0.6 nm	1.2 nm
C	32.0	32.0	32.0	32.0	32.0	32.0
N	8.0	7.7	7.9	8.1	7.7	7.8
Cl	1.0	1.4	1.5	1.2	1.2	1.0
Film stoichiometry AlClPc/TiO <sub>2</sub> (100) 16% Ti <sup>3+</sup>						
Thickness	AlClPc molecule	0.05 nm	0.1 nm	0.2 nm	0.3 nm	1.3 nm
C	32.0	32.0	32.0	32.0	32.0	32.0
N	8.0	7.7	7.2	7.5	7.5	7.5
Cl	1.0	1.4	1.0	1.3	0.9	0.7

Table 18. UPS parameters: work function, HOMO onset, ionization potential for the following systems: AlClPc/TiO<sub>2</sub>(100) treated with oxygen, AlClPc/TiO<sub>2</sub>(100) prepared in absence of oxygen.

AlClPc/TiO <sub>2</sub> (001): O <sub>2</sub> treatment			
Film thickness (nm)	Work function (eV)	Homo Onset (eV)	Ionization Potential (eV)
Substrate TiO <sub>2</sub>	5.3	x	8.3
0.1 nm	4.8	0.8	5.6
0.2 nm	4.6	0.9	5.5
0.4 nm	4.5	0.9	5.4
0.6 nm	4.5	0.9	5.4
1.2 nm	4.5	0.9	5.4
AlClPc/TiO <sub>2</sub> (001): Absence of O <sub>2</sub>			
Film thickness (nm)	Work function (eV)	Homo Onset (eV)	Ionization Potential (eV)
Substrate TiO <sub>2</sub>	5.1	x	8.3
0.05 nm	4.9	0.9	5.8
0.1 nm	4.8	0.9	5.7
0.2 nm	4.6	0.9	5.5
0.3 nm	4.4	0.9	5.3
1.3 nm	4.5	0.9	5.4

## 6. Appendix - 6.2 Fitting tables

### 6.2.5 AlClPc on TiO<sub>2</sub>(001)

Table 19. Fitting parameters of Ti 2p spectra of clean TiO<sub>2</sub>(001) at different reduction degree presented in Figure 4.50.

Doublet name		AlClPc/TiO <sub>2</sub> (001): O <sub>2</sub> treatment			AlClPc/TiO <sub>2</sub> (001): Absence of O <sub>2</sub>			
		Ti <sup>4+</sup>	Ti <sup>3+</sup>	Sat 1	Ti <sup>4+</sup>	Ti <sup>3+</sup>	Sat 1	
GP-FWHM/eV	P1	0.8	none	1.6	0.9	1.0	0.9	
	P2	1.7		1.6	1.6	1.2	0.9	
Position/eV	P1	459.4		462.4	459.5	457.6	462.5	
	P2	465.1		462.4	465.2	463.3	468.2	
LP-FWHM/eV	P1	0.5		0.5	0.5	0.5	0.5	
	P2	0.6		0.5	0.6	0.5	0.5	
Rel. Area	P1+P2	0.97	0	0.03	0.92	0.05	0.03	
(Ti <sup>3+</sup> +Ti <sup>2+</sup> )/(Ti <sup>4+</sup> +Ti <sup>3+</sup> +Ti <sup>2+</sup> )		0 %			5%			
Doublet name		AlClPc/TiO <sub>2</sub> (001): Absence of O <sub>2</sub>			AlClPc/TiO <sub>2</sub> (001): Absence of O <sub>2</sub>			
		Ti <sup>4+</sup>	Ti <sup>3+</sup>	Sat 1	Ti <sup>4+</sup>	Ti <sup>3+</sup>	Ti <sup>2+</sup>	Sat 1
GP-FWHM/eV	P1	1.0	1.1	2.0	1.4	1.6	1.6	2.9
	P2	1.8	1.3	2.0	2.1	2.7	2.7	2.9
Position/eV	P1	459.4	457.5	462.4	459.4	457.6	456.1	462.4
	P2	465.1	463.2	468.1	465.1	463.3	468.1	478.5
LP-FWHM/eV	P1	0.5	0.5	0.5	0.5	0.5	0.5	0.5
	P2	0.6	0.5	0.5	0.6	0.5	0.5	0.5
Rel. Area	P1+P2	0.86	0.11	0.03	0.46	0.38	0.9	0.06
(Ti <sup>3+</sup> +Ti <sup>2+</sup> )/(Ti <sup>4+</sup> +Ti <sup>3+</sup> +Ti <sup>2+</sup> )		12 %			50%			

Table 20. Fitting parameters: O 1s peak of TiO<sub>2</sub>(001) prepared with (0% Ti<sup>3+</sup>) and without oxygen treatment during annealing (5% Ti<sup>3+</sup>, 12% Ti<sup>3+</sup>, 50% Ti<sup>3+</sup>).

	TiO <sub>2</sub> (001): O <sub>2</sub> treatment		TiO <sub>2</sub> (001): Absence of O <sub>2</sub>		
	Clean Substrate 0% Ti <sup>3+</sup>		Clean Substrate 5% Ti <sup>3+</sup>		
Peak name	O-1	O-2	O-1	O-2	
Position/eV	530.8	531.9	530.7	531.8	
GP-FWHM/eV	1.0	1.1	1.0	1.1	
LP-FWHM/eV	0.1	0.1	0.1	0.1	
Relative Area	0.97	0.03	0.96	0.04	
	TiO <sub>2</sub> (001): Absence of O <sub>2</sub>		TiO <sub>2</sub> (001): Absence of O <sub>2</sub>		
	Clean Substrate 12% Ti <sup>3+</sup>		Clean Substrate 50% Ti <sup>3+</sup>		
Peak name	O-1	O-2	O-1	O-2	O-3
Position/eV	530.6	531.7	530.9	532.0	533.0
GP-FWHM/eV	1.0	1.1	1.3	1.3	1.3
LP-FWHM/eV	0.1	0.1	0.10	0.10	0.10
Relative Area	0.92	0.08	0.79	0.16	0.05

## 6. Appendix - 6.2 Fitting tables

Table 21. C 1s core level spectra fitting parameters of AlCIPc films on TiO<sub>2</sub>(001) surface treated with O<sub>2</sub> and prepared in absence of O<sub>2</sub>.

AlCIPc/TiO <sub>2</sub> (001): O <sub>2</sub> treatment												
Layer thickness 0.2 nm				Layer thickness 0.7 nm				Layer thickness 1.5 nm				
Peak name	C - 1	C - 2	S <sub>(C-1)</sub>	S <sub>(C-2)</sub>	C - 1	C - 2	S <sub>(C-1)</sub>	S <sub>(C-2)</sub>	C - 1	C - 2	S <sub>(C-1)</sub>	S <sub>(C-2)</sub>
GP-FWHM/eV	1.0	1.0	1.0	1.0	0.9	0.9	0.9	0.9	0.9	0.9	0.9	0.9
Position/eV	284.9	286.3	286.7	288.2	284.8	286.2	286.6	288.2	284.8	286.2	286.6	288.1
LP-FWHM/eV	0.1	0.1	0.1	0.1	0.1	0.1	0.1	0.1	0.1	0.1	0.1	0.1
rel. Area	0.67	0.20	0,08	0.05	0.67	0.20	0,08	0.05	0.67	0.20	0,08	0.05
	$(C-2+S_{C-2})/(C-1+S_{C-1})$			0.34	$(C-2+S_{C-2})/(C-1+S_{C-1})$			0.33	$(C-2+S_{C-2})/(C-1+S_{C-1})$			0.33
AlCIPc/TiO <sub>2</sub> (001): Absence of O <sub>2</sub>												
Layer thickness 0.2 nm				Layer thickness 0.5 nm				Layer thickness 1.3 nm				
Peak name	C - 1	C - 2	S <sub>(C-1)</sub>	S <sub>(C-2)</sub>	C - 1	C - 2	S <sub>(C-1)</sub>	S <sub>(C-2)</sub>	C - 1	C - 2	S <sub>(C-1)</sub>	S <sub>(C-2)</sub>
GP-FWHM/eV	1.2	1.2	1.2	1.2	1.1	1.1	1.1	1.1	0.9	0.9	0.9	0.9
Position/eV	284.8	286.0	286.6	288.0	284.8	286.1	286.6	288.1	284.7	286.1	286.5	288.1
LP-FWHM/eV	0.1	0.1	0.1	0.1	0.1	0.1	0.1	0.1	0.1	0.1	0.1	0.1
rel. Area	0.67	0.20	0,08	0.05	0.67	0.20	0,08	0.05	0.67	0.20	0,08	0.05
	$(C-2+S_{C-2})/(C-1+S_{C-1})$			0.34	$(C-2+S_{C-2})/(C-1+S_{C-1})$			0.34	$(C-2+S_{C-2})/(C-1+S_{C-1})$			0.33

Table 22. N 1s core level spectra fitting parameters of AlCIPc films on TiO<sub>2</sub>(001) surface treated with O<sub>2</sub> and prepared in absence of O<sub>2</sub>.

AlCIPc/TiO <sub>2</sub> (001): O <sub>2</sub> treatment									
Layer thickness 0.2 nm			Layer thickness 0.7 nm			Layer thickness 1.5 nm			
Peak name	N-1	S <sub>(N-1)</sub>	N-3	N-1	S <sub>(N-1)</sub>	N-3	N-1	S <sub>(N-1)</sub>	N-3
GP-FWHM/eV	1.2	1.2	1.2	1.0	1.0	1.0	1.0	1.0	1.0
Position/eV	399.4	401.0	401.1	399.3	400.9	401.0	399.3	400.9	401.0
LP-FWHM/eV	0.1	0.1	0.1	0.1	0.1	0.1	0.1	0.1	0.1
Relative Area	0.94	0.06	0.00	0.94	0.06	0.00	0.94	0.06	0.00
AlCIPc/TiO <sub>2</sub> (001): Absence of O <sub>2</sub>									
Layer thickness 0.2 nm			Layer thickness 0.5 nm			Layer thickness 1.3 nm			
Peak name	N-1	S <sub>(N-1)</sub>	N-3	N-1	S <sub>(N-1)</sub>	N-3	N-1	S <sub>(N-1)</sub>	N-3
GP-FWHM/eV	1.3	1.3	1.3	1.1	1.1	1.1	1.0	1.0	1.0
Position/eV	399.2	400.8	400.9	399.2	400.8	400.9	399.2	400.8	400.9
LP-FWHM/eV	0.1	0.1	0.1	0.1	0.1	0.1	0.1	0.1	0.1
Relative Area	0.77	0.05	0.19	0.90	0.05	0.05	0.93	0.06	0.02

## 6. Appendix - 6.2 Fitting tables

Table 23. Stoichiometric relations C:N:Cl for AlClPc on (001) surface at different reduction degree: 0%  $Ti^{3+}$  (prepared with  $O_2$  treatment) and 12%  $Ti^{3+}$  (prepared in absence of  $O_2$ )

Film stoichiometry AlClPc/TiO <sub>2</sub> (001): O <sub>2</sub> treatment								
Thickness	0.2 nm	0.7 nm	1.5 nm	AlClPc molecule				
C	32.0	32.0	32.0	32.0				
N	8.1	7.6	8.4	8.0				
Cl	1.0	1.6	1.5	1.0				
Film stoichiometry AlClPc/TiO <sub>2</sub> (001): Absence of O <sub>2</sub>								
Thickness	0.07 nm	0.17 nm	0.2 nm	0.3 nm	0.5 nm	1.3 nm	4.2 nm	AlClPc molecule
C	32.0	32.0	32.0	32.0	32.0	32.0	32.0	32.0
N	8.0	7.1	7.9	7.2	7.2	7.8	8.1	8.0
Cl	1.9	1.2	2.0	1.4	1.3	1.4	1.5	1.0

Table 24. Thickness dependent work function, HOMO onset and ionization potential values of AlClPc films on oxygen treated (0%  $Ti^{3+}$ ) and reduced (12%  $Ti^{3+}$ ) TiO<sub>2</sub>(001) surfaces.

AlClPc/TiO <sub>2</sub> (001): O <sub>2</sub> treatment	Work function (eV)	Homo Onset (eV)	Ionization Potential (eV)
TiO <sub>2</sub>	4.7	x	8.1
0.2 nm	4.5	1.0	5.5
0.7 nm	4.5	1.0	5.5
1.5 nm	4.4	1.0	5.4
AlClPc/TiO <sub>2</sub> (001): Absence of O <sub>2</sub>	Work function (eV)	Homo Onset (eV)	Ionization Potential (eV)
TiO <sub>2</sub>	4.7	x	8.1
0.07 nm	4.6	0.9	5.5
0.17 nm	4.4	1.0	5.4
0.2 nm	4.3	1.0	5.3
0.3 nm	4.2	1.0	5.2
0.5 nm	4.2	1.1	5.3
1.3 nm	4.2	1.1	5.3
4.2 nm	4.4	1.0	5.4

## 6. Appendix

### 6.3 Supporting information – AlClPc on TiO<sub>2</sub>(001) (5% Ti<sup>3+</sup>)

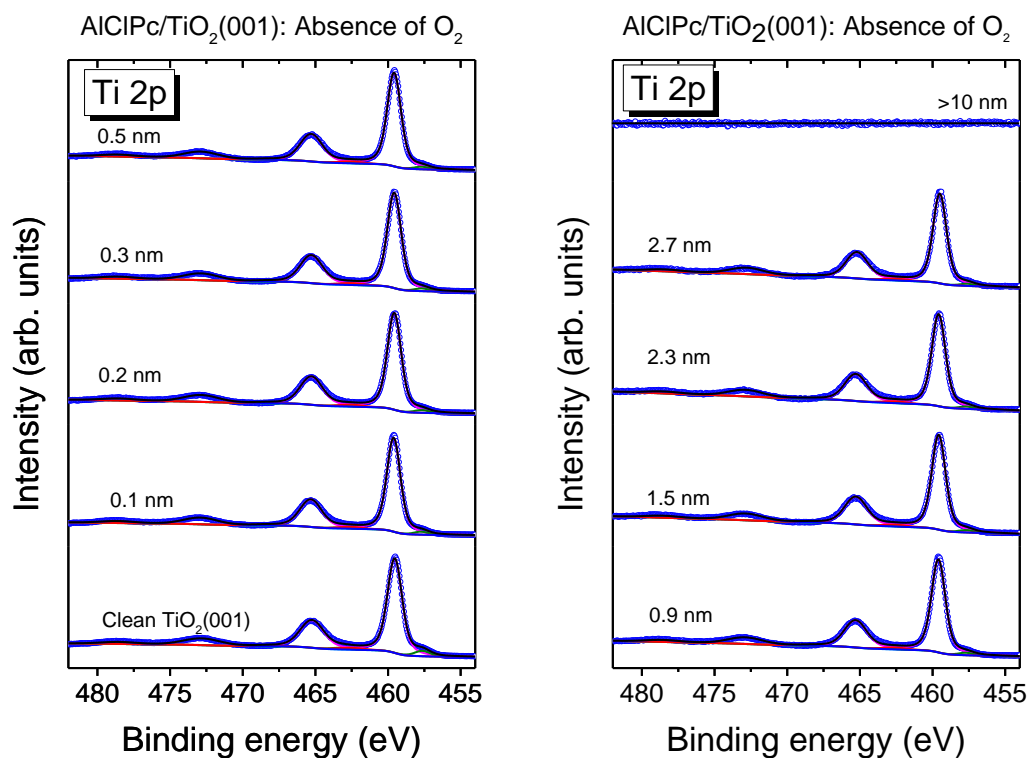


Figure 6.1. Thickness dependent Ti 2p core level spectra of AlClPc on TiO<sub>2</sub>(001) prepared in absence of oxygen (5% Ti<sup>3+</sup>). Spectra measured with Al K $\alpha$  radiation,  $h\nu = 1486.7$  eV.

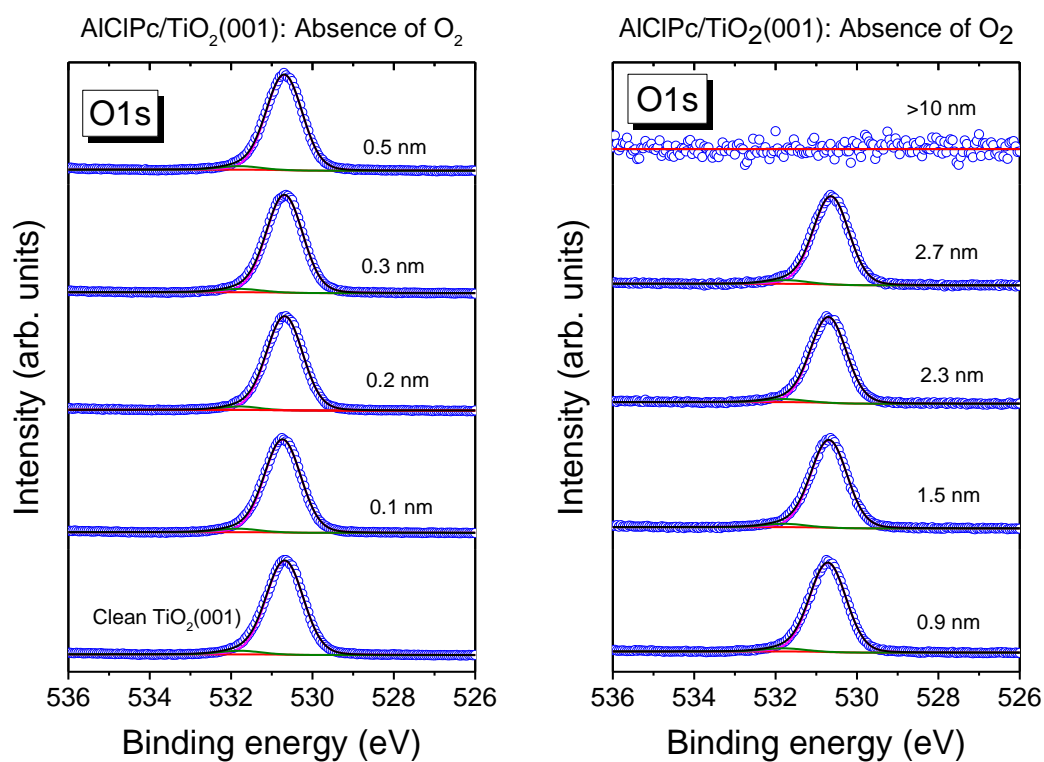


Figure 6.2. Thickness dependent O 1s core level spectra of AlClPc on TiO<sub>2</sub>(001) prepared in absence of oxygen (5% Ti<sup>3+</sup>). Spectra measured with Al K $\alpha$  radiation,  $h\nu = 1486.7$  eV.

## 6. Appendix - 6.3 Supporting information – AlClPc on TiO<sub>2</sub>(001) (5% Ti<sup>3+</sup>)

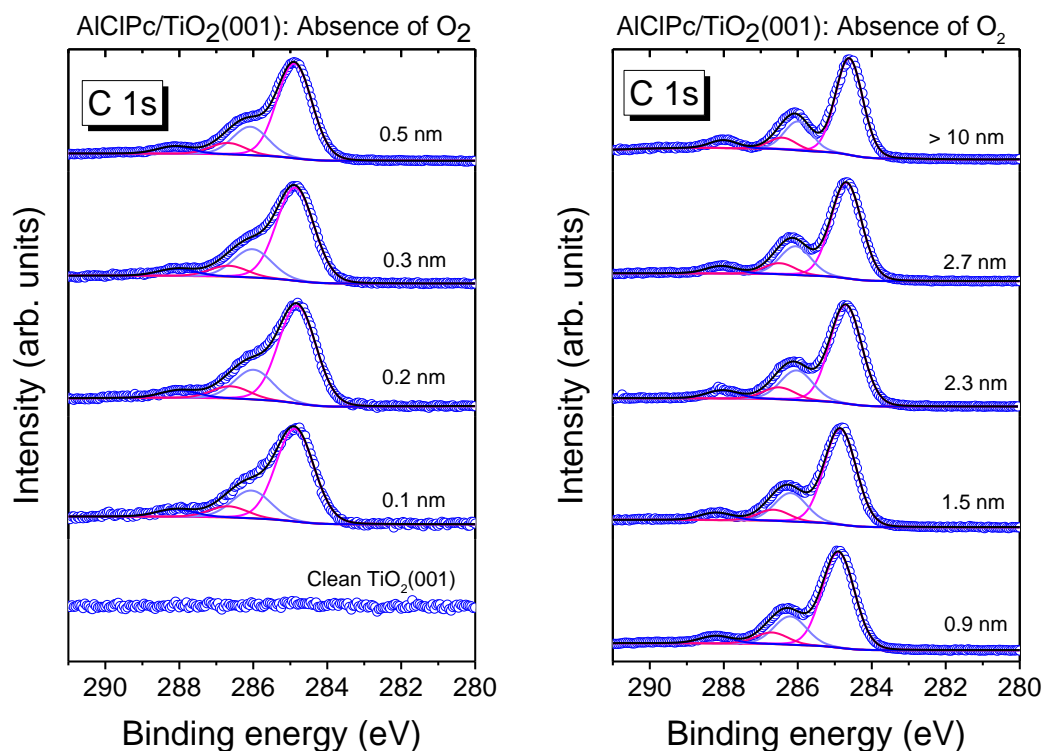


Figure 6.3. Thickness dependent C 1s core level spectra of AlClPc on TiO<sub>2</sub>(001) prepared in absence of oxygen (5% Ti<sup>3+</sup>). Spectra measured with Al K $\alpha$  radiation,  $h\nu = 1486.7$  eV.

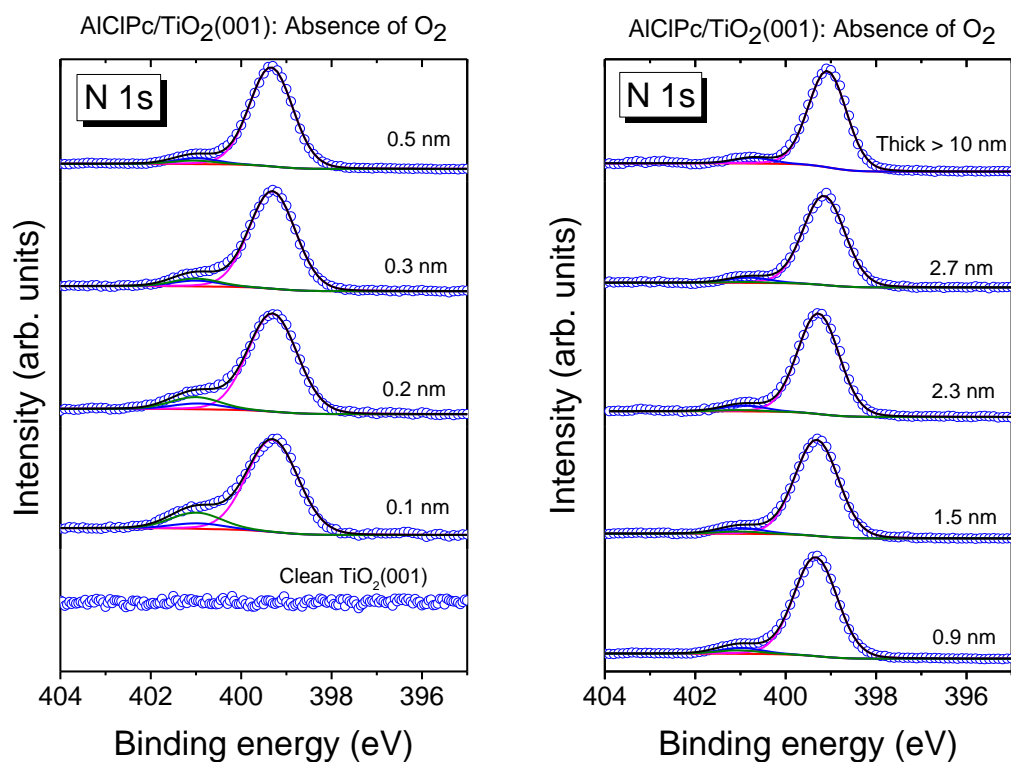


Figure 6.4. Thickness dependent N 1s core level spectra of AlClPc on TiO<sub>2</sub>(001) prepared in absence of oxygen (5% Ti<sup>3+</sup>). Spectra measured with Al K $\alpha$  radiation,  $h\nu = 1486.7$  eV.

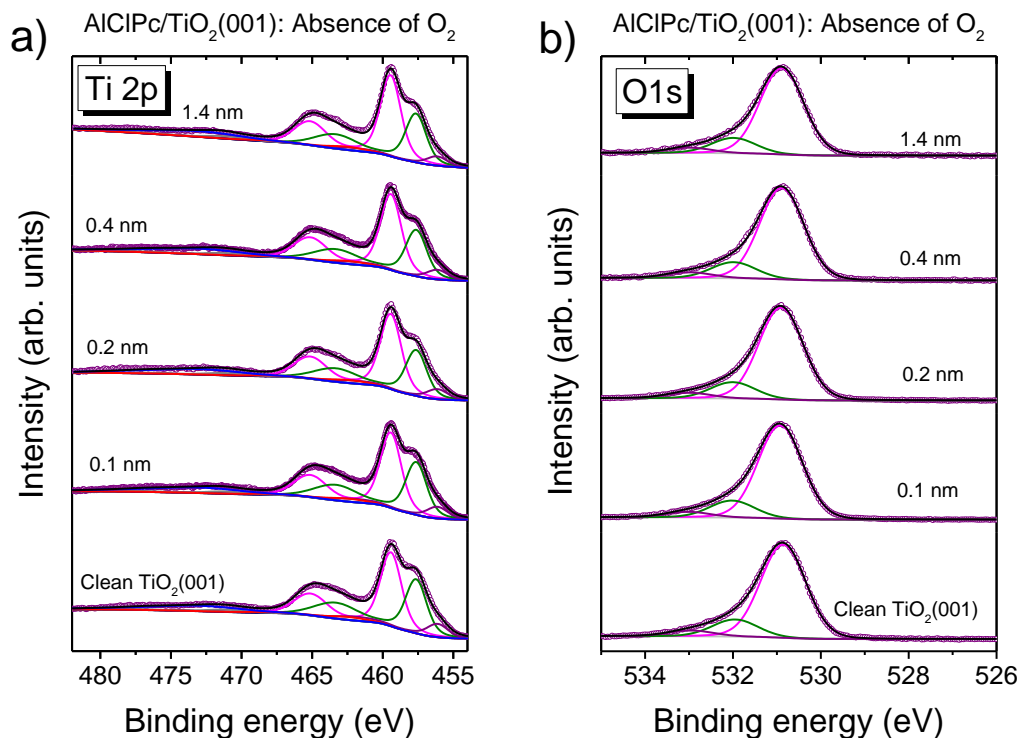
6.4 Supporting information – AlClPc on TiO<sub>2</sub>(001) (50% Ti<sup>3+</sup>)

Figure 6.5. Thickness dependent core level spectra of AlClPc on TiO<sub>2</sub>(001) prepared in absence of oxygen (50% Ti<sup>3+</sup>): a) Ti 2p and b) O 1s. Spectra measured with Al K $\alpha$  radiation,  $h\nu = 1486.7$  eV.

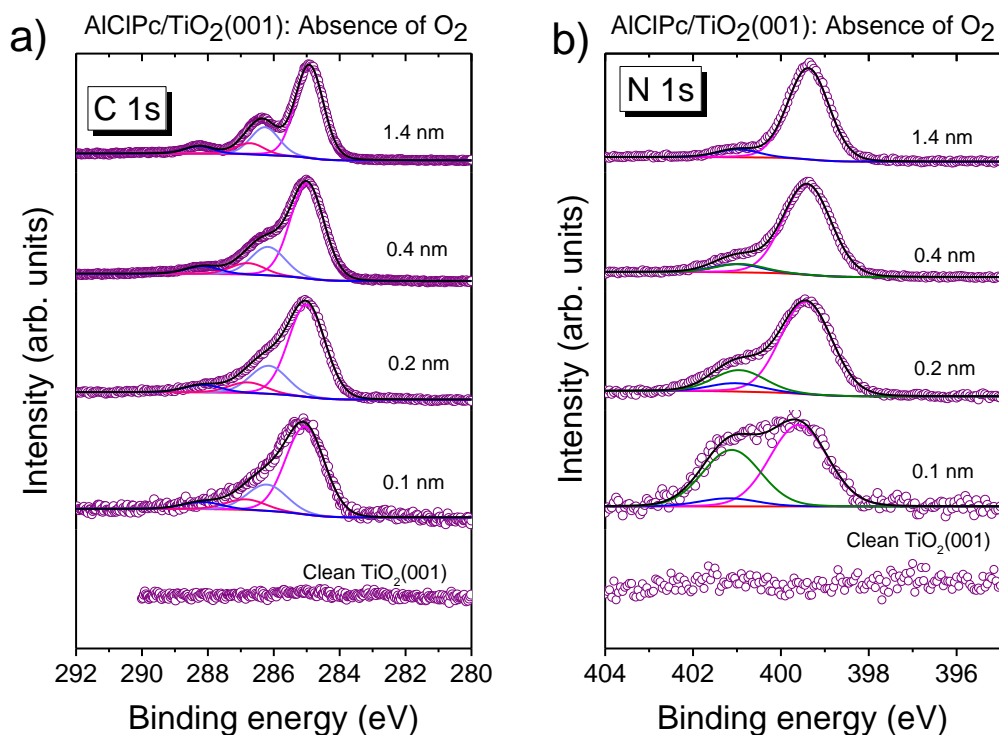


Figure 6.6. Thickness dependent core level spectra of AlClPc on TiO<sub>2</sub>(001) prepared in absence of oxygen (50% Ti<sup>3+</sup>): a) C 1s and b) N 1s. Spectra measured with Al K $\alpha$  radiation,  $h\nu = 1486.7$  eV.

## 7. List of References

1. Basova, T.; Plyashkevich, V.; Petraki, F.; Peisert, H.; Chassé, T., Magnetic field-induced reactions on the surface of chloroaluminum phthalocyanine thin films. *The Journal of Chemical Physics* **2011**, *134* (12), 124703.
2. Yoon, Y.; Koo, J. Y.; Oh, J.; Kim, S.; Choi, H. C.; Yoon, S. M., Surface-guided polymorphism control of titanyl phthalocyanine single crystals. *Inorganic Chemistry Frontiers* **2020**, *7* (11), 2178-2187.
3. Ibach, H.; Lüth, H., *Fizyka ciała stałego*. Wydawnictwo Naukowe PWN: 1996.
4. Sun, S.-S.; Dalton, L. R., *Introduction to organic electronic and optoelectronic materials and devices*. Second Edition ed.; CRC Press, Taylor; Francis Group: Boca Raton, FL, 2017.
5. Brütting, W., *Physics of organic semiconductors*. Wiley-VCH: Weinheim, 2004.
6. Smith, D. L., Electronic Properties of Inorganic and Organic Semiconductors and Their Application to National Security Needs. *MRS Bulletin* **2004**, *29* (9), 647-652.
7. Sorokin, A. B., Phthalocyanine Metal Complexes in Catalysis. *Chemical Reviews* **2013**, *113* (10), 8152-8191.
8. Zhang, Y.; Dong, H.; Tang, Q.; Ferdous, S.; Liu, F.; Mannsfeld, S. C. B.; Hu, W.; Briseno, A. L., Organic Single-Crystalline p-n Junction Nanoribbons. *Journal of the American Chemical Society* **2010**, *132* (33), 11580-11584.
9. Kenta, A.; Kenji, H., Small-molecule organic solar cells with multiple-layer donor. *Japanese Journal of Applied Physics* **2015**, *54* (9), 094102.
10. Huang, Y. L.; Chen, W.; Bussolotti, F.; Niu, T. C.; Wee, A. T. S.; Ueno, N.; Kera, S., Impact of molecule-dipole orientation on energy level alignment at the submolecular scale. *Physical Review B* **2013**, *87* (8), 085205.
11. Singh, V. K.; Kanaparthi, R. K.; Giribabu, L., Emerging molecular design strategies of unsymmetrical phthalocyanines for dye-sensitized solar cell applications. *RSC Advances* **2014**, *4* (14), 6970-6984.
12. Fukagawa, H.; Hosoumi, S.; Yamane, H.; Kera, S.; Ueno, N., Dielectric properties of polar-phthalocyanine monolayer systems with repulsive dipole interaction. *Physical Review B* **2011**, *83* (8), 085304.
13. Kera, S.; Yamane, H.; Honda, H.; Fukagawa, H.; Okudaira, K. K.; Ueno, N., Photoelectron fine structures of uppermost valence band for well-characterized ClAl-phthalocyanine ultrathin film: UPS and MAES study. *Surface Science* **2004**, *566-568*, Part 1, 571-578.
14. Mao, H. Y.; Wang, R.; Wang, Y.; Niu, T. C.; Zhong, J. Q.; Huang, M. Y.; Qi, D. C.; Loh, K. P.; Wee, A. T. S.; Chen, W., Chemical vapor deposition graphene as structural template to control interfacial molecular orientation of chloroaluminium phthalocyanine. *Applied Physics Letters* **2011**, *99* (9), 093301.
15. Niu, T.; Zhou, M.; Zhang, J.; Feng, Y.; Chen, W., Dipole Orientation Dependent Symmetry Reduction of Chloroaluminum Phthalocyanine on Cu(111). *The Journal of Physical Chemistry C* **2013**, *117* (2), 1013-1019.
16. Semyannikov, P. P.; Basova, T. V.; Grankin, V. M.; Igumenov, I. K., Vapour pressure of some phthalocyanines. *Journal of Porphyrins and Phthalocyanines* **2000**, *4* (3), 271-277.
17. Polek, M.; Latteyer, F.; Basova, T. V.; Petraki, F.; Aygül, U.; Uihlein, J.; Nagel, P.; Merz, M.; Schuppler, S.; Chassé, T.; Peisert, H., Chemical Reaction of Polar Phthalocyanines on Silver: Chloroaluminum Phthalocyanine and Fluoroaluminum Phthalocyanine. *The Journal of Physical Chemistry C* **2016**, *120* (43), 24715-24723.
18. Sienko, M. J.; Plane, R. A., *Chemia Podstawy i zastosowania*. Wydawnictwo Naukowo-Techniczne: Warszawa, 1980.
19. Meng, X.; Xu, Y.; Wang, Q.; Yang, X.; Guo, J.; Hu, X.; Tan, L.; Chen, Y., Silver Mesh Electrodes via Electroless Deposition-Coupled Inkjet-Printing Mask Technology for Flexible Polymer Solar Cells. *Langmuir* **2019**, *35* (30), 9713-9720.

## 7. List of References - 6.4 Supporting information – AlCl<sub>3</sub> on TiO<sub>2</sub>(001) (50% Ti<sup>3+</sup>)

20. Michaelson, H. B., The work function of the elements and its periodicity. *Journal of Applied Physics* **1977**, *48* (11), 4729-4733.
21. Giacomazzo, C.; Giacomazzo, C.; Monaco, H. L.; Artioli, G.; Viterbo, D.; Milanese, M.; Gilli, G.; Gilli, P.; Zanotti, G.; Ferraris, G.; Catti, M., *Fundamentals of Crystallography Second Edition, International Union of Crystallography*. Oxford Science Publications: 2002.
22. Hanaor, D. A. H.; Sorrell, C. C., Review of the anatase to rutile phase transformation. *Journal of Materials Science* **2011**, *46* (4), 855-874.
23. Cronmeyer, D. C., Electrical and Optical Properties of Rutile Single Crystals. *Physical Review* **1952**, *87* (5), 876-886.
24. Wen, B.; Hao, Q.; Yin, W.-J.; Zhang, L.; Wang, Z.; Wang, T.; Zhou, C.; Selloni, A.; Yang, X.; Liu, L.-M., Electronic structure and photoabsorption of Ti<sup>3+</sup> ions in reduced anatase and rutile TiO<sub>2</sub>. *Physical Chemistry Chemical Physics* **2018**, *20* (26), 17658-17665.
25. Göpel, W.; Anderson, J. A.; Frankel, D.; Jaehrig, M.; Phillips, K.; Schäfer, J. A.; Rocker, G., Surface defects of TiO<sub>2</sub>(110): A combined XPS, XAES AND ELS study. *Surface Science* **1984**, *139* (2), 333-346.
26. Diebold, U., The surface science of titanium dioxide. *Surface Science Reports* **2003**, *48* (5–8), 53-229.
27. Hollas, J. M., *Moderne Methoden in der Spektroskopie*. Vieweg & Sohn Verlagsgesellschaft mbH: Braunschweig/Wiesbaden, 1995.
28. *Phoibos Hemispherical Energy Analyzer Series Manual*. SPECS GmbH: Berlin, 2008.
29. Marder, M. P., *Condensed Matter Physics*. John Wiley & Sons: Hoboken, New Jersey, USA, 2010.
30. Briggs, D., Practical Surface Analysis second edition Vol. 1, Auger and X-ray Photoelectron Spectroscopy. *John Wiley & Sons Ltd., New York* **1990**.
31. Helander, M. G.; Greiner, M. T.; Wang, Z. B.; Lu, Z. H., Pitfalls in measuring work function using photoelectron spectroscopy. *Applied Surface Science* **2010**, *256* (8), 2602-2605.
32. Hesse, R. Verbesserung der qualitativen und quantitativen Analyse von Photoelektronenspektren und deren Verifizierung mittels mathematisch-numerischer Verfahren – Entwicklung und Test einer Bearbeitungs- und Analyse-Software. Universität Leipzig, Leipzig, 2006.
33. *SpecsLEED Optics and Electron Source, User's Guide*. Version 4.3 ed.; Omicron NanoTechnology: Germany, 2003.
34. Brillson, L. J., *An Essential Guide to Electronic Material Surfaces and Interfaces*. John Wiley & Sons: 2016; p 379.
35. Niemantsverdriet, J. W., *Spectroscopy in Catalysis: An Introduction*. Wiley: 2007.
36. Binnig, G.; Quate, C. F.; Gerber, C., Atomic Force Microscope. *Physical Review Letters* **1986**, *56* (9), 930-933.
37. Vickermann, J. C.; Gilmore, I. S., *Surface Analysis The Principal Techniques*. John Wiley & Sons: 2009.
38. *MultiMode Manual RevB, di MultiMode SPM Instruction Manual, NanoScope Software*. Version5 ed.; NanoScope Software 2004.
39. Training Notebook v 3.book, Scanning Probe Microscopy Training Notebook. [http://www.nanophys.kth.se/nanophys/facilities/nfl/afm/dim3100/Trng\\_Ntb\\_v3.0.pdf](http://www.nanophys.kth.se/nanophys/facilities/nfl/afm/dim3100/Trng_Ntb_v3.0.pdf)
40. Napier, A.; Collins, R. A., Phase behaviour of halogenated metal phthalocyanines. *physica status solidi (a)* **1994**, *144* (1), 91-104.
41. Yu, N.-H. Nanocluster defects and their properties on TiO<sub>2</sub>(110) and (001) surfaces. Baylor University, 2012.
42. Muryn, C. A.; Tirvengadam, G.; Crouch, J. J.; Warburton, D. R.; Raiker, G. N.; Thornton, G.; Law, D. S. L., TiO<sub>2</sub>(100) structure-reactivity relationship. *Journal of Physics: Condensed Matter* **1989**, *1* (SB), SB127.
43. Hesse, R.; Chassé, T.; Streubel, P.; Szargan, R., Error estimation in peak-shape analysis of XFS core-level spectra using UNIFIT 2003: How significant are the results of peak fits? *Surface and Interface Analysis* **2004**, *36*, 1373-1383.

## 7. List of References - 6.4 Supporting information – AICIPc on TiO<sub>2</sub>(001) (50% Ti<sub>3</sub><sup>+</sup>)

44. Horcas, I.; Fernández, R.; Gómez-Rodríguez, J. M.; Colchero, J.; Gómez-Herrero, J.; Baro, A. M., WSXM: A software for scanning probe microscopy and a tool for nanotechnology. *Review of Scientific Instruments* **2007**, *78* (1), 013705.
45. Nečas, D.; Klapetek, P., Gwyddion: an open-source software for SPM data analysis. In *Open Physics*, 2012; Vol. 10, p 181.
46. Seah, M. P.; Dench, W. A., Quantitative electron spectroscopy of surfaces: A standard data base for electron inelastic mean free paths in solids. *Surface and Interface Analysis* **1979**, *1* (1), 2-11.
47. Yeh, J. J.; Lindau, I., Atomic subshell photoionization cross sections and asymmetry parameters:  $1 \leq Z \leq 103$ . *Atomic Data and Nuclear Data Tables* **1985**, *32* (1), 1-155.
48. Heuberger, M.; Dietler, G.; Schlapbach, L., New aspects in Volmer-Weber 3D growth: an XPS intensity study applied to thin films of Au and Ce on polypropylene. *Surface Science* **1994**, *314* (1), 13-22.
49. Yeh, J. J., *Atomic Calculation of Photoionization Cross-sections and Asymmetry Parameters*. Gordon & Breach Science: 1993.
50. Gottfried, J. M., Surface chemistry of porphyrins and phthalocyanines. *Surface Science Reports* **2015**, *70* (3), 259-379.
51. Barth, J. V.; Costantini, G.; Kern, K., Engineering atomic and molecular nanostructures at surfaces. *Nature* **2005**, *437* (7059), 671-679.
52. Huang, Y.; Wruss, E.; Egger, D.; Kera, S.; Ueno, N.; Saidi, W.; Bucko, T.; Wee, A.; Zojer, E., Understanding the Adsorption of CuPc and ZnPc on Noble Metal Surfaces by Combining Quantum-Mechanical Modelling and Photoelectron Spectroscopy. *Molecules* **2014**, *19* (3), 2969-2992.
53. *Handbook of X-ray Photoelectron Spectroscopy*. Perkin-Elmer Corp., Physical Electronics Division: Eden Prairie, Minnesota, USA, 1979.
54. Henzler, M., LEED studies of surface imperfections. *Applications of Surface Science* **1982**, *11-12*, 450-469.
55. Teichert, C.; Ammer, C.; Klaua, M., Step formation on the ion-bombarded Ag(100) surface studied by LEED and Monte Carlo simulations. *physica status solidi (a)* **1994**, *146* (1), 223-242.
56. Peisert, H.; Knupfer, M.; Fink, J., Electronic structure of partially fluorinated copper phthalocyanine (CuPCF<sub>4</sub>) and its interface to Au(100). *Surface Science* **2002**, *515* (2), 491-498.
57. Latteyer, F.; Peisert, H.; Uihlein, J.; Basova, T.; Nagel, P.; Merz, M.; Schuppler, S.; Chasse, T., Chloroaluminum phthalocyanine thin films: chemical reaction and molecular orientation. *Analytical and Bioanalytical Chemistry* **2013**, *405* (14), 4895-4904.
58. Lin, M.-K.; Nakayama, Y.; Zhuang, Y.-J.; Su, K.-J.; Wang, C.-Y.; Pi, T.-W.; Metz, S.; Papadopoulos, T. A.; Chiang, T. C.; Ishii, H.; Tang, S. J., Control of the dipole layer of polar organic molecules adsorbed on metal surfaces via different charge-transfer channels. *Physical Review B* **2017**, *95* (8), 085425.
59. Petraki, F.; Peisert, H.; Aygül, U.; Latteyer, F.; Uihlein, J.; Vollmer, A.; Chassé, T., Electronic Structure of FePc and Interface Properties on Ag(111) and Au(100). *The Journal of Physical Chemistry C* **2012**, *116* (20), 11110-11116.
60. Helander, M. G.; Greiner, M. T.; Wang, Z. B.; Lu, Z. H., Effect of electrostatic screening on apparent shifts in photoemission spectra near metal/organic interfaces. *Physical Review B* **2010**, *81* (15), 153308.
61. Peisert, H.; Petershans, A.; Chassé, T., Charge Transfer and Polarization Screening at Organic/Metal Interfaces: Distinguishing between the First Layer and Thin Films. *The Journal of Physical Chemistry C* **2008**, *112* (15), 5703-5706.
62. Petraki, F.; Peisert, H.; Uihlein, J.; Aygül, U.; Chassé, T., CoPc and CoPcF<sub>16</sub> on gold: Site-specific charge-transfer processes. *Beilstein Journal of Nanotechnology* **2014**, *5*, 524-531.
63. Lindner, S.; Treske, U.; Knupfer, M., The complex nature of phthalocyanine/gold interfaces. *Applied Surface Science* **2013**, *267*, 62-65.

## 7. List of References - 6.4 Supporting information – AlClPc on TiO<sub>2</sub>(001) (50% Ti<sup>3+</sup>)

64. Papageorgiou, N.; Ferro, Y.; Salomon, E.; Allouche, A.; Layet, J. M.; Giovanelli, L.; Le Lay, G., Geometry and electronic structure of lead phthalocyanine: Quantum calculations via density-functional theory and photoemission measurements. *Physical Review B* **2003**, *68* (23), 235105.
65. Briggs, D.; Marbrow, R. A.; Lambert, R. M., An XPS and UPS study of chloride chemisorption on Ag(110). *Chemical Physics Letters* **1978**, *53* (3), 462-464.
66. Strydom, C. A.; van Staden, J. F.; Strydom, H. J., An XPS investigation of silver chloride coated ion-selective electrodes. *Journal of Electroanalytical Chemistry and Interfacial Electrochemistry* **1990**, *277* (1), 165-177.
67. Latteyer, F.; Peisert, H.; Aygul, U.; Biswas, I.; Petraki, F.; Basova, T.; Vollmer, A.; Chasse, T., Laterally Resolved Orientation and Film Thickness of Polar Metal Chlorine Phthalocyanines on Au and ITO. *Journal of Physical Chemistry C* **2011**, *115* (23), 11657-11665.
68. McGuire, G. E.; Schweitzer, G. K.; Carlson, T. A., Core electron binding energies in some Group IIIA, VB, and VIB compounds. *Inorganic Chemistry* **1973**, *12* (10), 2450-2453.
69. van Attekum, P. M. T. M.; Trooster, J. M., Bulk- and surface-plasmon-loss intensities in photoelectron, Auger, and electron-energy-loss spectra of Al metal. *Physical Review B* **1978**, *18* (8), 3872-3883.
70. Petraki, F.; Peisert, H.; Biswas, I.; Chassé, T., Electronic Structure of Co-Phthalocyanine on Gold Investigated by Photoexcited Electron Spectroscopies: Indication of Co Ion-Metal Interaction. *The Journal of Physical Chemistry C* **2010**, *114* (41), 17638-17643.
71. Peisert, H.; Uihlein, J.; Petraki, F.; Chasse, T., Charge transfer between transition metal phthalocyanines and metal substrates: The role of the transition metal. *J Electron Spectrosc* **2015**, *204*, 49-60.
72. Latteyer, F. Einflüsse auf die molekulare Orientierung von Phthalocyaninen in dünnen Schichten. PhD Thesis, Tübingen University, 2013.
73. Li Huang, Y.; Lu, Y.; Niu, T. C.; Huang, H.; Kera, S.; Ueno, N.; Wee, A. T. S.; Chen, W., Reversible Single-Molecule Switching in an Ordered Monolayer Molecular Dipole Array. *Small* **2012**, *8* (9), 1423-1428.
74. Ying Mao, H.; Wang, R.; Wang, Y.; Chao Niu, T.; Qiang Zhong, J.; Yang Huang, M.; Chen Qi, D.; Ping Loh, K.; Thye Shen Wee, A.; Chen, W., Chemical vapor deposition graphene as structural template to control interfacial molecular orientation of chloroaluminium phthalocyanine. *Appl Phys Lett* **2011**, *99* (9), 093301.
75. Huang, Y. L.; Wang, R.; Niu, T. C.; Kera, S.; Ueno, N.; Pflaum, J.; Wee, A. T. S.; Chen, W., One dimensional molecular dipole chain arrays on graphite via nanoscale phase separation. *Chem. Commun.* **2010**, *46* (47), 9040-9042.
76. Peisert, H.; Biswas, I.; Knupfer, M.; Chasse, T., Orientation and electronic properties of phthalocyanines on polycrystalline substrates. *Phys Status Solidi B* **2009**, *246* (7), 1529-1545.
77. Trelka, M.; Medina, A.; Ecija, D.; Urban, C.; Groning, O.; Fasel, R.; Gallego, J. M.; Claessens, C. G.; Otero, R.; Torres, T.; Miranda, R., Subphthalocyanine-based nanocrystals. *Chem. Commun.* **2011**, *47* (36), 9986-9988.
78. Liu, X. J.; Wei, Y. Y.; Reutt-Robey, J. E.; Robey, S. W., Dipole-Dipole Interactions in TiOPc Ad layers on Ag. *J Phys Chem C* **2014**, *118* (7), 3523-3532.
79. Xie, W.; Xu, J.; An, J.; Xue, K., Correlation between Molecular Packing and Surface Potential at Vanadyl Phthalocyanine/HOPG Interface. *The Journal of Physical Chemistry C* **2010**, *114* (44), 19044-19047.
80. Adler, H.; Paszkiewicz, M.; Uihlein, J.; Polek, M.; Ovsyannikov, R.; Basova, T. V.; Chassé, T.; Peisert, H., Interface Properties of VOPc on Ni(111) and Graphene/Ni(111): Orientation-Dependent Charge Transfer. *The Journal of Physical Chemistry C* **2015**, *119* (16), 8755-8762.
81. Berner, S.; de Wild, M.; Ramoino, L.; Ivan, S.; Baratoff, A.; Güntherodt, H. J.; Suzuki, H.; Schlettwein, D.; Jung, T. A., Adsorption and two-dimensional phases of a large polar molecule: Sub-phthalocyanine on Ag(111). *Physical Review B* **2003**, *68* (11), 115410.

## 7. List of References - 6.4 Supporting information – AICIPc on TiO<sub>2</sub>(001) (50% Ti<sub>3+</sub>)

82. Ilyas, N.; Harivyasi, S. S.; Zahl, P.; Cortes, R.; Hofmann, O. T.; Sutter, P.; Zojer, E.; Monti, O. L. A., Sticking with the Pointy End? Molecular Configuration of Chloro Boron-Subphthalocyanine on Cu(111). *The Journal of Physical Chemistry C* **2016**, *120* (13), 7113-7121.
83. Gaarenstroom, S. W.; Winograd, N., Initial and Final-State Effects in Esca Spectra of Cadmium and Silver-Oxides. *J Chem Phys* **1977**, *67* (8), 3500-3506.
84. Kaushik, V. K., Xps Core Level Spectra and Auger Parameters for Some Silver Compounds. *Journal of Electron Spectroscopy and Related Phenomena* **1991**, *56* (3), 273-277.
85. Wolan, J. T.; Hoflund, G. B., Surface characterization study of AgF and AgF<sub>2</sub> powders using XPS and ISS. *Applied Surface Science* **1998**, *125* (3), 251-258.
86. Schwieger, T.; Peisert, H.; Knupfer, M., Direct observation of interfacial charge transfer from silver to organic semiconductors. *Chemical Physics Letters* **2004**, *384* (4), 197-202.
87. Heimel, G.; Duhm, S.; Salzmann, I.; Gerlach, A.; Strozecka, A.; Niederhausen, J.; Bürker, C.; Hosokai, T.; Fernandez-Torrente, I.; Schulze, G.; Winkler, S.; Wilke, A.; Schlesinger, R.; Frisch, J.; Bröker, B.; Vollmer, A.; Detlefs, B.; Pflaum, J.; Kera, S.; Franke, K. J.; Ueno, N.; Pascual, J. I.; Schreiber, F.; Koch, N., Charged and metallic molecular monolayers through surface-induced aromatic stabilization. *Nature Chemistry* **2013**, *5* (3), 187-194.
88. Palmgren, P.; Nilson, K.; Yu, S.; Hennies, F.; Angot, T.; Layet, J. M.; Le Lay, G.; Göthelid, M., Strong Interactions in Dye-Sensitized Interfaces. *The Journal of Physical Chemistry C* **2008**, *112* (15), 5972-5977.
89. Polek, M.; Basova, T. V.; Chassé, T.; Peisert, H., The interface between chloroaluminum phthalocyanine and titanium dioxide: the influence of surface defects and substrate termination. *Physical Chemistry Chemical Physics* **2021**, *23* (23), 13370-13380.
90. Oku, M.; Matsuta, H.; Wagatsuma, K.; Waseda, Y.; Kohiki, S., Removal of inelastic scattering part from Ti2p XPS spectrum of TiO<sub>2</sub> by deconvolution method using O1s as response function. *Journal of Electron Spectroscopy and Related Phenomena* **1999**, *105* (2), 211-218.
91. Pouilleau, J.; Devilliers, D.; Groult, H.; Marcus, P., Surface study of a titanium-based ceramic electrode material by X-ray photoelectron spectroscopy. *Journal of Materials Science* **1997**, *32* (21), 5645-5651.
92. Karstens, R.; Glaser, M.; Belser, A.; Balle, D.; Polek, M.; Ovsyannikov, R.; Giangrisostomi, E.; Chassé, T.; Peisert, H., FePc and FePcF<sub>16</sub> on Rutile TiO<sub>2</sub>(110) and (100): Influence of the Substrate Preparation on the Interaction Strength. *Molecules* **2019**, *24* (24), 4579.
93. Nolan, M.; Elliott, S. D.; Mulley, J. S.; Bennett, R. A.; Basham, M.; Mulheran, P., Electronic structure of point defects in controlled self-doping of the TiO<sub>2</sub> (110) surface: Combined photoemission spectroscopy and density functional theory study. *Physical Review B* **2008**, *77* (23), 11.
94. Wang, L.-Q.; Baer, D. R.; Engelhard, M. H., Creation of variable concentrations of defects on TiO<sub>2</sub>(110) using low-density electron beams. *Surface Science* **1994**, *320* (3), 295-306.
95. Jackman, M. J.; Thomas, A. G.; Muryn, C., Photoelectron Spectroscopy Study of Stoichiometric and Reduced Anatase TiO<sub>2</sub>(101) Surfaces: The Effect of Subsurface Defects on Water Adsorption at Near-Ambient Pressures. *The Journal of Physical Chemistry C* **2015**, *119* (24), 13682-13690.
96. Fan, J. C. C.; Goodenough, J. B., X-ray photoemission spectroscopy studies of Sn-doped indium-oxide films. *Journal of Applied Physics* **1977**, *48* (8), 3524-3531.
97. Sang-Joon, P.; Jeong-Pyo, L.; Jong Shik, J.; Hyun, R.; Hyunung, Y.; Byung Youn, Y.; Chang Soo, K.; Kyung Joong, K.; Yong Jai, C.; Sunggi, B.; Woo, L., In situ control of oxygen vacancies in TiO<sub>2</sub> by atomic layer deposition for resistive switching devices. *Nanotechnology* **2013**, *24* (29), 295202.
98. Sham, T. K.; Lazarus, M. S., X-ray photoelectron spectroscopy (XPS) studies of clean and hydrated TiO<sub>2</sub> (rutile) surfaces. *Chemical Physics Letters* **1979**, *68* (2), 426-432.
99. Fan, C.; Chen, C.; Wang, J.; Fu, X.; Ren, Z.; Qian, G.; Wang, Z., Black Hydroxylated Titanium Dioxide Prepared via Ultrasonication with Enhanced Photocatalytic Activity. *Scientific Reports* **2015**, *5* (1), 11712.

## 7. List of References - 6.4 Supporting information – AlClPc on TiO<sub>2</sub>(001) (50% Ti<sup>3+</sup>)

100. Ghobadi, A.; Ulusoy, T. G.; Garifullin, R.; Guler, M. O.; Okyay, A. K., A Heterojunction Design of Single Layer Hole Tunneling ZnO Passivation Wrapping around TiO<sub>2</sub>Nanowires for Superior Photocatalytic Performance. *Scientific Reports* **2016**, *6* (1), 30587.
101. Wang, L.-Q.; Baer, D. R.; Engelhard, M. H.; Shultz, A. N., The adsorption of liquid and vapor water on TiO<sub>2</sub>(110) surfaces: the role of defects. *Surface Science* **1995**, *344* (3), 237-250.
102. Sasahara, A.; Pang, C. L.; Tomitori, M., Atomic Scale Analysis of Ultrathin SiO<sub>2</sub> Films Prepared on TiO<sub>2</sub>(100) Surfaces. *The Journal of Physical Chemistry C* **2010**, *114* (47), 20189-20194.
103. Murnyn, C. A.; Hardman, P. J.; Crouch, J. J.; Raiker, G. N.; Thornton, G.; Law, D. S. L., Step and point defect effects on TiO<sub>2</sub>(100) reactivity. *Surface Science* **1991**, *251-252*, 747-752.
104. Murray, P. W.; Leibsle, F. M.; Murnyn, C. A.; Fisher, H. J.; Flipse, C. F. J.; Thornton, G., Interrelationship of structural elements on TiO<sub>2</sub>(100)-(1x3). *Physical Review Letters* **1994**, *72* (5), 689-692.
105. Chambers, S. A.; Gao, Y.; Thevuthasan, S.; Liang, Y.; Shivaparan, N. R.; Smith, R. J., Molecular beam epitaxial growth and characterization of mixed (Ti,Nb)O<sub>2</sub> rutile films on TiO<sub>2</sub>(100). *Journal of Vacuum Science & Technology A* **1996**, *14* (3), 1387-1394.
106. Lu, Y.; Jaeckel, B.; Parkinson, B. A., Preparation and Characterization of Terraced Surfaces of Low-Index Faces of Anatase, Rutile, and Brookite. *Langmuir* **2006**, *22* (10), 4472-4475.
107. Murray, P. W.; Leibsle, F. M.; Murnyn, C. A.; Fisher, H. J.; Flipse, C. F. J.; Thornton, G., Extended defects on TiO<sub>2</sub>(100) 1 × 3. *Surface Science* **1994**, *321* (3), 217-228.
108. Zschack, P.; Cohen, J. B.; Chung, Y. W., Structure of the TiO<sub>2</sub>(100) 1 × 3 surface determined by glancing angle X-ray diffraction and low energy electron diffraction. *Surface Science* **1992**, *262* (3), 395-408.
109. Henzler, M., Atomic steps on single crystals: Experimental methods and properties. *Applied physics* **1976**, *9* (1), 11-17.
110. Serrano, G. B., B.; Kosmala, T.; Di Giovannantonio, M.; Diebold, U.; Wandelt, K.; Goletti, C., In situ scanning tunneling microscopy study of Ca-modified rutile TiO<sub>2</sub>(110) in bulk water. *Beilstein J. Nanotechnol.* **2015**, *6*, 438-443.
111. Cao, Y.; Yu, M.; Qi, S.; Ren, Z.; Yan, S.; Hu, S.; Xu, M., Nitric Oxide Reaction Pathways on Rutile TiO<sub>2</sub>(110): The Influence of Surface Defects and Reconstructions. *The Journal of Physical Chemistry C* **2018**, *122* (41), 23441-23450.
112. Zajonz, H.; Meyerheim, H. L.; Gloege, T.; Moritz, W.; Wolf, D., Surface X-ray structure analysis of the TiO<sub>2</sub>(100)-(1 × 3) reconstruction. *Surface Science* **1998**, *398* (3), 369-378.
113. Lindan, P. J. D.; Harrison, N. M., The structure of the reduced rutile TiO<sub>2</sub>(1 0 0) 1x3 reconstruction. *Surface Science* **2001**, *479* (1-3), L375-L381.
114. Wang, Y.; Lee, S.; Vilmercati, P.; Lee, H. N.; Weitering, H. H.; Snijders, P. C., Atomically flat reconstructed rutile TiO<sub>2</sub>(001) surfaces for oxide film growth. *Applied Physics Letters* **2016**, *108* (9), 091604.
115. Tero, R.; Fukui, K.-i.; Iwasawa, Y., Atom-Resolved Surface Structures and Molecular Adsorption on TiO<sub>2</sub>(001) Investigated by Scanning Tunneling Microscopy. *The Journal of Physical Chemistry B* **2003**, *107* (14), 3207-3214.
116. Fukui, K.; Tero, R.; Iwasawa, Y., Atom-Resolved Structures of TiO<sub>2</sub>(001) Surface by Scanning Tunneling Microscopy. *Japanese Journal of Applied Physics* **2001**, *40* (Part 1, No. 6B), 4331-4333.
117. Wang, J. Y.; Wang, J. Y.; Dougherty, D. B., Direct molecular quantification of electronic disorder in N,N'-Di-(1-naphthyl)-N,N'-diphenyl-1,1'-biphenyl-4,4'-diamine on Au(111). *J. Vac. Sci. Technol. B* **2020**, *38* (5), 7.
118. Evangelista, F.; Ruocco, A.; Gotter, R.; Cossaro, A.; Floreano, L.; Morgante, A.; Crispoldi, F.; Betti, M. G.; Mariani, C., Electronic states of CuPc chains on the Au(110) surface. *The Journal of Chemical Physics* **2009**, *131* (17), 174710.
119. Gruninger, P.; Polek, M.; Ivanovic, M.; Balle, D.; Karstens, R.; Nagel, P.; Merz, M.; Schuppler, S.; Ovsyannikov, R.; Bettinger, H. F.; Peisert, H.; Chasse, T., Electronic Structure of Hexacene and Interface Properties on Au(110). *J. Phys. Chem. C* **2018**, *122* (34), 19491-19498.

## 7. List of References - 6.4 Supporting information – AICIPc on TiO<sub>2</sub>(001) (50% Ti<sub>3+</sub>)

120. Kashiwaya, S.; Morasch, J.; Streibel, V.; Toupance, T.; Jaegermann, W.; Klein, A., The Work Function of TiO<sub>2</sub>. *Surfaces* **2018**, *1* (1), 73-89.
121. Kilinc, N.; Ozturk, Z. Z.; Berber, S., Adsorption of Phthalocyanines on Stoichiometric and Reduced Rutile TiO<sub>2</sub> (110). *ECS Journal of Solid State Science and Technology* **2020**, *9* (6), 061021.
122. Matencio, S.; Palacios-Rivera, R.; Martinez, J. I.; Ocal, C.; Barrera, E., Chiral Organization and Charge Redistribution in Chloroaluminum Phthalocyanine on Au(111) Beyond the Monolayer. *Journal of Physical Chemistry C* **2018**, *122* (28), 16033-16041.
123. Wruss, E.; Hofmann, O. T.; Egger, D. A.; Verwuster, E.; Gerlach, A.; Schreiber, F.; Zojer, E., Adsorption Behavior of Nonplanar Phthalocyanines: Competition of Different Adsorption Conformations. *Journal of Physical Chemistry C* **2016**, *120* (12), 6869-6875.
124. Rogala, M.; Bihlmayer, G.; Dabrowski, P.; Rodenbücher, C.; Wrana, D.; Krok, F.; Klusek, Z.; Szot, K., Self-reduction of the native TiO<sub>2</sub> (110) surface during cooling after thermal annealing – in-operando investigations. *Scientific Reports* **2019**, *9* (1), 12563.
125. Zojer, E.; Taucher, T. C.; Hofmann, O. T., The Impact of Dipolar Layers on the Electronic Properties of Organic/Inorganic Hybrid Interfaces. *Adv. Mater. Interfaces* **2019**, *6* (14).
126. Boileau, N. T.; Cranston, R.; Mirka, B.; Melville, O. A.; Lessard, B. H., Metal phthalocyanine organic thin-film transistors: changes in electrical performance and stability in response to temperature and environment. *RSC Advances* **2019**, *9* (37), 21478-21485.
127. Basova, T. V.; Jushina, I. V.; Ray, A. K., Influence of post-deposition annealing under magnetic field on the structure of phthalocyanine thin films. *Journal of Materials Science: Materials in Electronics* **2015**, *26* (7), 4716-4721.
128. Santerre, F.; Côté, R.; Veilleux, G.; Saint-Jacques, R. G.; Dodelet, J. P., Highly Photoactive Molecular Semiconductors: Determination of the Essential Parameters That Lead to an Improved Photoactivity for Modified Chloroaluminum Phthalocyanine Thin Films. *The Journal of Physical Chemistry* **1996**, *100* (18), 7632-7645.
129. Adepalli, K. K.; Kelsch, M.; Merkle, R.; Maier, J., Enhanced ionic conductivity in polycrystalline TiO<sub>2</sub> by “one-dimensional doping”. *Physical Chemistry Chemical Physics* **2014**, *16* (10), 4942-4951.
130. Catalysis and Electrocatalysis at Nanoparticle Surfaces. In *Catalysis and Electrocatalysis at Nanoparticle Surfaces*, Wieckowski, A., Savinova, E., Vayenas, C., Ed. CRC Press: 2003; p 94.
131. Chen, M.; Goodman, D. W., Catalytically Active Gold: From Nanoparticles to Ultrathin Films. *Accounts of Chemical Research* **2006**, *39* (10), 739-746.
132. Jupille, J.; Thornton, G., *Defects at Oxide Surfaces*. Springer: 2015.
133. Sun, R.; Wang, Z.; Shibata, N.; Ikuhara, Y., A dislocation core in titanium dioxide and its electronic structure. *RSC Advances* **2015**, *5* (24), 18506-18510.
134. Cubillas, P.; Anderson, M. W., Synthesis Mechanism: Crystal Growth and Nucleation. In *Zeolites and Catalysis*, 2010; pp 1-55.
135. Maras, E.; Saito, M.; Inoue, K.; Jónsson, H.; Ikuhara, Y.; McKenna, K. P., Determination of the structure and properties of an edge dislocation in rutile TiO<sub>2</sub>. *Acta Materialia* **2019**, *163*, 199-207.
136. Clancy, P., Application of Molecular Simulation Techniques to the Study of Factors Affecting the Thin-Film Morphology of Small-Molecule Organic Semiconductors. *Chemistry of Materials* **2011**, *23* (3), 522-543.
137. Olson, I. A.; Shtukenberg, A. G.; Kahr, B.; Ward, M. D., Dislocations in molecular crystals. *Reports on Progress in Physics* **2018**, *81* (9), 096501.
138. Szot, K.; Rogala, M.; Speier, W.; Klusek, Z.; Besmehn, A.; Waser, R., TiO<sub>2</sub>—a prototypical memristive material. *Nanotechnology* **2011**, *22* (25), 254001.
139. Stoyanov, E.; Langenhorst, F.; Steinle-Neumann, G., The effect of valence state and site geometry on Ti L<sub>3,2</sub> and O K electron energy-loss spectra of Ti<sub>x</sub>O<sub>y</sub> phases. *American Mineralogist* **2007**, *92* (4), 577-586.

## 7. List of References - 6.4 Supporting information – AlClPc on TiO<sub>2</sub>(001) (50% Ti<sup>3+</sup>)

140. Karstens, R. G., M.; Belser, A.; Balle, D.; Polek, M.; Ovsyannikov, R.; Giangrisostomi, E.; Chassé, T.; Peisert, H., FePc and FePcF16 on Rutile TiO<sub>2</sub>(110) and (100): Influence of the Substrate Preparation on the Interaction Strength. *Molecules* **2019**, *24*, 4579.
141. Saito, Y., Two-Dimensional Nucleation with Edge and Corner Diffusions. *Journal of the Physical Society of Japan* **2003**, *72* (8), 2008-2014.
142. Panina, N.; Meekes, H.; van Enckevort, W. J. P.; Deroover, G.; Vlieg, E., Analysis of Growth Spirals on Vapor-Grown Metal-free  $\beta$ -Phthalocyanine Crystals. *Crystal Growth & Design* **2009**, *9* (5), 2409-2414.
143. Diebold, U.; Madey, T. E., TiO<sub>2</sub> by XPS. *Surface Science Spectra* **1996**, *4* (3), 227-231.
144. Wu, L.; Wang, Z.; Xiong, F.; Sun, G.; Chai, P.; Zhang, Z.; Xu, H.; Fu, C.; Huang, W., Surface chemistry and photochemistry of small molecules on rutile TiO<sub>2</sub>(001) and TiO<sub>2</sub>(011)-(2 × 1) surfaces: The crucial roles of defects. *The Journal of Chemical Physics* **2020**, *152* (4), 044702.
145. Yamamoto, Y.; Nakajima, K.; Ohsawa, T.; Matsumoto, Y.; Koinuma, H., Preparation of Atomically Smooth TiO<sub>2</sub> Single Crystal Surfaces and Their Photochemical Property. *Japanese Journal of Applied Physics* **2005**, *44* (No. 17), L511-L514.
146. Firment, L. E., Thermal faceting of the rutile TiO<sub>2</sub>(001) surface. *Surface Science* **1982**, *116* (2), 205-216.
147. Kubo, T.; Sayama, K.; Nozoye, H., Microfaceting Explains Complicated Structures on Rutile TiO<sub>2</sub> Surfaces. *Journal of the American Chemical Society* **2006**, *128* (12), 4074-4078.
148. Ariga, H.; Taniike, T.; Morikawa, H.; Tero, R.; Kondoh, H.; Iwasawa, Y., Lattice-work structure of a TiO<sub>2</sub>(001) surface studied by STM, core-level spectroscopies and DFT calculations. *Chemical Physics Letters* **2008**, *454* (4), 350-354.
149. Busiakiewicz, A.; Klusek, Z.; Rogala, M.; Dabrowski, P.; Kowalczyk, P. J.; Datta, P. K., The new high-temperature surface structure on reduced TiO<sub>2</sub>(001). *Journal of Physics: Condensed Matter* **2010**, *22* (39), 395501.
150. Ariga, H.; Taniike, T.; Morikawa, H.; Tada, M.; Min, B. K.; Watanabe, K.; Matsumoto, Y.; Ikeda, S.; Saiki, K.; Iwasawa, Y., Surface-Mediated Visible-Light Photo-oxidation on Pure TiO<sub>2</sub>(001). *Journal of the American Chemical Society* **2009**, *131* (41), 14670-14672.
151. Adler, H.; Paszkiewicz, M.; Uihlein, J.; Polek, M.; Ovsyannikov, R.; Basova, T. V.; Chasse, T.; Peisert, H., Interface Properties of VOPc on Ni(111) and Graphene/Ni(111): Orientation-Dependent Charge Transfer. *J. Phys. Chem. C* **2015**, *119* (16), 8755-8762.
152. Zupalova, M.; Prochazka, J.; Bastl, Z.; Duchoslav, J.; Rubacek, L.; Havlicek, D.; Kavan, L., Facile Conversion of Electrospun TiO<sub>2</sub> into Titanium Nitride/Oxynitride Fibers. *Chemistry of Materials* **2010**, *22* (13), 4045-4055.
153. Duncan, D. A.; Pfisterer, J. H. K.; Deimel, P. S.; Acres, R. G.; Fritton, M.; Feulner, P.; Barth, J. V.; Allegretti, F., Formation of a thermally stable bilayer of coadsorbed intact and deprotonated thymine exploiting the surface corrugation of rutile TiO<sub>2</sub>(110). *Physical Chemistry Chemical Physics* **2016**, *18* (30), 20433-20442.
154. Hirakawa, H.; Hashimoto, M.; Shiraishi, Y.; Hirai, T., Selective Nitrate-to-Ammonia Transformation on Surface Defects of Titanium Dioxide Photocatalysts. *ACS Catalysis* **2017**, *7* (5), 3713-3720.
155. Benson, E. E.; Miller, E. M.; Nanayakkara, S. U.; Svedruzic, D.; Ferrere, S.; Neale, N. R.; van de Lagemaat, J.; Gregg, B. A., Semiconductor-to-Metal Transition in Rutile TiO<sub>2</sub> Induced by Tensile Strain. *Chemistry of Materials* **2017**, *29* (5), 2173-2179.
156. Reckers, P.; Dimamay, M.; Klett, J.; Trost, S.; Zilberberg, K.; Riedl, T.; Parkinson, B. A.; Brötz, J.; Jaegermann, W.; Mayer, T., Deep and Shallow TiO<sub>2</sub> Gap States on Cleaved Anatase Single Crystal (101) Surfaces, Nanocrystalline Anatase Films, and ALD Titania Ante and Post Annealing. *The Journal of Physical Chemistry C* **2015**, *119* (18), 9890-9898.
157. Tucker, N. P.; Blyth, R. I. R.; White, R. G.; Lee, M. H.; Robinson, A. W. & Barrett, S. D., Utilization of Photoemission Cross-Section Effects for Monitoring Thin-Film Growth in UHV. *Journal of Synchrotron Radiation* **1995**, *2*, 252-255.

## 7. List of References - 6.4 Supporting information – AlCIPc on TiO<sub>2</sub>(001) (50% Ti<sup>3+</sup>)

158. Kolotovska, V.; Friedrich, M.; Zahn, D. R. T.; Salvan, G., Magnetic field influence on the molecular alignment of vanadyl phthalocyanine thin films. *Journal of Crystal Growth* **2006**, 291 (1), 166-174.
159. Wang, Y.; Kröger, J.; Berndt, R.; Hofer, W. A., Pushing and Pulling a Sn Ion through an Adsorbed Phthalocyanine Molecule. *Journal of the American Chemical Society* **2009**, 131 (10), 3639-3643.
160. Hong, I. P.; Li, N.; Zhang, Y.-J.; Wang, H.; Song, H.-J.; Bai, M.-L.; Zhou, X.; Li, J.-L.; Gu, G.-C.; Zhang, X.; Chen, M.; Gottfried, J. M.; Wang, D.; Lü, J.-T.; Peng, L.-M.; Hou, S.-M.; Berndt, R.; Wu, K.; Wang, Y.-F., Vacuum synthesis of magnetic aluminum phthalocyanine on Au(111). *Chemical Communications* **2016**, 52 (68), 10338-10341.

## 8. List of publications

Throughout my PhD studies I have contributed to publications listed below.

### 8.1 Peer-reviewed papers

**[1] Communication: Influence of graphene interlayers on the interaction between cobalt phthalocyanine and Ni (111)**, J. Uihlein, H. Peisert, M. Glaser, M. Polek, H. Adler, F. Petraki, R. Ovsyannikov, M. Bauer, T. Chassé, *The Journal of chemical physics* 138 (8), 081101, (2013)

**[2] Interface between FePc and Ni (111): Influence of Graphene Buffer Layers**, J. Uihlein, H. Peisert, H. Adler, M. Glaser, M. Polek, R. Ovsyannikov, T. Chassé, *The Journal of Physical Chemistry C* 118 (19), 10106-10112, (2014)

**[3] Strong interaction of MnPc on Ni (111): influence of graphene buffer layer**, J. Uihlein, H. Peisert, H. Adler, M. Glaser, M. Polek, R. Ovsyannikov, M. Bauer, T. Chassé, *The Journal of Physical Chemistry C* 118 (49), 28671-28678, (2014)

**[4] Interface Properties of VOPc on Ni (111) and Graphene/Ni (111): Orientation-Dependent Charge Transfer**, H. Adler, M. Paszkiewicz, J. Uihlein, M. Polek, R. Ovsyannikov, T.V. Basova, T. Chassé, H. Peisert, *The Journal of Physical Chemistry C* 119 (16), 8755-8762, (2015)

**[5] Influence of graphene on charge transfer between CoPc and metals: The role of graphene–substrate coupling**, J. Uihlein, M. Polek, M. Glaser, H. Adler, R. Ovsyannikov, M. Bauer, M. Ivanovic, A. B. Preobrajenski, A. V. Generalov, T. Chassé, H. Peisert, *The Journal of Physical Chemistry C* 119 (27), 15240-15247, (2015)

**[6] Transition-Metal Phthalocyanines on Transition-Metal Oxides: Iron and Cobalt Phthalocyanine on Epitaxial MnO and TiOx Films**, M. Glaser, H. Peisert, H. Adler, M. Polek, J. Uihlein, P. Nagel, M. Merz, S. Schuppler, T. Chassé, *The Journal of Physical Chemistry C* 119 (49), 27569-27579, (2015)

**[7] Chemical reaction of polar phthalocyanines on silver: chloroaluminum phthalocyanine and fluoroaluminum phthalocyanine**, M. Polek, F. Latteyer, T.V. Basova, F. Petraki, U. Aygül, J. Uihlein, P. Nagel, M. Merz, S. Schuppler, T. Chassé, H. Peisert, *The Journal of Physical Chemistry C* 120 (43), 24715-24723, (2016)

**[8] Electronic structure and self-organization properties of low band gap polymers: The effect of the introduction of additional thiophene moieties**, M. Ivanović, U. Aygül, U. Dettinger, A. Tournebize, M. Polek, D. Batchelor, S. Mangold, M. Forster, U. Scherf, H. Peisert, T. Chassé, *Solar Energy Materials and Solar Cells* 157, 286-294, (2016)

**[9] Electronic structure of hexacene and interface properties on Au (110)**, P. Grüninger, M. Polek, M. Ivanović, D. Balle, R. Karstens, P. Nagel, M. Merz, S. Schuppler, R. Ovsyannikov, H. F. Bettinger, H. Peisert, T. Chassé, *The Journal of Physical Chemistry C* 122 (34), 19491-19498, (2018)

**[10] FePc and FePcF16 on Rutile TiO2 (110) and (100): Influence of the Substrate Preparation on the Interaction Strength**, R. Karstens, M. Glaser, A. Belser, D. Balle, M. Polek, R. Ovsyannikov, E. Giangrisostomi, T. Chassé, H. Peisert, *Molecules* 24 (24), 4579, (2019)

**[11] The interface between chloroaluminum phthalocyanine and titanium dioxide: The influence of surface defects and substrate termination**, M. Polek, T.V. Basova, T. Chassé, H. Peisert, *Physical Chemistry Chemical Physics*, 23 (2021) 13370–13380.

### 8.2 Conference contributions

**[1] Investigation of the influence of graphene interlayers on the interaction between cobalt phthalocyanine and Ni(111) by X-ray photoemission and absorption spectroscopies** (Poster), J.

## 8. List of publications - 8.2 Conference contributions

Uihlein, H. Peisert, M. Glaser, M. Polek, H. Adler, F. Petraki, R. Ovsyannikov, M. Bauer, and T. Chassé, DPG-Frühjahrstagung, Regensburg, Deutschland, 10 – 15 März 2013.

**[2] Investigation of electronic and structural properties of cobalt phthalocyanine on graphene interlayers on Ni(111)** (Poster), H. Adler, J. Uihlein, H. Peisert, M. Polek, F. Petraki, and T. Chassé, Institut für Physikalische und Theoretische Chemie, Auf der Morgenstelle 18, 72076 Tübingen, Germany, DPG-Frühjahrstagung, Regensburg, Deutschland, 10 – 15 März 2013.

**[3] Interface properties of polar phthalocyanines on silver substrates** (Poster), M. Polek, F. Petraki, F. Latteyer, H. Peisert, T. Chassé, DPG-Frühjahrstagung, Regensburg, Deutschland, 10 – 15 März 2013.

**[4] Interface properties of polar phthalocyanines on silver substrates** (Poster), M. Polek, T.V. Basova, F. Petraki, F. Latteyer, H. Peisert, T. Chassé, VIII International Workshop on Semiconductor Surface Passivation, Krakau, Polen, 8 – 12 September 2013.

**[5] Investigation of electronic and structural properties of vanadyl phthalocyanine on graphene interlayers on Ni(111)**, (Poster), H. Adler, H. Peisert, M. Paszkiewicz, J. Uihlein, M. Polek, and T. Chassé, DPG-Frühjahrstagung, Dresden, Deutschland, 30 März – 4 April 2014.

**[6] FePc and CoPc on Ni(111) and graphene/Ni(111): Influence of the central metal atom** (Poster), J. Uihlein, H. Peisert, H. Adler, M. Glaser, M. Polek, and T. Chassé, DPG-Frühjahrstagung, Dresden, Deutschland, 30 März – 4 April 2014.

**[7] AlClPc on silver: Influence of substrate surface** (Poster), M. Polek, T. V. Basova, F. Petraki, F. Latteyer, H. Peisert, T. Chassé, DPG-Frühjahrstagung, Dresden, Deutschland, 30 März – 4 April 2014.

**[8] Strong Interaction of MnPc on Ni(111): Influence of Graphene Buffer Layer** (Poster), J. Uihlein, H. Peisert, H. Adler, M. Glaser, M. Polek, R. Ovsyannikov, M. Bauer, T. Chassé, DPG-Frühjahrstagung, Berlin, Deutschland, 15 – 20 März 2015.

**[9] Influence of graphene interlayer on CoPc/Pt(111) interface** (Poster), M. Polek, H. Adler, A. Generalov, M. Glaser, M. Ivanović, A. Preobrajenski, J. Uihlein, H. Peisert, T. Chassé, Frühjahrstagung der Deutschen Physikalischen Gesellschaft (DPG-Frühjahrstagung), Berlin, Deutschland, 15 – 20 März 2015.

**[10] Tuning of the interactions of transition metal phthalocyanines with metal surfaces - influence of graphene buffer layers and intercalation**, H. Peisert, J. Uihlein, H. Adler, M. Glaser, D. Balle, M. Polek, T. Chassé, XUVX 2016 Zürich, Switzerland, 03 - 08 Juli 2016.

**[11] Interactions of transition metal phthalocyanines at metal surfaces – influence of intercalated graphene buffer layers** (Poster), J. Uihlein, D. Balle, H. Adler, M. Glaser, M. Polek, J. Schmid, T. Chassé, ICSFS 18, Chemnitz, Deutschland, 28 August – 02 September 2016.

**[12] Tuning of interactions of transition metal phthalocyanines at metal surfaces by intercalated graphene buffer layers** (Talk), D. Balle, J. Uihlein, M. Polek, H. Adler, T. Chassé, H. Peisert, ASOMEA-VIII Workshop, Okazaki, Aichi, Japan, 23 - 25 November 2016.

**[13] Influence of the Fluorination of CoPc on interfacial charge transfer**, D. Balle, H. Adler, P. Grüninger, R. Karstens, M. Polek, M. Glaser, T. Chassé, H. Peisert, BESSY Nutzertreffen 2016, Berlin, Deutschland, 07 - 09 Dezember 2016

**[14] Chemical interaction of chloroaluminum phthalocyanine on silver and TiO<sub>2</sub>**, (Poster) M. Polek, D. Balle, M. Ivanovic, P. Nagel, M. Merz, S. Schuppler, T. Chassé, H. Peisert, KNMF und ANKA Nutzertreffen 2017, Karlsruhe, Deutschland, 21 - 22 Februar 2017.

**[15] Interactions at the interface of Cobalt phthalocyanine and graphene covered metal surfaces: Influence of Fluorination of CoPc**, D. Balle, M. Polek, R. Karstens, P. Grüninger, H. Adler, T. Chassé, H. Peisert, DPG Frühjahrstagung 2017 Dresden, Deutschland, 19 - 24 März 2017.



# Acknowledgements

---

I thank Prof. Thomas Chassé and app. Prof. Heiko Peisert for giving me the opportunity to do my PhD and the possibility to learn about ultra-high vacuum based techniques. I forward my gratitude to Prof. Tamara V. Basova for providing the phthalocyanines, her help in discussion of data and preparation of manuscripts.

I am grateful for all the technical support from Mr. Wolfgang Neu. Thank you for always allowing me to take a look at your work. I have learned a lot and was able to give this knowledge further to my younger colleagues.

My gratitude goes to all of IPTC secretary office members who have always supported me with their work and who brought a lot of good atmosphere into our work place. I also could not do without all the known and unknown heroes of university workshops, whom I visited frequently for repairs of old and construction of new laboratory equipment.

Many thanks to Mathias, for his support as a fellow PhD student and a great friend, as well as my guardian angels Benedetta, Elke and Leonora for their friendship, motivation and scientific support.

I want to thank all members of AG Chassé and AG Casu for good working atmosphere at 5<sup>th</sup> floor, with special thanks to Caroline: for sharing her scientific and life wisdom, together with Team BESSY: Johannes, Hilmar and Mathias. We had a lot of work, but also a lot of fun.

Thank you to all of the students who were in my care. I really enjoyed working with you.

I wish to thank my wonderful flat-mates: Hasina and Aurélien (Team Derendingen) as well as Joana, Neeraja, Julien, Kushal, Prateek (Team Erlenweg) along with Fabienne, Diana and Francesco who were always adding to the good atmosphere of Erlenweg-WG. Thank you for great shared flat experience.

I am deeply grateful to my dear friends: Joanna, Karolina, Katarzyna, Renata, Kamil, Marcin and their dear families who, although so far away, never forgot about me, as well as Team HI: Jerzy, Artur, Jakub, Mieczysław and Karol. Thank you for your understanding and patience.

I want to thank my Tübingen sisters Faezeh and Elham, together with Markus for all our small adventures, cooking and renovation projects.

I would particularly like to thank Thorsten. Thank you for everything.

Last but not least, I want to thank my grandmother, parents and brother, who supported me from the very beginning.